Kinetics and mechanistic studies in the HIRAC chamber

Luke Nicholas Farrugia

Submitted in accordance with the requirements for the degree of
Doctor of Philosophy

The University of Leeds
School of Chemistry

September 2013

The candidate confirms that the work submitted is his own. Where work which has formed part of jointly-authored publications has been included, the contribution of the candidate to this work has been explicitly indicated overleaf. The candidate confirms that appropriate credit has been given within the thesis where reference has been made to the work of others.

Acknowledgements

Where to begin? First and foremost, a big thank you goes to my mentors Paul Seakins and Dwayne Heard for their constant support and dedication throughout my studies. I have learnt so much from you both, and am grateful for all your patience and attention during these past four years.

I would have probably lost it several times more if it weren't for the great company and support of my good friend Fred Winiberg. We have been through this whole experience together. I will miss our loud debates, and wish you all the best in getting your thesis in. I will make sure I leave some spare duct tape and neoprene in case the chamber leaks again.

I came to Leeds with a limited experimental background and could not thank Mark Blitz, Andy Goddard and Trevor Ingham enough for teaching me the ropes. My postdoc Shona Smith also deserves mention for her time and dedication during the first few years of my PhD. The bustling basement and Dainton offices have pretty much been my home over the past few years and have given me some good friends and I feel happy to have met you all: Hannah, Steph, Rebecca, Robin, James, Dan, Shona, Pete, Lisa, Ingrid, Danny, Ingvaar, Jadgwiga, and Pascale. I also wish to thank Dave Fogarty for his printing services and enjoyable chats as well as his guidance during my laboratory demonstration duties in the Porter Labs, and for offering me extra shifts when my PhD funding had run out.

Outside of the workplace, I am also very lucky to have made good friends in my time here in Leeds, which is still going on and I would have probably gone cuckoo if it wasn't for all the great company and moments I have shared with them all. Special mention goes to my girlfriend Kristina for her love, patience, care and cooking (2014 will be ours), and all my good friends Michal, Raul, Javi, Benito, Tolo, Laura, Benjamin, Cristina, Guillermo, Monica, Alfonso, Ivana, Ivan, Viktor, Mindaugas and Ugne. You are all amazing people and I love you all so much and thank you for all the great times we've shared and hope they will go on!

Mike Vella and Nicholas Flores Martin, my two oldest friends, you are like brothers to me and you were both so kind enough to offer to proof read this thesis for me, much appreciated. Also, thanks to the Natural Environment Research Council

(NERC) for funding my PhD. Last but not least, a small message in Maltese/Klingon for those dearest in my heart, my parents:

"Grazzi papa u mama tal-appogg kontinwu u mħabba li dejjem wrejtuni! Għandi u dejjem kelli rispett kbir lejkhom, u peress li din ser tkun misprobabli l-akbar kitba ta hajti, ma xtaqt niddedikaha lil ħadd ieħor ħliefkom! Nħobbkom ħafna u vera kburi u ffurtunat li għandi ġenituri bħalkom! Grazzi ta kull ma għamiltu miegħi!"

Energise!

Abstract

Atmospheric chambers are integral in the understanding of key issues surrounding the atmosphere. Atmospheric chemical processes can be studied both kinetically and mechanistically under predetermined and controlled conditions to better understand VOC oxidation processes occurring in the atmosphere. Wide arrays of atmospheric chambers enable the underpinning of key issues surrounding the behaviour of atmospheric trace gases and aerosols. Moreover, their input has also spread increasingly into mechanism development and development of new methods for detecting and investigating trace gases by intercomparison of different measuring instruments. The Highly Instrumented Reactor for Atmospheric Chemistry (HIRAC) chamber at the University of Leeds is a 2.25 m^3 stainless steel reactor that allows the study of a wide range of kinetics and mechanistic investigations over the full range of tropospheric temperatures and pressures.

A temperature control system has been setup and tested in HIRAC. Absolute rate measurements ozonolysis reactions with propene were performed over a temperature range of ~220 – 320 K to characterise this system. Relative rate measurements have also been used to measure the kinetics of a number of reactions, using Gas Chromatography (GC-FID) and Fourier Transform Infra-red (FTIR) spectrometry detection. An investigation of chlorine atom reactions with butanes and pentanes over a similar temperature range relevant to the entire troposphere were performed and branching ratios calculated over varying temperatures using GC and FTIR detection. High precision measurements were also obtained for several chlorine atom reactions and the rate coefficients of a series of higher ketones, esters and alkanes were generated in HIRAC using this method. GC-FID and FTIR were also useful in a preliminary investigation on the reaction of chlorine atoms with ethanol, and initial results on HCl and DCl ratios were obtained from this study.

Relative rate experiments were also useful in the assessment of different OH radical generation techniques under low NO_x conditions. A characterisation of *tert*-butyl hydroperoxide photolysis in HIRAC was performed under low NO_x conditions utilising the HIRAC FAGE for absolute OH measurements.

Table of Contents

List of Figures

List of Tables

Chapter 1 – Introduction to atmospheric chemistry and chamber studies

1.1 Introduction

The study of the detailed chemistry of atmospheric processes is of fundamental importance to fully understand both current and future global environmental problems. Increased concentrations of gas pollutants and particulate matter have arisen from increased transport emissions as well as industrial, land use changes and biomass burning processes, leading to several consequences including climate change and the degradation of air quality (Monks et al., 2009). Atmospheric chemistry is a broad field of study, both in the problems addressed and in the approaches taken to understand them. The genesis of the field lies in air pollution in the troposphere, for which there is documentation dating as far back as the 13th century (Finlayson-Pitts, 2010). There are various examples of air pollution phenomena that have occurred in the 20th century, such as smog formation. Nitrogen oxides are one of the key ingredients required for smog formation, and these are emitted along with Volatile Organic Compounds (VOCs) from the combustion of fossil fuels.

The analysis of the behaviour of polluted air and its oxidation processes by directly taking samples from the atmosphere has several downfalls including different sources, weather and transport conditions rendering the interpretation extremely difficult. Atmospheric chambers are capable of replicating the atmospheric conditions under more controlled environments without any issues on transport factors. Section 1.3 of this chapter will go through the pros and cons of studying the processes leading to air pollution and smog formation using atmospheric chambers.

It took a number of decades to understand the gas-phase chemistry of these processes, and it was not until the 1970's that the OH radical was recognised as the key driver of chemistry throughout the atmosphere (Finlayson-Pitts and Pitts, 2000, Heard and Pilling, 2003). Since this discovery, the role of O_3, NO_3 and halogen atoms as oxidants has also become evident (Finlayson-Pitts, 2010), and further studies into

the fundamental chemistry of this kind of pollution revealed that similar intermediates and processes were occurring as well in photochemical smog formation.

These discoveries expanded the scientific interest in the field, and were followed by further interest in the close linkage between the chemistry of the troposphere and stratosphere in the 1970's. This led to studies of species that could be transported from the troposphere to the stratosphere, such as chlorofluorocarbons (CFCs), which had sufficiently long lifetimes to reach this altitude. The photolysis of CFCs in the stratosphere would lead to the destruction of O_3, and the discovery and understanding of this destruction mechanism brought about by anthropogenic emissions was credited to Crutzen, Molina and Rowland. The latter authors were awarded a Nobel Prize in Chemistry in 1995 for their contributions to the understanding of halogen chemistry in the stratosphere, as well as NO_x and O_3 destruction (Molina and Rowland, 1974, Crutzen, 1971). This milestone has led to further studies on NO_x and O_3 loss phenomenon and to the need to further understand the heterogeneous chemistry involved, which was clearly playing a key role along with photochemistry.

Despite this gain in knowledge, much more work remains in order to better understand these processes on a molecular level, and in most cases this still remains quite challenging. All forms of atmospheric research (laboratory, theoretical, field work and modelling) must be brought together in order for the complexity of atmospheric processes to be better understood, and indeed the full integration of these approaches is needed in order to obtain a molecular level insight that would otherwise be even more challenging. In a similar manner, inter-comparison of results in the field with model and laboratory studies has been vital in reducing the uncertainties of our understanding of these processes. Chamber studies have come into play as well as will be mentioned further on, as they bridge the gap between fieldwork and laboratory studies, and are an important recent addition to the field of atmospheric chemistry to be demonstrated gradually over the course of this thesis. The main aims of this thesis are highlighted at the end of this chapter.

1.2 Tropospheric chemistry

1.2.1 Composition and structure

The major constituents of the atmosphere are nitrogen 78% (N_2), 21% oxygen (O_2) and 1% argon (Ar), with liquid water (H_2O) varying between ~0 – 4% by latitude, lower in the polar regions and higher in the tropics, as well as by altitude, being low in the dessert surface and high near the tropopause. Small amounts of a wider range of species are also present, such as ~400 ppm carbon dioxide (CO_2) and ~1.8 ppm methane (CH_4) (Tarasova et al., 2013). These are known as trace species, and their concentrations are dependent upon altitude and geographical location.

The pressure and temperature variations of the atmosphere as a function of altitude are illustrated in Figure 1.1. The region of the atmosphere of most relevance to the work reported in this thesis is the troposphere which is the lowest level of the atmosphere, of topical interest due to its direct effect on human health. The temperature in the troposphere falls at a rate of ~4 – 7 K km^{-1} until a minimum of ~220 – 230 K at ~10 – 17 km in a region of the atmosphere known as the tropopause. Pressures in the troposphere vary from ~1000 – 100 mbar.

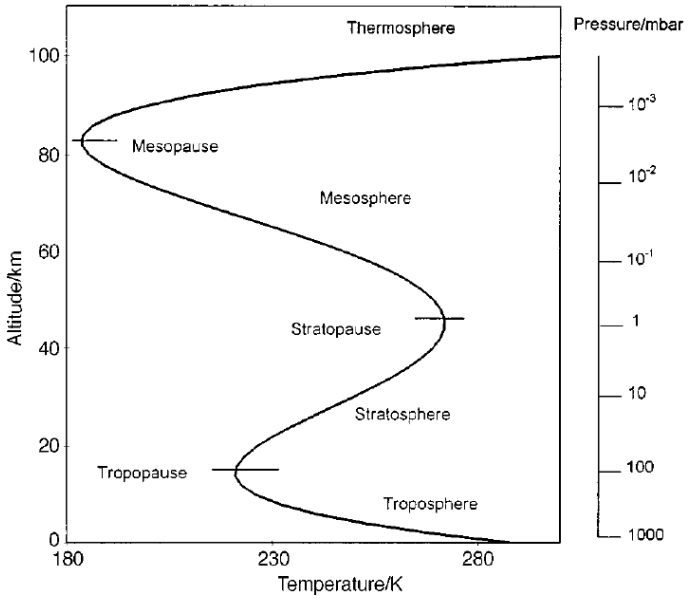

Figure 1.1: The temperature profile of the Earth's atmosphere at varying altitude (km) and pressure (mbar) (Wayne, 2000).

The temperature drop in the troposphere is due to strong heating effects arising from UV radiation absorbed at Earth's surface. This heat rises as hot air parcels that expand as they rise due to the drop in pressure at higher altitudes and these air parcels do work against the surroundings but do not gain heat in exchange, hence energy is lost resulting in a decrease in temperature. This process results in strong vertical mixing and causes the emitted gases and particles from the Earth's surface to travel to the higher troposphere and tropopause, depending on their reactivity (Finlayson-Pitts and Pitts, 2000).

On average it will take 1 – 2 days to exchange between the boundary layer and the free troposphere, and around a month to the tropopause (Seinfeld, 1998). Stratospheric temperature inversion significantly limits vertical mixing between the troposphere and the stratosphere, limiting transport of many ground level VOCs to the stratosphere. This limitation results in mixing times being in the order of years between the lowest two strata of the atmosphere (Wayne, 2000). The temperature profile of the stratosphere means it is much more stable than the troposphere.

The temperature at the tropopause changes upwards into the stratosphere due to the Chapman cycle (Chapman, 1930) involving the two most abundant oxidants in the atmosphere, ozone and molecular oxygen. The ozone layer at this stratum of the atmosphere absorbs solar radiation which is liberated as heat. This ozone layer is formed from molecular oxygen present in the stratosphere that photodissociates through absorption of low energy photons present in this region of the atmosphere. The oxygen atoms formed collide with oxygen molecules in the presence of a third body to form ozone. The bonds in ozone molecules are weaker than those in oxygen molecules and therefore photolysis resulting in dissociation is achieved with lower energy photons present in the stratosphere (Finlayson-Pitts and Pitts, 2000).

The ability to reproduce the full range of tropospheric conditions *i.e.* pressure, temperature and light in a controlled manner allows for important investigations into the chemistry of the troposphere that will help to improve our understanding of key processes such as climate change and air quality.

1.2.2 VOC oxidation

VOCs are the major gas pollutants emitted in large quantity by both anthropogenic and biogenic sources and have a major influence on the chemistry of the troposphere, which is of most interest to humans due to the direct impact to human and plant health. This has led to the development of detailed VOC oxidation schemes explaining the degradation processes of these pollutants in the troposphere. Figure 1.2(a) shows a flow of the different stages of VOC oxidation in the troposphere, and the secondary VOCs formed from this degradation process. A major component in the atmospheric oxidation of gas pollutants in the troposphere is the extremely reactive hydroxyl (OH) radical. The importance of OH chemistry is highlighted in the next section, and work done on assessing different OH generation methods under low NO_x conditions in atmospheric chambers is reported in chapter 7.

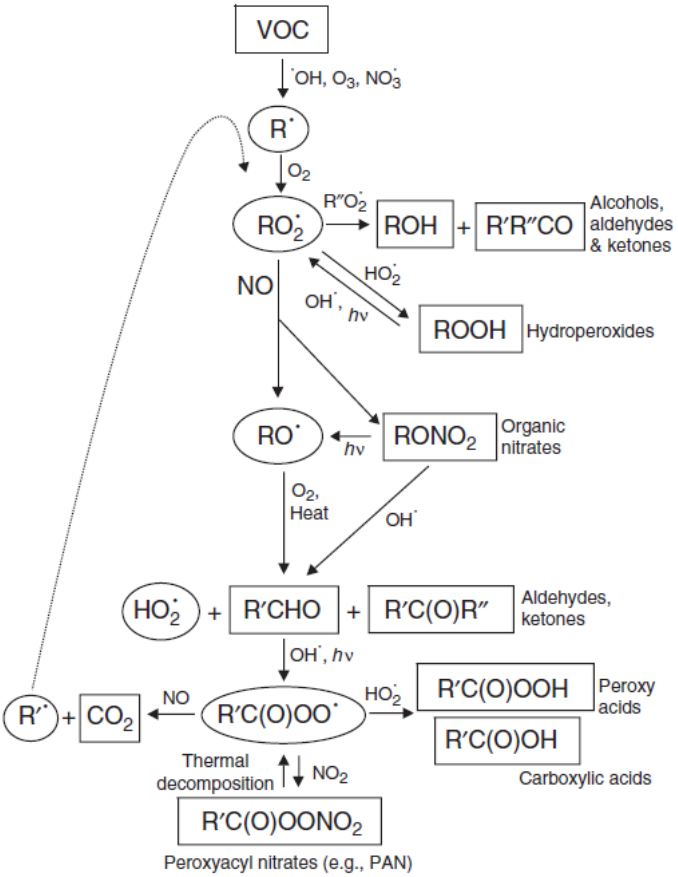

Figure 1.2(a): Flow diagram showing the VOC oxidation processes and end products at different stages of the degradation in the troposphere (Blake et al., 2002).

VOC oxidation is initiated by a range of oxidants, with OH, NO_3 and O_3 being the most important. An EKMA diagram, or ozone isopleth, shown in Figure 1.2(b)

was devised by the EPA (Environmental Protection Agency, USA) and is a useful regulatory control of ozone using two known precursors (NO_x and VOCs) and looking at the sensitivity of ozone production for different mixing ratios.

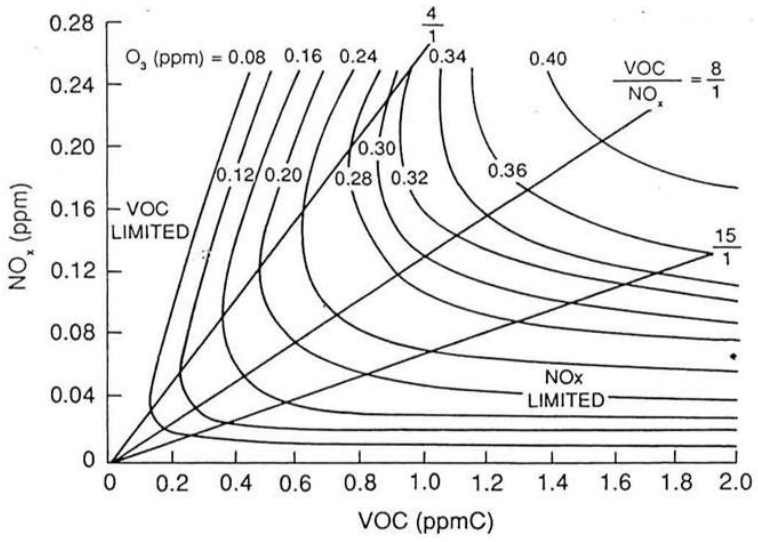

Figure 1.2(b): Typical ozone isopleth plot (Dodge, 1977)

In general, NO_x limited areas are located downwind of urban areas while VOC limited areas are typically in highly polluted urban areas. As has been already highlighted, the dominant oxidising agent during daytime is the hydroxyl radical, which is key to ozone formation and both VOCs and NO_x (mainly as NO_2) will compete for OH. VOC oxidation processes (as shown in Figure 1.2(a)) are initiated by OH radicals and produce an alkyl radical (R·), which reacts in the presence of oxygen to form a peroxyl radical (RO_2·), as is shown in R1.1 – 1.2:

$$OH\cdot + VOC \rightarrow R\cdot \qquad \text{(R1.1)}$$

$$R\cdot + O_2 \rightarrow RO_2\cdot \qquad \text{(R1.2)}$$

In urban polluted environments the presence of NO_x (nitrogen dioxide, NO_2 and nitrogen monoxide, NO), are high and RO_2· radicals react with NO to produce alkoxy radicals (RO) and NO_2. NO_2 is photolysed by sunlight to give NO and $O(^3P)$, which reacts with O_2 to give O_3:

$$RO_2\cdot + NO \rightarrow RO\cdot + NO_2 \qquad \text{(R1.3)}$$

$$NO_2 + h\upsilon(< 420nm) \rightarrow NO + O(^3P) \qquad \text{(R1.4)}$$

$$O(^3P) + O_2 \rightarrow O_3 \qquad (R1.5)$$

O_3 photolysis is the main precursor of OH, as it gives $O(^1D)$ radicals which may react with H_2O to give two OH radicals as is shown in R1.6 – 1.7, which is however a minor pathway, shown in R7.1a (10% conversion), and only occurs if it is not quenched back to its ground state through a collision with a third body (nitrogen or oxygen molecules). The quenching process, resulting in the formation of $O(^3P)$, is the major pathway, shown in R1.7b, accounting for 90% conversion (Wayne, 2000):

$$O_3 + h\upsilon \rightarrow O_2 + O(^1D) \qquad (R1.6)$$

$$O(^1D) + H_2O \rightarrow 2OH\cdot \qquad (R1.7a)$$

$$O(^1D) + M \rightarrow O(^3P) + M \qquad (R1.8b)$$

The photolysis of NO_2 also leads to the formation of $O(^3P)$ and NO, which reacts with O_2 to make O_3. RO· radicals formed in R1.3 may later react with oxygen to give HO_2 and a carbonyl product, RO as is shown in R1.8. The carbonyl product may undergo further oxidation in the presence of OH and other oxidants (R1.1) while the HO_2radical produced reconverts to OH (R1.9) in a similar manner to the RO_2 radical reaction with NO (R1.3):

$$RO\cdot + O_2 \rightarrow RO + HO_2 \qquad (R1.9)$$

$$HO_2\cdot + NO \rightarrow OH\cdot + NO_2 \qquad (R1.10)$$

By rapidly converting the hydroperoxide radical (HO_2) to OH, NO increases tropospheric OH abundances and thus indirectly reduces the atmospheric burdens of carbon monoxide (CO), methane (CH_4), and halofluorocarbons (HFCs) (Hallett, 2002). VOCs found in the troposphere can be transformed by several processes, such as photolysis, as well as reactions with OH, NO_3, halogens and O_3(Atkinson, 2000). The VOC oxidation cycle shown in Figure 1.2 demonstrates the further oxidation steps that give rise to subsequent oxidation products, each undergoing further oxidation processes. VOC oxidation proceeds until both parent and generated VOCs are completely oxidised to carbon dioxide and water. The complexity of understanding fully VOC oxidation processes in the troposphere lies in the importance in simultaneously knowing the oxidation of all the subsequent products generated

from the parent VOC, and this is where mechanistic studies become important. A number of mechanistic investigations will be highlighted in chapters 5 and 6. The lifetimes and consequent influence of both parent and generated VOCs on different parts of the troposphere are dependent upon their sources, sinks and concentration ranges. Table 1.1 gives an overview of the typical sources, sinks and concentration ranges of a select range of VOCs present in the troposphere. The majority of these classes of compounds have been investigated in kinetic and mechanistic investigations to be reported in this thesis.

Class of compound	**Formula**	**Atmospheric lifetime (reaction with OH)***	**Principal source**	**Principal sinks**	**Typical mixing ratios (ppb)**
Alkanes			Fossil fuel burning, biomass, vehicle emissions	OH	
methane	CH_4	10 years			$1.7 – 1.9 \times 10^3$
ethane	C_2H_6	80 days			0.2 – 2.0
propane	C_3H_8	17 days			0 – 1.0
n-butane	C_4H_{10}	6 days			0 – 0.5
n-pentane	C_5H_{12}	4 days			0 – 0.3
Alkenes			Vehicle emissions, Biomass, Biogenic, Vegetation	OH, NO_3, O_3	
ethene	C_2H_4	1.7days			0 – 0.1
propene	C_3H_6	7 hours			0.01
isoprene	C_5H_8	1.5 hours			0 – 1.0
Carbonyls			Biogenic, VOC oxidation	OH, *hυ*	0.3 – 1.0
formaldehyde	HCHO	4 hours			
acetone	CH_3COCH_3	16 days			
glyoxal	OCHCHO	2.9 hours			
methylglyoxal	CH3C(O)CHO	1.6 hours			
Peroxides			VOC oxidation	OH, *hυ*	0 – 1.0
methyl hydro-peroxide	CH_3OOH	2 days			
Alcohols			Biogenic, VOC oxidation	OH, NO_3	0 – 0.2
methanol	CH_3OH	16 days			

Table 1.1: Typical global atmospheric sources sinks and concentrations of select classes of tropospheric VOC species that are investigated in this thesis. Atmospheric lifetimes are calculated from IUPAC recommended kinetic data(Atkinson et al., 2006a) and based on mean global [OH] = 10^6 molecules cm^{-3} (Stone et al., 2012).

1.2.3 Hydroxyl radical chemistry

The hydroxyl (OH) radical is of fundamental importance in the understanding of tropospheric chemistry. OH is the key species in that it controls the removal rate of the majority of atmospheric pollutants. VOCs major loss process in the troposphere is from reaction with the OH radical and this in turn has its effect on local, regional and global scales. OH reactivity with VOCs results in OH being very short-lived (τ_{OH}<few seconds) and playing a major role in radical chemistry in the troposphere, with reactions often resulting in the formation of peroxy radicals. The average daytime concentration of OH radicals in the troposphere measured from various field campaigns was found to be ~1 × 10^6 molecule cm^{-3} (Stone et al., 2012). Figure 1.3 represents the cycling of OH in the troposphere.

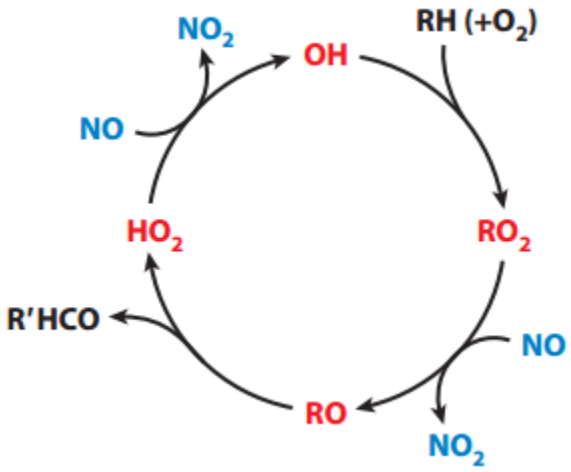

Figure 1.3: Diagram representing the HO_x cycle, showing the creation, termination and regeneration of HO_x radicals (Seakins and Blitz, 2011)

OH is involved in the formation of tropospheric ozone as well as secondary organic aerosols (SOAs). It is also responsible for controlling the major atmospheric trace gases' lifetimes due to its high reactivity (Ehhalt et al., 1998, Ehhalt, 1998, Hausmann et al., 1998), and is regarded as being the primary cleansing agent of the troposphere as it provides the dominant sink for the majority of greenhouse gases and pollutants. Due to all these contributions, it is important to accurately understand all the sources and sinks of this radical in the troposphere. OH is commonly used as a probe of our understanding of fast photochemistry (Heard, 2006) through comparison with model calculations (Stone et al., 2012). There are uncertainties that need

addressing with regards to sources and sinks of OH in rural environments (Di Carlo et al., 2004, Stone et al., 2012, Whalley et al., 2012).

Photodissociation of VOCs such as peroxides and carbonyls are also thought to be a significant source of OH radicals, particularly in the upper troposphere (Singh et al., 2004). Field measurements over the lower troposphere have also suggested contribution from acetone photolysis and other unsaturated hydrocarbons sustaining a large pool of radicals in continental regions (Heard et al., 2004). Acetone photolysis will be discussed in chapters 3 and 7 as a source of OH radicals in chamber studies.

Nitrous acid (HONO) photolysis can be a dominant OH source in the urban environment. HONO accumulates at night due to high NO_2 levels resulting in it being a major source in the early morning when the high zenith angle of the sun prevents short-wavelength UV-B from penetrating the troposphere (Alicke et al., 2003). Its importance has also been measured in low NO_x environments in forest canopies (Kleffmann et al., 2005) during daylight through heterogeneous formation on surfaces treated with nitric acid (Harris et al., 1982).

$$H_2O + 2\ NO_2 \rightarrow HNO_3 + HONO \qquad \text{(R1.11)}$$

$$HONO + h\upsilon \xrightarrow{\lambda \geq 400\ nm} OH + NO \qquad \text{(R1.12)}$$

HONO has been tested as a photolytic source of OH radicals in atmospheric chambers (Rohrer et al., 2005), and similar tests will be described in chapter 7 on low NO_x alternatives.

OH radicals react with the majority of atmospheric trace gases, often leading to the formation of HO_2, which reacts further with ozone or NO recycling back to OH as has been discussed in the previous section (R1.9). The major loss processes of OH radicals in the troposphere are through radical-molecule reactions resulting in the formation of peroxides (under low NO_x conditions) as is shown in R1.12 and R1.13, or through reaction with NO_2 forming nitric acid (R1.14):

$$HO_2 + HO_2 \rightarrow H_2O_2 + O_2 \qquad \text{(R1.13)}$$

$$CH_3O_2 + HO_2 \rightarrow CH_3OOH + O_2 \qquad \text{(R1.14)}$$

$$OH + NO_2 + M \rightarrow HNO_3 + M \qquad \text{(R1.15)}$$

VOC emissions from vegetation, particularly in tropical forests, are a significant contributor of VOCs in the troposphere (Goldstein and Galbally, 2007). These are

generally removed by oxidation by OH and deposition, and it was previously assumed that their atmospheric oxidation would reduce the oxidative capacity in these unpolluted environments (Lelieveld et al., 2002). However several field campaigns found discrepancies between the modelled and measured OH in these low NO_x environments. Figure 1.4 shows the mechanism of OH recycling in polluted and clean air environments. Termed as "missing OH", this has been a topic of great discussion in the atmospheric chemistry world, with several looking deeper into the oxidation of important biogenic VOCs such as isoprene and α-pinene as possible contributors to OH recycling which has as of yet not been fully understood.

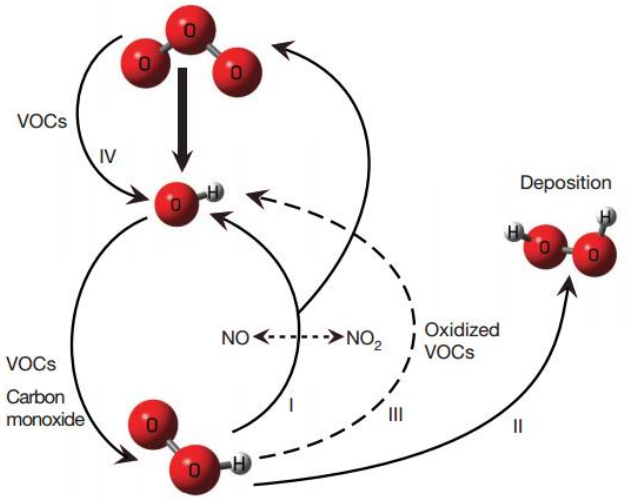

Figure 1.4: Mechanism of OH recycling. O_3 photolysis produces the hydroxyl radical (OH) and subsequent oxidation by VOCs, such as isoprene, generates peroxy radicals, for example, HO_2. Possible fates of HO_2 include OH production and catalytic O_3 generation *via* NO to NO_2 conversion in polluted regions (pathway I). Pathway III shows OH regeneration in clean-air environments *via* reaction of hydroperoxyl radicals with organic peroxy radical species. Pathway III shows deposition of peroxides and a net loss of OH (Lelieveld et al., 2008)

Several pathways have been proposed that may influence the fate of OH in non-polluted environments. It is apparent that isoprene chemistry is directly responsible in the recycling of OH via pathway III in Figure 1.4, and further products yield OH more than previously thought (Whalley et al., 2012). These hypotheses are based on OH radical studies in the field as well as laboratory and modelling studies that have been looking into the low NO_x chemistry of biogenic VOC oxidation processes, particularly isoprene, to answer the questions surrounding this OH recycling in tropical forests. Due to this increased interest in low NO_x chemistry, chapter 7 will examine the

characterisation of suitable generation methods of OH radicals under low NO_x conditions in HIRAC, a stainless steel atmospheric chamber to be discussed in Section 1.3.

1.2.4 Nitrate radical chemistry

There has been extensive documentation on the properties of NO_3 including its atmospheric formation and consumption, which are well characterised (Hahn et al., 2000). The NO_3 radical plays an important role in chemical transformation processes in the atmosphere (Wayne, 2000). NO_3 is the predominant night-time radical, since the majority of OH radicals are produced through photolytic processes and are therefore not as abundant during night-time.

Nitrogen oxides have a short lifetime (~1 day) with respect to conversion to nitric acid, and are removed from the atmosphere by direct dry or wet deposition, contributing to acid deposition (Wayne, 2000). Daytime [NO_3] concentrations are very low (3 ppt) (Wayne, 1991) as most of it rapidly photolyses, however night-time measurements could reach~300 ppt in the urban troposphere (Atkinson, 1990b). NO_3 has been shown to contribute to the oxidation of terpenes and other very reactive VOCs (e.g.: phenol) during the daytime (Geyer et al., 2003, Brown et al., 2004).

The NO_3 radical is formed in the upper and lower atmosphere in one of two ways: (i) from the reaction of NO_x with O_3 (R1.15– 1.16) or (ii) from the dissociation of N_2O_5 (R1.17):

$$NO + O_3 \rightarrow NO_2 + O_2 \qquad (R1.16)$$
$$NO_2 + O_3 \rightarrow NO_3 + O_2 \qquad (R1.17)$$
$$NO_2 + NO_3 + M \leftrightarrow N_2O_5 + M \qquad (R1.18)$$

The equilibrium reaction (R1.17) is the major nocturnal NO_3 sink, which is dependent on the concentration of NO_2. NO_3 also reacts with $HO_2$and $RO_2$to produce OH under low NO conditions. Several side-products are formed from the oxidation processes of VOCs by NO_3 radicals, including the night-time production of HO_2, which is converted to OH by NO_x (Finlayson-Pitts and Pitts, 2000).

$N_2O_5 \rightarrow NO_3 + NO_2$ (R1.19)
$N_2O_5 + 2\ H_2O \rightarrow 2\ HNO_3 + H_2O$ (R1.20)
$NO_3 + \text{organic} \rightarrow \text{products}$ (R1.21)

Several groups have used an inexpensive compact instrument known as cavity ring-down spectroscopy (CRDS) for detection of NO_3 in the field. This ultra-sensitive method of measuring NO_3 has been employed by various atmospheric research groups (Simpson, 2003, Brown et al., 2002, Dorn et al., 2013) and has been a successful way of studying NO_3 radical chemistry both in the field as well as in the laboratory. Some cavity ring down flow tube experiments have been carried out during the course of these studies in an attempt to obtain a suitable NO_3 generation method in HIRAC (from the decomposition of N_2O_5). The results obtained however were inconclusive and only relative rate measurements for the reaction of NO_3 with alkenes and aldehydes could be obtained. These are presented in Appendix A.

1.2.5 Atomic chlorine chemistry

Tropospheric halogen chemistry has been extensively reviewed over the past decade (Carpenter, 2003, Simpson et al., 2007, Saiz-Lopez and von Glasow, 2012, Faxon and Allen, 2013). Reactive halogen species are generally associated with stratospheric chemistry (Prather et al., 1984), however are also known to play an important role in tropospheric chemistry and influence oxidising capacities of a number of reactive species (Saiz-Lopez and von Glasow, 2012). Several different halogen species exist in the troposphere, mainly halides that are readily activated by sunlight in order to play an important role in the chemistry of the troposphere (Platt and Honninger, 2003). This section will focus on the chemistry of chlorine (Cl) atoms in the troposphere, since it is reported extensively in this thesis. Chapters 4 – 6 are devoted solely to work carried out on Cl atom chemistry in the Highly Instrumented Reactor for Atmospheric Chemistry (HIRAC).

Chlorine-containing compounds in the environment originate predominantly from the coastal boundary layer (aerosols and from marine organisms, *i.e.* inorganic halides and methyl halides respectively) (Graedel and Keene, 1996, Ravishankara, 2009). Molecular chlorine (Cl_2) is emitted directly through industrial processes as well as *in situ via* multiphase chemistry of reactive chlorine reservoirs (e.g.: $ClONO_2$ and

HOCl) (Riedel et al., 2012). Other anthropogenic sources, such as biomass burning and power stations are also known to contribute to molecular chlorine in the troposphere (Cuevas et al., 2005a). A number of reactive chlorine species exist in the troposphere, with the most abundant being CH_3CCl_3 and CH_3Cl, accounting for 62% of the total reactive species according to emissions inventories (Khalil et al., 1999; Montzka and Reimann, 2010). Reactive halides account for around 7% while the remainder of reactive species include HCl, Cl_2, HOCl, $CHClF_2$, CH_2Cl_2, $COCl_2$ and $CHCl_3$.HCl is predominantly formed from the reaction of OH radicals with HCl. According to a recent field and model study in Los Angeles, the relative contributions of $ClNO_2$, Cl_2 and HCl to Cl production are 45%, 10% and 45%, respectively (Riedel et al., 2012).

Cl atoms are formed from all these precursors, and are an important reactive species in the troposphere, particularly in the marine boundary layer and polar regions, but also recently identified sources have been uncovered in urban mainland environments such as in mainland USA, Colorado (Thornton et al., 2010). The activation or photolysis of these reactive species leads to the formation of Cl atoms. The nitryl chloride nocturnal source of chlorine is produced by the reaction of N_2O_5 on chloride containing aerosols. There is significant uncertainty concerning the sources and sinks of Cl atoms in the troposphere (Monks et al., 2009). The dominant source of Cl atoms in the troposphere is believed to be sea salt activation, given the large abundance of chlorine in the oceans, present as sea salt. There is also significant debate concerning the magnitude of the Cl atoms present in the marine environment since there is little direct evidence for Cl atom chemistry as it is generally inferred from the differential losses of non-methane hydrocarbons (NMHCs) with respect to OH and Cl reactivity (Wingenter et al., 1996), or from the concentration of its stable precursors such as $ClNO_2$ (Riedel et al., 2012, Phillips et al., 2012). The sources of Cl atoms also remain highly uncertain, however the potential consequences for air quality in polluted coastal regions is evident and clearly undisputed (Riedel et al., 2012).

The competition of OH and Cl atom chemistry is a topic of much debate given the great uncertainties associated with unknown sources of Cl atoms in polluted environments, and it is apparent from recent evidence the Cl atom influence on VOC oxidation processes could be much greater than initially thought (Finlayson-Pitts et

al., 1989, Thornton et al., 2010). According to Riedel (2012), the contribution of Cl atoms to the oxidation of alkanes can be as high as ~25% of the total during the day urban marine environments, and that Cl atom chemistry dominates in the early morning chemistry of alkanes (Riedel et al., 2012). These are based on the assumption that precursors for both OH and Cl atoms are collocated over the same air mass volume during the entire day. This work was based on continuous measurements of $ClNO_2$ and Cl_2 concentrations in California. A significant finding from this campaign was that of well-confined Cl_2 plumes observed largely independent of $ClNO_2$, which the author correlated with localised industrial emissions of reactive chlorine (Riedel et al., 2012). Riedel concluded that Cl atoms, especially during the early morning, can affect the chemistry of polluted marine environments especially that of alkane oxidation given the higher reactivity of Cl atoms with respect to OH.

A recent study in London predicted ~56% Cl-atom driven oxidation for alkanes (Riedel et al., 2012). A comparison of the rate coefficients for reactions of Cl atoms with alkanes are up to 2 orders of magnitude faster than with OH radicals as is shown in Table 1.2 for C_1 – C_6 alkanes, and this has been shown to promote the formation of ozone in the presence of VOCs and NO_x (Tanaka et al., 2000), which is limited by the lifetime of NO_2.

	k / (10^{-14} cm^3 molecule^{-1} s^{-1})	
Compound	**OH**	**Cl**
methane	0.64	10
ethane	24	5,900
Propane	110	14,000
n-butane	244	22,000
n-pentane	400	28,000
n-hexane	545	34,000

Table 1.2: A comparison of the rate coefficients for the reactions of alkanes with OH radicals and Cl atoms at 298 K taken from IUPAC recommendations (Atkinson et al., 2006a). Table adapted from: (Tanaka et al., 2000).

In polar regions during springtime a unique photochemical process (due to greater UV intensity) converts halide salt ions such as Cl^- and Br^- into reactive halogen species such as Cl, Br, ClO and BrO species that are responsible for the depletion of O_3 in the polar boundary layer (Simpson et al., 2007). The main consequence of these

processes is quite severe given the destruction of O_3 results in the less OH being formed in these environments, and therefore halogen atoms and oxides result as primary oxidants. Since the discovery of these ozone depletion events in the 1980s, key advances have been made in understanding the central role played by bromine photochemistry (Pratt et al., 2013), however there is a lack of knowledge on how salts are transported and oxidised to become reactive halogen species (Simpson et al., 2007). The activation of Cl atoms from halides is now known to be coupled to bromine chemistry (Mielke et al., 2011, Thornton et al., 2010).

The difference in reactivity between halogen reactive species and OH has broad impacts on polar atmospheric chemistry, including removal of mercury from polar environments (Stephens et al., 2012), as well as altering the oxidative fates for different VOCs (Simpson et al., 2007). These ozone depletion processes resemble the halogen chemistry taking place in the stratosphere, where Cl atom chemistry plays a major role in ozone depletion processes (Solomon, 1999). This however is due to a larger pool of stable chlorine-containing molecules that make it to the stratosphere and are photolysed by a wider range of UV radiation to produce Cl atoms. In the troposphere the conditions are slightly different given the different radiation and scarce stable precursors available for Cl atoms to be sustained. Moreover Cl atoms are highly reactive and thus immediately end up forming HCl which precipitates out of the troposphere by rainout (Ravishankara, 2009).

Two different pathways shown in Figure 1.5 have been proposed to explain the mechanism that leads to the formation of $ClNO_2$ in the troposphere. The latest proposed heterogeneous reactions of HCl on surfaces in the presence of NO_2 and N_2O_5 leading to the formation of ClNO and $ClNO_2$ respectively (Raff et al., 2009) (R1.21). The photolysis of these species results in the formation of Cl atoms in the troposphere. The mechanism shown on the right of Figure 1.5 shows the gas phase N_2O_5 entering an aerosol leading to the formation of aqueous nitric acid (shown in R1.22) or $ClNO_2$.

$$N_2O_{5\,(g)} + Cl^-_{(aq)} \rightarrow ClNO_{2(g)} + NO_3^-{}_{(aq)} \qquad (R1.21)$$

$$N_2O_{5\,(g)} + H_2O_{\,(aq)} \rightarrow 2HNO_{3(aq)} \qquad (R1.22)$$

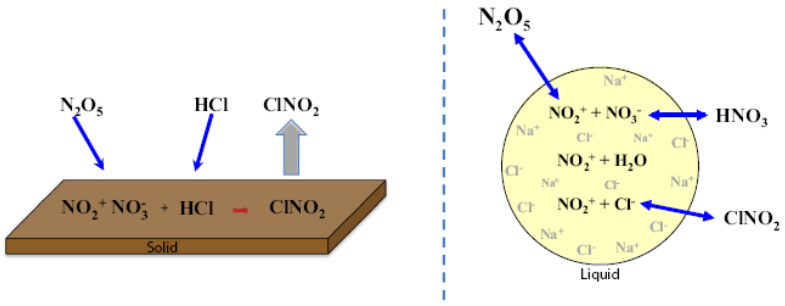

Figure 1.5: Two mechanisms leading to formation of $ClNO_2$ in the troposphere. The mechanism on the right shows gas phase reactants entering an aerosol or water particle; mechanism on the left shows the new proposed mechanism involving surface chemistry (Ravishankara, 2009)

In a paper by Thornton *et al.*, a novel direct method for simultaneous measurements of $ClNO_2$ (product) and N_2O_5 (reactant) was reported using chemical ionisation mass spectroscopy (CIMS) (Thornton et al., 2010). Work was carried out as part of the ICEALOT 2008 Field Campaign which focussed on $ClNO_2$ measurements. The same group have also published a report in Nature on their observation of a large Cl atom source inferred from mid-continental nitrogen chemistry (Thornton et al., 2010). These observations were made 1,400 km from the nearest coastline. A persistent and significant production of $ClNO_2$ was observed relative to the consumption of its nitrogen oxide precursors.

Thornton and his group suggest that from comparison of their results and comparison with models that the composition data obtained from long-term monitoring suggests $ClNO_2$ production in mid-continental regions is at a similar level to global estimates for marine and coastal areas. Moreover, they suggest that Cl atoms may also arise directly from anthropogenic sources (Thornton et al., 2010). Although Cl atom concentrations are still typically lower than OH radicals, the higher reactivity relative to OH mainly with most VOCs leads to an observable affect in the influence Cl atoms have on air quality particularly due to the increase in ozone production rates (von Schneidemesser and Monks, 2013).

1.3 Atmospheric chemistry in the laboratory

1.3.1 Absolute gas phase kinetic techniques

Two main types of conventional experimental techniques may be distinguished for use in gas phase kinetics studies: laser flash photolysis and flow reactors (discharge flow systems). Laser flash photolysis is a basic technique that requires the flow of a pre-mixture of reactants and precursors into a photolysis cell at a defined pressure. It normally employs two different laser sources, a fixed frequency pulsed laser that generates the reactive species being studied (e.g.: excimer laser), and a wavelength tunable species (e.g.: excimer pumped dye laser) that excites the reactive species, making it fluoresce. The atom or radical reacting is formed *in-situ* in a photolysis cell *via* a pulse of light from a pulsed laser or lamp. The concentration of the latter species would then be monitored using LIF detection in the case of OH radicals, which are commonly studied using this technique. Alternatively, the appearance of product with time could be monitored using an optical detector. This technique has been employed for several Cl atom investigations with ketones and acetates (Albaladejo et al., 2003, Cuevas et al., 2005a, Cuevas et al., 2004), which will be detailed further in chapter 4.

Mixing times in the region of milliseconds to a few seconds exist in such systems and timescales of only a few seconds to a couple of minutes are studied, depending on the pulse repetition rate of the laser. High-powered laser pulses enable studies at nanoseconds or even femtosecond timescales. The reactant species from the photolysis is generated in the centre of the photolysis cell, and therefore excludes any wall reactions. Flash photolysis can be used to study elementary reactions over a wide range of pressures and temperatures, however the number of reactions that can be studied is limited to reactants that have a photolytic precursor and must be detectable in at least millisecond timescales.

A typical flow tube system consists of a movable injector used to add the reactant to the radical or atom source, present constantly in the flow tube usually in a nitrogen or argon bath gas (Figure 1.6). The reactant gas is usually introduced in excess of the radical or atom source in order to approach a pseudo-first order condition

for radical removal. The flow of the bath gas is set high enough to avoid any back mixing within the flow tube.

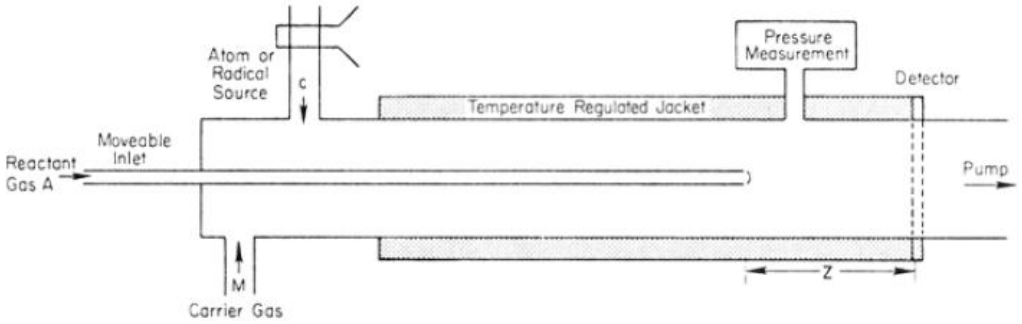

Figure 1.6: Schematic of flow tube systems with moveable inlet (Howard, 1979).

The flow in discharge tubes is described by the Reynolds number, which in the majority of studies of elementary reactions has been in the laminar flow regime. The contact time between the reactant and radical or atom can be calculated from the distance between the point at which the reactant come out of the injector and the detector (distance Z) if the velocity of gas in the flow tube is known. The operation of flow tubes is typically based on the relation between reactant concentration and contact time, and is achievable through the shifting of the position of the moveable inlet. The relative concentration of radicals is plotted relative to time which is changed by the moved inlet, resulting in a decay profile that is pseudo first order, *i.e.* could be calculated from $k = k'$ [reactant] or from the bimolecular rate coefficient obtained through varying reactant concentrations and plotting a graph of k' against reactant concentration.

Flow tube studies normally involve *in-situ* generation of radicals or atoms during the experiment. NO_3 radicals are, for instance, produced by either having an excess of NO_2, introducing O_3, or by thermal decomposition of N_2O_5 prepared beforehand. OH radicals are generated by either photolysis of HONO or through introducing a mixture of hydrogen in helium, which is passed over a microwave discharge lamp giving H atoms, which are injected in the flow tube with an excess NO_2 giving OH and NO products. The reactions producing radicals *in-situ* are generally very fast and lead to conversion before subsequent introduction of reactant species.

Several detection techniques may be used for flow tube studies, depending on the radical or atoms that are being studied. In the case of OH radicals laser-induced fluorescence (LIF) is the most common method of detection, while for NO_3 absorption spectroscopy is commonly used, particularly cavity ring down spectroscopy (CRDS) which is a relatively new technique compared to LIF, with pulsed-laser (CRDS) only being developed in the late 1980s (Dorn et al., 2013). Cl atoms are commonly measured indirectly using hydrocarbon ratios. A direct way of measuring Cl atoms does exist, but the problem faced with regeneration of Cl atoms is a hard issue to overcome. The reaction of Cl atoms with hydrocarbons (shown in R1.23 and R1.24) is the same as for OH. The subsequent reaction of the alkyl radical with Cl_2 present as a precursor of Cl atom chemistry results in the regeneration of the Cl atoms in the system.

$$Cl + RH \rightarrow HCl + R \qquad (R1.23)$$

$$R + Cl_2 \rightarrow RCl + Cl \qquad (R1.24)$$

Adding O_2 to the system is commonly used to minimise this since the reaction of the alkyl radical with O_2 would outcompete the reaction with Cl_2, however the subsequent reaction of the alkylperoxy radical with Cl atoms would interfere instead.

Although less common than OH given the precursors available for Cl atoms in gas phase kinetics are more straight forward to prepare than for OH and other reactive radicals in the laboratory. A recent technique used in such systems has shown that the reactions of peroxy radicals with HO_2 radicals can generate OH radicals (shown in R1.25c) (Dillon et al., 2008; Jenkin et al., 2007; Hasson et al., 2004):

$$R + Cl_2 \rightarrow CH_3C(O)O_2H + O_2 \qquad (R1.25a)$$

$$\rightarrow CH_3C(O)OH + O_3 \qquad (R1.25b)$$

$$\rightarrow OH + CH_3C(O)O + O_2 \qquad (R1.25c)$$

Fast flow reactors have been coupled to laser induced fluorescence, LIF (Parker et al., 2007) and chemical ionisation mass spectrometry, CIMS (Suh and Zhang, 2000) to detect the reactants and products in the reaction of Cl atoms with various VOCs. The two studies cited investigate two important species in the troposphere, methane and isoprene respectively. These absolute kinetic experiments

differ from OH absolute kinetic experiments in that it is the reactants and/or products that are detected, while for majority of OH absolute rate experiments, most of which employ LIF detection, it is the OH radical that is probed directly. In contrast, the relative rate method, used widely in modern kinetics and mechanistic, to be discussed extensively in chapters 4 and 5, differs in the way it obtains kinetic data as it is not the radical but the reactants and/or product decays that are monitored.

The timescales at which most flow tube studies are generally carried out range from a few milliseconds to several seconds. This often requires high concentrations of radicals or atoms which could be problematic in diffusion-limited reactions owing to difficulty in obtaining proper mixing in such short timescales. Higher concentrations of radicals or atoms may also lead to secondary chemical reactions taking place, which could potentially compete with the reaction being studied, and thus may lead to non-linearity between the radical or atom concentration and reaction time. Flow tubes can be used to study a great number of elementary reactions owing to the facility in introducing radicals in different generation methods, and using several different detection systems that could be implemented into the flow tube.

The main advantage of flash photolysis is the ability to study reactions over a wider range of both temperatures and pressures. It is also a direct way of monitoring the loss of a reactant species, and also excludes any wall losses. However being a laser based method, it is limited to reactants that have a photolytic source, and must be able to react over rapid timescales. Flow tubes on the other hand are able to study a greater number of reactions since they can use several different methods of generating radicals or atoms *in-situ*. It is a very cheap technique, but reactions studied cannot be characterised to a full range of temperature and pressure, owing to limitation in going to higher pressures in laminar flow regimes. Moreover at lower temperatures wall losses become quite large.

Due to limitations of both techniques, a large number of reactions, particularly radical-radical reactions which are complicated owing to the difficulty of generating two different radicals, have been studied at a small range of temperatures and pressures. Several direct observations at wider ranges of these conditions are often based on extrapolations. With so many gas phase bimolecular reactions displaying temperature and pressure dependences, further experimental work is required in order

to achieve a better understanding of several elementary reactions of importance to the atmosphere.

1.3.2 Atmospheric chambers

Atmospheric chambers (also referred to as smog chambers) bridge the gap between traditional laboratory studies and large outdoor field campaigns in obtaining information on complex chemical processes in the atmosphere (Seakins, 2010a). The earliest atmospheric chambers were intended to study the smog phenomena occurring in Los Angeles in the early 1970s. The success of these studies, which provided fundamental knowledge on VOC and NO_x reactions in the troposphere (Atkinson, 2000), led to the development of a broad range of chambers which have aimed at covering wider applications and targeting different aspects of atmospheric chemistry.

Modern day chambers are useful tools in addressing gaps in the current knowledge of atmospheric processes such as the impact of biogenic VOCs on the ozone budget, contribution of aromatic VOCs to photooxidation processes, biofuel combustion and photoxidation products, and response of oxidising capacities of HO_x and NO_x to anthropogenic emissions (Seakins, 2010a).

Chamber studies are useful in studying such reactions with greater control over predetermined conditions than field campaigns. The greater size of atmospheric chambers when compared to flow tubes and other small scale kinetic setups allows for larger timescales and also the use of a wider range of instrumentation. Large atmospheric chambers have several other advantages over flow tubes and other smaller scale vessels. Figure 1.7 illustrates the largest European atmospheric chamber facility at present, known as EUPHORE.

A distinct advantage of EUPHORE and other similarly large atmospheric chambers is the ability to allow the use of a large variety of analytical detection instruments which provide *in-situ* detection of both stable molecules but also free radicals such as OH and HO_2. In the case of the EUPHORE chamber shown in Figure 1.7, a Fourier Transform Infrared (FTIR) spectrometer (optical path length of 560 m), UV spectrometer (optical path length of 1100 m) detect the majority of trace elements

present in the chamber in parts per billion (ppb) levels (Siese et al., 2001). FAGE is also present for the detection of HO_x radicals (HO_2 and OH), while other instruments are present to measure other conditions such as intensity of solar spectrum, NO_x, and other trace gases.

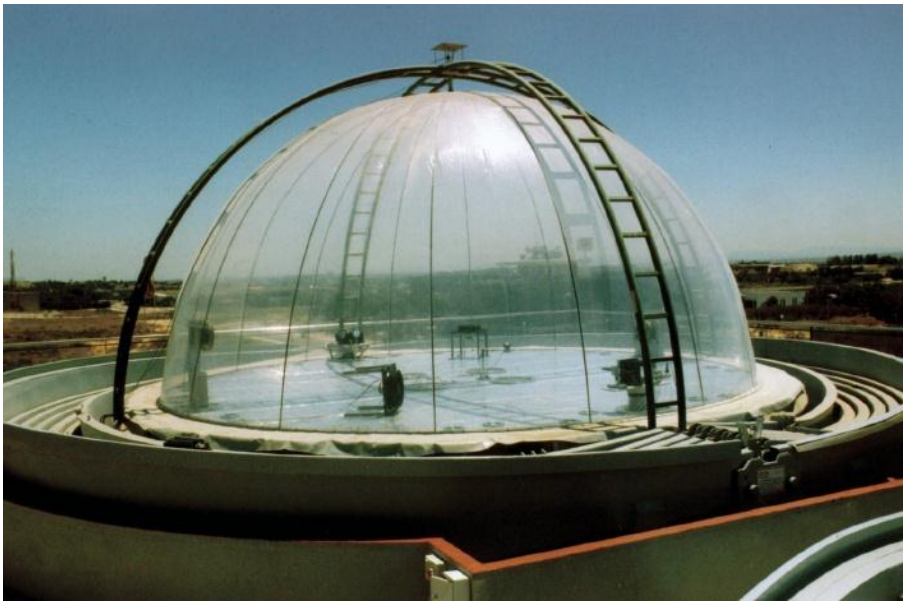

Figure 1.7: The EUPHORE (European Photoreactor) facility at CEAM, Valencia, Spain.

The ability to carry out experiments under predetermined and controlled conditions, with the extra advantage of indoor chambers along with the ability to vary temperature and pressure conditions; in most cases enables chambers to generate information relevant over the entire range of the troposphere. This characteristic, in addition to the ability to perform over longer timescales, results in more detailed kinetic and mechanistic information, such as rate coefficients branching ratios, which are inputted into complex atmospheric models such as the Master Chemical Mechanism (discussed in Section 1.4). Chambers are also used as test beds for calibration and characterisation of field instrumentation. A use to which they are particularly suited owing to their large volume and their ability to control the conditions and concentrations of species introduced, thus providing the best possible reproduction of the atmosphere in the laboratory.

Some limitations do however exist with large atmospheric chambers. This includes the dilemma of chamber instrumentation detection limits and the requirement to often have to investigate trace gas chemistry at higher than ambient concentrations.

This can be a significant limitation in the utility of certain VOC oxidation data obtained for mechanism evaluation and the range of conditions that studies may take place in chambers (Carter et al., 2005).

An example of an atmospheric chamber to be mentioned frequently in this thesis, is the Highly Instrumented Reactor for Atmospheric Chemistry (HIRAC for short), developed at the University of Leeds in 2007. HIRAC (Figure 1.8) forms part of an integrated European consortium of atmospheric simulation chambers known as EUROCHAMP. Chapter 2 will describe this atmospheric chamber in further detail and describe the different instrumentation available for use in this vessel.

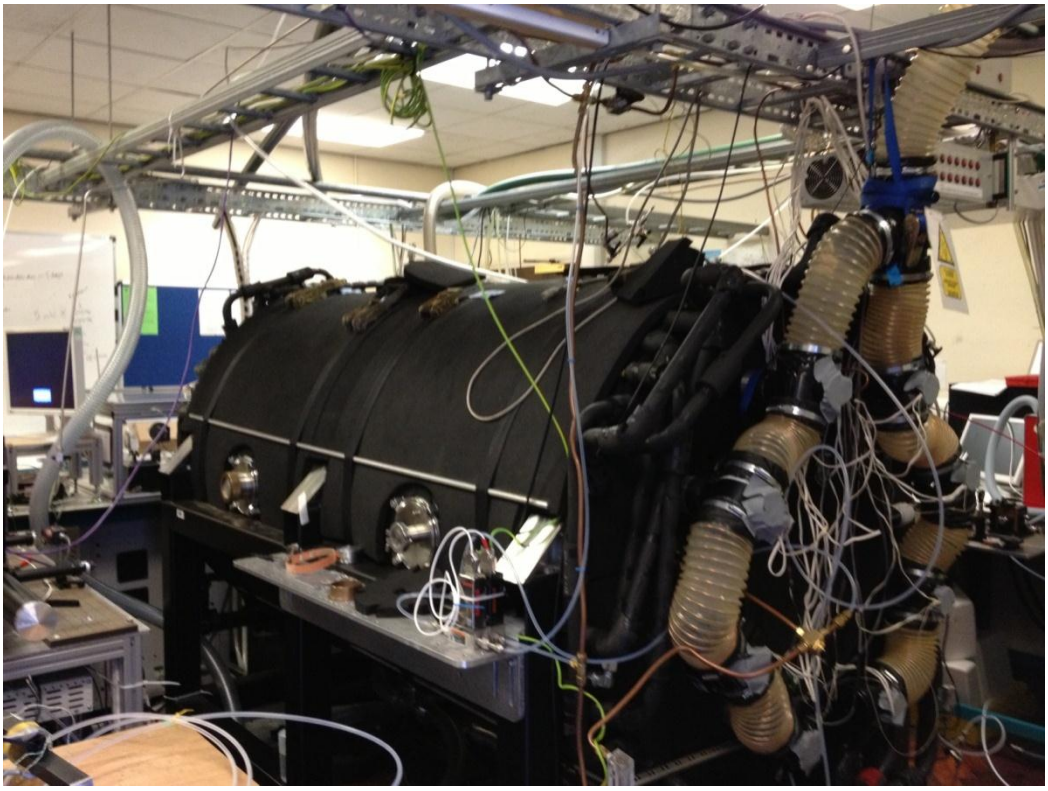

Figure 1.8: Highly Instrumented Reactor for Atmospheric Chamber (HIRAC) at the University of Leeds.

HIRAC, as its name suggests, is interfaced with a number of different instruments, including two gas chromatography instruments with flame ionisation detection (GC-FID), a Fourier Transform Infra-Red spectrometer (FTIR), a Cavity ring-down spectrometer (CRDS), a Fluorescence Assay by Gas Expansion (FAGE) instrument and commercial NO_x, ozone and water analysers. Table 1.3 gives all the different techniques used in HIRAC as well as the detection limit ranges and time resolutions of commonly detected organic species in the HIRAC chamber. A distinct

advantage of chambers over smaller scale experiments is the ability to make use of multiple instruments, enabling simultaneous detection of both stable and radical species.

Instrument	**Species detected**	**Detection limit**	**Time resolution**
GC-FID	organic species (e.g.: hydrocarbons and oxygenated compounds)	0.01 - 0.05 ppmv	20 s averages
FTIR	O_3, organic species (CH_3CHO, CH_4, HCHO)	60 - 80 ppbv	60 s
CRDS	NO_3	6 pptv	4 s
FAGE	OH and HO_2	0.1 - 0.02 pptv	1 - 30 s
Commercial Analysers	NO_x	50 pptv	120 s
	O_3	1 ppbv	20 s
	H_2O	2.5 %	10 s

Table 1.3: HIRAC instrumentation and known detection limits and time resolutions of detectable stable and radical species.

As has already been highlighted, HIRAC forms part of EUROCHAMP, a European-wide consortium of chambers that integrates the existing atmospheric chambers and aims at initiating collaboration between different communities for studying atmospheric processes. A wide range of chambers form part of this consortium, with 17 countries forming part of this European collaboration, and some details of a selection of chambers in EUROCHAMP are highlighted in Table 1.4.

	Chamber	Temperature ranges/ K	Pressure ranges/ mbar	Volume/ m^3	Reference
Aluminium/ Steel chambers	HIRAC, Leeds	~220 – 330	~10^{-3} – 1000	2.25	(Glowacki et al., 2007a)
	LISA/CESAM, Paris	~230 - 450	10^{-7} – 1500	4.20	(Wang et al., 2011)
	AIDA, Karlsruhe	~180 - 330	10^{-2} -1100	84.3	(Möhler et al., 2003)
Glass/ Quartz chambers	QUAREC, Wuppertal	~265 - 315	1 – 1000	1.08	(Barnes et al., 1983, Barnes et al., 1994)
	UCPH, Copenhagen	~240 – 350	10^{-3} -1000	0.10	(Nilsson et al., 2009)
Teflon/ FEP* chambers	EUPHORE, Valencia	298 - 308	Atmospheric pressure	187	(Siese et al., 2001)
	SAPHIR, Jülich	293 – 298	Atmospheric pressure	270	(Rohrer et al., 2004)
	CRAC1, Cork	293 – 298	Atmospheric pressure	3.91	(Thuner et al., 2004)
	PSI, Villigen	290 – 298	Atmospheric pressure	27	(Paulsen et al., 2005)

Table 1.4: Comparison of a number of different atmospheric simulation chambers that form part of the European simulation chambers (EUROCHAMP). (*FEP: fluorine ethene polymer).

Table 1.4 shows the different ranges of pressure and temperature operational in each chamber. Atmospheric chambers are generally categorised as evacuable and collapsible chambers, depending on their construction. Various materials have been used in construction of these chambers, including Teflon (collapsible), stainless steel, quartz and aluminium (evacuable). A brief understanding of the diversity of these atmospheric chambers as well as the advantages and disadvantages in comparison to our HIRAC chamber will be reviewed in this section.

Other well-known examples of atmospheric chambers elsewhere outside of Europe are tabulated in Table 1.5 and include the Ford smog chamber in Dearborn, UCR chamber in Riverside, NCAR chamber in Boulder and NIES chamber in Tsukuba.

Chamber	Wall Material	Temperature ranges/ K	Pressure ranges/ mbar	Volume/ m^3	Reference
Ford Smog Chamber, Dearborn	Pyrex	~200 – 350	~10^{-3} – 1000	2.25	(Wallington and Japar, 1989)
UCR Chamber, California Riverside	FEP Teflon bag	~280 – 320	Atmospheric pressure	180	(Carter et al., 2005)
NCAR chamber, Boulder	Aluminium alloy	~215 – 470	~10^{-3} – 10^{4}	0.05	(Shetter et al., 1987, Orlando and Tyndall, 2002)
NIES, Tsukuba	Stainless steel	~273 – 473	~10^{-3} – 1000	6.07	(Volkamer et al., 2002, Akimoto et al., 1979b)
Caltech Chamber, California Institute of Technology	FEP Teflon bag	~280 – 320	Atmospheric pressure	56	(Cocker et al., 2001)

Table 1.5: Comparison of a number of different atmospheric simulation chambers outside of Europe.

The majority of atmospheric chambers are made of Teflon (essentially Teflon bags). Teflon chambers, such as the SAPHIR chamber shown in Figure 1.9, are generally larger in volume than metal or glass chambers (due to construction limitations and cost), and the fact that they are outdoor chambers.

Figure 1.9: The SAPHIR simulation chamber in Jülich Research Centre, Germany.

Teflon film chambers are easily constructed in comparison to metal and glass chambers, and the size of these constructions is easily varied owing to the flexibility of these FEP/Teflon materials. Due to this property, they are not very rigid structures and are therefore are only able to operate under room temperatures and pressures. Out-gassing of organics from the chamber walls is less predominant than metal chambers in particular and also glass chambers, however can still result in contamination during experiments, and in contrast with other chambers, Teflon bags are not easily cleaned, given they cannot be scrubbed or heated to degas the organics on the walls. This would make them less suitable in investigating low NO_x chemistry for instance, given the need for the chamber walls to be clean and rid of any contamination (such as HNO_3) that could lead to NO_x evolution. HIRAC is particularly suitable for such experiments, and chapter 7 is devoted to the characterisation of a low NO_x source of OH for use in future isoprene oxidation studies.

In contrast, metal or glass chambers are able to conduct experiments over a wider range of temperatures and pressures; however these chambers are generally kept indoors. Indoor chambers require a light source to simulate photochemistry and therefore depend on artificial light which may be different from solar radiation and result in different photochemistry. In contrast, outdoor chambers rely on sunlight;

however this varies primarily due to clouds and zenith angle, rendering the photolytic conditions difficult to model and characterise.

Glass and quartz reactors such as the QUAREC chamber at Wuppertal, Ford motor company smog chamber and the UCPH chamber at Copenhagen (Figure 1.10) are generally constructed out of borosilicate or quartz and are relatively inexpensive and convenient reactors. Glassware is also readily available and repairable. Similar to metal chambers like HIRAC, they are evacuable chambers. This means experiments can be carried out over a larger range of pressures. One consequence of evacuable chambers, however, is their size limitation during construction: the smaller the size of the chamber the higher the surface area to volume ratio, and in turn the higher the rate of heterogeneous reactions occurring on chamber walls.

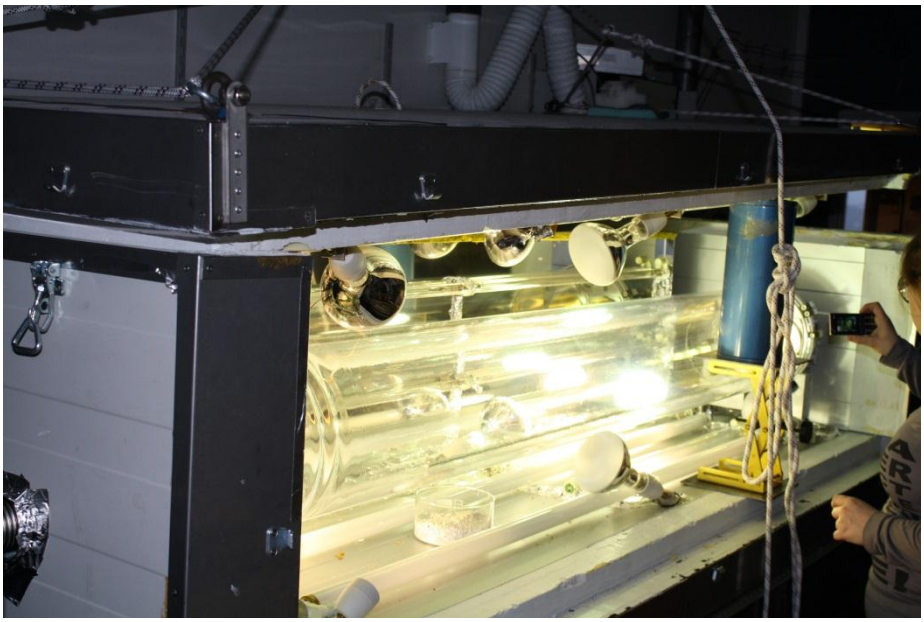

Figure 1.10: The UCPH chamber in Copenhagen, Denmark.

A major difficulty with the use of glass chambers is that glass absorbs light at critical wavelengths for atmospheric photochemistry. This depends on the transparency and the thickness of the glass used, but in some cases the absorption of light ≤350 nm by glass reactors has been reported in several investigations (Wildt, 2013), therefore making it only possible to study photochemistry under longer wavelength radiations. A way around this is to have lamps present inside the glass chamber rather than externally. Metal chambers do not possess this problem and have the facility to study photolysis experiments over the full range of wavelengths relevant

to the troposphere. In contrast glass is able to transmit some natural light which is a better representation of the real atmosphere than artificial light sources used in metal chambers. The photolysis sources of HIRAC will be further discussed in Chapter 2.

Metal chambers are generally either made of stainless steel or aluminium and a few examples are shown in Tables 1.4 and 1.5. Stainless steel chambers are used at the National Institute for Environmental Studies (NIES), Japan, the National Center for Atmospheric Research (NCAR), Boulder, USA and HIRAC at the University of Leeds while aluminium alloy with FEP/Teflon coated walls is used at Air Pollution Research Center (APRC), University of California, Riverside, USA. Similar to glass reactors, metal chambers allow the control of pressure and temperature, however are a more expensive option since internal artificial lighting is required and the designing of ports for coupling instruments to chamber increases design time and cost. In contrast however the wavelength of light used in a metal chamber is not an issue as for glass chambers and lamps can be altered in intensity.

Few other differences exist between metal and glass chambers. Wall effects are the other major difference since the two materials are expected to have different surface chemistries. In the case of metal chambers, this disadvantage can be minimised by surface coating with inert polymers, such as Teflon (polytetrafluoroethylene – most commonly used) or polyethylene and polypropylene coatings. Following experiments in metal or glass chambers, adsorption of hydrocarbons and other compounds occur at the chamber walls. This can be removed by "baking out" by pumping to low pressures, and where possible heating the walls prior to pumping. Chemical treatment is another possibility and is either carried out by introducing a reactive gas in the chamber such as O_3 or by manually cleaning the surface of the walls with soap and water, ensuring the removal of any contaminants on the chamber walls.

The development and widespread use of atmospheric chambers has led to important advances in atmospheric chemistry in particular in mechanistic studies and model development. Prior to their contributions to atmospheric chemistry, kinetic data were only obtainable through laboratory studies of elementary reactions and field measurements. Elementary kinetic techniques are useful tools for obtaining kinetic data, however their inability to look into mechanistic implications and secondary

chemistry of atmospheric processes is a major limitation that is hard to address on such a small scale given instrumental limitations. On the other hand, the high degree of uncertainty in field measurements from physical variables (e.g.: transport and cloud coverage) as well as complexity from the multitude of reactive species that need measuring provide quite a difficult task to understand the chemistry of the atmosphere. This is where atmospheric chambers are able to bridge the gap and obtain knowledge of mechanistic interest that could be used to back both field measurements and elementary kinetic experiments.

The main limitations of atmospheric chambers discussed in this section are the instrument sensitivity for investigating trace gases and NO_x concentrations in concentrations similar to ambient, secondary chemistry due to high concentrations used in experiments, and heterogeneous surface reactions that are difficult to characterise. Wall effects and background reactivity may affect the gas phase chemistry and introduce unknown uncertainties. Despite all this, chamber studies are an integral tool in the understanding of VOC oxidation processes, as well as other areas of atmospheric chemistry such as aerosol chemistry. At present the best way to test and investigate the data collected from chamber studies is through modelling the data obtained and refining the oxidation mechanism. Due to its importance, atmospheric models will be briefly discussed in the following section, and their use in analysing the discrepancies between experimental VOC oxidation data and model predictions. The predictions and uncertainties obtained from these comparisons are useful in improving the scope and design of further investigations, both experimental and theoretical.

1.4 Atmospheric models and the Master Chemical Mechanism (MCM)

Detailed chemical mechanisms are useful tools in atmospheric chemistry, as they serve for modelling the chemistry and are also useful for knowledge of the several chemical processes. The Master Chemical Mechanism (MCM) is a highly detailed benchmark box model widely used in Europe and the US for research and

policy applications (Jenkin et al., 1997; Saunders et al., 2003). This chemical mechanism currently details the gas phase tropospheric degradation of 143 primary emitted volatile organic compounds (VOCs). Commonly used in conjunction with field measurements, the MCM has also found recent use in the evaluation of reduced mechanisms required for chemistry-climate models. The accuracy of the MCM is dependent on the accuracy of kinetic and photochemical data inputted into this model (Jenkin et al., 1997).

The latest version of the Master Chemical Mechanism (MCM) consists of over 140 volatile organic compounds (VOCs) present in the troposphere (Fuentes et al., 2000, Guicherit, 1997, Brewer et al., 1983). There are several lines of evidence pointing towards this being only a mere fraction of the real number of VOC species present. It is now known from 2D GC measurements that there are over a thousand VOCs present in the troposphere (Hamilton, 2010), most of which have not been measured. Advances in gas chromatography, a technique mentioned quite frequently in this thesis and detailed in Chapter 2, have enabled the detection and characterisation of more detailed VOC inventories, with the growing use of quadropole mass spectrometry enabling up to 200 VOCs to be isolated and identified (Yassaa et al., 2001), which can however add additional complexity owing to the practical aspects of simultaneously analysing such a large amount of VOCs.

A wide range of models are available for describing the chemistry of the troposphere, from box models to detailed 3-D models. Detailed transport models are not as necessary for the understanding of the main VOC oxidation processes occurring in the troposphere as they are primarily influenced by HO_x cycles, which have short lifetimes and thus very limited transport. For this reason, the MCM is sufficient for describing the chemistry of the troposphere and VOC oxidation processes (Saunders et al., 2003). Atmospheric chambers are useful tools in obtaining data suitable for testing VOC oxidation models prior to compiling chemical mechanisms, to predict the major features of VOC oxidation processes. It is an ideal environment for such experiments since experiments can be carried out under controlled and well-characterised conditions. The experimental results can later be compared with those predicted by models and used as an indicator on how well the chemistry is known. Several indoor and outdoor chambers have been used in the development of chemical

mechanisms and their ability to test different aspects of the chemical mechanism have linked chamber studies very strongly with mechanism and model building.

All conditions of potential interest for control strategies cannot be simulated experimentally. Consequently, the development and application of mathematical models capable of accurately describing both the chemical and physical aspects of atmospheric processes is critical in development and assessment of effective control strategies.

1.5 Thesis outline

This chapter has outlined the advantages of atmospheric chambers in the study of atmospheric chemistry as well as the importance of obtaining a better understanding of various aspects of atmospheric chemistry. In conclusion, atmospheric chambers enable the investigation under predetermined controlled conditions of complex atmospheric processes enhancing the application of the results obtained to the understanding of the real atmosphere. Their use as test beds for field instruments as well as for inter-comparison of different measuring techniques has enhanced the importance of these vessels in the study of atmospheric chemistry, and resulted in several breakthroughs in the knowledge of atmospheric trace species and aerosol chemistry.

The importance of understanding VOC oxidation processes has been highlighted in this chapter and is essential in the predictions made on air quality and climate change and decisions made in setting emission limits as well as for interpreting the effects to human health of these pollutants (Ravishankara et al., 2012, Ravishankara, 2005). VOC oxidation mechanisms play an important role in the understanding the chemistry and fates of oxygenated organics formed during the oxidation of parent VOCs which play a role in secondary aerosol formation (Baltensperger et al., 2005).

The work described in this thesis aims at accomplishing the main aims of HIRAC which are: to validate mechanisms of VOC oxidation and provide a test bed

for instrument calibration and development. Chapter 2 will describe in further detail the HIRAC chamber and its existing suite of instrumentation. Chapter 3 follows on instrumentation and goes through improvements made to HIRAC and instrument development carried out during these studies aimed at increasing the potential for studying wider atmospheric chemistry applications. Chapters 4 and 5 both deal with relative rate studies of VOC reactions with Cl atoms, with chapter 4 describing reactions with oxygenated hydrocarbons aimed at demonstrating the capability of HIRAC for use in kinetic experiments. Chapter 5 provides a further demonstrating of the capabilities of HIRAC for both kinetic and mechanistic applications, and also extends to investigate temperature dependence of hydrocarbon reactions with Cl atoms.

Chapter 6 also involves Cl atom chemistry with ethanol and consists of an isotopic branching ratio study of ethanol and deuterated ethanols, and is aimed at demonstrating the capabilities of HIRAC to carry out similar experiments. Chapter 7 is dedicated to the characterisation and testing of an OH generation method in HIRAC under low NO_x conditions.

Chapter 2 – Highly Instrumented Reactor for Atmospheric Chemistry (HIRAC): Instrumentation

2.1: Introduction

Atmospheric simulation chambers aim at bridging the gap between the study of elementary reactions in the laboratory and atmospheric field studies. Mechanism evaluation of VOC oxidation requires studies over a range of temperature and pressure, a limiting factor for several existing chambers. The Highly Instrumented Reactor for Atmospheric Chemistry (HIRAC) was designed at the University of Leeds (Glowacki et al., 2007b) and was intended to address these limitations, allowing for control of temperature, pressure and photolytic conditions, which are important variables that affect the rates of reactions in atmospheric processes.

The controlled conditions of environmental chambers provide an ideal test bed for characterising field instrumentation and examples of studies range from inter-comparison of physical instrumentation such as spectral radiometers (Bohn et al., 2008), through oxygenated VOCs (Apel et al., 2008), to calibrations of OH radical detection systems (Hard et al., 1984, Bloss et al., 2004, Schlosser et al., 2007, Schlosser et al., 2009). Many field instruments draw significant sample volumes and hence some studies are limited to larger chambers such as EUPHORE or SAPHIR, shown in Figure 2.1 (Seakins, 2010b).

The purpose of this chapter will be to highlight the details of the HIRAC chamber and the instrumentation available, and to discuss recent instrument development, with a particular focus on gas chromatography. Chapter 3 will follow on the latter and extend to further instrument development carried out over the past few years at the University of Leeds.

Figure 2.1: EUPHORE chamber in Valencia and SAPHIR chamber in Jülich.

2.2 HIRAC

2.2.1 Introduction

The Highly Instrumented Reactor for Atmospheric Chemistry, HIRAC (shown in Figure 2.2), is a ~2.25 m^3 stainless steel indoor chamber consisting of 4 circulating fans and 8 rows of photolysis lamps. This chamber is built out of grade 304 stainless steel. This was chosen over glass for manufacturing reasons to allow easier construction of ports and access holes for the inclusion and accessibility of instrumentation. Furthermore stainless steel tubes could be easily welded in this way in order to allow for a heating and cooling fluid to flow on the outer body of the chamber. HIRAC enables studies over varying pressures ranging from ~50 – 1050 mbar, and more recently temperatures through these aforementioned stainless steel channels welded to the outer body of HIRAC connected to a Huber thermostat Model 690W temperature control unit, and filled with a thermal fluid (DW-Therm) evenly circulated to cover the full range of temperatures relevant to the troposphere of ~220 – 330 K. This setup has been recently set up and characterised and the discussion of this work is to be highlighted in chapter 3. Chapter 5 will look at the first extensive temperature dependent studies carried out in HIRAC, and this thesis will demonstrate the chamber's potential to carry out similar experiments in future planned research.

Figure 2.2: The HIRAC chamber at the University of Leeds showing the stainless steel channels through which the thermofluid is circulated and black neoprene for insulation of the chamber. The inlet manifold is also shown, which is a series of taps used to isolate particular sections of the steel tubes.

The chamber has also been covered with an insulating double layer of 20 mm thick neoprene as is shown in Figure 2.2. The temperature control system in HIRAC facilitates detailed mechanistic studies of tropospherically relevant reactions. This system also makes HIRAC invaluable in that it can vary both temperature and pressure. The installation and testing of this temperature control system is detailed in Chapter 3.

The various instrumental ports and flanges around the chamber (Figure 2.3) were cut and welded to the stainless steel skin of HIRAC, allowing a range of instruments to be simultaneously connected, including: Gas Chromatography by Flame-Ionisation Detection (GC-FID) and Fourier Transform Infra-Red spectroscopy (FTIR) for VOC detection, Fluorescence Assay by Gas Expansion (FAGE) for HO_x radical detection, Cavity ring down spectroscopy (CRDS) for NO_3 detection and various commercial analysers (O_3, NO_x, H_2O and CO).

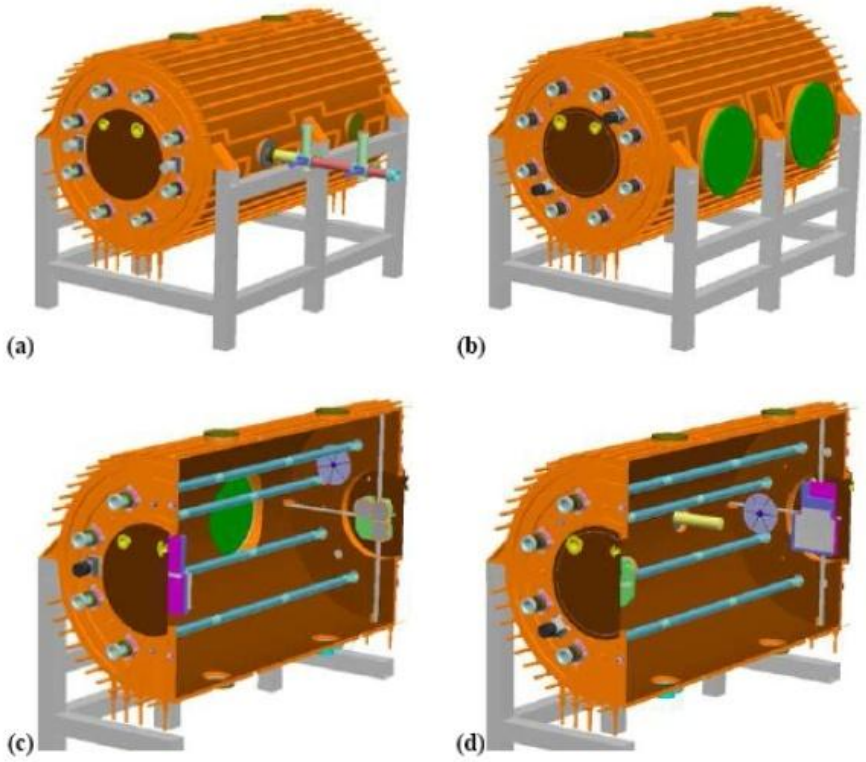

Figure 2.3: SolidWorks 2004 views of HIRAC chamber showing interior and external flanges and ports in its frame; (a) and (d) show the FAGE instrument coupled to HIRAC (Glowacki et al., 2007a).

The design approach taken was to develop a chamber capable of performing under varying conditions of temperature and pressure, and being able to monitor both free radicals and stable species. In doing so, HIRAC is now utilised as a useful tool for carrying out both kinetic and mechanistic studies (Malkin, 2010, Malkin et al., 2010), and also in the development and calibration of field apparatus (Winiberg, 2014).

The pressure of the chamber is monitored by a Leybold Ceravac CTR90 (0 – 100 Torr). HIRAC may be pumped from 1000 mbar down to ~2.5×10^{-3} mbar within ~60 – 70 minutes by using a combination of a rotary pump (Leybold Trivac D40B) backed roots blower (Leybold Ruvac WAU251) with a charcoal filled catchpot trap (BOC Edwards, ITC300) to avoid oil backflush into the evacuated chamber (Malkin 2010).

HIRAC contains 8 rows of 2 mm thick quartz tubes that run the length of the chamber and can house up to 24 lamps (dependant on length) mounted on the circular faces of the chamber. These tubes are flushed using a purge of nitrogen gas to avoid

any condensation or ice formation. The purge also reduces the likelihood of lamp overheating, which is more common when HIRAC is heated up. Lamp output has an optimal operational temperature of ~310K.The purge flow is adjustable depending on the reading given by the thermocouples also mounted within the quartz tubes. Quartz is used since it does not absorb in the UV range, which is important given that the majority of VOCs absorb in this region.

Four different types of lamps are available for use in HIRAC: Philips TLK40W/05 actinic UV lamps, GE G55T8 / OH 7G UV-C lamps, Philips TL 40W/12 RS SLV UV-B medical therapy lamps and Philips TL-D 36W/BLB mercury UV lamps. The spectral outputs of these lamps are shown in Figure 2.4.

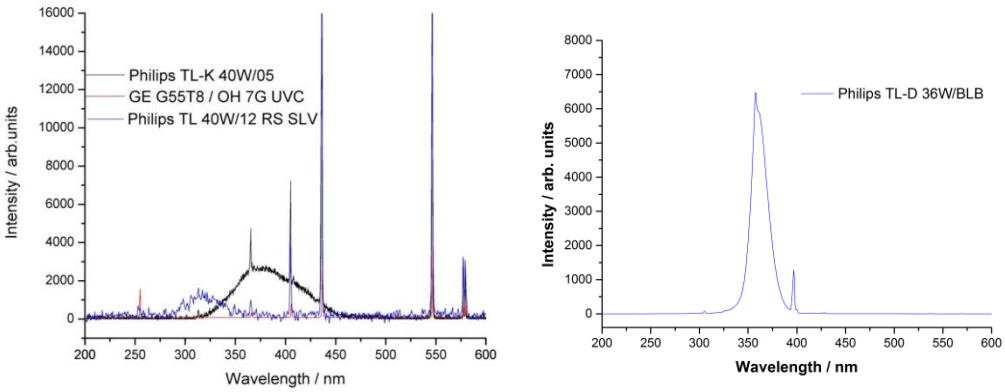

Figure 2.4: Output spectrum of all four lamps within HIRAC measured using a spectral radiometer with a resolution of 0.25 nm. The spectrum on the right is for a new set of lamps used in Chapter 7 for photolysis of peroxides.

The homogeneity of the radiation profile within HIRAC is important as this greatly simplifies analysis and modelling of results of photolytic studies, and moreover in the case of radical measurement, it is necessary in order to avoid radical gradients within HIRAC. Modelling of the radiation distribution in HIRAC was performed for the purpose of designing a light arrangement that maximised the volume of uniform light in the chamber, shown in Figure 2.5. The model consisted of the generation and evaluation of an NO_2 photolysis map (Glowacki et al., 2007a). Through a combination of experimental, analytical and ray tracing results it has been shown that J_{NO2} is within ±15% of the average for ~75% of HIRAC's volume. Additionally, measurements of OH across the chamber diameter showed that there is no significant radical gradient (Malkin, 2010).

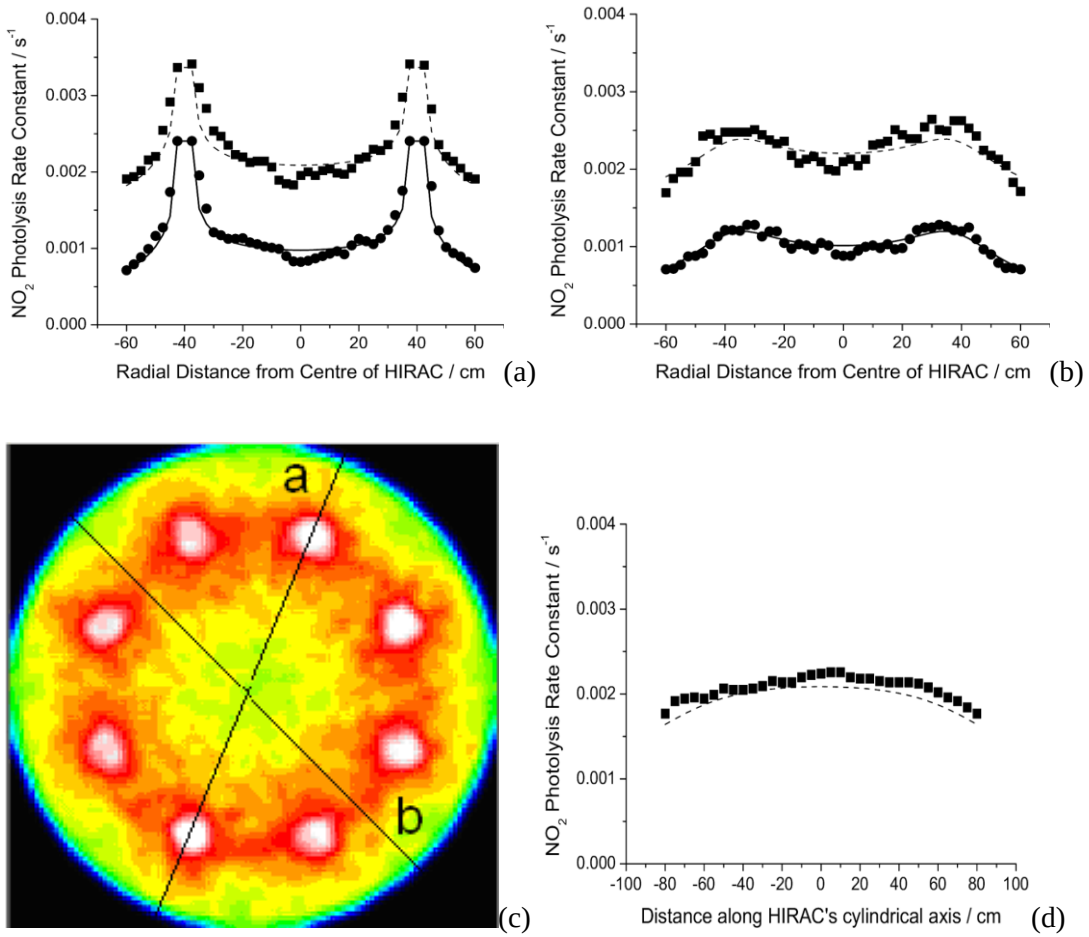

Figure 2.5: At a plane located at the centre of HIRAC, the above plots indicate that the region of ±15% radiation homogeneity represents ca. 86% of the cross sectional area of HIRAC. (a) and (b) Are comparison of the analytical form derived to describe NO_2 photolysis with the ray trace simulations for two radial transects on (a) line a and (b) line b in Figure 2.3(c) and (d) Comparison of the analytical form derived to describe NO_2 photolysis as a function of position along HIRAC's cylindrical symmetry axis (Glowacki et al., 2007a).

2.2.2 Gas delivery and mixing

In order to ensure good mixing of gases, HIRAC has four circulation fans, with two mounted on each end plate. The fans are made of aluminium, 225 mm in diameter, and coupled to externally-mounted variable speed DC motors *via* ferro fluidic feedthroughs (Ferrotec SS-250-SLBD). A flexible coupling between the motors and the feedthroughs, in conjunction with the neoprene pads between the motor housing and the end plates leads to significant reduction in vibrations, which

gives improved signal to noise ratios (S/N) in the spectra obtained by the FTIR optical system (which is described in Section 2.4).

Measurements were performed to investigate mixing times in HIRAC (Glowacki et al., 2007a). Mixing time is defined as τ_{95}, the time required for the concentration of a stable species to reach 95% of its maximum value (Pinelli et al., 2001). NO in N_2 (474 ± 14 ppbv NO in N_2, NPL certified) was measured with a commercial NO_x analyser, and several combinations of injection and sampling points around the chamber were investigated with respect to the number of fans running as well as the speed at which the fans were run.

Mixing measurements were insensitive to the particular locations of the injection and sampling points. Furthermore, the measurements indicate that at lower fan speeds (<1500 rpm), mixing time is reduced significantly by running all of the fans whereas at higher fan speeds, mixing time is insensitive to the number of fans that are running. With all fans running at 1500 rpm and 3000 rpm (100%), mixing times are ~70 s and ~60 s, respectively, and show good reproducibility. In the majority of experiments carried out in HIRAC all fans were running at a speed of 1500 rpm, with the exception of the isotopic branching ratio study in Chapter 6.

2.3 Chromatographic techniques

2.3.1 Introduction

Gas chromatography is a versatile technique capable of separating a sample into individual components, and at the same time qualitatively and quantitatively analysing the separated components. Separation of gases and volatile substances is achieved through their distribution between a mobile and stationary phase, and they are registered through transport by the mobile phase to the detector. The output from chromatographic separation is observed as peaks, which give both quantitative and qualitative information in a chromatogram as the intensity of the detector signal for each compound against their time spent in the column.

This technique can be used for a wide range of organics, and a good portion of the work presented in this thesis has been performed using this technique. For this reason this section will go through the basic theory of gas chromatography in sufficient detail highlighting the main areas of interest whilst comparing and contrasting the different techniques available for sampling, inlets, column selection, and detector performance, with a particular emphasis on the HIRAC Agilent 6890N Gas Chromatograph instrument shown in Figure 2.6 is available with Flame Ionisation Detection (FID).

Figure 2.6: HIRAC GC-FID (Agilent HP 6890N series Gas Chromatograph).

2.3.2 Gas management in GC systems

High purity gas (~99.999%) flows into the injector and through the sampling line, column and detector, with noble gases being commonly used as carrier gases due to their inertness. The HIRAC GC-FID system uses helium carrier gas (Fluka, ≥99.999%) with a number of gas filters installed prior to entry into the GC-FID instrument (Figure 2.7) preventing any contamination of the column and any interference in chromatograms from the carrier gas. Impurities such as oxygen and water are damaging to the GC column, and are a common problem with GC columns systems. Hydrocarbon traps are also useful to ensure the high purity gases used are free from any contaminants, and are commonly filled with activated charcoal, while oxygen and moisture traps are normally adsorbent cartridges.

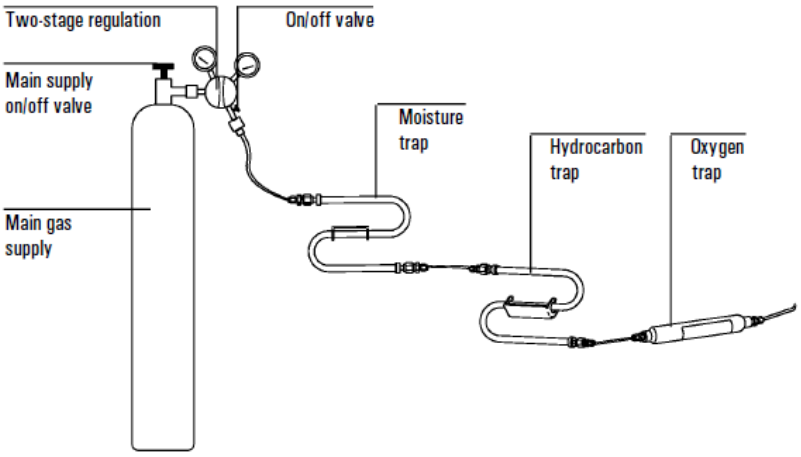

Figure 2.7: Gas management system for helium carrier gas (Agilent, 2000).

These traps are regularly maintained and routinely leak tested. In the helium supply used for the HIRAC GC-FID the moisture and oxygen traps are combined into one multifunctional adsorbent trap.

2.3.3 Chromatographic theory

All chromatographic processes can be regarded as a continuous repetition of partition steps between two phases, the stationary and mobile phase. Numerous separating steps take place and individual components elute out one after the other from these series of partitions, commonly referred to as plates (McNair and Miller, 2009). The separating capacity of the column on each partition corresponds to a theoretical plate, with the length of each plate called the height to equivalent to a theoretical plate (HETP). HETP is calculated from the column length divided by number of plates:

$$HETP = L / N \qquad \text{(Eq 2.1)}$$

The theoretical plate number, *N* shows the relation between retention time and peak width and describes column quality and separation power. The number of plates (*N*) can be calculated from the peak profile on the chromatogram (peak maximum and width); the more plates a column has the more effective it is in separating individual components:

$$N = 16 (t_r / W_b)^2 \qquad \text{(Eq 2.2)}$$

Where t_r is retention time and W is peak width. Retention time may be defined as the width at half maximum. The factors affecting HETP are described in the Van Deemter equation:

$$HETP = A + (B/u) + C + u \qquad \text{(Eq 2.3)}$$

Where A is the eddy diffusion term, B is the longitudinal diffusion term, u is the linear velocity and C is the resistance to mass transfer coefficient. An important factor that affects column efficiency is the mobile phase velocity, which varies all these terms effectively, as do particle size and morphology. The optimum mobile phase velocity is therefore achieved from the understanding of the van Deemter equation. HETP is affected by various factors such as column length, linear velocity in column (flow rates), particle size, retention factor and dead volume (instrument quality).

Figure 2.8 shows the ideal linear velocities for different carrier gases for a specific column. The smaller the plate height, the greater the number of plates and therefore the greater the efficiency of the column; this would be defined as the optimum flow.

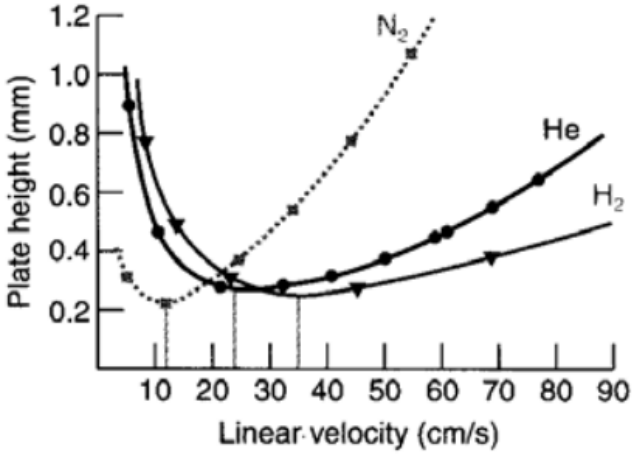

Figure 2.8: Van Deemter curves for gas chromatography of *n*-$C_{17}H_{36}$ at 448 K using N_2, He, or H_2 in a 0.25 mm diameter x 25m long wall-coated column with OV-101 stationary phase (Freeman, 1979).

Stationary phase particle size is another of the most important factors in the van Deemter equation. For a given column length, the plate number is inversely

related to the particle size of the column packing. Therefore the smaller the particles are the higher the plate number and the separation power.

Molecular dispersion, diffusion and slow mass transfer are the three main factors that govern the peak heights and peak broadenings in a GC chromatogram, and these are all kinetic processes described in the van Deemter equation. Identical molecules travel differently in the column due to probability processes. Column packing, and column thickness affect these kinetic processes since different packing and particle shapes alter the speed of the mobile phase and in turn the flow rate through the column.

Molecules traverse the column under influence of the flowing mobile phase resulting in slight dispersions in the mean flow rate due to molecular diffusion. A chromatographic system is in dynamic equilibrium. As the mobile phase is moving continuously, the system has to restore this equilibrium continuously. Since it takes some time to restore equilibrium (resistance to mass transfer), the concentration profiles of sample components between mobile and stationary phase are always slightly shifted. This results in additional peak broadening (McNair and Miller, 2009).

2.3.4 GC inlet systems

Inlets are the interface through which samples are introduced onto the GC column. Various different inlet systems are available, some specifically designed for purpose, and correct choice is essential for obtaining best quality data.

Inlet systems are generally classified according to the temperature at which they operate, thus the two main classes are: (a) hot inlets and (b) cold inlets; the former being the only system employed in our instrument. Injector temperature should be high enough to volatilise all of the analytes. The initial column temperature should be just below the temperature at which the first compound elutes (Sparkman et al., 2011). A split/splitless mode inlet is the most widely used inlet system for GC capillary columns, and is the one present in the HIRAC GC-FID instrument. A schematic of a typical split/splitless inlet is shown in Figure 2.9. A total flow controller external to the inlet system controls the flows of gas going into the inlet.

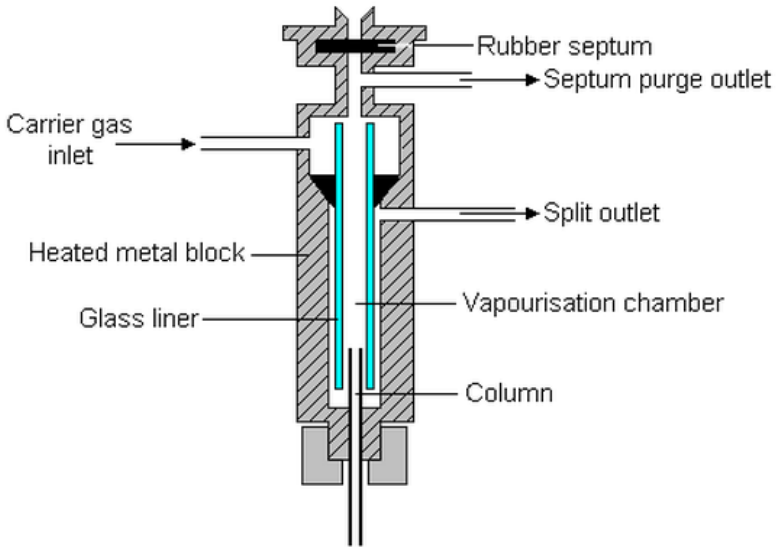

Figure 2.9: Split/splitless split mode inlet system (Taken from: http://www.chromatography-online.org).

Glass liners in split injection setups usually contain a glass frit or cup that promotes mixing of the sample. Quartz wool is often used in these liners in order to prevent non-volatile components from entering the column. This is not necessary for the HIRAC GC-FID given all vapour phase studies do not condense at 523 K, which is the temperature at which the injector is typically kept. Split mode is generally used for samples that are fairly concentrated, at levels greater than 100 μg mL^{-1}.

The split ratio is determined by dividing the sum of the column flow and vent flow by the column flow. Typical split ratios range from 10:1 to 400:1 (Sparkman et al., 2011).

$$\text{Split ratio} = \frac{\text{column flow + vent flow}}{\text{column flow}} \qquad \text{(Eq 2.4)}$$

Typical helium flows used for the HIRAC GC-FID inlet system are ~53 mL $minutes^{-1}$, with 3 mL $minutes^{-1}$ of helium entering the column, and 50 mL $minutes^{-1}$ acting as a purge for the inlet system. The purge flow makes its way through the split vent outlet. With the purge turned off, the entire sample flowing down the inlet enters the column. In a splitless mode, which is what is used in gas phase detection in HIRAC GC-FID, when the purge is turned on; the split vent is opened to purge the inlet during injection. This reduces the overload on the column and sharpens peaks in the GC chromatogram.

2.3.5 Gas sampling system

The HIRAC GC-FID instrument uses a Valco 6-way rotary gas sampling valve, which is shown in Figure 2.11. This mechanism is the method for continuous sampling in most chamber experiments and is used in all experiments presented here. The HIRAC GC-FID gas sampling system was developed due to the high uncertainties that were associated with syringing samples into a GC-FID instrument.

The sampling valve is connected to HIRAC and the pump *via* quarter inch copper sampling lines that are opened and closed by a set of two solenoid valves (Figure 2.10). The pump valve is opened and the chamber valve closed under normal operation in order to evacuate the copper tubing as well as the stainless steel sample loop. The sample loop is filled by opening the chamber valve and closing the pump valve, allowing ~30 s for a gas sample from HIRAC to be transferred into the sampling loop at the current chamber pressure.

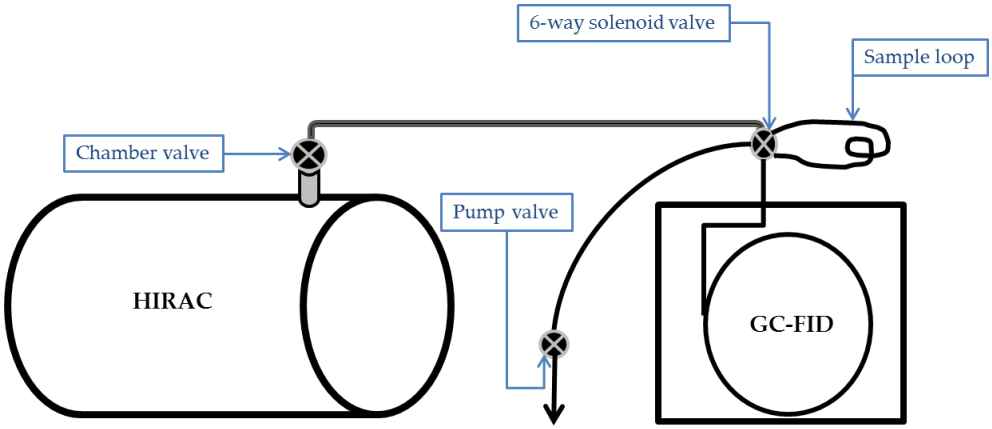

Figure 2.10: GC sampling system present in HIRAC.

A continuous flow is taking place through a sample loop when in inject position, the volume of which is interchangeable depending on the volume of sample desired to be analysed using the GC-FID. Varying the volume of the loop enables an increased amount of sample available for trace analysis. Several considerations should be taken into account prior to this being changed. It is important to balance out the carrier gas flow rate (using Van Deemter curve) with the pressure at the head of the column in order to determine the optimal time to allow for the sample loop to load the sample onto the column. Large volume loops reduce separation of chromatographic

peaks, since they result in a longer time for the sample to be loaded onto the column, which will in turn result in larger peak widths.

There are two operational positions for the 6-wayrotary valve; load and inject. In the load position, the volume of the sampling loop is connected to the chamber sample line, labelled “sample in” and “out”. In the “in” position, an automatic pump fills the sample loop and the sample is pulled through the valve. A sufficient flush of gas (generally 10 times greater than the volume of the sample loop installed) is necessary to ensure that the sample loop contains enough sample for analysis. The valve is then timed to shift position to inject long enough for introduction of the sample onto the column. The sample is pushed by the He carrier gas into the inlet and onto the column.

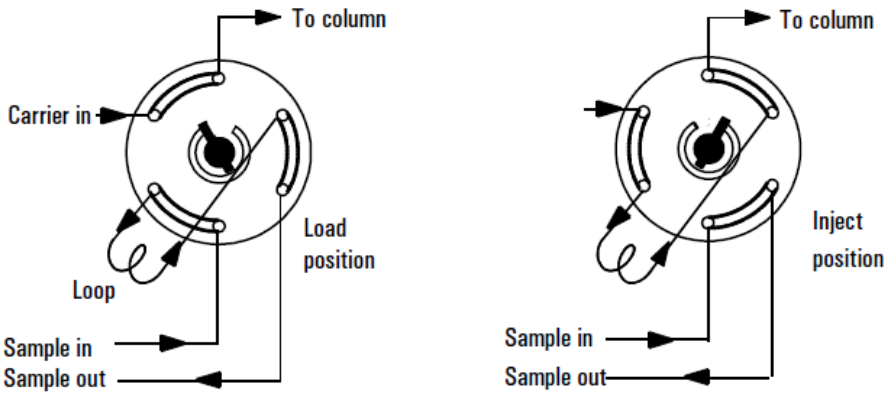

Figure 2.11: “Load” and “Inject” positions of the Valco 6-way solenoid valve. At Load position – the sample gas is expanded into the loop. The column is flushed with carrier gas; At Inject position – the filled loop is inserted into the carrier gas stream and the sample is flushed onto the column *via* the inlet. The run is controlled using an in-house LabView software which automates solenoid sampling in the HIRAC GC-FID. (Agilent, 2000)

As shown in Figure 2.11, the gases in the sampling loop are transferred to the column *via* the six-way gas sampling valve, and the sample loop is purged by resetting the chamber and pump valve. This automated sampling method is generally set to ~120 s for an entire cycle. The sampling rate is ~100 sccm (standard cubic centimetres per minute). All valves used to control sampling in the GC are controlled by in-house written LabView software, which controls the sampling and timing of the pump and chamber valves. The Chemstation software controls the timings for the 6-way gas-sampling valve. Temperature and pressure conditions must be held constant during

the entire run. A 3 K difference or ~7 Torr difference will cause a 1% change in the amount of gas sample (Grob and Barry, 2004). Shorter run cycles keep these uncertainties low, owing to lower variability in pressure or temperature parameters. If the samples are at a different temperature from the sample lines and valve, it is recommended to maintain them at an elevated temperature in order to minimise sample loss, which could occur through adsorption and loss to walls.

2.3.6 GC columns and stationary phases

Solutes are separated in the column, primarily by their physical properties, such as mass and polarity. Temperature and composition of the column walls also influence separation. There are two different types of columns: packed and capillary columns. The latter is the most common and modern GC column, and is a capillary tube coated with stationary phase leaving a small inner diameter for the analytes to flow through. Stationary phases can be either liquid or solid phase and present on the inside of the tubular column. Figure 2.12 shows the different types of stationary phases available in GC capillary columns: WCOT (wall-coated open tubular column), SCOT (Support-coated open tubular column) and PLOT (porous-layer open tubular column) columns.

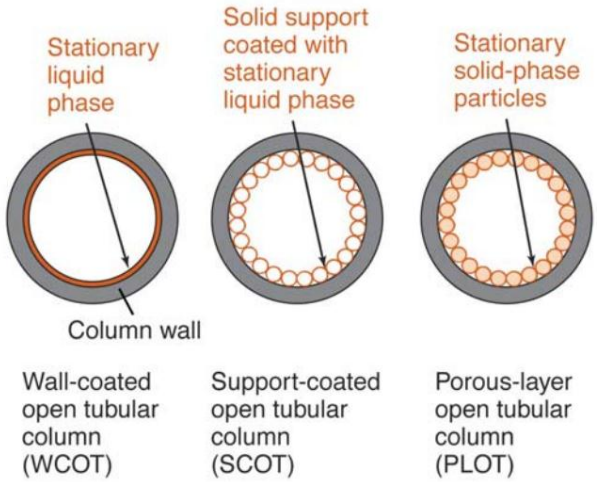

Figure 2.12: Types of stationary phases in GC capillary columns: stationary liquid phase (WCOT), solid supported liquid phase (SCOT), and solid phase particles (PLOT) (Taken from: http://www.chem.uidaho.edu)

There are a number of columns available for GC-FID analyses in the HIRAC lab. The most used are a J&W DB-1 column (50 m, 0.53 mm i.d. and film thickness of 5.00 μm,) and a Varian Chrompack CP-Sil 5CB column (50 m, 0.32 mm i.d. and film thickness of 5μm). These two columns are both non-polar columns coated with 100% dimethylpolysiloxane and can be used for separation of a wide range of organics. Separation of mixtures in these columns occurs by volatility.

Figure 2.13 shows the polymeric chain in polysiloxane columns, which is the stationary phase present in all the general purpose columns made use of in the HIRAC lab. It is also present in the majority of polar and polarisable columns, functionalised accordingly with cyanopropyl, trifluoropropyl and others depending on required selectivity.

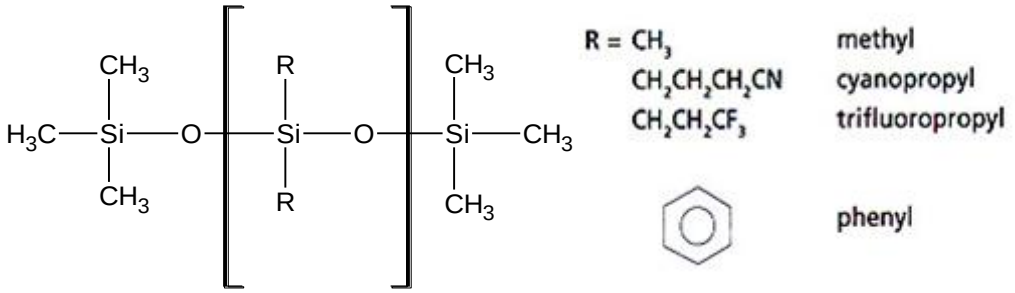

Figure 2.13: Common polysiloxane stationary phases and respective R groups used in modern gas chromatography columns (Hemavibool, 2009).

100% Dimethylsiloxane, 5% phenyl/95% dimethylsiloxane and columns are good general purpose phases that find numerous applications since they are non-polar and separate mainly by mass and boiling point of analyte. If the latter characteristics are similar for the analytes being studied, then polar columns are more selective towards their polarities. Examples of some polar stationary phases include polyethylene glycol (CarboWax columns).

2.3.7 Detectors

There are various kinds of detectors used in gas chromatography, and the choice of detector depends on the sample being studied. It is important to note that the

choice of carrier gas used also depends upon the detector being used. The most common carrier gases used are helium, nitrogen and hydrogen. The most commonly used detectors are flame-ionisation detectors, electron-capture detectors, mass spectroscopy and thermal conductivity detectors. Other examples of detectors used in gas chromatography include Pulsed discharge detectors (PDD), Electron Capture detectors (ECD) and Thermal Conductivity detectors (TCD). Mass spectrometers (GC-MS) and Fourier Transform Infrared instruments (GC-FTIR) are also commonly found coupled with modern GCs.

FID detectors are mostly used for organics and are mass sensitive detectors particularly sensitive towards organic analytes. Modern day FIDs are sensitive to ~10^{-13} g/s for most organics (Harris, 2003). Flame ionisation detection is much less sensitive to any oxygen/nitrogen containing compounds (carbonyl, alcohol, amine groups), thus the FID signal is expected to be significantly lower for these species. Most FIDs consist of hydrogen/air flames or hydrogen enriched with helium or nitrogen, burning at a capillary jet. Hydrogen is thoroughly mixed with the compounds being analysed and carrier gas within the column prior to contact with flame, as is shown in Figure 2.14.

The detector used for the HIRAC GC is a flame-ionisation detector (FID). The HIRAC GC-FID normally operates at a flow of 400 mL $minutes^{-1}$ of air and 40 mL $minutes^{-1}$ of hydrogen and 20 mL $minutes^{-1}$ of helium makeup gas; the latter also acting as a carrier gas. The FID detector used is maintained at 523 K.

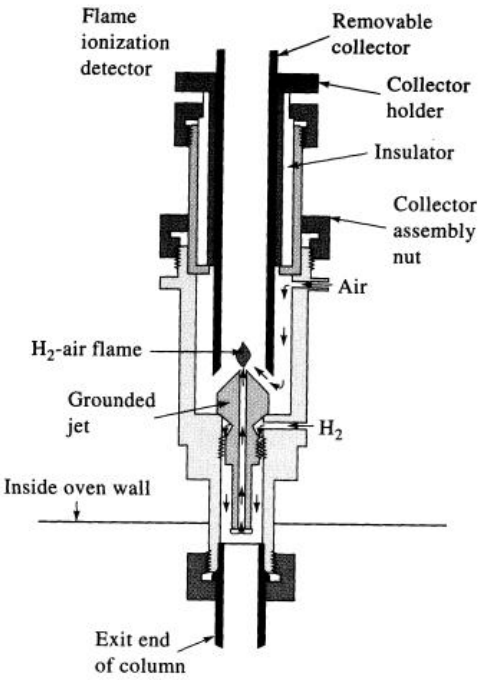

Figure 2.14: FID system in the HIRAC GC-FID instrument (Taken from: http://www.cem.msu.edu/).

Once the analytes elute from the column, they mix with the makeup gas and hydrogen, before pyrolysis in the flame breaks apart the analytes into ion fragments. The ionised fragments are directed onto a collector plate; a biased electrode, which produces an electrical signal that is detected by an electrometer.

The intensity of the signal is proportional to carbon number of the components, since the rate of ion formation would depend on the size of the sample upon injection. The magnitude of the electrode potential recorded depends therefore on the organic chain size and nature of the organic species. The output of the detector (converted from current to voltage) is sent to an integrating recorder that plots, stores, and analyses the data. The detector voltage (*y*-axis) is plotted as a function of time (*x*-axis). Each peak corresponds to a separate component. The time it takes for a given peak to appear after injection is called the retention time. If the column conditions are kept constant, the retention time for each component is quite reproducible from one sample and injection to the next. The identity of each peak can be determined by injecting pure samples of the individual components of the mixture and noting their retention times.

The HIRAC lab possesses two different pulsed discharge detectors, one used to detect formaldehyde in the in-built GC-HID instrument (Pulsed Discharge Helium Ionisation Detector, pdHID) and another in an Agilent 6890N GC (Pulsed Discharge Photoionisation detector, PDPID). The Leeds GC-HID was purposely built for achieving high sensitivity of detection of formaldehyde in the field with a good time resolution for determination (Hunter et al., 1999, Hunter et al., 1998, Hopkins et al., 2003). This method utilises the trapping of analytes in a loop cooled by a cold trap of liquid nitrogen, separation by GC and subsequent detection using the pulsed discharge helium ionisation detector doped with argon (Hemavibool, 2009).

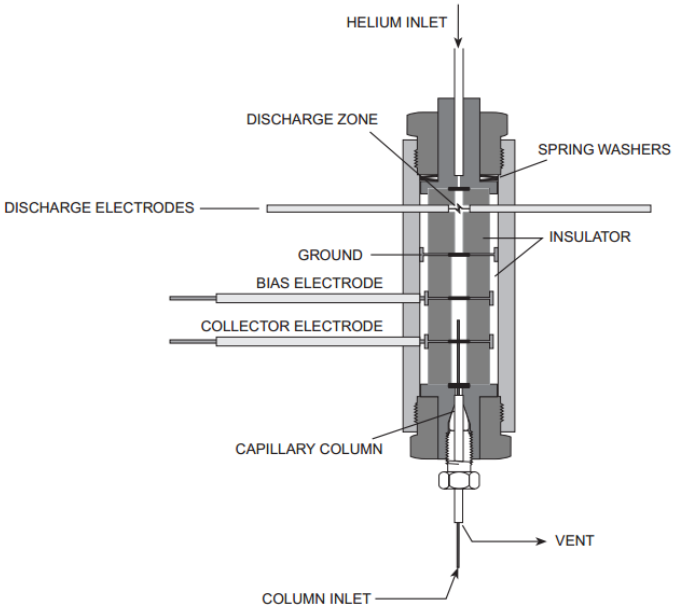

Figure 2.15: Schematic of a Pulsed discharge detector (Taken from: http://www.vici.com/support/manuals/d4_var.pdf).

Both pulsed discharge detector types mentioned work in a similar manner, and have several advantages over FID detection. They are non-destructive (0.01 - 0.1% ionisation) and highly sensitive, more so than an FID, with detection limits in the subpicogram ranges, and the response to organic compounds being linear over five orders of magnitude. Ionisation of the analytes is believed to occur by a combination of two mechanisms, the Penning Effect and the Hopfield emission (Whalley et al., 2004). The response is obtained from the ionisation potentials of the analyte relative to that of the discharge gas, which can be changed from pure helium doped with any of the noble gases depending on the desired discharge emission profile. This results

in resonance of atomic and diatomic noble gases. Response is constrained to samples possessing an ionisation potential less or equal to that of the dopant emission.

Electron Capture detectors (ECD) make use of radioactive beta emitters in order to ionise the carrier gas. A current is produced this way and this flow in between a biased pair of electrodes. When the carrier gas and organic analyte travel through the detector, the electronegative functional groups of the analyte will pass by the detector capturing electrons and reducing the current measured between the two electrodes. The analytes however have to contain an electronegative functional group in order to be detected, such as halogens, phosphorus and nitro groups. These detectors are as sensitive as FIDs, and commonly used for halogen compound detection, but can detect smaller ranges of compounds than FIDs.

A TCD detector consists of an electrically-heated wire or thermistor. The temperature of the sensing element depends on the thermal conductivity of the gas flowing around it. Changes in thermal conductivity, such as when organic molecules displace some of the carrier gas, cause a temperature rise in the element which is sensed as a change in resistance. The TCD is not as sensitive as other detectors but it is non-specific and non-destructive.

2.3.8 Peak Optimisation

Peak optimisation refers to the efforts made in obtaining higher resolution, shorter retention time and lower detection limit while at the same time separating at high throughput and economically. The three first-named goals may be most important, and of these the improvement of the resolution is the prime concern (Kromidas et al., 2008).

The effects of changing the purge flow in a split/splitless split mode inlet system are shown in Figure 2.16. This was a quick test on the HIRAC GC-FID while optimising conditions for experiments involving propane and cyclohexane. As can be seen from the chromatogram, the increase in purge flow results in a narrowing of the peaks widths, making them look sharper, however the peak heights and areas decrease since less sample is being loaded onto the column. Further testing of the effects of

these conditions on the output chromatograms is necessary and this is planned to be incorporated into a report outlining the modifications performed and their effects on the HIRAC GC-FID.

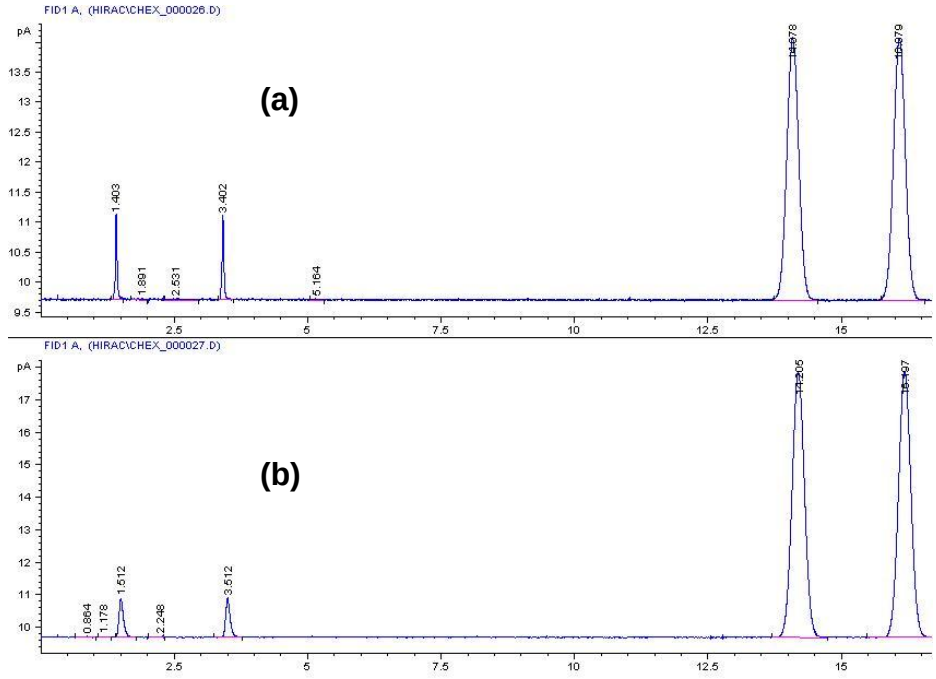

Figure 2.16: Effects of varying purge flow on a GC-FID chromatogram for two injections of propane (first two peaks) and cyclohexane (last two peaks): (a) purge flow at 25 mL minutes^{-1} (b) purge flow set to 5 mL minutes^{-1}.

The peak width determines the resolution of two components at a given distance between the peak maxima (Hubschmann, 2009), while the quality of the chromatographic separation (resolution) is measured as the retention difference divided by the peak width:

$$R \approx \frac{\Delta t}{\text{Width}} \qquad \text{(Eq 2.5)}$$

Where R is the resolution of two peaks, which is dependent upon the mean of the two peak widths and their respective Δt:

$$R = 1.198 \times \frac{t_{R2} - t_{R1}}{W_{h1} + W_{h2}} \qquad \text{(Eq 2.6)}$$

Where W_h is the full width half maximum. Resolution is related to the capacity factor, k', number of plates, N, and selectivity, α, by:

$$R = \frac{\sqrt{N}}{4}(\alpha - 1)\frac{k'}{1+k'} \qquad \text{(Eq 2.7)}$$

Chromatographic resolution therefore depends on three important terms: selectivity, retardation (fraction of a compound in the mobile phase) and dispersion (such as hydrophobic interactivity). The resolution is mostly dependent upon selectivity, as more plates are required in order to achieve better peak separation. Selectivity is improved by changing the column stationary phase, such as changing to a more polar column if the sample contains components with different polarities.

Decreasing the operating temperature of the column also increases the selectivity, since species take longer in the column under these conditions therefore allowing more time for separation, but also results in wider peaks. Other ways of improving resolution include increasing film thickness of stationary phase of GC column since this increases the number of theoretical plates for separation. Increasing the length of the column increases the resolution: doubling the length increases the resolution by a factor of 1.4 using the above equation, since it doubles the efficiency (number of plates) and doubles analysis time.

Figure 2.17 shows the effects of varying inject time (*i.e.:* time allowed for sample loop to flush sample into column) on peak shape. As can be seen, the lower the inject time, the less time the sample takes to elute, resulting in sharper peaks.

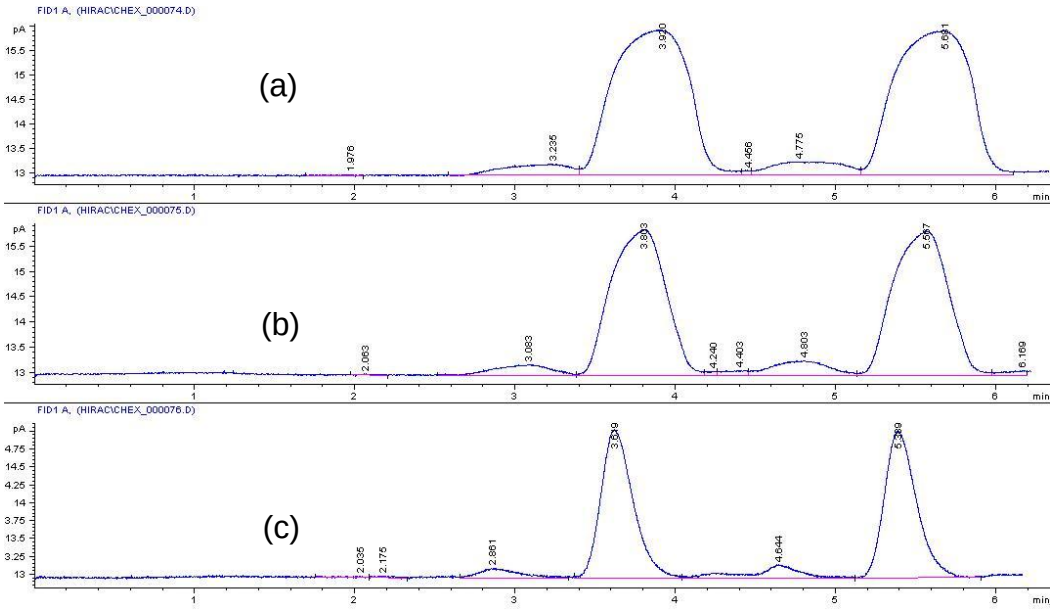

Figure 2.17: Varying the injection time ((a) 1 minutes (b) 0.8 minutes (c) 0.6 minutes) for GC-FID measurements of methane and propane.

2.3.9 Cryofocusing

Cryogenic trapping or cryofocusing is a technique commonly used in gas chromatography to overcome peak distortion and problems with resolution of chromatographic peaks. Trapping does not directly occur; rather the migration time of the sample is slowed down by the inclusion of a cold trap is incorporated into a GC system (Hagman and Jacobsson 1988). The utility of these cryogenic traps has been reviewed clearly by Brettel and Grob (Brettell and Grob, 1985a, Brettell and Grob, 1985b, Grob and Barry, 2004).

This technique has been extensively used to improve separation during the analysis of VOCs in the real environment (Simmonds, 1984, Wylie, 1986, Kolb et al., 1986, Shimoda and Shibamoto, 1990, Buser et al., 1982, Hagman and Jacobsson, 1988, Pankow, 1983, Werkhoff and Bretschneider, 1987, Mehran et al., 1990), with majority of reported studies using a "conventional" GC-FID instrument similar to that used for experiments in HIRAC.

Cryofocusing can be carried out by either cooling the entire column to sub-ambient temperatures during sample injection, or more conveniently by using the first coil of the capillary column (Kolb et al., 1986). The former has a few shortcomings as it takes a longer time to cool down the entire column and will also consume copious amounts of coolant, generally liquid nitrogen or carbon dioxide. Cooling the whole column is a still regarded as a viable "simpler" method as no trapping loop connections is necessary and this method has been shown to provide good chromatographic efficiency (Pankow, 1983). According to the literature, it is thought that cryofocusing occurs primarily by slowing down the migration rates of the sample components by increasing their capacity factors, which can be expressed as:

$$R_F = 1 / (1 + k) = u_s / u_c \qquad \text{(Eq 2.8)}$$

where R_F is the migration rate, k is the capacity factor of the solute, and u_s and u_c are the respective velocities of the sample vapour and the carrier gas respectively (Kolb et al., 1986).

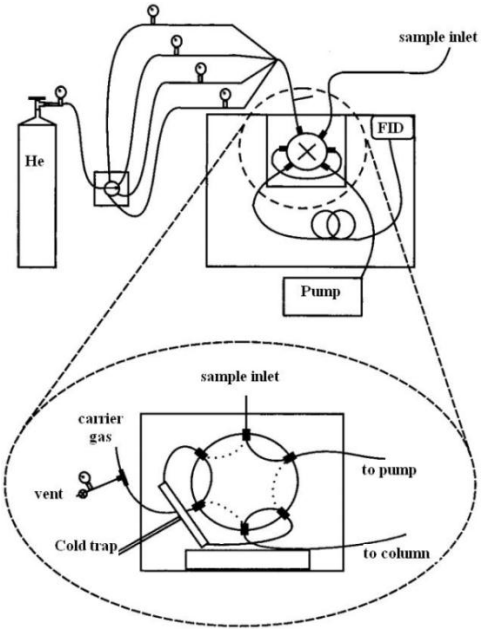

Figure 2.18: Cold trap installation in sampling loop; Adapted from (Borgerding and Wilkerson, 1996).

The most common method of cryofocusing makes use of a high-pressure liquid that can reduce the column temperature to as low as ~230 K within seconds, as is shown in Figure 2.18. This is similar to a recently installed liquid carbon dioxide cryogenic cold trap in the HIRAC GC-FID system (Figure 2.19). This section will describe the function and purpose of this recently installed cold trap, and discuss recent tests using *n*-alkanes.

The efficiency of a cold trap, measured on its ability to retain compounds, is dependent upon a number of factors, including the lowest temperature achievable. This is the reason liquid nitrogen and liquid carbon dioxide are used since they are inexpensive and can cool a trap to low enough temperatures to retain the majority of VOCs. Other factors include the temperature of the GC oven, the amount of analyte loaded onto column, timing of cooling and temperature gradients in the column. Compounds with very low capacity factors have also been found to exhibit problems as a short portion of the column may not be sufficient for the trapping of these analytes. Increasing the sampling time and trapping time can make this problem less pronounced, but if the capacity factor is too small, some of the compound could break through the trap.

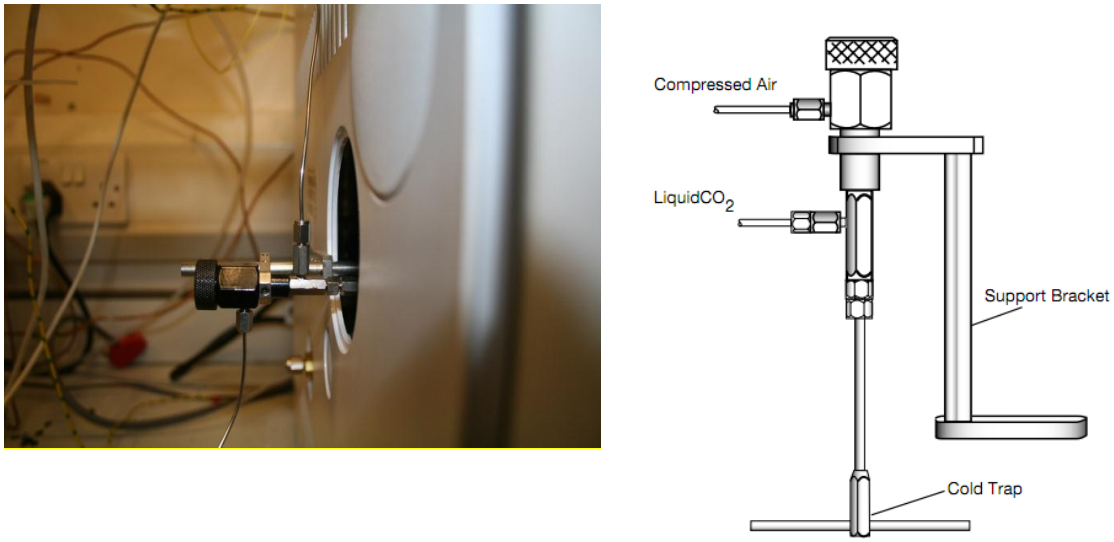

Figure 2.19: Liquid CO_2 system installed on the wall of the HIRAC GC-FID instrument (Taken from: http://www.sge.com/).

The aim of this cold trap was to improve the separation of peaks in GC-FID chromatograms, which would be beneficial for more elaborate product studies in HIRAC. This setup aims at improving the quality of chromatographic peaks observed during runs by giving ideal peak shapes through focusing of components into a narrow band resulting in reduced peak tailing and band broadening, depending on the cause of the poor peak shape in the chromatography.

This SGE CO_2 cold trap system installed works by controlling the flow of liquid CO_2 to a low thermal mass trap through a pneumatically actuated valve. Focusing takes place at the head of the column through cooling the first section of the column using liquid CO_2. The cold trap is designed to rapidly cool and efficiently reheat afterwards. The cold trap setup consists of a tee that is mounted in the GC-FID oven and connected to the cooling CO_2 liquid *via* insulated transfer lines. The flows are controlled by a pneumatic head switching valve that requires an actuating gas (nitrogen) pressure of ~4 bar. A three-way solenoid valve has been installed in order to automate this system by switching on and off the pneumatic nitrogen gas flow which in turn controls the switching valve for the cold trap which switches on and off the flow of CO_2 into the tee. This is controlled using an in-house National Instruments LabView software added on to the already existing solenoid program used to control the GC solenoids described earlier.

Initial tests of the cold trap were performed on a series of *n*-alkanes in HIRAC. The results presented in Table 2.1 were obtained in HIRAC at 1000 mbar and 292 K for *n*-pentane, hexane and *n*-octane.

	***n*-pentane**				**hexane**				***n*-octane**			
	Ret time	**width**	**area**	**height**	**Ret time**	**width**	**area**	**height**	**Ret time**	**width**	**area**	**height**
Cold trap on	2.19	0.04	4518	1774	2.96	0.05	292	86.6	7.18	0.12	3835	507
Cold trap off	2.05	0.11	4290	664	2.77	0.11	278	39.9	6.84	0.15	3400	357
Ratio	**1.07**	**0.36**	**1.05**	**2.67**	**1.07**	**0.46**	**1.05**	**2.17**	**1.05**	**0.80**	**1.13**	**1.42**

Table 2.1: Chromatographic data (retention time, width, area and height) for a series of *n*-alkanes with the cold trap turned on and off. The ratio reflects the change due to the cold trap being on.

These results demonstrate the potential for using a cold trap in the effect it has on the width of the peaks, particularly for the smaller alkanes used. This seems to point toward a trade-off between the time the cold trap is "holding" the analytes in the column with their retention times (Hagman and Jacobsson, 1988). As can be noted the cold trap is having a more pronounced effect on the *n*-pentane peaks; this is due to a higher vapour pressure compared to *n*-octane. The timings used for the cold trap were the same for every consecutive injection and the peak parameters shown in Table 3.1 are taken from the average of 7 injections. In fact the width decreases by a factor of 2.67 for *n*-pentane, while the height increases by the same factor. For the hexane the width roughly halves while the height roughly doubles, and for *n*-octane the change noted is much less evident, with a decrease by 20% for the width and an increase by a factor of 42% for the height.

Small changes in the peak areas (5%) are also noted, and it is not clear what could be the reason for this, possibly due to retardation of elution for any possible contaminants present in HIRAC or in sample line that may overlap with the hydrocarbons. A thermocouple was attached to the cold trap during these experiments and an average temperature of ~223 – 233 K was reached within a few seconds of the cold trap being turned on. Other authors report lower temperatures would be more suitable to focus all VOCs, since if the temperature is not low enough, the focusing is not as pronounced, and hence the efficiency of the cold trap is minimised this way.

2.3.10 Chromatographic techniques in other chambers

A brief review of chromatographic techniques used in different chambers was deemed appropriate in order to compare and contrast the different methods used and to what benefit and use these are being put to. The separating power of chromatography is invaluable during mechanistic studies with a large range of primary, secondary and tertiary products where FTIR would struggle due to overlapping IR peaks (Seakins, 2010b). GC and GC-MS instruments are therefore a standard benchtop instrument present in the majority of atmospheric chambers. In fact most chamber groups classify their GC instruments along with conventional analytical instrumentation such as O_3 and NO_x analysers and actinometers.

GC-MS is used by a number of atmospheric chamber groups owing to its ability to directly identify and quantify compounds being monitored, which is a valuable tool in mechanistic studies. The NIES chamber in Japan make use of both GC-FID and GC-MS in their chamber studies (Akimoto et al., 1979a), as does the aluminium alloy reactor at the Air Pollution Research Centre (APRC) in the University of California (Atkinson et al., 1980). Recent experiments by a group from Toledo performed in the EUPHORE chamber focused on product studies of the reaction of chlorine atoms with unsaturated alcohols (Rodriguez et al., 2012). GC-FID was used to quantify products from the relative rate study of unsaturated alcohols, whilst GC-MS was used to qualitatively identify other unknown products formed. Both instruments sampled from the chamber *via* 6-way sampling valves kept in the GC oven, and into a 1 mL loop that was evacuated with a vacuum pump. This setup is similar to the current setup in our HIRAC GC-FID, with HIRAC possessing a larger sample loop of 10 mL.

The EUPHORE chamber in Valencia has been used by various groups for kinetic and mechanistic studies using GC-FID and GC-MS (Cabanas et al., 2005, Borras and Tortajada-Genaro, Vivanco et al., 2011). A study on the photo-oxidation products of alkylbenzenes made use of a comprehensive GC×GC system. This work was carried out by groups from the University of Leeds, York and Newcastle as part of the EXACT project (Hamilton et al., 2003). Two litre air samples were taken from

the 190 m^3 Teflon chamber and were cryofocused using a cold trap (stainless steel sample loop held above liquid nitrogen) with a sampling frequency of 30 minutes, allowing the evolution of species during the photo-oxidation process to be followed over 3 – 6 hours. Likely photo-oxidation products were synthesised and used as reference standards for easier identification by the gas chromatographs. Comparison of GC×GC measurements with FTIR showed good agreement (Hamilton et al., 2003). The columns used were a very long (50m) BP-1 polysiloxane column and a second very short (10m) BP-20 polar column. The high polarity of the second columns' stationary phase ensured good 2D separation and narrow peak shapes.

GC systems have also been coupled to other instruments in chamber studies. The CRAC1 chamber at the University College Cork have a GC-MS instrument coupled to a novel denuder-filter system for simultaneous measurement of gas and particle phase oxidation products (Temime et al., 2007). They also have a GC-FID instrument coupled to their chamber that regularly monitors the concentrations of the organics being analysed (Thuner et al., 2004).

2.4 Spectroscopic techniques

2.4.1 Fourier transform infra-red spectroscopy (FTIR)

The importance of characterising VOC oxidation mechanisms has already been highlighted in Chapter 1. Environmental chambers provide a suitable environment for the study of these processes, and the availability of a Fourier transform Infra-Red (FTIR) absorption spectrometer is one of the most essential detection systems for chamber studies. IR absorption is an almost universal detection method with high selectivity.

FTIR is based on measuring absorption of IR radiation by a sample. An interferometer enables the measurement of all IR frequencies simultaneously. The only requirement for a molecule to be detectable is that it must have a vibrational mode that changes its dipole moment. Contrary to the HIRAC GC-FID, the HIRAC FTIR system is non-destructive since the sample remains intact during measurements.

An advantage of the FTIR system over GC-FID is the measurements are done *in-situ* compared to the direct sampling of GC-FID, which is beneficial as it does not dilute the chamber and also reduces the uncertainties associated with sampling and gas samples making it through a sample loop. Being such a versatile tool for analytical purposes, it is a useful quantitative and continuous technique that makes it a universal detection method for most trace gases in the atmosphere.

A Bruker IFS/66 FTIR spectrometer (CaF_2 beam splitter, Si diode detector, measurement range 4,000 – 400 cm^{-1}), is coupled to HIRAC and the multipass optical arrangement on the interior of the chamber *via* a series of transfer optics housed in a sealed purged box. This multipass optics system was developed by Glowacki and Goddard (Glowacki et al., 2007b), and a diagram of the arrangement is shown in Figure 2.20.

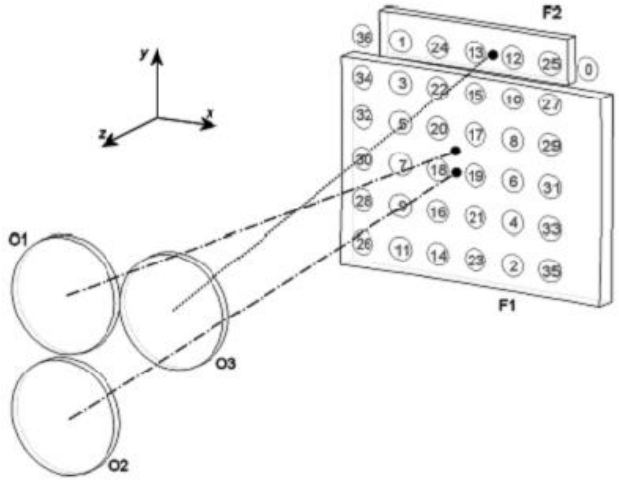

Figure 2.20: Modified multipass Chernin cell optics in HIRAC (Glowacki et al., 2007b).

This optical system is known as a modified multipass Chernin type cell, and is a modified multipass matrix system that features three objective mirrors with input and output apertures placed on opposite sides of the small field mirror(Chernin, 2001). The latter publications give a description of the modified multipass system which differs from the original system in that it separates input and output beams to opposite sides of the field mirror, thus making it a more convenient arrangement. Figure 2.20 shows a schematic of the 72 pass arrangement for this modified multipass Chernin type cell optics developed by Glowacki and Goddard (Glowacki et al., 2007b). The above figure also shows the image pattern on the field mirror and points the centre of

curvature for each objective mirror (F1 located at midpoint of O1 and O2, while F2 located at midpoint of centres of O1 and O3). Some temperature effects due to expansion of mirrors may lead to loss in alignment of the FTIR optical system; this can be minimised by selecting mirrors with materials that have low thermal expansion coefficients.

Under normal operation, IR beams pass in and out of HIRAC *via* two 6 mrad wedged potassium bromide (KBr) windows, in order to avoid etalon effects (Glowacki et al., 2007b). The transfer optics are housed in a sealed purged Perspex box flushed with nitrogen to avoid absorption by laboratory air. Alignment of the FTIR system is done using a near-infrared (NIR) output from the Bruker FTIR spectrometer, which is visible on the mirrors surfaces and field mirror spots may be easily counted this way. The colinearity of the NIR and MIR beams ensured the aligned NIR beam almost exactly positioned as the aligned MIR beam (Glowacki et al., 2007b). A sample volume or approximately 0.083 m^3 of HIRAC is illuminated by this FTIR optical system, corresponding to around 3.6% of the volume of the chamber.

The importance of the mirror systems to be robust and able to handle ranges of temperatures and pressures is an important consideration that needed to be taken into account during design of the HIRAC FTIR system. This would ensure the system developed would maintain alignment through pressure and temperature variations. The HIRAC mixing fans and pumping systems described previously result in vibration that could also have an effect on the FTIR alignment. The mirrors used in the HIRAC FTIR system are made of zerodur glass which has a very small thermal expansion coefficient.

The sensitivity of the FTIR instrument is related to absorbance, (I_o/I), *via* the Beer-Lambert law:

$$A = \ln\left(\frac{I_o}{I}\right) = \sigma \, c \, l \qquad \text{(Eq 2.9)}$$

Where A is the absorbance, I_o and I are the initial and detected intensities respectively, σ the absorption cross-section, c the concentration and l the path length. According to Eq 2.9, a long path length clearly enhances the sensitivity of the system and this is achievable in HIRAC with a multipass system by-passing the chamber 72 times. This means that long path lengths (up to 140 m) achieved in the HIRAC-FTIR

increases the sensitivity of the instrument, explaining why a multipass system is used in HIRAC. The robustness of the system developed in HIRAC also influences the capabilities of this system to withstand various conditions of temperature and pressure, and all the time and effort put into the design of this system has ensured it can withstand such conditions. HIRAC is mounted on a stainless steel frame that rests on neoprene and cork pads to damp vibrations that otherwise affect the performance of the optical system (Glowacki et al., 2007a).

The FTIR has been a useful technique in the work reported in this work. The unavailability of the HIRAC FTIR system at the start of these studies meant relative rate experiments in chapter 4 could not make use of this facility. Experiments described in chapter 5 reports both GC-FID and FTIR measurements of the product branching ratios from the reaction of Cl atoms with butanes and chapter 6 will also involve use of FTIR to investigate HCl/DCl ratios from the reaction of Cl atoms with ethanol and its deuterated isotopologues.

2.4.2 Cavity ring down spectroscopy (CRDS)

A CRDS system was installed in HIRAC in October 2009 to study NO_3 radical chemistry, particularly reactions with alkenes. Figure 2.21 shows a schematic of the CRDS system coupled to the HIRAC chamber. This system utilised a medium pulse repetition frequency (PRF) red light source for the detection of NO_3 radical at λ = 623 nm. The probe light was generated using a Nd:YAG (Litron Nano TRL, 200 Hz PRF) pumped dye laser (Lambda Physik LPD3000) and delivered *via* fibre optic cables (OZ optics, QMMJ-55-UVVIS-200/240-3-15, 15m, core diameter 200 ± 4μm) was introduced into the cavity *via* a focussing lens (focal length of 25 mm at 355 nm), a collimating unit and an optical system consisting of a lens (Thorlabs, LA1908) and 3 tuning mirrors (Thorlabs, BB2-EO2) that direct light through the optical mounts (Malkin 2010). The cavity was set up across the diameter of HIRAC (1.4 m) using two high reflectivity mirrors (Los Gatos Research, R = 99.9995%, radius of curvature = 1.0 m, λ = 590 – 650 nm) mounted onto the chamber flanges in fine tunable CRDS mirror mounts (Los Gatos Research).

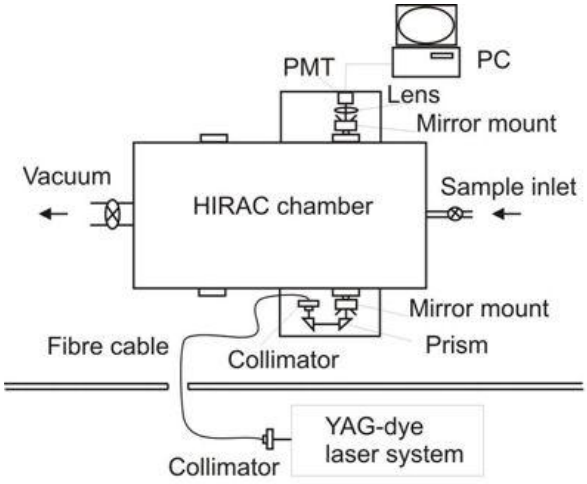

Figure 2.21: Schematic of the HIRAC CRDS system (Malkin 2010).

The theoretical longest ring-down time (τ_{max}) for this CRDS system is 93 μs, determined by equation 3.1, which shows the relationship of τ_{max} with mirror reflectivity (R), path length (*l*) and the speed of light (c):

$$\tau_{max} = l/c \ln R \approx 1/c (1-R) \qquad \text{(Eq 2.10)}$$

This value could be greater as it is calculated using the lowest estimate of mirror reflectivity quoted by the manufacturer. The HIRAC CRDS system was tested by Malkin (2010) using a short set of NO_3 radical reactions with a series of C_1– C_4 aldehydes (Figure 2.22). NO_3 radicals were generated *in-situ* in HIRAC by the reaction of $NO_2 + O_3$. The detection limit for NO_3 was 6 pptv (time resolution of 4 seconds and chamber pressure of 1000 mbar).

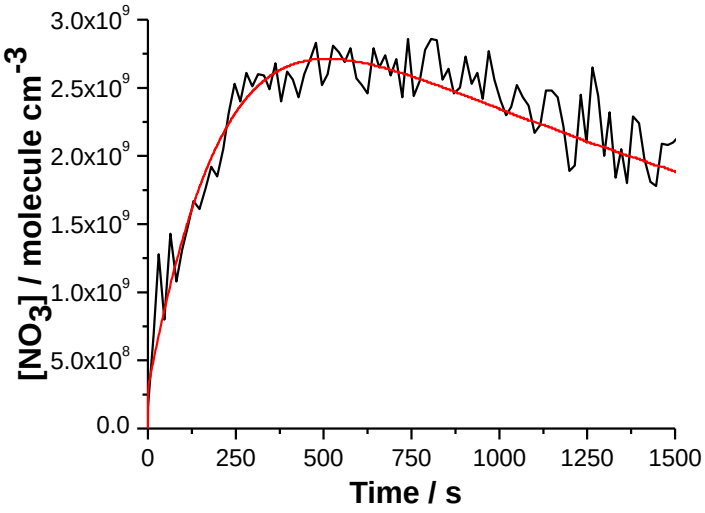

Figure 2.22: NO_3 detection synthesised from NO_2+O_3*in-situ* using HIRAC CRDS (Malkin 2010).

The setup consists of a tuneable pulsed laser source, two concave mirrors, a photosensitive detector and a data acquisition device. A laser beam is aligned to the mirrors along the axis of the cavity creating an optical cavity consisting of two highly reflective (>99.9%) di-electric coated concave mirrors as illustrated in Figure 2.23.

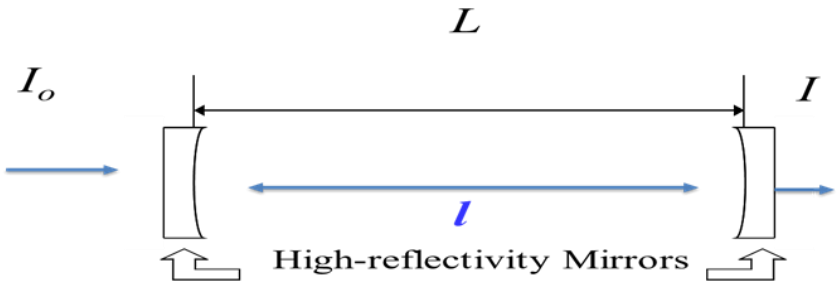

Figure 2.23: Schematic illustrating the principles of CRDS. (L = length of flow tube; I_o = initial light intensity going into cavity; I = light intensity leaking out of cavity; l = path length of light).

The high reflectivity mirrors used are not perfectly reflective, resulting in a small fraction (0.1%) of light transmitting through the mirror. The mirrors are aligned in such a way that an optical cavity is formed. The light intensity slowly begins to diminish due to both transmission of the laser light through the mirrors, and molecular absorption of species present within the cavity. The measure of the ring-down process, τ, is taken as the time it takes the light in the cavity to decay to 1/e of its initial value. This is known as the ring-down lifetime, τ, which is extracted by a weighted least squares fit:

$$\tau = t_r / [1\ (1 - R) - \varepsilon C l] \qquad \text{(Eq 2.11)}$$

τ is related to the round trip time, *t*r, mirror reflectivity, R, molar extinction coefficient, ε, path length, l, and concentration of absorbing species, C. This is picked up by a photo-sensitive detector located at the back of the second mirror. A computer then determines the decay time constant by fitting the data from the light intensities recorded to a first order exponential, measuring the decay of light leaking out of the cavity as a function of time. The intensity of light after the cavity, I, is related to the intensity of light before the cavity, I_o, the residence time of the light, t, the speed of light, c, the path length, l and the ring-down time in the absence of an absorber, τ_o:

$$I = I_o \exp(-t / \tau_o) \qquad \text{(Eq 2.12)}$$

Change in light intensity leaving the cavity is also caused by sample absorption, and, based on the assumption that light in the cavity is obeying the Beer-Lambert law, exponential decay of light will remain constant with time. This is used to calculate the absorption coefficient, α:

$$\Delta k = 1/\tau - 1/\tau_0 = \alpha c \qquad \text{(Eq 2.13)}$$

$$I_t = I_o \exp(- t / \tau - \alpha c t) \qquad \text{(Eq 2.14)}$$

where α is the molar absorption coefficient, which is the product of the concentration of the absorbing species, C and the absorption cross-section of the species at a given wavelength, σ ($\alpha = \sigma C$) and Δk is the change in the decay rate constant. In the absence of any absorbing species within the cavity, *i.e.* $\alpha = 0$, the decay rate is simply $1/\tau_o$, however when sample is present, it is given as $1/\tau_o + \alpha c$. The sensitivity of a CRDS system is measured by the fractional loss of light intensity per pass along the cavity, δI, which may be determined using the Beer-Lambert law (Wheeler et al., 1998):

$$\delta I = \frac{I_o - I}{I_o} \cong \alpha l \qquad \text{(Eq 2.15)}$$

2.4.3 Fluorescence assay by gas expansion (FAGE)

Fluorescence Assay by Gas Expansion, FAGE (Hard et al., 1986), is another spectroscopic method that has been coupled to HIRAC. This is a low pressure, on-resonance laser-induced fluorescence (LIF) technique used for the detection of OH and HO_2 radicals.

The HIRAC FAGE system shown in Figure 2.24 operates by drawing air from the chamber through a pin-hole nozzle of 1.0 mm diameter into the sampling inlet (300 mm length, 50 mm diameter) towards the low pressure detection cells maintained at $\leq$4 mbar by a rotary pump backed roots blower combination.

The OH detection axis is reached directly after the inlet. At this stage, the OH radicals in the air sample are excited by the fibre coupled, second harmonic UV output from the laser used in this LIF setup. The Nd:YAG pumped dye laser is employed for HIRAC FAGE at 308 nm.

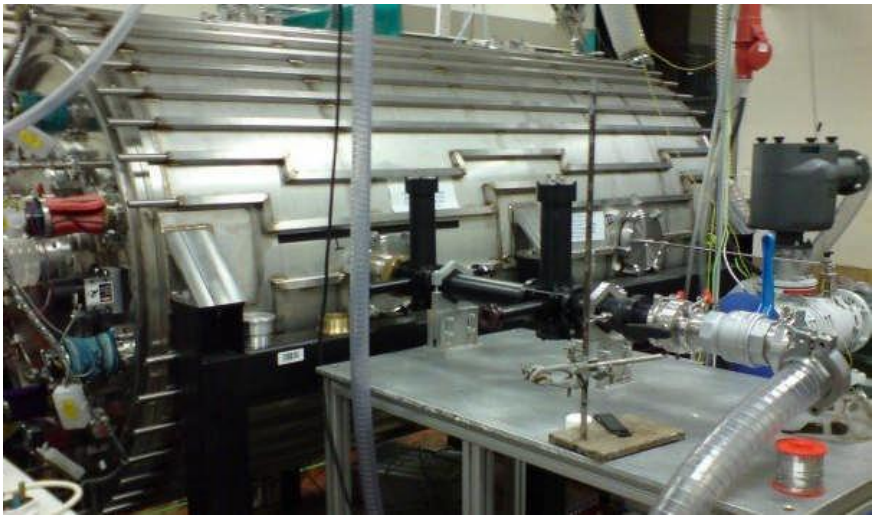

Figure 2.24: FAGE cells coupled to HIRAC chamber.

The OH absorption cross-section at 308 nm is about 6 times stronger than at 282 nm, which was the wavelength used in earlier FAGE instruments, thus improving the sensitivity of detection of OH by working under these conditions (Heard, 2006). The rather large pulse energies at 282 nm led to considerable photolysis of O_3, initiating OH production *via*:

$$O_3 + h\upsilon\ (282\ nm) \rightarrow O(^1D) + O_2 \qquad \text{(Eq 2.16)}$$

$$O(^1D) + H_2O \rightarrow 2\ OH \qquad \text{(Eq 2.17)}$$

This ironically was the same way OH is formed by solar photolysis in the atmosphere, and this led to the end of this method in the tropospheric field community (Heard and Pilling, 2003). A schematic diagram of LIF detection schemes for OH is shown in Figure 2.25. HO_2 radicals are detected indirectly in the second detection axis following chemical conversion to OH using a small flow of NO ($HO_2 + NO \rightarrow OH + NO_2$).

OH fluorescence resulting from this excitation at 308 nm is filtered and collected by a photomultiplier tube that is fixed stationary on the third axis

perpendicular to the laser beam. The fluorescence is analysed by gated photon counting. This on-resonance form of detection is able to distinguish between OH fluorescence and any unwanted signal scatter from other gaseous constituents present.

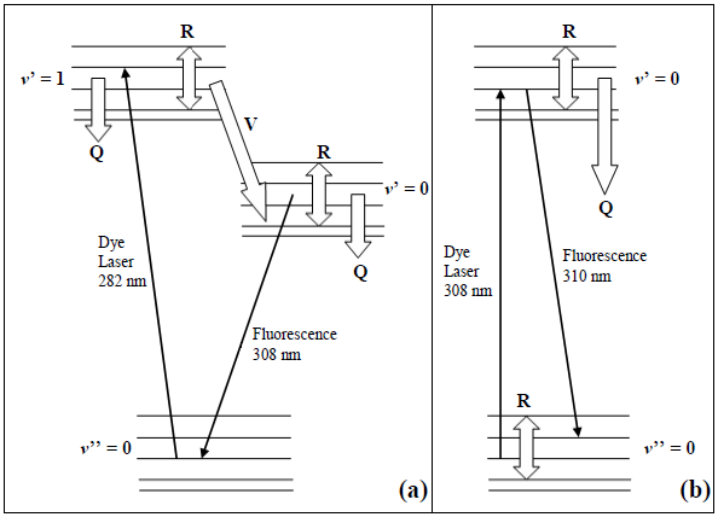

Figure 2.25: A schematic of the laser used to detect OH using LIF. (a) The $v'= 1$ level is pumped $\lambda = 282$ nm. V: vibrational energy transfer, induced by collisions with ambient N_2 and O_2. Fluorescence detected at $\lambda = 308$ nm. (b) The $v'= 0$ level is pumped with $\lambda = 308$ nm and fluorescence detected at 308 nm. Q and R denote collisional quenching and rotational energy transfer (Crosley, 1995).

OH and HO_2 measurements in the field using LIF were performed using a small flow of NO to convert HO_2 into OH, and detecting the additional signal from OH formed (Heard and Pilling, 2003). In HIRAC OH and HO_2 data are collected with a time resolution of ~1 second at which the instrument has detection limits of the order ~10^6 to 10^8 molecule cm^{-3} for OH and HO_2.

2.4.4 Spectroscopic techniques in other chambers

Fourier transform infrared (FTIR) spectrometers are probably as ubiquitous in chambers as gas chromatographs discussed in Section 2.3.10 for other chambers. FTIR is one of the most useful techniques for the purpose of monitoring reactants and primary products in chambers and is easily coupled to chambers of any size and make by introducing the optics through windows in chamber. Most evacuable stainless steel chambers, such as the one at the National Institute for Environmental Studies (NIES) in Japan (Akimoto et al., 1979a) are equipped with long-path FTIR with a multipass

system similar to the Chernin setup present in HIRAC. The FTIR in this NIES chamber has a path length of 221.5 m. The multipass cell is an eight mirror system. A similar setup is available in the NCAR chamber (Bacher et al., 2001, Orlando et al., 2002).

The Air Pollution Research Centre (APRC) in the University of California (Atkinson et al., 1980) possesses both an FTIR and a Differential Optical Absorption Spectroscopy (DOAS) rapid-scanning device as is shown in Figure 2.26.

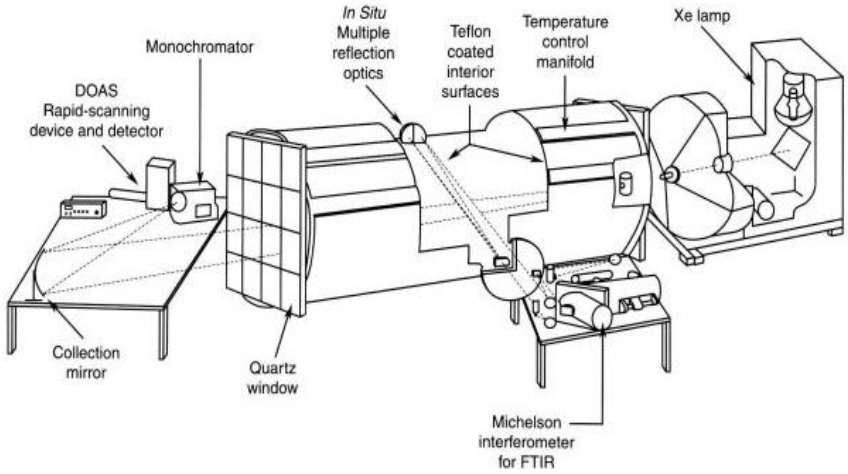

Figure 2.26: Schematic diagram of the evacuable chamber at APRC, University of California, Riverside (Finlayson-Pitts and Pitts, 2000)

The above chamber uses a three mirror White-type multipass system for its FTIR, coupled to a Michelson interferometer. The base path between the two mirrors is 1.33 m and the system can have path lengths up to 85 m using gold coated mirrors.

The Centre for Research into Atmospheric Chemistry (CRAC1) chamber in Cork and the QUAREC chamber in Wuppertal both use *in-situ* FTIR systems same as HIRAC but with a slightly different arrangement designed in conjunction with Dr. Klaus Brockmann (Thuner et al., 2004). The CRAC1 and QUAREC chambers both consist of a White Cell with two circular field mirrors and a rectangular objective mirror, both sets of mirrors being gold-plated pyrex mirrors. The mirrors are interfaced to the FTIR instrument *via* an optical arrangement of gold-coated mirrors through a KBr window.

The SAPHIR chamber in Jülich has a large range of spectroscopic instruments, including and *in-situ* FTIR, DOAS and LIF instrument. DOAS and LIF are been used

in the SAPHIR chamber and have been compared prior to taking the instruments on field campaigns (Schlosser et al., 2007, Fuchs et al., 2010). SAPHIR, same as HIRAC, has a wide range of standard equipment for trace gas measurements. The LIF instrument and DOAS in the SAPHIR chamber are positioned the same way the FTIR and FAGE (LIF) instrument are positioned in HIRAC. The DOAS cross the full length of the chamber, while the LIF instrument samples perpendicular to the DOAS path, as is shown in Figure 2.27.

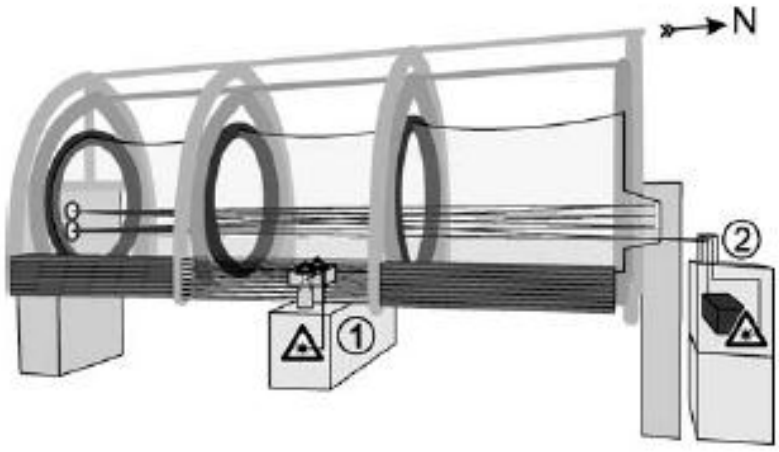

Figure 2.27: A schematic of the SAPHIR chamber and the positioning of ①LIF and ② DOAS instrumentation

CRDS is a fairly recent technique to be used in atmospheric chambers. Aside from HIRAC, only a few other chambers make use of the technique. The CRAC1 chamber in Cork makes use of a custom-built cavity enhanced absorption spectroscopy (CEAS) system for the detection of nitrate radicals (Venables et al., 2006).

2.5 Commercial Analysers

HIRAC is also equipped with a suite of commercial analysers for the measurement of O_3, NO_x, H_2O and CO. All the analysers are monitored using a Lab View v10.1 software developed on a computer in the laboratory that is used solely to control these analysers, temperature, pressure and the fans in HIRAC.

The Thermo Electron Environmental instruments Model 49C O_3 analyser uses UV photometry to measure O_3. This instrument has been calibrated using a commercial primary standard O_3 analyser Thermo Electron Corporation 49i-PS (Malkin, 2010) and has been a very useful instrument used in ozonolysis experiments carried out in HIRAC. This instrument is quite sensitive to pressure changes and can operate well between 500 mbar and ambient pressure. It has a detection limit of 1.0 ppb and a sample flow rate of 1 L/minutes (Thermo Electron Corporation, 2005). A particular limitations to the use of this instrument is the presence of some artefacts that arise from the absorption of UV radiation by VOCs present within the sample.

A Thermo Electron Corporation Model 42C NO_x box has been used for detection of NO and NO_2 in HIRAC. This instrument is able to operate down to approximately 725 mbar. The detection limits for NO and NO_2 using this instrument are 50 ppt. The sample rate at atmospheric pressure is set to 0.6 L/minutes and the response time is every 40 seconds with 10 second averaging (Thermo Electron Corporation, 2004). Some limitations with these converters do exist as well, particularly dependent on the type of converter the NO_x box possesses. Molybdenum converters catalytically convert NO_2 to NO and subsequently measure its chemiluminescence by reaction with O_3. These converters are known to overestimate the NO_2 because of other oxidized nitrogen compounds such as peroxyacetyl nitrate and nitric acid that are also partly converted to NO (Steinbacher, 2007). Other photolytic converters using UV light can be used as an alternative for long term measurements, but these can under estimate the NO_2 through interference (production of OH through photolysis of e.g.: glyoxal to give HO_2 which reacts with NO).

The CO analyser is a commercial gas chromatographic reduction gas analyser (Trace Analytical Model RGA3), and has a detection limit of 10 ppbv and a sample flow rate of 35 mL/minutes.

Numerous inter-comparisons were carried out for these analysers in order to confirm linearity of the instrument detection with other instruments (Malkin, 2010, Hemavibool, 2009, Glowacki, 2008). The O_3 and CO analysers were tested both in HIRAC in conjunction with the FTIR instrument (Malkin, 2010), and using three different commercial O_3 analysers outdoors around the Chemistry building (Hemavibool, 2009). In the case of the FTIR inter-comparisons, both CO and O_3

results gave linear correlation plots with respect to concentration. The results obtained from ambient air sampling also correlated well with each other and showed similar trends in ozone throughout the monitoring period.

2.6 Summary

The entire suite of analytical instrumentation available in HIRAC has been highlighted in this chapter, demonstrating the full capabilities of this atmospheric chamber for the study of tropospheric VOC oxidation processes.

Its main features include a commercial GC-FID, a multipass FTIR system, a FAGE instrument, CRDS system, and a range of commercial analysers. The FTIR and GC-FID instruments highlighted in greater detail are to feature prominently in the remainder of this thesis; with a particular emphasis on work using GC-FID and the relative rate method, which will be presented in Chapters 4 and 5. HIRAC's potential to perform detailed pressure and temperature dependent studies will also be demonstrated in Chapter 5, and the details and characterisation of HIRAC's recently installed temperature control system developed specifically for this purpose will be elaborated in the following chapter on instrument development.

Chapter 3 – Instrument development and characterisation

3.1 Introduction

Laboratory studies of gas phase chemistry are crucial in the understanding of atmospheric processes of relevance in tackling issues such as climate change and air quality (Seakins and Blitz, 2011, Finlayson-Pitts, 2010). Instrument development plays a crucial role in improving techniques and experimentation used in the study of atmospheric chemistry. One can improve several characteristics in an experimental setup, including the instrument detection, the versatility of the chamber or flow tube, and how controlled the conditions are for studies of atmospheric chemistry.

All recent contributions made to the developing new techniques and instruments during the course of this study are highlighted in this chapter. The setting up and characterisation of a recently refurbished mini photolysis chamber will be discussed first. This chamber was setup and characterised with the support of Stephanie Orr, who characterised the wall losses and heterogeneous effects of the walls, and carried out several alkene ozonolysis experiments probing O_3 using a commercial O_3 analyser. The potential to interface various detection systems to this chamber (GC-FID, FTIR, and gas analysers) made this setup an attractive addition to the HIRAC lab. The main aim of this work was to eventually use this chamber as a test-bed for experiments prior to them being performed in HIRAC, as well as to carry out photolysis experiments of interest such as for characterising or identifying suitable alternative radical precursors for chamber studies.

The last portion of the chapter will focus on the recent installation of a temperature control system in the HIRAC chamber. This is an important component of this research as one of the main objectives was to obtain temperature dependent kinetics in HIRAC. Chapter 5 will go through some chlorine atom temperature dependent studies carried out with a series of butanes and pentanes. In this chapter, a full characterisation and testing of the temperature control system is outlined, and the

results obtained for the ozonolysis of propene over a temperature range of 233 – 323 K, which is the full range of the troposphere as has been highlighted in chapter 1. This system has increased HIRAC's capabilities to conduct experiments not just over various pressures, but also over temperatures.

3.2 Mini photolysis chamber

3.2.1 Design

A 35 L mini photolysis chamber shown in Figure 3.1 has been recently refurbished in the HIRAC lab. This stainless steel chamber has a volume of 35 litres, approximately 66 times smaller than the HIRAC chamber, making it an ideal test bed prior to experiments being performed in HIRAC. A 4 L Edwards scroll pump was used to evacuate the chamber between experiments. This pump is able to fully evacuate the mini photolysis chamber from atmospheric pressure to 0.1 mbar in less than 5 minutes, compared to ~1 hour in HIRAC. The pressure of the chamber is measured using an MKS 1000 Torr pressure transducer connected to an MKS PR4000 dual channel power supply, readout and control unit with an accuracy of 0.2%.

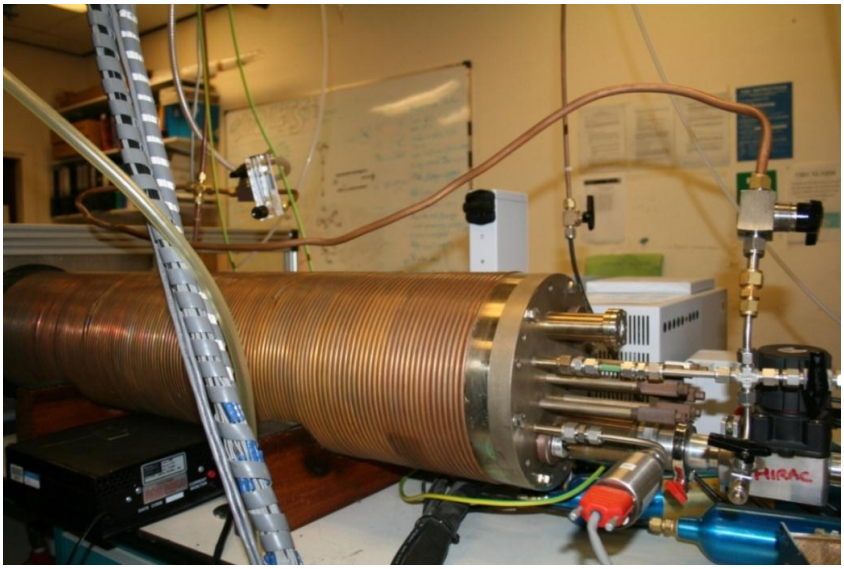

Figure 3.1: A side view of the recently refurbished mini photolysis chamber.

The mini photolysis chamber has a 2 mm Teflon coating on its walls that reduces the heterogeneous chemistry taking place on the surface of such a small metal chamber with a high surface area to volume ratio. The outer chamber walls are covered by hollow copper coils that were intended in design for circulation of a thermo-fluid to offer temperature control similar as in HIRAC. There were some complications that needed addressing regarding the uniformity of the temperature control given the likely conductance effects of continuous copper coils. A high capacity thermoregulator (Huber Unistat 360) has been fitted for the purpose of testing the full capabilities of this mini photolysis chamber and to control the chamber temperature in the near future. Insulating the walls of the chamber with 20 mm thick neoprene would be beneficial in reducing heat losses and is recommended should temperature dependent studies be carried out, as this has already been used for HIRAC successfully.

The temperature in this mini photolysis chamber is read using three K-type thermocouples, configured to a JENCO-765 temperature readout box, which are arranged along the chamber walls and inlets to monitor temperature homogeneity. A program written by Stephanie Orr using National Instruments LabVIEW v.10.0.02 software is used to log temperature, pressure, O_3 and NO_x data in this chamber. A computer fan is attached to one of the brass ends achieving homogenous mixing in <60 s. A cross-sectional diagram of the mini photolysis chamber and its equipment can be seen in Figure 3.2.

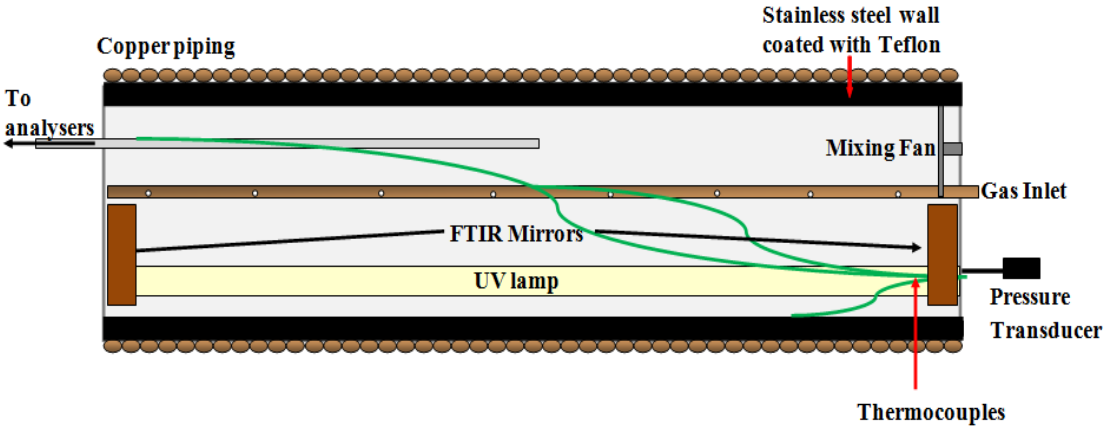

Figure 3.2: Cross-section of the mini photolysis chamber (Orr, 2012).

VOCs are first introduced in a glass vacuum line using an Edwards 1000 Torr pressure transducer which measures the concentration of the organics, and later flushed into the chamber through a length of copper tube (volume = 4.3 cm^3)filled at the same pressure as the vacuum line. Gases are introduced into the mini photolysis chamber through a long stainless steel tube with several apertures to release gas at different points in the chamber, thus aiding in mixing. A circulating fan was recently attached to one of the end flanges on the pump end in order to better circulate the gases in the chamber. Homogeneity of VOCs introduced into the chamber can be achieved within a few seconds, and this has been shown from initial calibrations and tests that have been carried out using GC-FID.

3.2.2 Instrumentation

The mini photolysis chamber is comparable both in size and function to the EXTRA (EXTreme RAnge) chamber based at the University of Manchester (Leather et al., 2010). A comparison of the two chambers is shown in Table 3.1. Previous studies in this chamber have included higher alkene ozonolysis kinetics and temperature dependent investigations (McGillen et al., 2011b). Similar ozonolysis experiments have been characterised in our mini photolysis chamber using both the GC-FID to measure the kinetics from organic decays and an O_3 box to measure the kinetics from O_3 decays.

	EXTRA chamber	**Mini Photolysis chamber**
Material	Teflon-coated stainless steel	Teflon-coated stainless steel
Volume / L	123	35
S/V / cm-1	0.12	0.21
Pressure range / bar	0.01 – 5	0.0003 – 1.3
Temperature range / K	180 – 395	~240 – 320 K*
Presently operating Instrumentation	GC-ECD/FID, GC-MS, CIMS, O_3 analyser, CO_2 sensor, CO analyser	GC-FID, O_3 and NO_x analysers

Table 3.1: Comparison of the Mini photolysis chamber with the EXTRA chamber (Leather et al., 2010). (*projected performance).

The mini photolysis chamber is also equipped with two gold-plated FTIR mirrors in a White cell arrangement that can be used for FTIR spectroscopic

analysis(White, 1942). This White cell arrangement is a similar system to the Chernin cell used for FTIR detection in HIRAC and greatly enhances the path length of the system (~140 m). Constructed from three concave mirrors, the White cell is a multipass optical arrangement that uses a field mirror on one end and two objective mirrors on the other end of the chamber opposite to the entrance aperture allowing FTIR spectroscopic probing of reactions taking place in the mini photolysis chamber with a multipass enhanced detection of infra-red (IR) active species. Detection limits for such systems are in the sub-ppmv levels for the majority of VOCs analysed from knowledge of previous experiments performed in HIRAC, which would be ideal for kinetics and mechanistic studies in the mini photolysis chamber. This would be favourable for using the chamber for measuring temperature and pressure dependent kinetics in the future, in particular if the compounds being studied are difficult to study in HIRAC and need to be tested on a smaller scale prior to being introduced into HIRAC. Unfortunately a recoating of the mirrors is necessary given their poor state at present, however once recoated this system could potentially be aligned and characterised in the mini photolysis chamber.

The mini photolysis chamber has also been connected to the HIRAC GC-FID instrument through ~1.5 m Teflon tubing and a series of solenoid valves which control the sampling from the chamber in a similar system as has been described for HIRAC in chapter 2. Another strong motive for pursuing to refurbish this chamber was the time GC-FID calibrations took to be performed in HIRAC. Calibrations for compounds studied using the GC-FID instrument are performed prior to every different set of experiments in order to quantify the concentrations being sampled from HIRAC. Carrying this out in the HIRAC chamber takes ~3 – 4 hours, particularly owing to the time it takes to fill and evacuate a ~2.25 m^3 chamber. Calibrations are performed by repeatedly diluting the chamber volume with the compounds for analysis. Each successive dilution would result in a different concentration of these compounds, and is expected to correspond to a linear decrease in GC-FID peak heights and areas. Calibration plots are obtained from the linear relationship between peak areas or heights and known concentration of samples introduced into the chamber. Calibrations in this mini photolysis chamber (Figure 3.3) can be carried out quicker ~1 hour and are performed using up smaller quantities of gases.

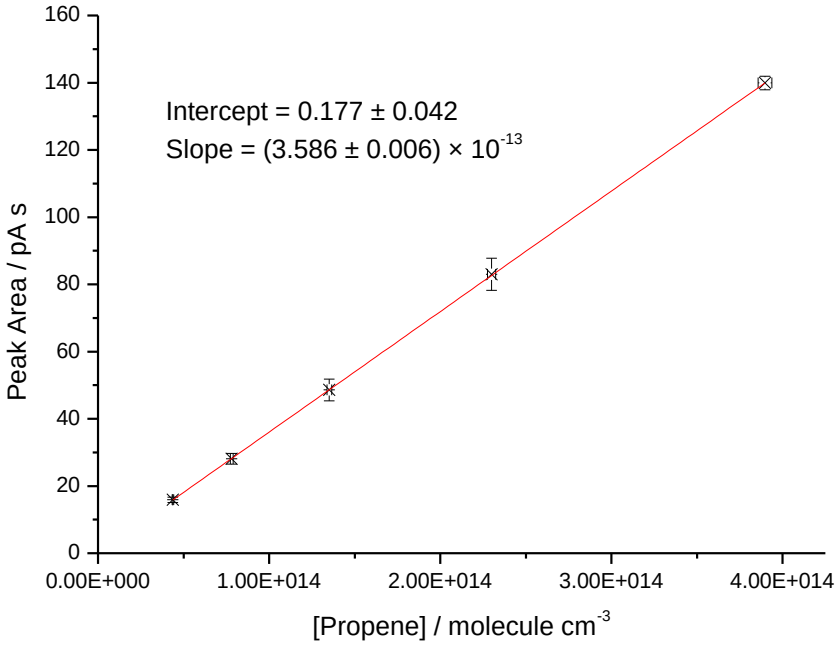

Figure 3.3: Example of GC-FID calibration plot for propene in the mini photolysis chamber at 290 ± 3 K and 1000 mbar (error bars represent 1σ).

3.2.3 Photolysis lamps

Another advantage of the mini photolysis chamber is the possession of two ports allowing direct insertion of lamps spanning the entire length of the chamber. In contrast to the HIRAC chamber, no casings are present to hold these lamps in place and as a result the process of changing lamps is much less laborious than in HIRAC which holds the lamps in quartz tubes flushed with a nitrogen gas purge to avoid overheating or formation of condensation in the tubes. There were some concerns about localised heating effects of the lamps within the mini photolysis chamber. However in contrast with HIRAC which is a much larger vessel and where reactions take place for longer timescales (1 – 1.5 hours), the aim of the mini chamber was to carry out shorter timescale experiments (10 – 20 minutes), within which time the temperature reached for the lamps was not expected to be too high to cause any major localised effects.

Therefore both photolysis experiments and generation of free radicals could be performed at specific wavelengths, and the lamps present could be easily changed accordingly. If non-photolytic experiments are being carried out, these ports could be

easily blanked off by insertion of stainless steel sealing plates. A set of Philips TLK40 W/05 actinic UV black lamps and Philips TUV 75W/HO T8 UV C lamps are currently available for this chamber. The latter set of lamps photolyse at 254 nm and have been recently installed in order to assess the generation of OH radicals in this chamber in a NO_x - free environment by photolysis of acetone at low pressures. This would be further evaluated in the HIRAC chamber to test for a suitable low NO_x source of OH radicals for isoprene oxidation studies, which will be described further in chapter 7.

3.2.4 Mixing fans

Tests were also carried out to assess the sampling and circulation within the mini photolysis chamber. Despite its small size compared to HIRAC, it is evident from plots of propene decay experiments (Figure 3.4) how a fan does improve the mixing and this is clear from the comparison of the scatter of GC-FID measurements of propene obtained in the chamber for with and without fan. There are some dilution effects evident over the course of 20 minutes, which are likely to be a combination of the dilution of the chamber during sampling as well as some losses to the chamber walls. It must be noted also that these characterisations were performed in order to address any improvements to the mini photolysis chamber and some modifications were carried out to minimise the problems with dilution and wall losses.

The presence of a fan has also improved the mixing time (time required for all compounds introduced in the chamber to be stable on the GC-FID) from 5 minutes to less than 60 seconds, which is ideal for sufficiently quick experiments with lifetimes shorter than a few minutes. Moreover, O3 wall losses have also been characterised as well as the effects the heterogeneous chemistry occurring on the walls have been investigated by Stephanie Orr in the mini photolysis chamber.

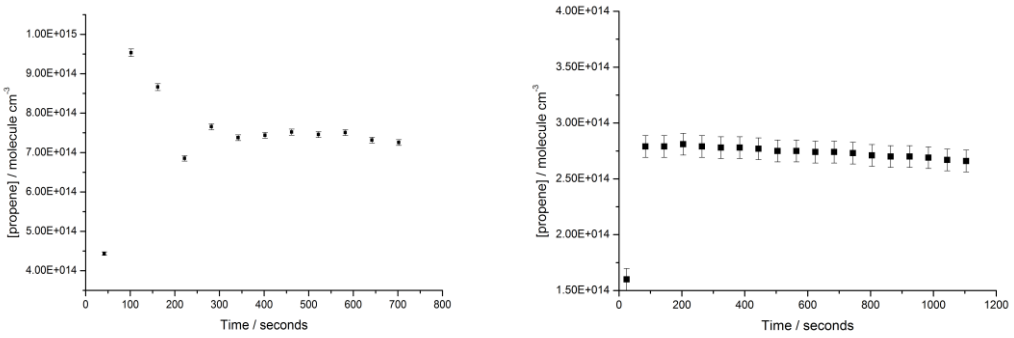

Figure 3.4: Plots of peak area vs. time for a dark propene dilution monitored using a GC-FID before mixing fan installed (left) and after mixing fan installed (right) (Orr, 2012).

3.2.5 Ozone analyser

Alkene ozonolysis experiments to be discussed in the following section have been carried out using GC-FID to probe the [alkene] and using an ozone analyser to probe [O_3], with the former to be presented in this section. Several problems were encountered regarding sampling when testing the ozone analyser in the mini photolysis chamber, particularly given the small size of the chamber and the high sample rate of the O_3 analyser (1.5 L minutes^{-1}). A counter flow of N_2 into the chamber was tested but this led to problems with dilution, with the chamber volume essentially being completely diluted within the first 25 minutes of sampling. This has not been a problem previously faced in HIRAC given its larger volume. The installation of a Bruker mass flow controller directing 1.2 L minutes^{-1} of N_2 into the O_3 analyser has minimised reactant dilutions significantly and allowed longer timescales to be studied for kinetic experiments in the mini photolysis chamber.

3.3 Mini photolysis chamber characterisation

3.3.1 Alkene Ozonolysis

Alkene ozonolysis reactions were studied to better characterise the mini photolysis chamber system and ensure the setup was suitable for similar investigations using amines. Ozonolysis of alkenes in the atmosphere was not introduced in Chapter 1 and for this reason a brief introduction on the chemistry of these reactions is important first. These reactions provide a direct oxidation pathway for unsaturated VOCs that compete with OH and NO_3 radical-initiated processes and lead to the production of important reactive intermediates, in particular HO_x radicals (Paulson and Orlando, 1996, Malkin et al., 2009). O_3 cleaves the double bond of alkenes, forming various different products, including OH in the case of some species. The kinetics of the ozonolysis of alkenes has been well reviewed in the literature (Atkinson, 1997, Paulson and Orlando, 1996, Atkinson et al., 2006a, Johnson and Marston, 2008). The mechanism for the ozonolysis of alkenes was first suggested by Criegee (Criegee, 1975) and is shown in Figure 3.5:

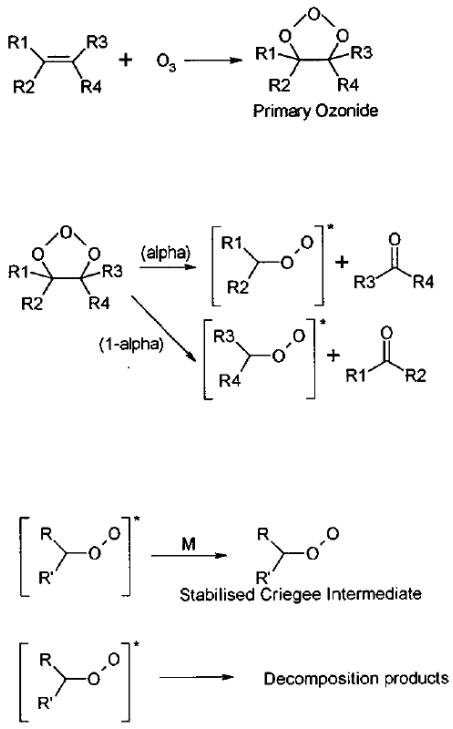

Figure 3.5: General mechanism for the reactions of O_3 with alkenes (Marston, 1999).

Alkene ozonolysis is of importance in the troposphere as it contributes directly to the oxidation of organic compounds. The Criegee intermediates may also react with other species such as water and SO_2. HO_x radicals are generated directly in this process, with this being a significant source of HO_x in polluted urban air during the early hours of the day (Johnson and Marston, 2008).

Ethene and propene ozonolysis relative rate experiments were performed in HIRAC using ethane as a reference compound. Both reactions have been well reviewed in the literature (Atkinson et al., 2006a) and are a suitable test for a straight forward kinetics experiment in this chamber. These experiments made use of GC detection to measure relative rate decays of the organics introduced into the mini photolysis chamber. Some ozonolysis kinetic experiments have also been performed by Stephanie Orr using absolute measurement of O_3 decays using a commercial O_3 analyser. The purpose of these characterisations were to confirm the chamber's suitability as a test-bed for quick relatively straight forward kinetic experiments as well as a test for complicated low vapour pressure compounds such as amines that have a tendency to stick to chamber walls, prior to them being performed in HIRAC.

3.3.2 Experimental method

The mini photolysis chamber was filled first with nitrogen gas (BOC Oxygen Free Nitrogen, OFN) up to 900 mbar and about 5 ppmv of O_3 was added using a flow of O_2 into a Fischer OZ 500MM O_3 generator. The introduction of this flow of oxygen and ozone would raise the pressure in the chamber up to ~940 mbar. Samples of purified analytical grade reagent were prepared in a 4.3 cm^3 copper tube and flushed into the chamber with a stream of OFN nitrogen gas to give alkene mixing ratios of 1 - 2 ppmv at the desired total chamber pressure of 1000 mbar. The HIRAC Agilent 6890N GC-FID (J&W DB-1 column, 50 m, 0.53 mm, 5.00μm at 305 K) was set to sample before introduction of alkenes. Starting concentrations could not be obtained on the GC-FID since the reaction starts as soon as the alkenes were introduced into the chamber, however this would not have any effect on the relative rate method. Experiments were all performed at room temperature and pressure.

The relative rate method, to be described in further detail in Chapter 4, relies on one important assumption that the reactant and reference are reacting only with one reactive species. Other important assumptions include no reformation of the compounds being investigated, or any intermediates reacting with the compounds (e.g.: Criegee intermediates during this alkene ozonolysis process). Based on these assumptions, it follows that:

Ethene (organic) + O_3 → products (R3.1)
propene (reference) + O_3 → products (R3.2)

$$\ln\left(\frac{[\text{reactant}]_0}{[\text{reactant}]_t}\right)=\left(\frac{k}{k_{ref}}\right)\ln\left(\frac{[\text{reference}]_0}{[\text{reference}]_t}\right) \quad \text{(Eq 3.1)}$$

A linear regression tool (Regres2) developed by Theo Brauers from Jülich Forschungszentrum was used in order to obtain the ratio: k_1/k_2. This regression analysis uses a linear least-squares regression, which takes into account random errors in [organic] and [reference], eliminating any systematic errors that may occur (Brauers and Finlayson-Pitts, 1997). The relative rate coefficient is obtained from the relative rate ratio of the organic and reference, and multiplied by the reference rate coefficient, which needs to be well documented and reviewed in the literature.

3.3.3 Results

Two experimental rate coefficients were obtained for the ozonolysis of propene in the mini photolysis chamber. A relative rate coefficient of (9.24 ± 0.58) × 10^{-18} molecule cm^{-3} s^{-1} was obtained for using GC-FID measurements of propene and ethene using the relative rate method and a reference rate coefficient of 1.6 × 10^{-18} molecule cm^{-3} s^{-1} for the reaction of ethene with O_3 (Atkinson et al., 2006a). The results were not corrected for dilution using GC-FID as this results in a dilution of less than 1%. In the case of the O_3 analyser, the sampling rate was kept to a minimum by flushing nitrogen into the analyser to minimise the amount of gas sampled from the chamber, but given the short timescales, this relative dilution over such a small period of time was not deemed significant (5%). Results were also obtained by measuring ozone decays using an ozone analyser and a rate coefficient of (8.59 ± 0.35) × 10^{-18} molecule cm^{-3} s^{-1} was obtained for the same propene ozonolysis

experiment in the mini photolysis chamber. The only difference with these experiments is that the rate coefficient was obtained from the pseudo first order rate of O_3 decay, as is described in Section 3.5.2. The results obtained using the O_3 decays are within error of the IUPAC recommendation of $(8.69 \pm 0.68) \times 10^{-18}$ molecule cm^{-3} s^{-1} (Atkinson et al., 2006a) and within error of the relative rate coefficient obtained.

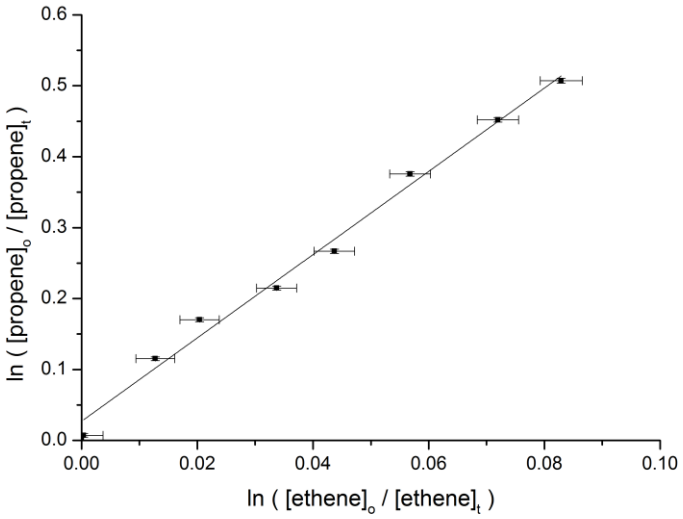

Figure 3.6: A relative rate plot of the reaction of propene with ozone using ethene as a reference compound at 292 ± 3 K and 1 bar.

	***k*propene+O_3 / 10^{-18} molecule cm^{-3} s^{-1}**	**Technique**
Mini photolysis chamber	8.59 ± 0.35	O_3 analyser (pseudo 1st order)
	9.24 ± 0.58	GC-FID (relative rate)
Literature (IUPAC)	8.69 ± 0.68	(Atkinson et al., 2006a)

Table 3.2: Relative and absolute rate coefficients obtained for the ozonolysis of propene in the mini photolysis chamber at 290 ±3 K and 1000 mbar of OFN nitrogen.

This work demonstrates the suitability of the mini photolysis chamber to carry out relative rate experiments for ideally suited compounds (may not stand as enough evidence for low volatility compounds or more complex systems) and be able to carry out kinetics experiments much quicker than HIRAC. Moreover the ability to also calibrate for the compounds being studied in less than half the times as HIRAC provides an efficient tool for future experiments.

3.4 Acetone Photolysis

3.4.1 Introduction

Photolysis is a significant removal process and an important source of HO_x radicals in the upper troposphere(Seakins and Blitz, 2011). Acetone (CH_3COCH_3) is present in relatively large amounts in the atmosphere (0.4 – 1.3 ppb), probably being the most abundant oxygenated hydrocarbon (Singh et al., 1994) along with formaldehyde, acetaldehyde and methanol. Acetone originates from both natural (vegetation) and anthropogenic (biomass burning) emissions, as well as from the oxidation processes of non-methane hydrocarbons (Gierczak et al., 1998).

The two loss processes of acetone in the atmosphere are photodissociation (R3.3 and 3.6) and its reaction with OH (R3.7).

$$CH_3COCH_3 + h\upsilon\ (\leq 299\ nm) \rightarrow CH_3CO + CH_3 \quad (R3.3)$$
$$CH_3COCH_3 + h\upsilon\ (\geq 338\ nm) \rightarrow CH_3 + CH_3 + CO \quad (R3.4)$$
$$CH_3CO\cdot \rightarrow CH_3 + CO \quad (R3.5)$$
$$CH_3 + CH_3 + M \rightarrow CH_3CH_3 + M \quad (R3.6)$$
$$CH_3COCH_3 + OH + O_2 \rightarrow CH_3COCH_2O_2 + H_2O \quad (R3.7)$$
$$CH_3COO_2 + NO_2 + M \rightarrow CH_3C(O)O_2NO_2 + M \quad (R3.8)$$

Acetone photolysis also enhances the formation of PANs as is shown in R3.8. PAN formation in the upper troposphere through is generally dictated by this slow photolysis process, resulting in a typical lifetime of several months (Brühl, 2000).

Reaction 3.7 has been shown to be temperature dependent (Wollenhaupt et al., 2000), and proceeds *via* hydrogen abstraction at higher temperatures producing an acetonyl radical (Vasvari et al., 2001) as is shown in R3.9. A minor channel (R3.10) results in methyl elimination, and this used to be thought to be dominant below room temperature.

$$CH_3COCH_3 + OH \rightarrow CH_2COCH_3 + H_2O \quad (R3.9)$$
$$CH_3COCH_3 + OH \rightarrow CH_3 + CH_3COOH \quad (R3.10)$$

Wollenhaupt and Crowley provided evidence for an addition-elimination mechanism occurring from measuring CH_3 yields for this reaction, and more recent studies have confirmed this second product channel is also possible and results in the

production of acetic acid (Turpin et al., 2003, Tyndall et al., 2002, Vandenberk et al., 2002). This occurred *via* addition of OH to carbonyl carbon and subsequent elimination of the CH_3 from excited addition complex $(CH_3COH(O)CH_3)^*$. The photodissociation process leads to either the initial formation of methyl peroxy radicals, or another minor channel leading to two methyl radicals and carbon monoxide. The latter process is however orders of magnitude slower at wavelengths relevant to the lower atmosphere (Blitz et al., 2004). Net production of HO_x radicals for this process is up to 3.2 HO_x molecules from the collisional stabilisation of the peroxy radical by other species present in the atmosphere, or by internal abstraction of a hydrogen.

The purpose of carrying out acetone photolysis experiments was to test the mini photolysis chamber's potential to carry out photolysis experiments, and to investigate the use of this photolysis method as a source of OH radicals in chamber studies. This chapter will describe the pressure dependent study carried out in HIRAC and some initial photolysis rates for acetone in the mini photolysis chamber. Chapter 7 will go into further detail on the results obtained for testing this method as a source of OH under low NO_x.

3.4.2 Experimental method

The lamps used for these photolysis experiments were two 254 nm Philips 75W/HO TUV T8 UV C lamps. Figure 3.7 shows the output of the lamps being 100% at the desired wavelength for these experiments, based on the absorption cross section of acetone shown in Figure 3.8.

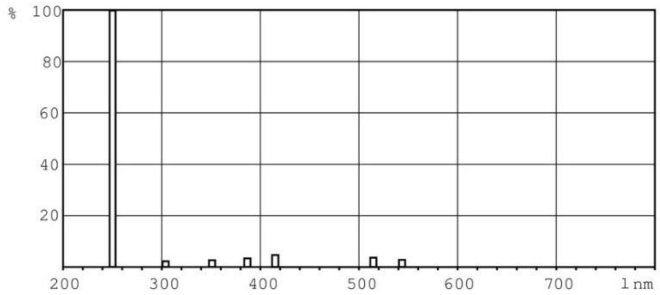

Figure 3.7: Output of 254 nm Philips 75W/HO TUV T8 UV C lamps.

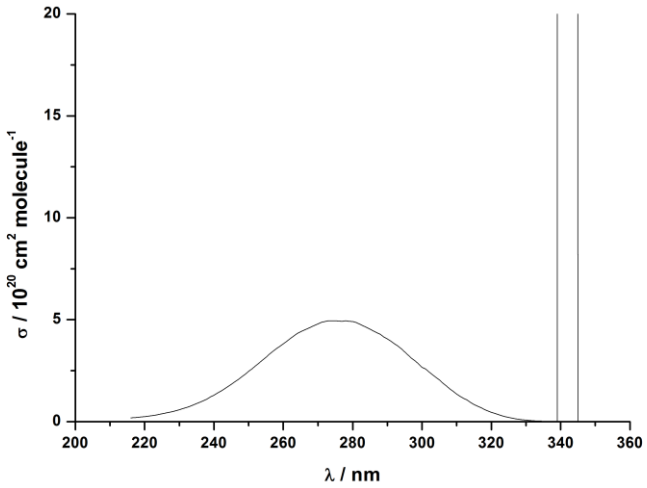

Figure 3.8: IUPAC reference absorption cross section of acetone. Vertical lines around 340 nm show σ outside the scale of this graph. Region of interest to the troposphere and this work is the region at ≤ 320 nm.

All these experiments were carried out in OFN nitrogen (BOC Oxygen Free Nitrogen). The presence of oxygen would result in the generation of OH which would compete with the photodissociation measurements. Initial difficulties were encountered for low pressure investigations due to a slight observed chamber leak that was causing air to enter into the chamber and resulting in fast acetone decays. This turned out to be a cracked quartz window (view port) that was replaced to make the chamber leak tight.

Several purification freeze-pump-thaw cycles were carried out for acetone (Sigma Aldrich, 99.5%) prior to it being introduced in the mini photolysis chamber to remove any likely contaminants that could affect the results obtained. Acetone decays and ethane production was monitored by the GC-FID instrument (J&W DB-1 column, 50 m, 0.53 mm, 5.00μm at 305 K) for the photodissociation of acetone in the chamber. A typical chromatogram of the experiments carried out is shown in Figure 3.9 with acetone and ethane peaks labelled. An unknown third peak could not be identified but is likely to be a photolysis product of the impurities present in the acetone used, given the high concentrations of acetone used for this experiment.

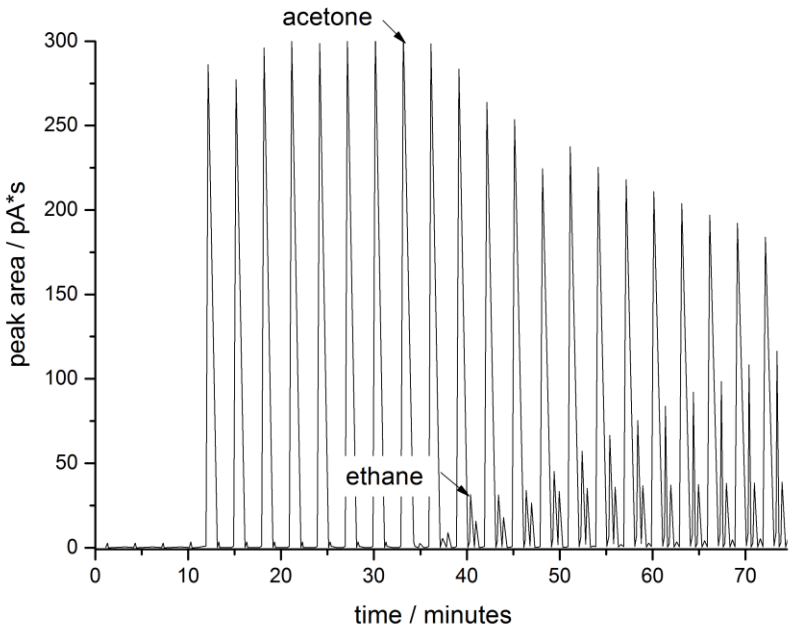

Figure 3.9: Typical chromatogram of acetone photodissociation experiments carried out in the mini photolysis chamber in OFN nitrogen at 270 mbar and 290 ± 3 K.

A recently set up LabView 10.1 software was used to read the thermocouples in the chamber. All experiments were carried out at 290 ± 3 K. Typical concentrations used were ~60 – 120 ppmv of acetone. Calibration of the GC-FID instrument was necessary prior to experiments in order to confirm validity of sampling and test the solenoids and LabView v10.1 software was used to automate the sampling process for the mini photolysis chamber.

The calibrations were carried out by repeat dilutions of a known amount of acetone and ethane introduced into the chamber, and measuring the peak areas and peak heights which should scale linearly with concentration. The measured amounts of organics were flushed into the mini photolysis chamber *via* a stream of nitrogen gas through a 4.33×10^{-3} L copper delivery vessel.

The quoted uncertainties in these measurements were estimated from the standard deviation of the GC-FID peak areas obtained from repeat measurements of the organics at the start of the experiment before photolysis is initiated. A typical quoted uncertainty of 0.2% for the pressure gauge readings (σ_p) was factored in, along with statistical uncertainties from the equipment. Temperature readings were assigned an uncertainty (σ_T) from the thermocouple manufacturer quoted uncertainty of ±3 K.

More accurate temperature readings of ±1 K are available and would therefore be advantageous to invest in such instruments for improving the precision for the mini photolysis chamber to read temperatures with lower uncertainty.

$$\sigma_{[\text{Species}]} = \sqrt{\left(n\sqrt{\frac{{\sigma_T}^2}{T} + \frac{{\sigma_p}^2}{p}}\right)^2 \times \left(\frac{N_A}{V_{\text{chamber}}(\text{cm}^3)}\right)^2} \qquad \text{(Eq 3.2)}$$

3.4.3 Preliminary results

The results obtained in this section are preliminary given the poor characterisation of the mini photolysis chamber at the time these experiments were carried out. Nevertheless these results provide evidence of potential application of this chamber and to further studies on this photodissociation process which is one of the most abundant oxygenated VOCs in the atmosphere and a known source of OH in the upper troposphere.

The results to be reported are compared to a FACSIMILE model set up using MCM chemical inputs for the known chemistry of acetone and its photodissociation (See Appendix B). The photodissociation rates of acetone have been determined over a pressure range of ~150 – 1040 mbar. The results obtained are tabulated in Table 2.2.

Pressure / ±2 mbar	$[CH_3COCH_3]$ / 10^{15} molecule cm^{-3}	$J(CH_3COCH_3)$/ 10^{-4} s^{-1}	FACSIMILE model $J(CH_3COCH_3)$ / 10^{-4} s^{-1}
1040	2.59	2.82 ± 0.03	3.14
775	3.49	2.82 ± 0.04	3.43
585	4.14	2.11 ± 0.10	3.52
425	3.47	2.27 ± 0.08	3.36
320	3.43	2.42 ± 0.10	3.45
150	3.51	2.31 ± 0.04	3.22

Table 3.3: Acetone ((2.59 – 4.14) x 10^{15} molecule cm^{-3}) photolysis experiments carried out over a range of pressures (150 – 1040 mbar) in the mini photolysis chamber using the GC-FID at 290 ± 3 K.

The results obtained vary by 10 – 15% for the majority of experiments. This is possibly due to a number of unassessed properties of the mini photolysis chamber, including the variation of the lamp output. A spectral radiometer has been made available for the purpose of assessing this; unfortunately due to time constraints it was not possible to carry this out to finalise these investigations. The results nevertheless demonstrate that the photodissociation of acetone does occur independent of pressure. Higher pressures are expected to favour the stabilisation of the acetylperoxy ($CH_3CO(O_2)$) radical while lower pressures leads to the formation of OH radicals, from this same radical's dissociation, which would mean the OH yield of this system might be pressure dependent. This will be further discussed in chapter 7.

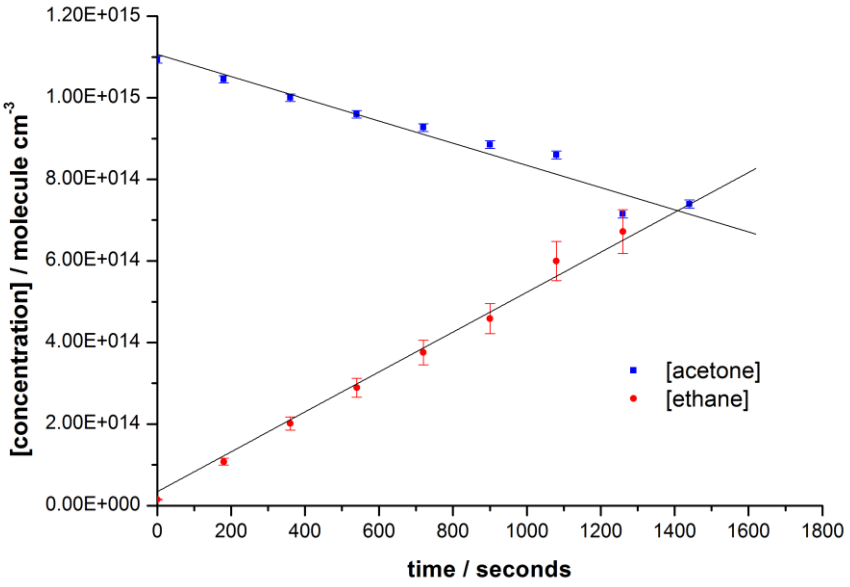

Figure 3.10: Measured acetone decay and ethane production in the photodissociation of acetone at 320 mbar at 290 ± 3 K in the mini photolysis chamber using GC-FID. Data taken from a single experiment (Errors quoted to 1σ).

The pressure dependence of the photodissociation of acetone (due to cross section) could also be assessed using the measured product yields of ethane (Figure 3.10). This however could not be investigated further in this study given the ethane produced in several of the runs was overestimated by the GC-FID. These photodissociation rates from the loss of acetone are evidence enough of the pressure independence of this process. Further studies could be carried out on the temperature dependence of acetone cross section in the presence and absence of oxygen, which

could not be carried out in the mini photolysis chamber due to the absence of a working temperature control system, but would be an interesting investigation based on reports by Wollenhaupt and Crowley that reported a possible temperature dependence of this photolysis process due to the temperature dependence in the absorption cross section (Wollenhaupt et al., 2000).

3.5: Temperature control system in HIRAC

3.5.1 Instrumentation

The final portion of this chapter will discuss the recent installation of a temperature control system in HIRAC which will enable studies at temperatures between ~220 – 330 K (covering the full temperature range of the troposphere). During the construction of HIRAC several steel tubes were welded into its outer skin to allow a cooling/heating thermofluid to flow through them. An inlet manifold and Huber thermostat unit Model 690W were installed in 2010. This thermostat is designed to circulate thermal fluid (DW-Therm) along the steel tubes welded to the chamber walls. The flow can be controlled using an inlet manifold (Figure 3.11), which has a series of taps used to isolate particular sections of the steel tubes flowing around the thermal fluid around HIRAC.

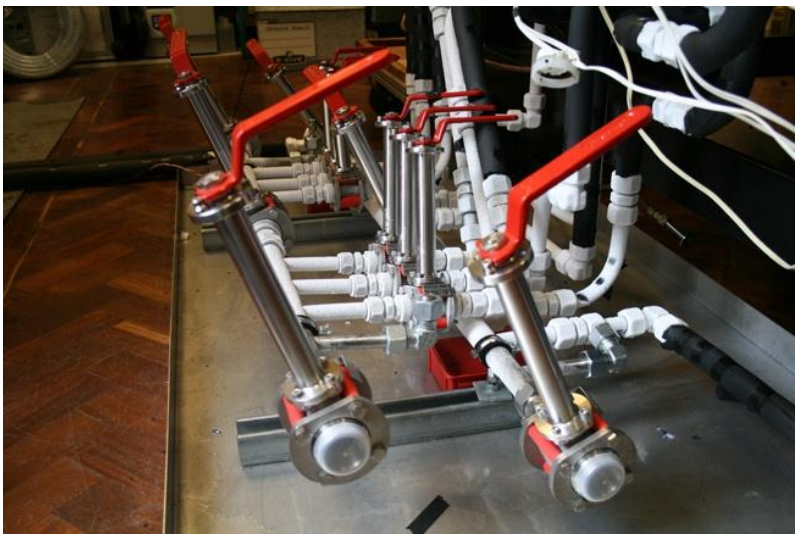

Figure 3.11: The thermofluid inlet manifold in HIRAC and the various taps used to control the flow of liquid through the temperature control system.

Allowing the thermal fluid to only circulate round selected sections of the chamber can slow the heating/cooling of the chamber which would be useful for ramping temperatures, but could lead to uneven temperature gradients. These temperature gradients were carried out by Fred Winiberg (School of Chemistry, University of Leeds).

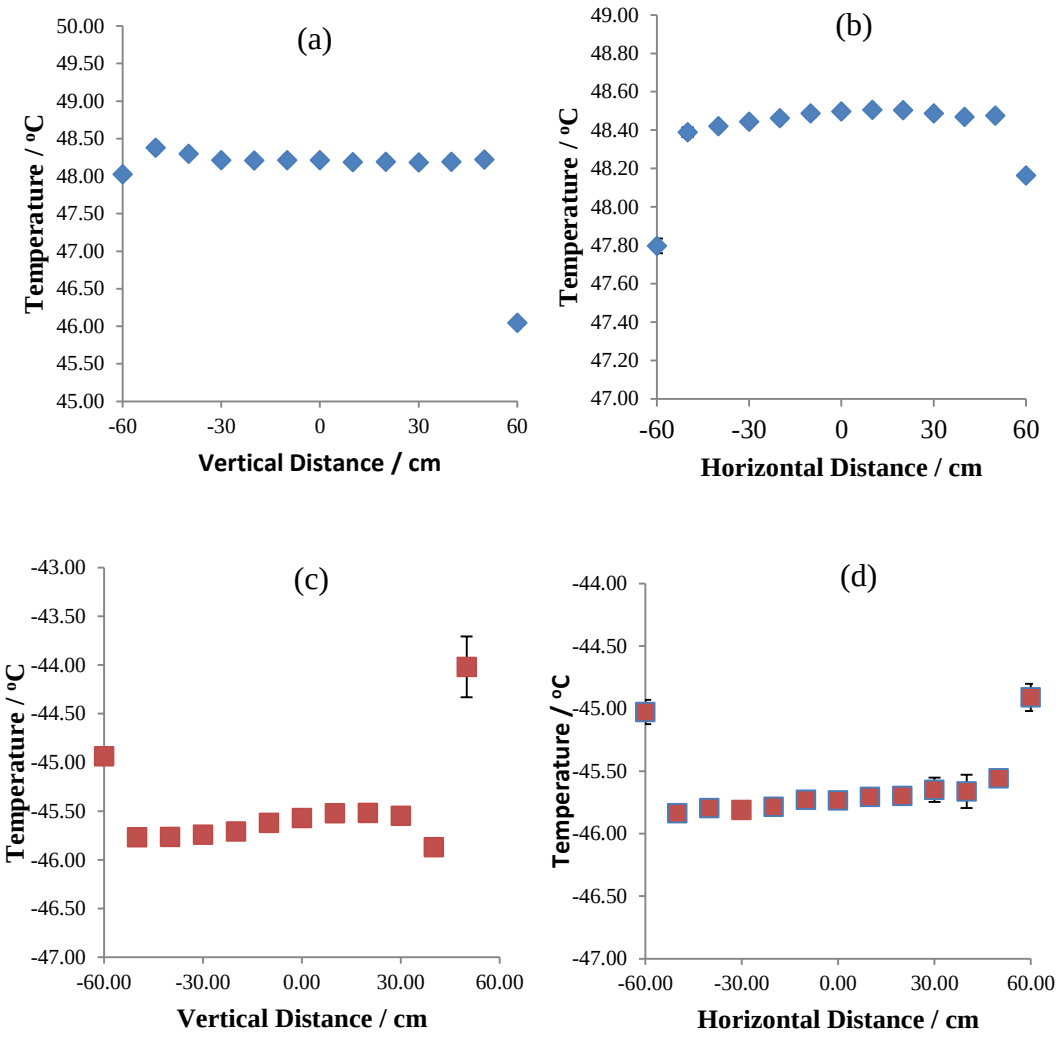

Figure 3.12: Temperature gradients measured at 321 ± 3 K (a + b) and 227 ± 3 K (c + d) at 1000 mbar across the length of HIRAC.

The temperature gradients measured across the length of the chamber have been shown to be uniform through most of the chamber, apart from the edges which did not have neoprene insulating the flanges (Figure 3.12). This was expected given the influence of the conducting steel walls with the outer laboratory environment, and insulation of the chamber was carried out prior to any future temperature dependent

studies being carried out in HIRAC. The next sets of temperature dependent studies are reported in chapter 5.

3.5.2 Characterisation

A validation of the HIRAC temperature control system was carried by studying the temperature dependent kinetics of the reaction of O_3 with propene, which is a well-documented reaction in the literature (Jia et al., 2006). This served as a useful test for the assessment of the suitability of HIRAC's temperature control system for being able to reproduce temperature dependent kinetic parameters accurately. This work was carried out with Stephanie Orr. Temperature dependence of rate of reactions in chemistry is described by the empirical Arrhenius expression (Eq. 3.3):

$$k = A\, e^{-Ea/RT} \qquad \text{(Eq. 3.3)}$$

where k is the rate coefficient, E_a is the activation energy, A is the Arrhenius parameter, T is temperature and R is the universal gas constant.

A temperature-dependent study under pseudo-first order kinetics with excess propene (2.5 – 34.7 ppmv) over O_3 (0.3 ppmv) was performed using a commercial O_3 analyser measuring O_3 decays at ~233 – 323 K and 1000 mbar. The temperature readings were made using K-type thermocouples and their precision was taken during the length of the experiment (± 3 K). An uncertainty in the thermocouples of 0.2% ± 5 K was also reported by manufacturer and factored into uncertainty of the temperature readings.

These pseudo first order experiments were based on the assumption that the propene concentration remains unchanged due to the large excess, and therefore the rate of reaction is dependent only on the decay of ozone in the reaction (Eq. 3.5):

$$\text{rate} = k_{O3+propene}\,[O_3]\,[\text{propene}] \qquad \text{(Eq. 3.4)}$$

$$k' = k\,[O_3] \qquad \text{(Eq. 3.5)}$$

A trace of the ozone decay with time is obtained from the reaction and a pseudo first order rate coefficient (k') can be calculated from Eq 3.6:

$$\ln([O_3]_t) = -k't + \ln([O_3]_o) \qquad \text{(Eq. 3.6)}$$

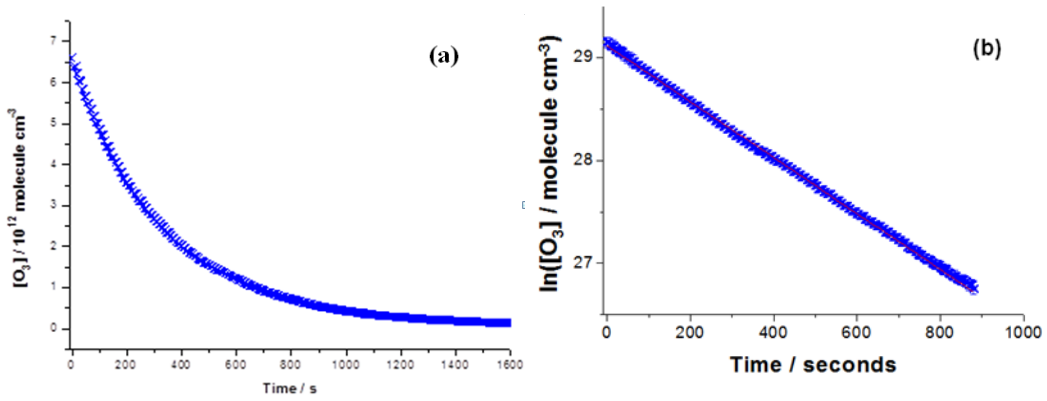

Figure 3.13: (a) Measured $[O_3]$ trace from the reaction with propene in excess (2.2×10^{14} molecule cm^{-3}) at 294 ± 3 K and 1000 mbar in HIRAC (b) Pseudo first order decay of O_3 for same reaction.

As is shown in Figure 3.13(b), the pseudo first order rate coefficient (k') obtained from the gradient of the ln $[O_3]$ as a function of time can be carried out over different [propene]. A bimolecular rate coefficient (k_{bim}) can be obtained for these reactions from the relationship of k' with [propene] at different temperatures, as is shown in Figure 3.14.

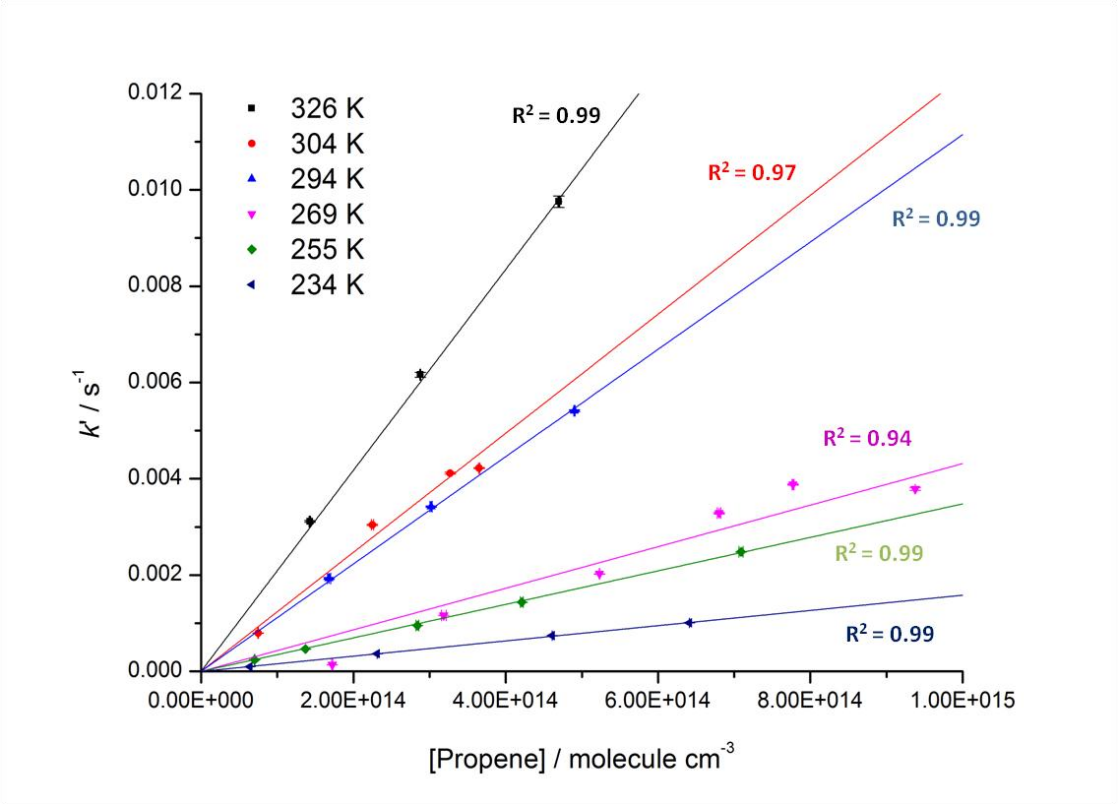

Figure 3.14: Bimolecular rate plots for the reaction of O_3 with propene (~1 $\times 10^{14}$ – 10^{15} molecule cm^{-3}) at 326, 304, 294, 269, 255 and 234 K and 1000 mbar in HIRAC.

Bimolecular rate constants at six different temperatures (326, 304, 294, 269, 255 and 234 K) between 234 – 326 K are shown in Table 3.3. The bimolecular plots obtained indicate that the HIRAC temperature control system is capable of generating accurate rate coefficients at a wide range of temperatures.

Figure 3.14 shows excellent bimolecular plots were obtained at all temperatures in HIRAC, with the exception of 269 K, for which the experimental uncertainty was almost 6%, higher than the experimental data for other experiments (1 – 2%). This may be attributed to a possible outlier evident for the experiment carried out using 2×10^{14} molecule cm^{-3} propene at this temperature.

Temperature / K	k_{bim} / molecule^{-1} cm^3 s^{-1}
326	(2.07 ± 0.04) x 10^{-17}
304	(1.25 ± 0.08) x 10^{-17}
294	(1.08 ± 0.02) x 10^{-17}
269	(6.49 ± 0.38) x 10^{-18}
255	(3.42 ± 0.05) x 10^{-18}
234	(1.61 ± 0.02) x 10^{-18}

Table 3.4: Experimentally determined bimolecular rate coefficient (k_{bim}) for the gas phase reaction of O_3 with propene at temperature range of 234 – 326 K and 1000 mbar in HIRAC.

This was the first time this system was tested, and the results obtained from these experiments have confirmed the suitability of this system to be used for generating rate coefficients at varying temperatures for different systems in HIRAC. O_3 decays due to reaction with propene were repeated 2 – 3 times each at six different temperatures, between 233 – 326 K, for [propene] of ~2.5 – 34.7 ppmv.

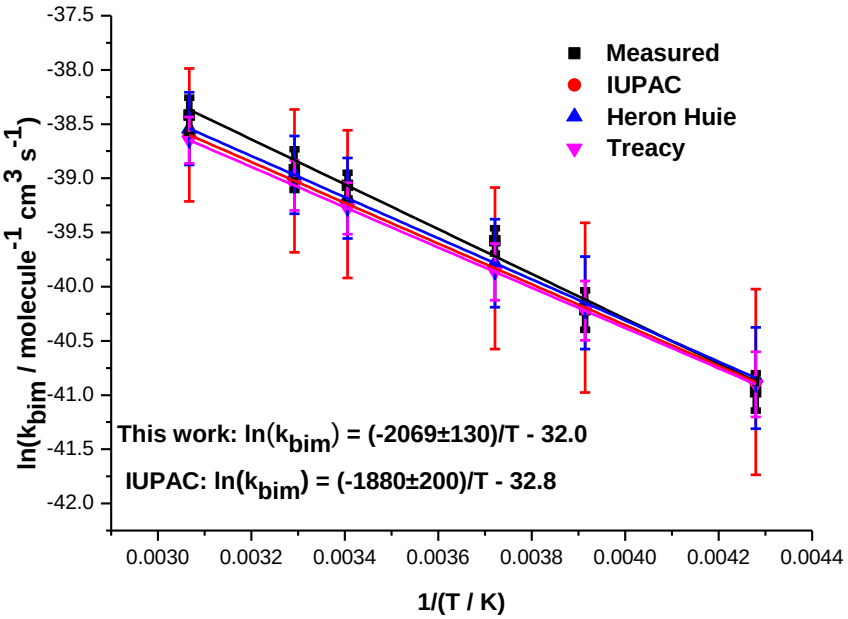

Figure 3.15: Arrhenius plot for propene at 1000 mbar and over a temperature range of 233 - 323 K.

An Arrhenius plot of the bimolecular rate constant for propene was obtained by plotting the natural log of the bimolecular rate constants against 1/Temperature (Figure 3.14). This gave an E_a = 17.69 ± 0.29 kJ mol^{-1}. Experimental uncertainties for the activation energy were reported from the weighted fit of the Arrhenius plot shown in Figure 3.15, and an estimated systematic uncertainty of 10% was added to this statistical error. These results are within error of IUPAC recommended values of E_a = 15.6 kJ mol^{-1} (Atkinson et al., 2006a). This temperature-dependent study demonstrates the suitability of HIRAC for further temperature-dependent studies.

3.5 Conclusions

This chapter has highlighted several new improvements that will enhance the potential to study different systems in the HIRAC laboratory. The availability of a mini photolysis chamber offers the advantage of carrying out initial testing of conditions for experiments prior to performing them in HIRAC. The smaller timescales possible in this chamber when compared to HIRAC may not render it beneficial for mechanistic studies; however this chamber does provide the advantage of carrying out instrument calibration (GC-FID in particular given the very small sample rate), photolysis and kinetic experiments. The photolysis lamps were tested using initial acetone photolysis experiments. Despite not yielding any new material, the potential of carrying out further photolysis experiments on a smaller scale than HIRAC has been demonstrated. Further kinetic experiments could be performed on higher alkenes (C_8 – C_{12}) which would be useful in obtaining information of use for structure activity relationships (SARs).

The successful characterisation of a temperature control system in the HIRAC chamber is a useful addition that will enable studies over the full range of tropospheric conditions of both temperature and pressure. The temperature limits have not been fully assessed in these experiments, since caution was taken to avoid any instrumental damage from overheating or overcooling the chamber. The thermofluid used has the potential to cool HIRAC down to 183 K and to heat it up to 363 K, however these would not be of atmospheric interest in HIRAC in any case given they lie well outside the limits of temperature conditions in the troposphere.

Chapter 5 is devoted to the first temperature dependent study of Cl atom reactions with butanes and pentanes, which is a more detailed investigation than the ozonolysis experiments described in this chapter. Other interesting temperature dependent studies that could be carried out include investigation of acetone photolysis and the temperature dependence of the reaction of acetone with OH discussed in this chapter, as well as Br atom chemistry, which is of particular relevance in Arctic and marine environments and has been reported to have a slight temperature dependence with certain VOCs in the atmosphere.

Chapter 4 – Relative rate studies and Structure Activity Relationships (SARs) of chlorine atoms with oxygenated hydrocarbons

4.1 Introduction

The relative rate method is a well-established technique used to obtain rate coefficients for chemical reactions. It has been used in several Cl atom gas-phase kinetic measurements of relevance to the oxidation mechanism of VOCs in the troposphere (Banco et al., 2012, Atkinson, 1991, Wallington et al., 1988b, Tyndall et al., 1997, Blanco et al., 2009). The relative rate technique, mentioned briefly in chapter 3, has been extensively reviewed in the work presented in this thesis: chapter 5 will focus on a more detailed study of Cl atom reactions with butanes and pentanes, making use of this technique, and chapters 6 and 7 also make use of this technique briefly for the characterisation of the method used (chapter 6) and for verifying OH reactivity is occurring (chapter 7). The relative rate experiments reported in this chapter are the earliest substantial kinetic data obtained in the HIRAC chamber. Prior to this work, the only kinetic data obtained was reported by Tamsin Malkin (Malkin, 2010) and Khuanjit Hemavibool (Hemavibool, 2009). Empirical approaches known as Structure Activity Relationships (SARs) have been found to be suitable in reproducing rate coefficients (Kerdouci et al., 2010, McGillen et al., 2011a, Atkinson, 1987, Kwok and Atkinson, 1995b) and are widely used in atmospheric models such as the master chemical mechanism (MCM) (Saunders et al., 2003).

This chapter will introduce the importance of the relative rate method and SARs as well as highlight the importance of Cl atom reactions with oxygenated volatile organic compounds, the latter being the most abundant of VOC classes present in the troposphere (Wedel et al., 1998, Greenberg et al., 1999). Cl atom chemistry has recently been shown to be of importance not only in the marine

boundary layer, where significant Cl atom concentrations arise from inorganic sea salt conversion (von Glasow, 2010a) but also in more inland urban environments (Thornton et al., 2010). This has already been discussed in chapter 1. Cl atoms and OH radicals react similar to each other with the majority of VOCs, however the increased abundance of Cl atoms and its higher reactivity with most VOCs with respect to OH would mean that Cl atoms are more likely to compete and therefore knowledge of the rate coefficients for these reactions as well as their degradation pathways are essential in order to better understand the full chemistry of tropospheric organic oxidation processes.

4.2 Chlorine in the atmosphere

The presence of Cl atoms in the lower atmosphere is mainly attributed to the photolysis of inorganic halogens from sea salt sprays (Finlayson-Pitts and Pitts, 2000). Indirect measurements of Cl atoms through their precursors, primarily ClO and $ClNO_2$, or hydrocarbon decays have been measured at various locations: coastal boundary layer – $ClNO_2$ (Pszenny et al., 1993, Finley and Saltzman, 2006, Lawler et al., 2009, Spicer et al., 1998, Riedel et al., 2012, Phillips et al., 2012), polar regions– ClO/NMHC (Wetzel et al., 2012, Hellen et al., 2012, Gilman et al., 2010, Cavender et al., 2008, Read et al., 2007, Hopkins et al., 2002, Kieser et al., 1993), volcanic environments – ClO/NMHC (Baker et al., 2011, von Glasow, 2010b) and urban cities– $ClNO_2$ (Riemer et al., 2008, Thornton et al., 2010). These latter observations inferred concentrations of a third to a half of the marine and coastal measurements (*i.e.*: ~10^4 atoms cm^{-3}), which is significant as it shifts the Cl:OH balance by 10 – 20% in the troposphere away from the marine environment.

These observations also indicate that there were unconsidered sources and sinks of Cl atoms in continental environments, not just transportation of sea salt particles *via* air masses, but possibly even industrial contributions. These findings also mean that Cl atoms may compete with OH radicals in VOC oxidation processes in the troposphere. A scheme shown in Figure 4.1 highlights the findings made by Thornton *et al.* and stresses the importance in better understanding the sources and sinks of Cl atoms in urban environments.

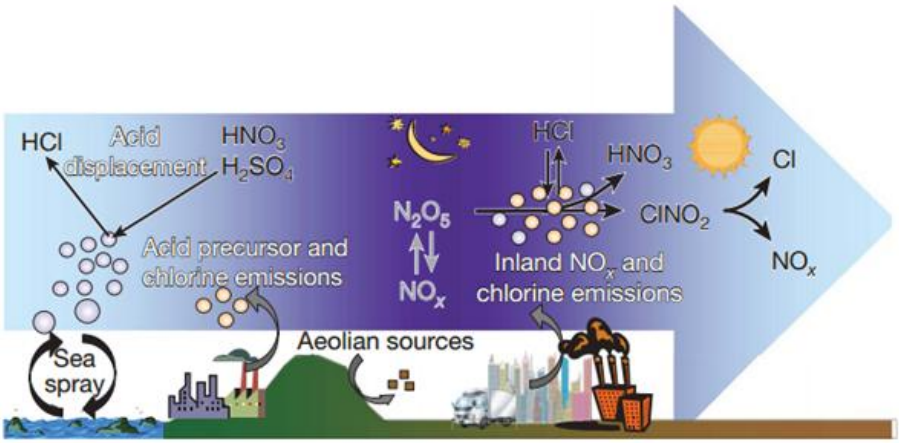

Figure 4.1: A schematic of night-time NO_x activation of chlorine in tropospheric urban environment (Thornton et al., 2010).

Cl atoms generated in the atmosphere react in a similar way to OH radicals with VOCs *via* hydrogen atom abstraction or addition across an unsaturated bond. The rates of reaction are considerably faster than OH, up to two orders of magnitude (Pszenny et al., 2007), making Cl atoms important in the troposphere even at low atomic concentrations (von Glasow, 2010a).

Aside from reacting with organics, Cl atoms will also extend the lifetime of nitrogen oxides (NO and NO_2), through nitryl chloride which is a major sink of Cl atoms; NO_x being the main precursors for ozone production in the troposphere (von Glasow, 2010a, Simpson et al., 2007), as has been highlighted in Chapter 1. Chlorine may also react with ozone to form ClO in the upper atmosphere, and reactions of Cl atoms with organics will eventually result in the formation of ozone in NO_x environments, implying Cl atoms will impact the ozone concentrations either way (Ezell et al., 2002).

The observations reported by Thornton emphasise an inland $ClNO_2$ production and results are consistent with models for coastal areas. Models incorporating R4.2 and R4.3 differ in their predicted impacts; however there is a trend in the summer ozone concentration spikes in coastal urban areas influenced by oxidants cycling from Cl atom reactions with organics in the environment (Thornton et al., 2010):

$$N_2O_5 + H_2O \rightarrow 2HNO_3 \qquad \text{(R4.1)}$$
$$N_2O_5 + Cl^- \rightarrow ClNO_2 + NO_3^- \qquad \text{(R4.2)}$$

$$ClNO_2 + h\upsilon \xrightarrow{\lambda \leq 300\ nm} Cl + NO_2 \qquad (R4.3)$$

Unusually high $ClNO_2$ measurements observed outside the coastal and marine environments away from sea spray and aerosols are indicative of anthropogenic sources contributing to a previously unknown significant Cl atom chemistry in inland environments. Despite these findings, the generation of sea salt aerosols by turbulence at the marine boundary layer remains the major source of reactive chlorine in the Earth's atmosphere (Graedel and Keene, 1995, Graedel and Keene, 1996, Lee et al., 2010) however if other continental regions also act as sources of $ClNO_2$ (Mielke et al., 2011, Riedel et al., 2012, Thornton et al., 2010), then the cycling of NO_x and Cl atoms through this compound is of a more global relevance (von Glasow, 2010a). Thornton and his group have provided compelling evidence that Cl atom chemistry is more widespread than initially thought, and sheds a greater importance into the study of the atmospheric chemistry of chlorine (Thornton et al., 2010). Their findings have demonstrated that the urban Cl atom levels could be as high as up to half the levels found in the marine environment (10^4 atoms cm^{-3}). This can have significant impact on the NO_x budget and O_3 levels.

4.3 Relative rate method

A vast majority of kinetic data obtained for gas phase experiments of interest have actually been reported not as absolute values but rather as a ratio of rate coefficients (Finlayson-Pitts and Pitts, 1986). The relative rate method is a major technique used for determination of rate coefficients. In order to derive useful rate data from this technique, either the investigated organic reactions occurs solely with one reactive species or, if another loss process such as photolysis or dilution is occurring, that this must be able to be taken into account (Atkinson, 1986). Tests can be carried out to ensure no other reactive species is reacting, or to assess photolysis and dilution effects accordingly. An internal standard is normally used to monitor dilution effects. This would be an organic that does not react or reacts at a sufficiently slower rate than organics being monitored to have no influence in time period of reaction being studied. As a result, the variation in their concentration would be correlated with dilution effects during the experiment.

The relative rate method is a simple yet effective way of obtaining rate coefficients from monitoring the competition of two organic compounds with a reactive species, one of which being a reference compound. Assuming the organic compounds monitored in the experiment are removed only by the reactive species, Cl atoms in this case, relative rate experiments are based on the simultaneous decay of a substrate of interest and a reference compound, in which both are removed by the same reactive species.

Cl + organic → product (R4.4)
Cl + reference → products (R4.5)

By following the simultaneous decay of both organic and reference compounds, the ratio k/k_{ref} may be derived from the known rate coefficient for the reference, thus calculating a relative value for k:

$$-\frac{d[reactant]}{dt} = k\ [Cl][reactant] \text{ or } -\frac{d\ ln[reactant]}{dt} = k_A\ [Cl] \quad \text{(Eq 4.1)}$$

$$-\frac{d[reference]}{dt} = k_{ref}[Cl][reference] \text{ or } -\frac{dln\ [reference]}{dt} = k_B[Cl] \quad \text{(Eq 4.2)}$$

Combining the two equations:

$$-\frac{1}{k}\, d\left(\frac{ln[reactant]}{dt}\right) = -\frac{1}{k_{ref}}\, d\left(\frac{ln[reference]}{dt}\right) \quad \text{(Eq 4.3)}$$

Integrating t=0 → t=t:

$$ln\left(\frac{[reactant]_0}{[reactant]_t}\right) = \left(\frac{k}{k_{ref}}\right) ln\left(\frac{[reference]_0}{[reference]_t}\right) \quad \text{(Eq 4.4)}$$

The rate coefficient for the organic species is calculated from the slope of the plot of ln $([reactant]_o/[reactant]_t)$ as a function of ln $([reference]_o/[reference]_t)$. The main advantages over the absolute-rate method are the ability to obtain high precision without the requirement of direct measurement of the radical species being investigated and the avoidance of secondary chemistry effects of the radicals. The use of multiple reference compounds at the same time is also possible, thus enabling comparison of two relative decays for the same rate coefficient determination simultaneously. This method also has the ability to cover wide ranges of initial concentrations and is insensitive to impurities. The reference compound, however, must possess a rate coefficient that is well reviewed in the literature, and it must also be easily detectable (Atkinson, 1991). The ideal reference compound would react with

the reactive species at similar concentrations and reaction times, and within one order of magnitude of the expected rate coefficient for the reaction of interest. It is particularly important to know whether any of the reference reactions are temperature or pressure dependent.

Another advantage that the relative rate technique possesses over absolute techniques, is that both fast and slow reactions can be studied, which is often a difficulty in absolute studies using flash or discharge flow photolysis techniques (Finlayson-Pitts and Pitts, 1986). One disadvantage with the relative rate technique over flash photolysis is that very fast kinetic reactions are much less easy to follow given the references used decay away at a fast rate and may be below the detection limits of the instruments used within seconds (depending on the detection used).

However, being a relative measure, the accuracy is dependent upon the reference rate coefficients. If the reference's rate coefficient is not so accurately known these relative rate ratios are still important values since they are true experimental values, and rate coefficients can be updated as better absolute rate coefficients appear in the literature. Some other disadvantages are:

1) Having another reactive species competing would render this method useless, since it relies on there being only one reaction occurring;

2) Secondary chemistry may also contribute to the evolving of such reactive species. In chamber studies this may well have a larger contribution owing to the size of the vessel and the typical starting concentrations for such experiments. This is observed as slightly curved relative rate plots after a significant amount of time elapses.

Relative rate techniques have the advantage that such relative measurements can often be made with greater precision than absolute rate coefficient measurements because only relative, not absolute, concentrations of organic and reference need be measured, thus increased precision, however this does not necessarily mean increased accuracy (Finlayson-Pitts and Pitts, 1986).

4.4 Cl atom relative rate experiments in HIRAC

Atmospheric simulation chambers play an important role in the study of atmospheric chemistry being excellent facilities to generate kinetic and mechanistic data (Seakins, 2010a) through use of the several types of different instrumentation interfaced for monitoring hydrocarbons and radical species. Several radical species are very difficult to either generate and/or monitor in an isolated system such as a flow tube or discharge flow system. Chambers provide a way to study such species with a level of control over the conditions and chemistry taking place and their larger size and longer timescales mean a wider variety of techniques may be employed (Blitz and Seakins, 2012).

This chapter discusses the Cl atom relative rate experiments performed in the HIRAC chamber, primarily making use of GC-FID. Cl atom chemistry is fast and Cl atoms can be generated from the relatively long wavelength photolysis of precursors such as oxalyl chloride, $(COCl)_2$, which is relatively unreactive and produces CO as the photolysis co-product (R4.6) or from the photolysis of molecular chlorine (R4.7):

$$(COCl)_2 + h\upsilon \xrightarrow{\lambda \leq 350\ \text{nm}} 2Cl\cdot + 2CO \qquad \text{(R4.6)}$$

$$Cl_2 + h\upsilon \xrightarrow{\lambda \leq 320\ \text{nm}} 2Cl\cdot \qquad \text{(R4.7)}$$

Three sets of Cl atom relative rate experiments are reported in this chapter. The reactions of propane and *n*-butane with Cl were carried out to test the references that will be used in the other relative rate studies and also to obtain relative rate ratios for important reactions that have been used as markers for [Cl] in several field campaigns such as the CHABLIS - Chemistry of the Antarctic Boundary Layer and the Interface with Snow that took place in Antarctica (Read et al., 2007, Read et al., 2008).

Reactions with ketones were carried out to further test and validate the relative rate method in HIRAC and to understand the discrepancy between relative rate and absolute data available for aliphatic ketones. An introduction to Structure Activity Relationships is (SARs) also given in this section. Ester reactions were performed to compare the results obtained with earlier work carried out in HIRAC and extend the SAR data previously reported for acetates to propionates (Malkin, 2010).

4.4.1 Apparatus

Cl atoms were generated *via* photolysis of molecular chlorine in HIRAC, using UV-B medical therapy lamps (Philips TL 40 W/12 RS SLV). Several tests were performed in order to determine the optimal lamp intensity used in these studies. All experiments were carried out at atmospheric pressure (1 bar) and temperature (292 ± 3 K). HIRAC was evacuated to ~1×10^{-3} mbar between each experiment, ensuring partial cleaning of the chamber. This was achieved by a rotary pump backed roots blower and took approximately 60 minutes each time.

Hydrocarbon experiments were all carried out in laboratory grade nitrogen, while oxygenated hydrocarbon experiments were carried out in ultra-high purity (U.H.P.) grade nitrogen, due to overlap on the GC-FID of methane present in laboratory grade nitrogen. HIRAC was first filled to ~970 mbar with nitrogen, and the reactant (~4 – 5 ppm), chlorine (~8 – 10 ppm) and the reference compound (~4 –5 ppm) were introduced shortly after by flushing a stainless steel delivery vessel containing the measured amounts of each constituent. This was obtained by knowing the volume of the delivery vessel and the glass line used to prepare the reactants, and using a calibrated pressure capacitance manometer to measure the pressure of the gas being introduced. All reagents were obtained from commercial sources, prepared in a vacuum line, and if liquids, purified prior to delivery into the chamber by successive freeze-pump-thaw cycles. Gases were used as provided by the supplier.

An Agilent HP 6890 GC-FID with a CP-Sil-5CB 100% dimethylpolysiloxane column (50 m length, 0.25 μm film and 0.32 mm internal diameter) was used in all experiments, and is referred to as HIRAC GC-FID or GC-FID henceforth. The GC-FID sampling was controlled by solenoid valves that opened HIRAC to a 5 mL stainless steel loop and then to a diaphragm pump after the sample had been introduced onto the column. Gas sampling was programmed to a loop volume of 5 mL, load time of 0.4 minutes and inject time of 0.3 minutes. This allowed sufficient time for the sample loop to fill between runs. The GC-FID column was usually maintained at a temperature within close range of the compound with the highest boiling point. The next experimental sections will discuss the investigations carried out for reaction of Cl atoms with hydrocarbons, ketones and esters.

4.4.2 Cl + hydrocarbons

Hydrocarbon relative rate experiments were carried out to test and validate the relative rate methodology as well as to test the HIRAC GC-FID following maintenance to the traps and conditioning of the GC column. The reactions of hydrocarbons with Cl atoms have been well characterised and also previously reported in HIRAC (Hemavibool, 2009) therefore particularly suitable for method validation since these compounds are also commonly used in relative rate studies as references, and are investigated further in chapter 5 and used as reference compounds in both chapters 6 and 7. The chemicals used in these experiments were acquired from the following commercial sources: propane (Sigma Aldrich, 98%), ethane (Sigma Aldrich, 99+%), *n*-butane (Sigma Aldrich, 99%), and chlorine (Sigma Aldrich, 99.5%). All the above gases were used as obtained from the supplier.

Rate coefficients were measured for the reaction of propane and *n*-butane with Cl, using ethane and propane respectively as references. Methane present in laboratory grade nitrogen (also referred to as departmental nitrogen) was used as an internal standard in all experiments. An internal standard reacts much slower than the organics being investigated and therefore serves as a useful marker for dilution during the experiment. The results obtained are shown in Table 4.1.

$Cl + CH_4 \rightarrow$ products (R4.8)
$Cl + C_2H_6 \rightarrow$ products (R4.9)
$Cl + C_3H_8 \rightarrow$ products (R4.10)
$Cl + n\text{-}C_4H_{10} \rightarrow$ products (R4.11)

Hydrocarbon	**Reference compound**	k / 10^{-10} cm^3 molecule^{-1}s^{-1}	**IUPAC** k/ 10^{-10} cm^{3}molecule^{-1}s^{-1}	k/k_{ref}	**IUPAC** k/k_{ref}
propane	ethane	1.35 ± 0.06	1.40 ± 0.13	2.36	2.43
n-butane	propane	1.90 ± 0.08	2.05 ± 0.10	1.59	1.46

Table 4.1: Measured rate coefficients for propane + Cl and *n*-butane + Cl from relative rate ratios obtained in HIRAC compared with current IUPAC recommendations (Atkinson et al., 2006a).

These results are in good agreement with the values recommended by IUPAC (Atkinson et al., 2006a). The linearity of the relative rate plots obtained from the regression analysis shown in Figure 4.2 and Figure 4.3 confirm the methodology used is satisfactory for relative rate experiments in HIRAC, and that there are small errors in both axes. This margin of error increases with the extent of reaction as is expected given it is a logarithmic relationship. These propagated errors are measured from the instrumental standard deviation by measuring the average and standard deviation of the peaks prior to the start of the experiment.

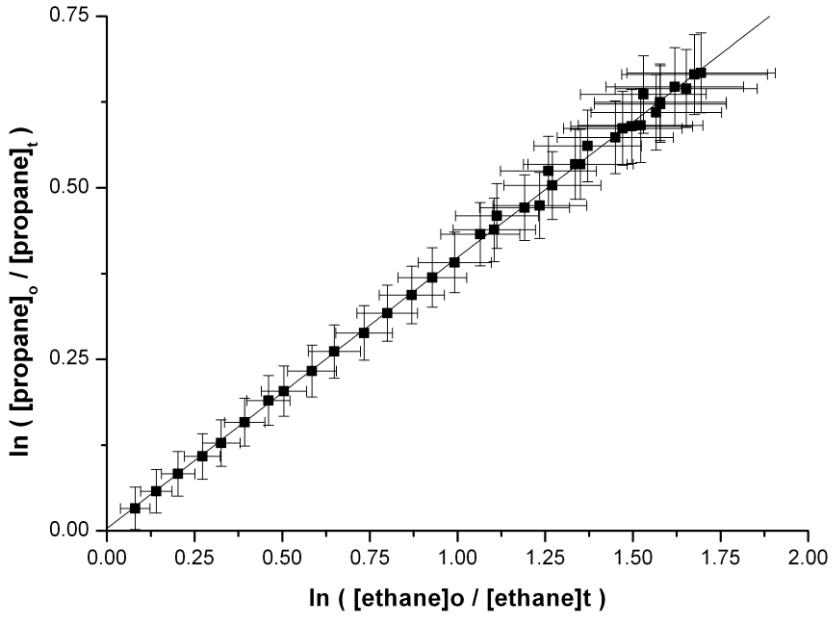

Figure 4.2: Relative rate data for reaction of Cl atoms with propane and ethane (reference) at 298 K and 1000 mbar in nitrogen, measured using GC-FID.

A linear regression tool, Regres2, was used to obtain the ratiok/k_{ref}. This regression analysis uses a linear least-squares regression, which takes into account random errors in both the [organic] and [reference], eliminating any systematic errors that may occur (Brauers and Finlayson-Pitts, 1997). The precision was taken as the standard deviation in repeat measurements of a known concentration of the organic, which is done before the photolysis of chlorine gas is initiated in the chamber.

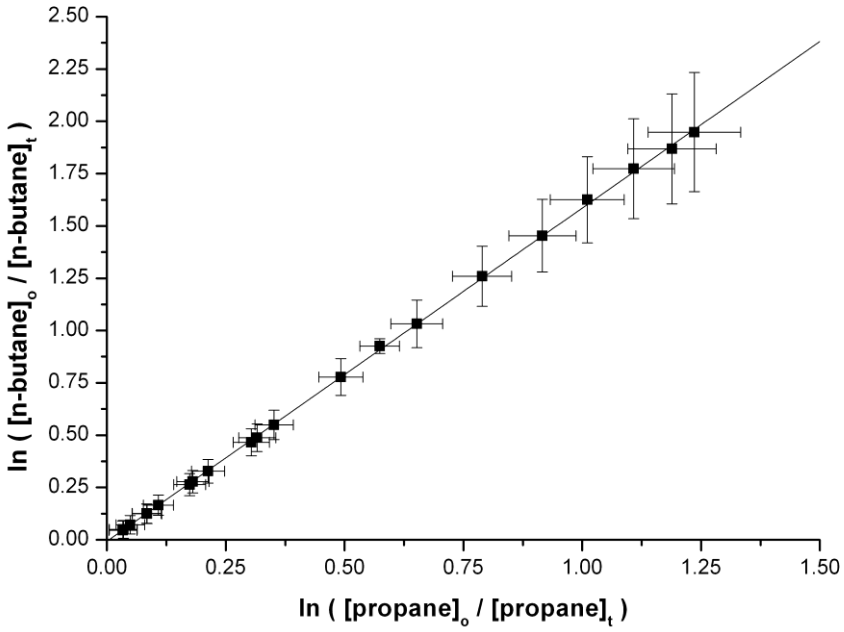

Figure 4.3: Linear regression plot for relative rate of *n*-butane reaction with Cl with propane as a reference compound.

4.4.3 Stability tests

In chamber experiments unwanted loss of reactants and products may occur *via* photolysis, dark chemistry, and wall reactions. Control experiments were performed to check for such unwanted losses prior to experiments. Concentrations of the reference compound and reactive species were monitored for ~30 minutes with the photolysis lamps off, and no evidence of unwanted reactions was observed with reactants and reference compound concentrations remaining constant as is shown in Figure 4.4.

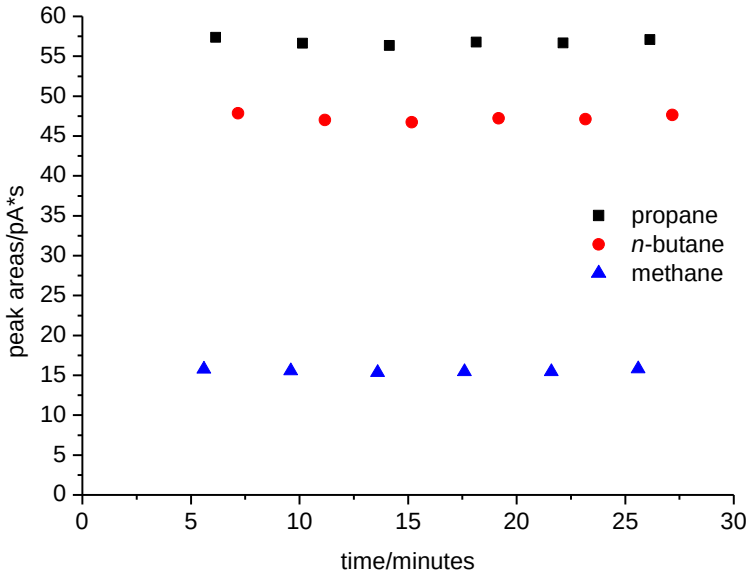

Figure 4.4: Stability tests carried out over a time period of 20 – 30 minutes for methane, propane and *n*-butane in the presence of molecular chlorine in HIRAC at 292 ± 2 K and 1 bar.

4.4.4 [Cl] estimation

An estimation of the Cl atom concentration in HIRAC was necessary primarily to understand how quickly chlorine gas is being photolysed in HIRAC and to be able to know how best to control the Cl atom concentrations for an experiment by altering lamps or adding molecular chlorine. A value for [Cl] generated from Cl_2 photolysis in HIRAC was estimated from the measurement of the rate of decay of propane. The relationship used for estimating the [Cl] was the following:

$$-\frac{d\,[C_3H_8]}{dt} = k_{C_3H_8}\,[C_3H_8]\,[Cl] \qquad \text{(Eq 4.5)}$$

Thus, using the known rate coefficient for C_3H_8+ Cl, $k_{C_3H_8}$, and the decay rate of propane from the relative rate plot shown in Figure 4.5, an estimate of the Cl atom concentration was made using equation R4.16. This was found to be ~3.0×10^6 atom cm^{-3} with all lamps on, and was calculated by obtaining the gradient from the decay of propane using IUPAC recommended rate coefficient of $(1.4 \pm 0.2) \times 10^{-10}$ molecule^{-1} cm^{-3} s^{-1}.

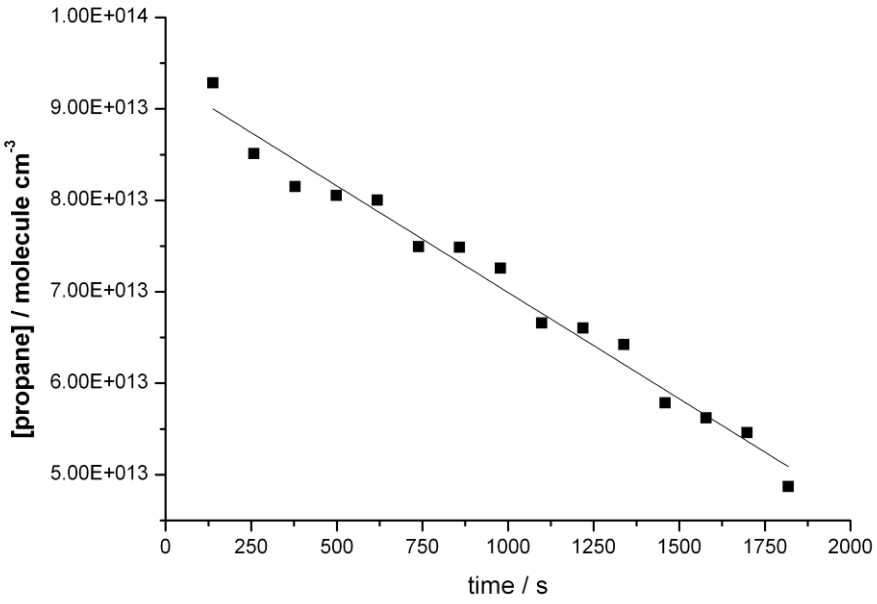

Figure 4.5: Example of decay plot of propane used to estimate [Cl] in HIRAC.

4.4.5 Error calculations

The error in the relative rate coefficient, σ_k, is obtained from the multiplication of the error from the gradient ($\sigma_{gradient}$) with the error from the reference rate coefficient (usually known and recommended, σ_{ref}). The value obtained is then converted to % error in quadrature using Eq4.6:

$$\sigma_{k'} = \sigma_{k(ref)} \times \sigma_{k(gradient)} \qquad \text{(Eq 4.6)}$$

The σ_{kref} value is usually recommended by chemical kinetic databases such as IUPAC. These values are generally derived from evaluations of all the data available and based on averages of errors from spread of values. The percentage error in k_a is achieved as follows, and the percentage value is divided by 100 to determine σ, and multiplied by 2 to quote 2σ:

$$\sigma_{k'} = k' \times \sqrt{(\sigma_{k_{reference}}/k_{reference})^2+(\sigma_{gradient}/k_{gradient})^2} \qquad \text{(Eq 4.7)}$$

The relative errors for the relative rate method increase exponentially with extent of reaction, as is shown in Table 4.2.In order to reduce errors in the relative

rate method as much as possible it is useful to have a reference compound that reacts roughly the same order of magnitude as the organic being investigated in order to make sure the extent of reaction is kept as low as possible. This is because errors grow exponentially as the reaction proceeds.

	Extent of Reaction	Relative Errors
$[A]_0/[A]_t$	t/τ_A	$\sigma_Y/(\sigma_A/[A]_0)$
1	0	1.41
2	0.69	2.34
5	1.6	5.1
10	2.3	10
100	4.6	100

Table 4.2: Relative increase in error in $\ln([A]_0/[A]_t)$ as a function of reaction time (Brauers and Finlayson-Pitts, 1997).

4.4.6 Discussion

Cl atom relative rate experiments with simple hydrocarbons have been carried out to validate the relative rate method in HIRAC. The relative rate results obtained were in good agreement (~5%) with IUPAC recommendations (Atkinson et al., 2006a), with both rate coefficients being within error of the IUPAC values. Previous experiments had already been reported in HIRAC on similar systems (Hemavibool, 2009), however a more recent account of the conditions in HIRAC as well as a better grasp of the method to be used was important in light of the use of relative rate experiments in all subsequent chapters in this thesis.

4.5 Cl atom reactions with oxygenated VOCs

Oxygenated volatile organic compounds represent the most abundant class of organics within the atmosphere, and their reactions have been extensively reviewed in the literature (Atkinson and Arey, 2003a, Mellouki et al., 2003). Large global contributions of oxygenates in the atmosphere have been shown to exist, which have contributed to an increased interest in these compounds in the recent literature (Singh et al., 2001, Lewis et al., 2000). The degradation of oxygenates leads to secondary

pollutants such as O_3, PANs and SOAs, and strategies to control the emissions of these O_3 precursors has been based on their individual contributions to tropospheric ozone formation (Mellouki et al., 2003).

The major sources of oxygenates are biogenic, primarily from plant emissions and biomass burning, with the main anthropogenic sources being solvent and fuel additive use, as well as from the oxidation processes of other VOCs. In recent years, owing to stricter industrial legislation, solvent use has shifted more towards oxygenated hydrocarbons from more toxic aromatic and halocarbon solvents (Liang et al., 2010). Another contributor that has increased the anthropogenic contributions of oxygenated compounds is biofuel consumption and diesel fuel blending. In the U.S. and Brazil, bioethanol is the most used biofuel, whereas in the EU fatty acid methyl and ethyl esters (FAMEs and FAEEs) are the dominant form of biofuel (Andersen et al., 2012, Schutze et al., 2010a).

Experiments were therefore carried out in order to obtain a better understanding of reactions of Cl atoms with two sets of oxygenates, saturated ketones and esters. Another motivation for carrying out this work was to further enhance the structure activity relationships available for Cl atom reactions with oxygenates, which in this chapter will be reported for formates, acetates, propionates and ketones and compared with the experimental rate coefficients obtained in this work and in previous work in HIRAC by Hemavibool and Malkin for acetates (Hemavibool, 2009, Malkin, 2010).

4.6 Cl + ketones

4.6.1 Ketones in the atmosphere

Ketones are an important group of oxygenates present in the atmosphere as products of other oxidation processes as well as through both natural and anthropogenic sources. Acetone is the most abundant ketone in the troposphere, averaging at 0.3 - 1 ppb(Sprung and Zahn, 2010). The main sources of ketones in the atmosphere are from rural and forested sites in nature, and through solvent use in

industry. Ketones are known to participate in photochemical transformations in the troposphere, as well as undergo efficient uptake into cloud droplets, leading to various transformation processes (Kaiser and Wallington, 2007, Wallington et al., 1988b).

Carbonyls are sources of free radicals and SOAs that lead to organic acids in the troposphere in the presence of NO_x, as well as ozone formation (Levart and Veber, 2001, Roberts, 1990). There have been numerous recent publications focused on the understanding the chemistry of unsaturated ketones (Banco et al., 2012), and ketone chemistry at higher temperatures (Lam et al., 2012), which stresses the interest in the atmospheric chemistry and combustion of these species, given their importance in the understanding of VOC oxidation mechanisms.

This work was carried out because there was a significant discrepancy between relative rate data quoted by Kaiser and Wallington (Kaiser and Wallington, 2007) and Taketani et al. (Taketani et al., 2006) and absolute rate data quoted by Notario et al. (Notario et al., 2000) and Cuevas et al. (Cuevas et al., 2004, Albaladejo et al., 2003) for Cl atom reactions with saturated ketones. Taketani et al. ascribed the regeneration of Cl atoms in the absolute rate studies by Notario et al. and Cuevas et al. as the cause of this discrepancy. Notario et al. and Cuevas et al. stated that significant amounts of molecular chlorine could be problematic in absolute-rate experiments as these may react with alkyl intermediates leading to the regeneration of Cl atoms.

In contrast to the absolute rate measurements, an appreciable loss of ketones was reported by Kaiser and Wallington in their relative rate investigations, owing to the low vapour pressures of these ketones. Wall losses and any experimental problems associated with the introduction of these ketones into the chamber were however ignored based on the assumption that any losses would be constant for all of the ketones during the duration of the experiment (Kaiser and Wallington, 2007). Longer chain ketones were allowed to mix for longer to ensure their peak heights were stable on the GC-FID prior to initiating photolysis, improving the precision of the results obtained. Due to these discrepancies and uncertainties in the literature it was found appropriate to further investigate these reactions in HIRAC.

4.6.2 Experimental method

The relative rate experiments were carried out in HIRAC and the ketones and reference compounds were monitored by GC-FID. Concentrations of reference compounds and organics used were the same as for the hydrocarbon experiments mentioned earlier. Similar experimental conditions were used in HIRAC as were used in the work by Kaiser and Wallington (Kaiser and Wallington, 2007). Each ketone was run with separate reference alkanes (propane and *n*-butane) at least three times for each run.

The chemicals obtained from commercial sources all had purities of ≥ 98%: 3-methyl-2-butanone (99%, Sigma Aldrich), 2-pentanone (≥ 99% Reagent Plus, Sigma Aldrich), 3-pentanone (99%, Alfa Aesar), 4-methyl-2-pentanone (99%, Alfa Aesar), 5-methyl-2-hexanone (99%, Alfa Aesar), propane (98%, Sigma Aldrich), n-butane (99%, Sigma Aldrich), chlorine (99.5%, Sigma Aldrich).

$Cl + CH_3C(O)C_3H_7 \rightarrow$ products (R4.12)
$Cl + C_2H_5C(O)C_2H_5 \rightarrow$ products (R4.13)
$Cl + CH_3CHCH_3C(O)CH_3 \rightarrow$ products (R4.14)
$Cl + CH_3C(O)CH_2CH(CH_3)CH_3 \rightarrow$ products (R4.15)
$Cl + CH_3C(O)CH_2CH_2CH(CH_3)CH_3 \rightarrow$ products (R4.16)
$Cl + C_3H_8$ (reference) $\rightarrow$ products (R4.14)
$Cl + n\text{-}C_4H_{10}$ (reference) $\rightarrow$ products (R4.15)

4.6.3 Results

The relative rate ratios obtained are shown in Table 4.3. The results obtained are all within 10% of the ratios reported previously by Kaiser and Wallington. These discrepancies are likely to be within the experimental uncertainty of these investigations, which may be attributed to the uncertainty in our vacuum line and stainless steel delivery vessel method used to introduce known concentrations of these compounds into our chamber, as well as losses of ketones to walls, which could explain why some of the relative rate plots do not all go through the origin. Kaiser and Wallington also reported difficulties in introducing certain ketones into their experimental system. Significant problems associated with delivery of some of the higher-carbon ketones investigated into HIRAC, particularly 4-methyl-2-pentanone

and 5-methyl-2-hexanone was unavoidable given their low vapour pressures and difficulty in getting them in the gas phase.

C_4 – C_6 Ketones	**Number of repeat runs (this work)***	**RR ratio**	**Reference**
2-pentanone	3	0.83 ± 0.04	(Kaiser and Wallington, 2007)
		0.77 ± 0.02	**This work**
3-pentanone	3	0.60 ± 0.03	(Kaiser and Wallington, 2007)
		0.51 ± 0.01	**This work**
3-methyl-2-butanone	3	0.44 ± 0.01	(Kaiser and Wallington, 2007)
		0.34 ± 0.02	**This work**
4-methyl-2-pentanone	2	0.91 ± 0.03	(Kaiser and Wallington, 2007)
		0.81 ± 0.03	**This work**
5-methyl-2-hexanone	2	**2.03 ± 0.13**	**This work**

Table 4.3: A comparison of relative rate ratios for the reaction of Cl atoms with ketones obtained in HIRAC with previous work by Kaiser and Wallington (*using propane as a reference compound in both studies).

Figure 4.6 shows that 4-methyl-2-pentanone has a slightly curved relative rate plot at the beginning of the experiment. The most likely explanation is losses in the delivery of these ketones into the GC, which was expected since their low vapour pressures do not make these compounds easy to be studied in a large stainless steel chamber like HIRAC. Such difficulties had been reported by Kaiser and Wallington in their work. This could not be picked up on the GC-FID as once mixed the stability of these ketones was evident, so the main difficulty was the introduction into the chamber and accurately knowing the starting concentrations of the ketones during these experiments. The uncertainty associated with wall losses within the copper tubing introducing the ketones into HIRAC and into the GC were difficult to estimate. Any wall losses within HIRAC were regarded as being negligible given the GC never showed any decays during the stability tests carried out before initiating the reaction. The GC-FID sampling loop losses would result in different volumes of ketone being sampled from the chamber; however, in relative rate investigations these are not as significant provided the loss is constant for the duration of the experiment. This would only be reflected in slightly higher margins of error for the ketones relative to the reference, as can be noted in the linear regression plots obtained from these

experiments in HIRAC. The uncertainty in the relative rate coefficients ranged from 4 – 6% for the majority of the experiments carried out.

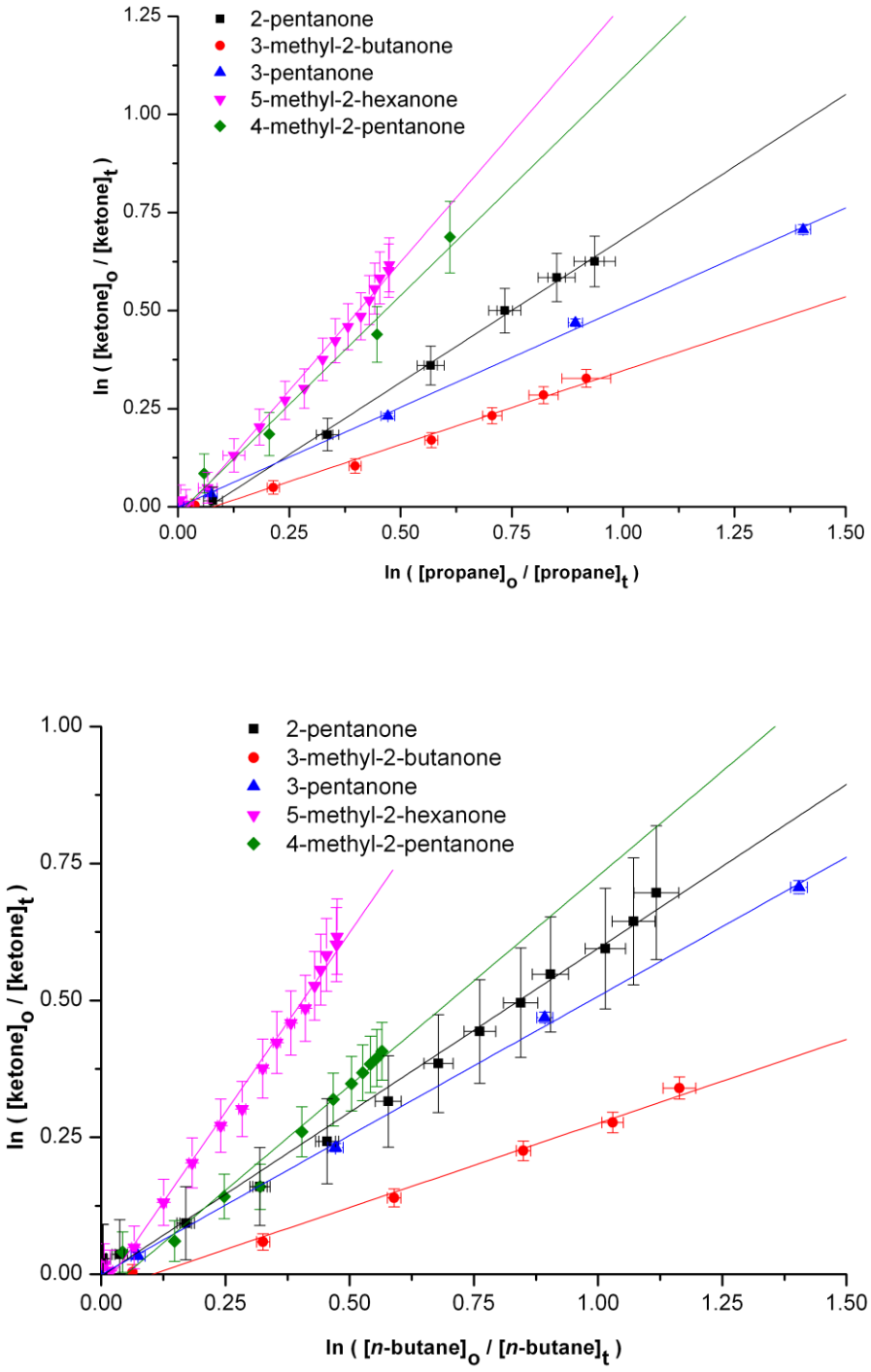

Figure 4.6: Relative rate plots for the reaction of Cl atoms with a series of ketones relative to propane and *n*-butane at 292 ± 3 K and 1000 mbar in U.H.P. nitrogen measured using GC-FID.

Ketones	$k_{ketones}$ (10^{-11} $cm^3molecule^{-1}$ s^{-1})	Technique	Reference
2-Pentanone	4.57 ± 0.28	PLP-RF	(Albaladejo et al., 2003)
	4.17 ± 1.21	PLP-RF	(Cuevas et al., 2004)
	11.1 ± 0.10	RR	(Taketani et al., 2006)
	12.3 ± 0.13	PLP-RF	(Takahashi et al., 2007)
	11.6 ± 1.0	RR (C_3H_8)	(Kaiser and Wallington, 2007)
	10.5 ± 0.95	**RR (C_3H_8)**	**This work**
	11.8 ± 1.04	**RR (C_4H_{10})**	**This work**
3-pentanone	4.50 ± 0.32	PLP-RF	(Albaladejo et al., 2003)
	5.9 ± 0.5	DF-MS	(Aranda et al., 2004)
	8.10 ± 0.85	RR	(Taketani et al., 2006)
	8.87 ± 0.92	PLP-RF	(Takahashi et al., 2007)
	7.47 ± 0.30	PLP-RF	(Zhao et al., 2008)
	8.3 ± 0.7	RR (C_3H_8)	(Kaiser and Wallington, 2007)
	9.81 ± 1.33	**RR (C_3H_8)**	**This work**
	8.66 ± 0.82	**RR (C_4H_{10})**	**This work**
3-Methyl-2-butanone	7.02 ± 0.89	PLP-RF	(Notario et al., 2000)
	4.50 ± 0.25	PLP-RF	(Cuevas et al., 2004)
	6.2 ± 0.5	RR (C_3H_8)	(Kaiser and Wallington, 2007)
	7.46 ± 0.74	**RR (C_3H_8)**	**This work**
	6.41 ± 0.84	**RR (C_4H_{10})**	**This work**
4-Methyl-2-pentanone	9.72 ± 1.2	PLP-RF	(Notario et al., 2000)
	8.52 ± 4.0	PLP-RF	(Cuevas et al., 2004)
	12.8 ± 1.0	RR (C_3H_8)	(Kaiser and Wallington, 2007)
	10.2 ± 1.37	**RR (C_3H_8)**	**This work**
	13.1 ± 1.03	**RR (C_4H_{10})**	**This work**
5-methyl-2-hexanone	10.6 ± 1.4	PLP-RF	(Notario et al., 2000)
	14.8 ± 1.0	PLP-RF	(Cuevas et al., 2004)
	19.9 ± 2.21	**RR (C_3H_8)**	**This work**
	25.8 ± 2.06	**RR (C_4H_{10})**	**This work**

Table 4.4: Measured rate coefficients for ketone+Cl reactions obtained by relative rate using hydrocarbon/ketone/Cl mixtures in UHP nitrogen measured using GC-FID.

Product overlap was however evident in some of the chromatograms, which seem to have led to poorer resolution of peaks leading to a greater uncertainty being proportional to extent of reaction. This was particularly evident in the case of 5-methyl-2-hexanone, for which the agreement between experiments carried out with propane and butane as references was poor in comparison with the other ketones. As can be seen from Figure 4.6, the curvature in some of the relative rate plots,

particularly in the case of the higher ketones (5-methyl-2-hexanone and 4-methyl-2-pentanone), is quite visible as the reaction progresses. This seems to indicate that perhaps some of the products from the reference compounds may have been missed and could have been lying under the ketone peaks leading to a sharper increase in the ketone and hence the curvature exhibited. There was also a discrepancy between the results obtained using different reference compounds, but it is noted that the values obtained are within error of each other for all except 5-methyl-2-hexanone. The latter was found to be very problematic to deliver into the chamber and showed a very small response on the chromatogram owing to its long retention time resulting in broader peaks that are not well resolved in the chromatogram. This could be why there is such a significant difference between the values obtained for the two references used in this case.

4.6.4 Discussion

This work shows how the relative rate method could be used to obtain rate coefficients for the reactions of Cl with ketones in HIRAC. The results obtained were in general within error of previous relative rate work reported by both Taketani et al. and Kaiser and Wallington (Kaiser and Wallington, 2007, Taketani et al., 2006), with the exception of 5-methyl-2-hexanone, demonstrating the strengths of the relative rate method over the absolute method for studying such systems and also the potential of HIRAC to be used to study the kinetics of oxygenates with Cl atoms.

According to Taketani et al. however seems to be an overestimation of the reactivity of the ketones studied using the relative rate method with respect to the absolute rate measurements (Taketani et al., 2006). Taketani's group ascribe this to the possible regeneration of Cl atoms in the absolute rate investigations, since significant amounts of molecular chlorine may be a problematic condition in absolute rate determinations since the alkyl intermediates may react with molecular chlorine leading to regeneration of chlorine atoms. They propose that further absolute rate experiments should be carried out under conditions where Cl atom regeneration does not exist, in order for these absolute rate results to be verified.

4.6.5 Structure activity relationships

Structure activity relationships (SAR) are useful in predicting rate coefficients that are difficult to measure or that have never been studied previously. This method is based on summing the cumulative processes that occur when a reactive species interacts with an organic compound, which in the case of OH and Cl atom reactions, is the different hydrogen abstractions that occur.

The SAR method has been fully validated for OH chemistry (Kwok and Atkinson, 1995b, Atkinson, 1987) at room temperature and atmospheric pressure. SARs have also been well characterised for NO_3 reactions (Kerdouci et al., 2010), O_3 reactions (McGillen et al., 2011a) and, with limited use, in understanding Cl atom chemistry (Aschmann and Atkinson, 1995, Ezell et al., 2002, Notario et al., 1998, Schütze et al., 2010). Such methods give important mechanistic insights and information on favoured routes leading to different radical production, through understanding site specificity of abstraction reactions.

There are several different types of SARs used, based on either group reactivity (Mellouki et al., 2003), as a function of the ionisation potential, or as a function of the highest occupied molecular orbital (HOMO). The former method is put into practice in this chapter, with the group rate coefficients reported by Aschmann and Atkinson (1995) being used for the Cl atom reactions investigated.

In order for rates of primary, secondary and tertiary hydrogen abstractions to be determined SARs need an accurate set of experimental rate coefficient measurements for prototypical compounds. Correction for effects of neighbouring groups on the hydrogen abstraction sites is also necessary in order to properly assess each abstraction site. A particular focus on Cl atom reactions with esters is relevant as previous studies have reported deactivating effects of the –C(O)-O- group (Notario 1998).

A review of the literature for these reactions also shows significant discrepancies in reported rate coefficients, even with studies using the same basic technique such as flash photolysis/resonance fluorescence, as well as between

absolute and relative rate techniques. For this reason, the SAR method has been applied to the reactions of Cl atoms with the studied esters.

The SAR method was developed by Atkinson for H-atom transfer reactions of the OH radical with a large variety of saturated VOCs (Kwok and Atkinson 1995). In the SAR method the calculation of the overall rate coefficient is based on the estimation of $–CH_3$, $–CH_2–$ and >CH– group rate coefficients for the reaction of Cl atoms with alkanes. These group rate coefficients depend only on the identity of the substituent bonded to these groups (e.g.: in α position):

$$k(CH_3\text{-}X) = k_{prim}\, F(X) \quad \text{(Eq 4.8)}$$
$$k(X\text{-}CH_2\text{-}Y) = k_{sec}\, F(X)F(Y) \quad \text{(Eq 4.9)}$$
$$k(X\text{-}CH(Y)(Z)) = k_{tert}\, F(X)F(Y)F(Z) \quad \text{(Eq 4.10)}$$

where, $k_{prim} = 3.32 \times 10^{-11}$, $k_{sec} = 8.34 \times 10^{-11}$, $k_{tert} = 6.09 \times 10^{-11}$ cm^3 $molecule^{-1}$ s^{-1}, $F(–CH_3) = 1.00$ and $F(–CH_2–) = F(>CH_2) = F(>C<) = 0.79$, at 296 K (Aschmann and Atkinson, 1995).

Table 4.5 below shows the calculations of the CH_x group rate coefficients for the reaction of Cl with ketones. The coefficients in brackets represent the values obtained by Atkinson and co-workers using the SAR method they proposed (Aschmannand Atkinson, 1995). The predictions made were based on the assumption that the 2° and 3° carbons are found adjacent to the CH_x in the case of β to >C=O, while the CH_x group is assumed to be in the inner position and the CH_3 group in the outer position in the case of γ or δ to >C=O.

CH_x group	**α–position**	**β–position**	**γ–position**	**≥δ–position**
$-CH_3$	0.10	0.53	0.17	0.17
$-CH_2-$	0.7	3.6	1.2	1.2
>CH-	1.3	7.1	2.3	2.3

Table 4.5: Structure activity predictions for CH_x group rate coefficients of Cl+ ketone reactions in 10^{-12} cm^3 $molecule^{-1}s^{-1}$ (Aschmann and Atkinson, 1995).

The above group rate coefficients represented by Aschmann and Atkinson are a clear demonstration that the carbonyl group activates both α and β sites in the molecule. These results are of use in predictions of possible sites of attack in the

reaction with Cl and therefore the possible products expected from these reactions. This is of importance in the better understanding of VOC oxidation mechanisms.

Table 4.6 below compares the experimentally obtained rate coefficients from this work and literature values (tabulated in (Calvert et al., 2011)) with those obtained through structure activity calculations using the above Table 4.5 values for the reaction of OH with ketones.

Compound	**k_{expt} / 10^{-11} $cm^3 molecule^{-1} s^{-1}$ (this work)***	**k_{expt} / 10^{-11} $cm^3 molecule^{-1} s^{-1}$ (Calvert et al., 2011)**	**$10^{11} \times k_{calc}$ (SARs) (Aschmann and Atkinson, 1995)**	**% Difference (this work)**
Acetone	-	0.21	0.21	-
Butanone	-	4.0	3.8	5
2-Pentanone	11.2	11.6	13.1	-14
3-Pentanone	9.2	7.9	7.3	26
3-Methyl-butanone	6.9	6.0	7.0	-2
2-Hexanone	-	20.0	18.2	-
3-Hexanone	-	14.4	16.7	-
4-Methyl-2-pentanone	11.7	9.1	12.5	-6
5-Methyl-2-hexanone	22.9	13.0	18.5	-24

Table 4.6: Comparison of experimental and calculated rate coefficients (k, cm^3 $molecule^{-1}$ s^{-1}) for Cl + ketone (Calvert et al., 2011).*results shown are the average of two separate relative rate determinations from results presented in Table 4.4.

The rate coefficients presented from this work were worked out as the mean for the two reference compounds. The percentage differences shown are for between this work and the SARs available and were calculated using $100 \times (k_{expt} - k_{calc})/ k_{expt}$. The results show good agreement with the SARs for butanone, 3-methyl-butanone and 4-methyl-2-pentanone, but poorer agreement for 2-pentanone, 3-pentanone, and 5-methyl-2-hexanone.

4.7 Cl + esters

4.7.1 Esters and the atmosphere

Esters are another very important class of oxygenates widely used in industrial products and feedstock. Large quantities are used as paint and varnish solvents in the manufacturing industry (Cuevas et al., 2005a), and also as a starting product for polymer production (Blanco et al., 2009). Esters are also common flavourings in the food industry and have been increasingly used in the EU as biofuel and diesel additives, which upon combustion give off several other oxygenated organic intermediates such as ethers (Xing et al., 2009). They are also emitted from vegetation and fruits, which still remains the primary source of esters in the atmosphere despite increase in consumption of biofuel and solvents.

Consequently these significant biogenic and anthropogenic emissions result in various esters being present in the atmosphere participating in subsequent oxidation processes that need to be fully understood. Oxidation of ethers and other volatile organic compounds result in further ester emissions in the atmosphere (Liang et al., 2010), such as methyl *t*-butyl ether which is used commonly as an oxygenated fuel additive in combustion engines in order to reduce CO emissions, results in methyl acetate (35% yield). Higher ethers can form correspondingly larger ester species. The oxidation of oxygenated species are currently a topic of significant interest due to both interesting mechanistic issues including the generation of OH (Peeters et al., 2009) and the potential to form low volatility compounds which may lead to particle formation or growth.

Wallington reported a systematic discrepancy of 20 – 30% between relative rate and absolute rate studies for Cl atom studies with acetates and formates, noting the values obtained using absolute techniques were higher (Wallington et al., 2006). Many other relative rate studies have suggested the same, with their being an overestimation of the rate coefficients, most likely due to an additional loss channel such as reaction with alkylperoxy radicals produced in the absolute technique setup (Schutze et al., 2010a) that had not been taken into consideration. Studies performed in flow tubes have encountered several wall adsorption/desorption problems. In larger

chambers these problems are minimised (Harry et al., 1999), making HIRAC an ideal test bed.

4.7.2 Experimental Method

All experiments were performed in HIRAC at 296 ± 3 K and at 1 bar. The same relative rate method was used in order to be able reproduce previous experiments carried out in HIRAC (Hemavibool 2009; Malkin 2010), thus validating the method and the experimental conditions, and to expand the range of esters studied in HIRAC to propionates. The chemicals obtained from commercial sources all had purities of ≥98%: methyl acetate (99%, Alfa Aesar), acetone (≥99%, Fisher), and chlorine (99.5%, Sigma Aldrich), methyl propionate (99+%, Fischer Scientific), ethyl propionate (99+%, Fischer Scientific), propyl propionate (99%, Sigma Aldrich), isobutyl propionate (98%, Acros Organics), *n*-butyl propionate (99%, Alfa Aesar), chlorine (99.5+%, Aldrich), propane (98%, Sigma Aldrich), *n*-butane (99%, Sigma Aldrich) and nitrogen (>99.995%, Dominick Hunter N_2 generator, MAX116).

$Cl + CH_3C(O)OCH_3 \rightarrow$ products	(R4.17)
$Cl + C_2H_5C(O)OCH_3 \rightarrow$ products	(R4.18)
$Cl + C_2H_5C(O)OC_2H_5 \rightarrow$ products	(R4.19)
$Cl + C_2H_5C(O)OC_3H_7 \rightarrow$ products	(R4.20)
$Cl + C_2H_5C(O)OCH(CH_3)_2 \rightarrow$ products	(R4.21)
$Cl + C_2H_5C(O)OC(CH_3)_3 \rightarrow$ products	(R4.22)
$Cl + C_3H_8$ (reference) → products	(R4.23)
$Cl + C_4H_{10}$ (reference) → products	(R4.24)

With the exception of the gases used, all chemicals were freeze-pump-thawed several times prior to use. This minimised the impurities introduced and gave a better accuracy of the concentrations of the ester that were being introduced into the chamber.

4.7.3 Results

Previous measurement of the rate of Cl + acetates reactions had been carried out by Malkin and Hemavibool using both GC-FID and FTIR instruments for detection of reactants and references (Malkin, 2010, Hemavibool, 2009). In this work the FTIR was unavailable so only GC-FID measurements are reported, and methyl acetate was the only ester to be studied, with acetone being used as the reference compound. Figure 4.7 demonstrates the high accuracy in the GC relative rate results obtained for methyl acetate in HIRAC, which are within error of Hemavibool and Malkin's previous work. A comparison of the results obtained with other reported data are shown in Table 4.7. Results for both GC-FID and FTIR measurements are in excellent agreement with the previously reported results from HIRAC and with previous literature, particularly Christensen, Ball and Wallington's relative rate results, indicating satisfactory conditions for carrying out relative rate experiments, and a good methodology.

Acetate	**Reference compound**	**Method used**	$k_{acetate}/k_{reference}$	$k_{acetate}$ **(10^{-11}cm^3 molecule^{-1} s^{-1})**	**Reference**
Methyl acetate	C_2H_5F, CH_3Cl, CH_3OCHO	RR	-	0.22 ± 0.03	(Christensen et al., 1999)
	-	PLP-RF	-	0.29 ± 0.04	(Notario et al., 1998)
	-	PLP-RF	-	0.28 ± 0.03	(Cuevas et al., 2005b)
	CH_3COCH_3	RR-GC	0.98 ± 0.12	0.22 ± 0.05	(Hemavibool, 2009)
		RR-FTIR	1.10 ± 0.16	0.23 ± 0.05	(Malkin, 2010)
		RR-GC	**0.99 ± 0.15**	**0.22 ± 0.08**	**This work**

Table 4.7: Measured rate coefficients for methyl acetate + Cl from relative rate ratios obtained in HIRAC compared to previous work from HIRAC and other laboratories. RR: relative rate method, PLP-RF: pulsed laser photolysis-resonance fluorescence technique.

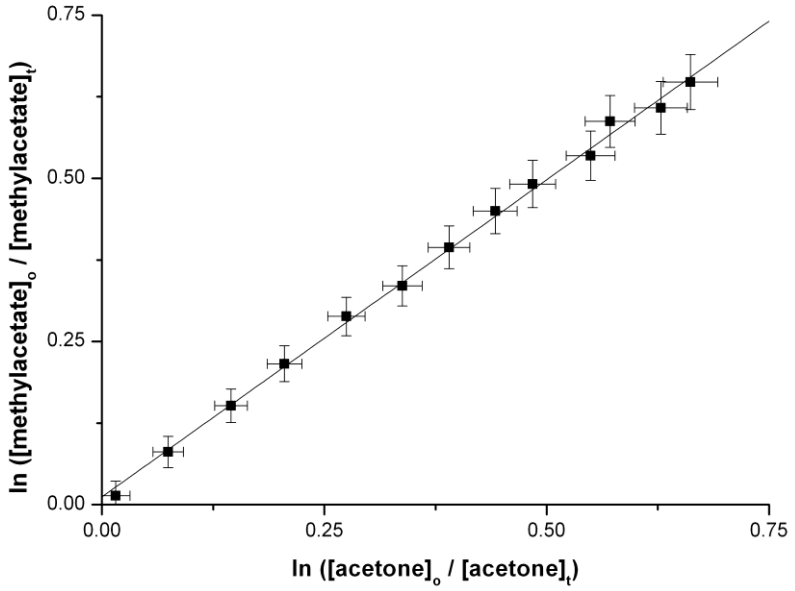

Figure 4.7: Relative rate data for reaction of Cl atoms with methylacetate at 298 K and 1000 mbar in U.H.P. nitrogen measured using GC-FID.

The relative rate plots for methyl propionate, ethyl propionate, propyl propionate, *n*-butyl propionate and *iso*-butyl propionate are shown in Figure 4.8 and 4.9. All experiments were conducted at least twice each for each propionate investigated. As can be noted for the propyl and butyl propionate plots, less data points were obtained. This was due to the operation of longer cycles of 6 minutes to avoid overlap of the unidentified product peaks with the propionate and reference. The decision to use fewer data points stems from the logarithmic increase in uncertainty associated with this method.

The results obtained for the propionates show good agreement (within 5%) with previous relative rate data for methyl propionate, but the rate coefficients obtained for the ethyl, propyl and *n*-butyl propionates all appear to be slightly higher than previously reported literature data, however are all within the experimental error. No previous literature data has to our knowledge been reported on *iso*-butyl propionate. As can be seen in Figure 4.8, fewer data points have been obtained for propyl propionate in comparison with methyl and ethyl propionates. This is due to longer sampling rates on the GC set for this compound (same for butyl analogues) to ensure adequate resolution of all peaks in the gas chromatogram.

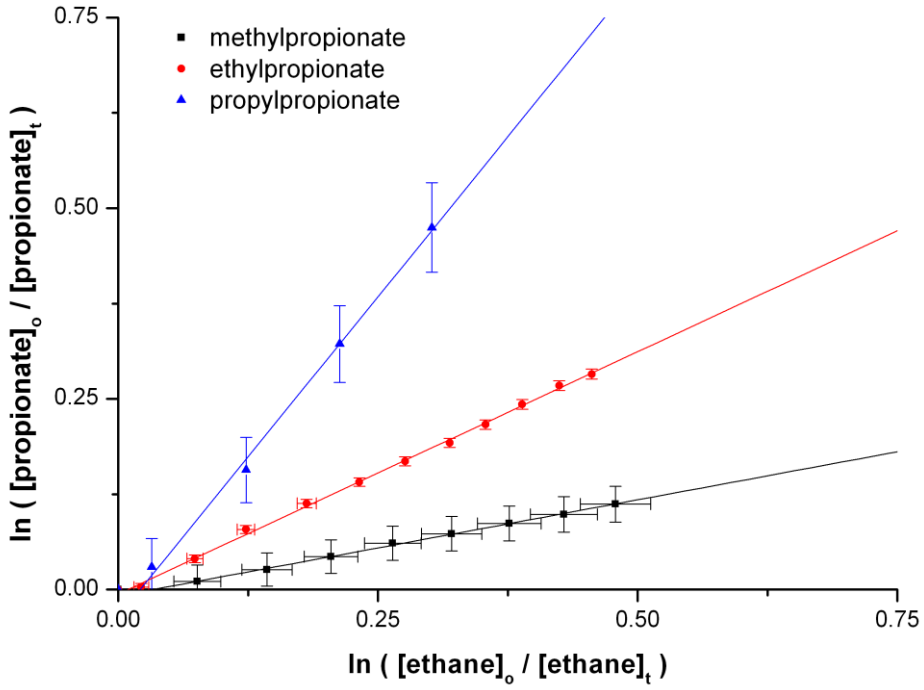

Figure 4.8: Relative rate plots for reaction of Cl atoms with methyl, ethyl and propyl propionates at 298 K and 1000 mbar in U.H.P. nitrogen measured using GC-FID.

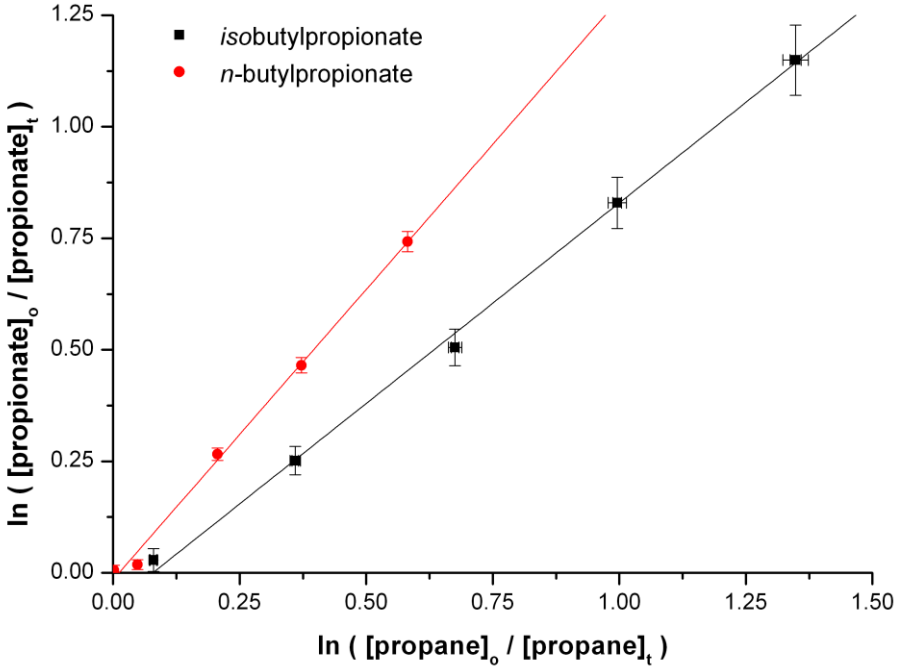

Figure 4.9: Relative rate plots for reaction of Cl atoms with *n*-butyl and *iso*-butyl of propionates at 298 K and 1000 mbar in U.H.P. nitrogen measured using GC-FID.

A comparison of the rate coefficients obtained for Cl atoms with propionates is shown in Table 4.8.

$$k_{\text{methyl propionate}} << k_{\text{ethyl propionate}} < k_{n\text{-propyl propionate}} < k_{i\text{-butyl propionate}} < k_{n\text{-butyl propionate}} \quad \text{(Eq 4.11)}$$

Propionate	$k_{propionate}/k_{reference}$	$k_{propionate}$ (10^{-11} cm^3 molecule^{-1} s^{-1})	Source
Methyl Propionate	0.27 ± 0.02	1.51 ± 0.22	(Cavalli et al., 2000)
	-	1.98 ± 0.26	(Notario et al., 1998)
	0.18 ± 0.43*	1.57 ± 0.23	(Andersen et al., 2011)
	0.265	**1.56 ± 0.36**	**(Schütze et al., 2010)**
	0.25 ± 0.01	**1.49 ± 0.30**	**This work**
Ethyl Propionate	0.50 ± 0.06	3.11 ± 0.35	(Andersen et al., 2012)
	0.63 ± 0.02	3.71 ± 0.11	(Cometto et al., 2009)
	0.64 ± 0.01	**3.74 ± 0.20**	**This work**
Propyl Propionate	1.40 ± 0.02	8.26± 0.12	(Cometto et al., 2009)
	0.61 ± 0.01**	8.50± 0.18	
	1.59 ± 0.02	**9.46 ± 0.91**	**This work**
n-Butyl Propionate	-	15.8 ± 1.30	(Liang et al., 2010)
	1.30 ± 0.05	**17.7 ± 1.28**	**This work**
iso-Butyl Propionate	**0.89 ± 0.02**	**12.2 ± 1.13**	**This work**

Table 4.8: Comparison of rate constants and relative rate ratios of reactions of Cl atoms with a series of propionates using ethane (for methyl, ethyl and propyl) and propane (for butyl) as a reference at 1000 mbar and 293 K (*relative to C_2H_5Cl; **relative to propane).

There is a clear trend as for the acetates reported by Malkin (2010) for the propionates with the rate of these reactions rapidly increasing in rate coefficient with size. The obtained values show a much lower reactivity for methyl propionate compared with the other propionates. Furthermore, one can note that the rate constant increases with the number of CH_x groups in the ester molecule. Excellent agreement is observed for the rate coefficient obtained for methyl and ethyl propionates with recent work by Schütze et al. (2010) and Cometto et al. (2009) respectively. Some discrepancies with the literature were noted for the rate coefficient obtained for propyl propionate which could have been improved by rerunning the experiment another time to obtain more data points on the relative rate plot presented in Figure 4.8. The same may apply for *n*-butyl propionate, which is however within error of the only other literature value by Liang et al. (2010). Iso-butyl propionate has to our best knowledge

never been reported in the literature and the value obtained seems to fit in well with the trend expected from the SARs of these group of compounds, which will be discussed further in the following section.

4.8 Structure activity relationships

The substituent factors specific for the acetates, which have been evaluated previously by Malkin have been determined as follows: F(CO) has been calculated from the rate coefficient $k(Cl + C_2H_5C(O)CH_3) = 3.30 \times 10^{-11}$ cm^3 molecule^{-1} s^{-1} (Albaladejo *et al.*, 2003): $F(CO) = k(Cl + C_2H_5C(O)CH_3)/2k_{prim} = 0.04$. The factor F(C(O)O–) has been derived by applying the SAR method to the reaction $Cl+C_2H_5C(O)OCH_3$ ($k_1 = 1.98 \times 10^{-11}$ cm^3 molecule^{-1} s^{-1}, Notario *et al.* 1998): $F(C(O)O–) = (k_1 - k_{prim}F(CO))/k_{prim} = 0.11$ (Malkin 2010) and using the F(-RC(O)O-) = 0.66 from Xing et al. (2009). The calculated SARs for the acetates and propionates are shown in Table 4.9.

Compound	$k_{expt}/10^{-11}$ **cm^3 molecule^{-1} s^{-1}**	k_{calc} [a]$/ 10^{-11}$ **cm^3 molecule^{-1} s^{-1}**	k_{calc} [b]$/ 10^{-11}$ **cm^3 molecule^{-1} s^{-1}**
Methyl Acetate	0.20 ± 0.04	0.199	0.199
Ethyl Acetate	1.68 ± 0.29[c]	2.922[c]	1.69[c]
Propyl Acetate	6.02 ± 0.41[c]	9.48[c]	6.39[c]
n-Butyl Acetate	15.8 ± 1.31[c]	14.7[c]	12.2[c]
t-Butyl Acetate	1.69 ± 0.15[c]	4.44[c]	1.65[c]
Ethyl Formate	0.95 ± 0.05[c]	2.79[c]	1.56[c]
Methyl Propionate	1.49 ± 0.06	2.00	2.00
Ethyl Propionate	3.74 ± 0.10	5.16	3.93
Propyl Propionate	9.46 ± 0.11	11.6	8.48
n-Butyl Propionate	17.7 ± 5.20	16.8	14.3
i-Butyl Propionate	12.2 ± 2.80	10.2	6.48

Table 4.9: Summary of the rate coefficients for the reaction of Cl atoms with the studied acetates and propionates: comparison between the experimental values and the calculated ones using the SAR method. [a] Calculated using factors F(-CO) and F(-C(O)O-), [b] Calculated using factor F(-C(O)OCH2-), [c] (Malkin 2010).

A comparison with the experimental values obtained in HIRAC seem to indicate a deactivating effect on the carbons in the β-position by the C(O)O- group, which was proposed by Notario et al. (1998), and confirmed by Xing et al. (2009) and Cuevas et al. (2005).

Reasonable agreement is found for the methyl esters but poorer agreement with the remainder although several of the esters lie within the experimental error. This is due to the SAR method not being able to account for this deactivating effect. This is observable from the larger differences when attempting the SAR method using factors F(-CO) and F(-C(O)O-) or factor F(-C(O)OCH2-).Schutze et al. (2010) applied the F(-RC(O)O-) = 0.66 from Xing et al. (2009), F(-C(O)O-CH_3) = 0.04 from Christensen et al. (2000) and the group rate coefficients by Aschmann and Atkinson (1995) for their work on Cl SARs of methyl alkyl esters.

The substituent factor F(C(O)OCH_2–) has been derived from $k_{\text{methylacetate+Cl}}$ (determined in this study) to take into account such an effect: F(C(O)OCH_3–) = (k_2 – k_{prim}F(CO)-k_{sec}F(C(O)O–)F(–CH_3))/k_{prim}= 0.04. The rate coefficients in ethyl, propyl and butyl acetates have been calculated by using this substituent factor, and its values are also shown in Table 4.9. These rate coefficients show better agreement between calculated and experimental results for ethyl and propyl, although butyl acetates do show reasonable agreement using factors F(-CO). A similar trend was observed for the propionates, with poorer better agreement between calculated and experimental using factor F(-C(O)OCH_2-) for methyl, ethyl and propyl and better agreement with using F(-CO) factor for butyl propionates.

Before a final conclusion to the deactivating effect of the C(O)O– group on the carbon groups in the β-position in these aliphatic acetates more Cl atom and acetates reactions should be investigated. Temperature and pressure studies of the reactions may be suitable in helping gain insight into this long range deactivating effect occurring for the ester group.

4.9 Atmospheric implications

The atmospheric lifetime, τ_X of a VOC with respect to chemical reaction with any of the reactive species (NO_3, OH, O_3 and Cl) may be determined by:

$$\tau_X = \frac{1}{k_X[X]} \qquad \text{(Eq 4.12)}$$

where X is NO_3, OH, O_3 or Cl and k_X is the rate of reaction with the VOC, τ_X is defined as the time take for the concentration of the VOC to fall to a fraction 1/e of its initial value.

Atmospheric degradation of VOCs can be initiated by reaction with OH, NO_3, O_3 and Cl, photolysis and/or wet and dry deposition, with the most important loss process thought to be the removal by chemical reaction primarily with the OH radical. Cl atom reactions may be negligible for typical concentrations of Cl atoms in the troposphere compared to OH (Cavalli et al., 2001). However as has been substantiated in the introduction, previously unknown sources of Cl atoms in urban environments have led to a shift in the balance and an increased importance in their reactivity (von Glasow, 2010a).

The lifetimes for aliphatic acetates and propionates are shown in Table 4.10 using rate coefficients obtained for reactions with Cl atom in HIRAC compared to OH rate coefficients obtained from literature. Atmospheric lifetimes are useful in assessing degree of transport and potential regional importance of particular species in the atmosphere.

Compound	k_{Cl} /10^{-11} cm^3 molecule^{-1}s^{-1}	k_{OH}[b] /10^{-12} cm^3 molecule^{-1}s^{-1}	τ_{Cl}[c]/ years	τ_{Cl}[d]/days	τ_{OH}[e]/days
Methyl Acetate	0.20 ± 0.04	0.32 ± 0.03	5.90	56.2	72.3
Ethyl Acetate	1.68 ± 0.29[a]	1.67 ± 0.22	0.72	6.90	13.9
n-Propyl Acetate	6.02 ± 0.41[a]	3.42 ± 0. 26	0.20	1.90	6.80
n-Butyl Acetate	15.8 ± 1.31[a]	5.52 ± 0.51	0.08	0.70	4.20
t-butyl Acetate	1.69 ± 0.15[a]	0.56 ± 0.03[f]	0.72	6.90	41.3
Ethyl Formate	0.95 ± 0.05[a]	0.96 ± 0.04[g]	1.28	12.2	24.0
Methyl Propionate	1.49 ± 0.06	0.93± 0.04[h]	0.82	7.77	6.22
Ethyl Propionate	3.74 ± 0.10	2.10 ± 0.20[i]	0.33	3.09	5.50
Propyl Propionate	9.46 ± 0.11	4.20 ± 0.30[i]	0.13	1.22	2.80
n-Butyl Propionate	17.7 ± 5.20	6.00 ± 0.10[j]	0.07	0.65	0.96
t-butyl Propionate	12.2 ± 2.80	-	0.10	0.95	-

Table 4.10: [a]Comparison of the rate coefficients at room temperature for the reactions of Cl and OH with the studied esters and the corresponding lifetimes.[a] Malkin 2010, [b] El Boudali *et al*., 1996 [c] Platt *et al*., 2004 ([Cl] = 2.6 × 10^3 molecule cm^{-3}) (24 hour global average) [d] Spicer *et al*., 1998 ([Cl] = 1 × 10^5 molecule cm^{-3}, high coastal concentration) [e] Dorn *et al*., 1996 (12 hour day/night cycle, daytime global average [OH] = 1 × 10^6 molecule cm^{-3}), [f]Picquet *et al*., 1998 [g]Szilagyi *et al*., 2004, [h] Cavalli *et al*., 2000, [i] Cometto *et al*., 2009, [j] Liang *et al*., 2010.

As can be noted from the atmospheric lifetimes shown above, Cl lifetimes for the acetates are much longer using normal global concentrations of 2.6 × 10^3 molecule cm^{-3} (Rudolph et al., 1996). This can be significantly shorter if recent findings by Thornton et al. (Thornton et al., 2010) and other authors prove to be a global effect, since this would raise the global concentration contributing to shorter lifetimes of these esters in the atmosphere. In higher Cl concentration areas such as the marine environment however, the processes may compete with the effective loss pathway by OH during the day and by NO_3 during the night (Riedel et al., 2012). This is clearly shown in the propionate lifetimes worked up here, which point towards greater lifetimes for Cl than OH for methyl propionate, and the lifetimes for the remainder of the propionates are also closer to the OH lifetimes than the acetates. In this way, these processes can compete. Also, the shorter lifetimes of these esters due to lower Cl concentrations in the atmosphere would mean that they will be subjected to long range transport, which could lead to further observations in inland urban environments.

5 – Kinetics and mechanistic study of chlorine atom initiated hydrogen abstraction reactions

5.1 Introduction

Oxidation reactions occurring at different sites due to different reactivities, known as site specific reactions, are important propagation reactions of interest in atmospheric and combustion chemistry due to the possibility of their subsequent chemistry from primary, secondary and tertiary radicals formed (Seakins, 2007). These reactions may be exemplified by the reaction of Cl atoms with a simple alkane such as propane. This reaction may proceed *via* either a primary or secondary hydrogen abstraction process:

$$Cl + C_3H_8 \rightarrow n\text{-}C_3H_7 + HCl \quad \text{(R5.1)}$$

$$\rightarrow i\text{-}C_3H_7 + HCl \quad \text{(R5.2)}$$

The primary and secondary radicals are converted into aldehydes and ketones, in air, respectively under high NO_x conditions. This has mentioned previously in chapter 1. These two different classes of compounds have different atmospheric chemistry due to their different reactivities. This completes the first step of their oxidation and eventual removal from the atmosphere. The products originating from such site-specific reactions have historically been studied by gas chromatography or FTIR analysis of the stable end products. As the oxidation process propagates, further products arise from reactions such as the recombination of peroxy radical (RO_2) that may lead to products such as *n*-hexane, 2,3-dimethylbutane and 2-methylpentane. Recombination would only occur in environments where oxygen is not present (such as chamber studies in nitrogen) as oxidation would compete with this process and result in the formation of peroxy radicals. However despite this, recombination reactions still result in mechanistic information relevant to atmospheric chemistry. The propagation stages of oxidation processes lead to great difficulty in obtaining

product branching ratios of the abstraction reaction which cannot be obtained without knowledge of the recombination kinetics, increasing the potential for error. In such complicated systems a direct way of measuring the radicals would be an advantage since it would rule out the need to look at end products of oxidation processes.

Hydrogen abstraction by chlorine atoms on hydrocarbons is an important elementary free-radical process and which leads to long-chain substitution processes when chlorine transfer takes place, or in presence of oxygen, leading to oxidation.

$$Cl + R_3CH \rightarrow R_3C + HCl \quad \text{(R5.3)}$$
$$R_3C + Cl_2 \rightarrow R_3CCl + Cl \quad \text{(R5.4)}$$
$$R_3C + O_2 \rightarrow R_3COO \rightarrow\rightarrow\rightarrow \quad \text{(R5.5)}$$

Despite a long history of relative reactivity and regioselectivity studies of these systems both in solution (Poutsma, 1968, Miller and Walling, 1957) and in the gas phase (Chiltz et al., 1963a, Chiltz et al., 1963b, Johnston and Goldfinger, 1962), a renewed interest in their absolute reactivity and gas phase kinetics in particular has resulted in a revisiting of these reactions. This has been in part due to increased importance in VOC oxidation processes in the atmosphere (Poutsma, 2013). For this reason, the first section of this chapter investigates reactions of Cl atoms with *n*-butane, *iso*-butane, *n*-pentane and *iso*-pentane studied experimentally in HIRAC. Another motivation for carrying out these experiments was to refine empirical approaches such as structure activity relationships used to determine the reactivity of Cl atoms towards hydrocarbons (Aschmann and Atkinson, 1995). From previous work the rate of hydrogen abstraction from a methyl group was found to not be influenced by neighbouring groups (Tyndall et al., 1997).

Relative rate experiments were carried out in HIRAC over a temperature range of ~220 – 320 K at atmospheric pressure and both FTIR and GC-FID detection were used concurrently whenever possible. The advantage of having two simultaneous measurements is the ability to compare both analytical techniques coupled to HIRAC allowing an assessment of the instrumental precision and accuracy (Malkin et al., 2010). Branching ratios have also been obtained for *n*-butane and *iso*-butane products seen on both GC-FID and FTIR.

5.2 Hydrogen abstraction of Cl atom reactions with butanes and pentanes

5.2.1 Introduction

The site specificity of chlorine reactions with alkanes have been shown to be temperature dependent (Sarzynski and Sztuba, 2002, Qian et al., 2001, Tyndall et al., 1997, Choi et al., 2006). These results also provide a good test bed for comparison with the predictions of various structure activity relationships (SAR) (Aschmann and Atkinson, 2013, Aschmann and Atkinson, 1995, Hooshiyar and Niki, 1995). An increasing proportion of primary abstraction with increasing temperature has been observed in several of these studies; however the temperature dependence of the rate coefficient itself is known to influence this site specificity. In fact, it is also reported that Cl reactions are either temperature independent such as the reaction with propane, or temperature dependent such as the reaction with *iso*-butane (Seakins, 2007). This would imply that the rate coefficients for the abstraction of secondary or tertiary hydrogen would be expected to have a relatively strong negative activation energy, however theoretical calculations show no effective barriers along any of the potential energy surfaces for C-H abstraction reactions (Fernandez-Ramos et al., 2003).

The importance of chlorine chemistry in the atmosphere has already been highlighted in the previous chapter. This chapter will investigate Cl atom hydrogen abstraction reactions further, identifying through product ratios whether these processes are selective for different volatile organic compounds. From a survey of the literature it was found that very few report detailed studies of hydrogen abstraction reactions from individual carbon atoms (Sarzynski and Sztuba, 2002). All these processes proceed through hydrogen abstractions yielding a hydrocarbon radical and HCl as is shown in R5.7 (Hickson et al., 2010, Taatjes, 1999). The kinetics and mechanisms of alkane C-H abstraction reactions with Cl atoms to produce HCl have been extensively studied and reviewed (Atkinson et al., 1997, Atkinson and Aschmann, 1985, Atkinson, 1990a).

$Cl_2 + h\upsilon\ (< 320\ nm) \rightarrow 2\ Cl$ (R5.6)

$RH + Cl \rightarrow HCl + R$ (R5.7)

Ratios of butanes and pentanes measured *in-situ* in the Arctic during springtime have demonstrated the importance of these volatile organic compounds in understanding the influence of Cl atoms in these environments (Jobson et al., 1994, Kieser et al., 1993, Cavender et al., 2008, Dhanya et al., 2012). An additional decrease in these hydrocarbons was correlated with Cl atom chemistry, and provided evidence for halogen chemistry importance during ozone depletion episodes in the Polar regions (Jobson et al., 1994, Cavender et al., 2008, Gilman et al., 2010). This also increases the importance to understand the kinetics and mechanisms of these processes at low tropospheric temperatures (~200 – 250 K). The significance of these studies is exemplified by oxidation of *n*-butane in air to produce a peroxyl radical:

$CH_3CH_2CH_2CH_3 + (OH\ or\ Cl) + O_2 \rightarrow CH_3CH_2CH(OO)CH_3 + (H_2O\ or\ HCl)$ (R5.8)

The peroxy radical can react with other peroxy radicals (R5.11 – R5.13) or react with NO (R5.9) or HO_2 (R5.10) to form methyl ethyl ketone and other products (Cavender et al., 2008). This sequence of reactions is shown in R5.9 – 5.14:

$CH_3CH_3CH(OO)CH_3 + NO \rightarrow CH_3CH_2CHOCH_3 + NO_2$ (R5.9)

$CH_3CH_2CH(OO)CH_3 + HO_2 \rightarrow CH_3CH_2CHOOHCH_3 + O_2$ (R5.10)

$CH_3CH_2CH(OO)CH_3 + RO_2 \rightarrow CH_3CH_2COCH_3 + ROH + O_2$ (R5.11)

$CH_3CH_2CH(OO)CH_3 + RO_2 \rightarrow CH_3CH_2CHOHCH_3 + RCOR' + O_2$ (R5.12)

$CH_3CH_2CH(OO)CH_3 + RO_2 \rightarrow CH_3CH_2CHOCH_3 + RO + O_2$ (R5.13)

$CH_3CH_2CHOCH_3 + O_2 \rightarrow CH_3CH_2COCH_3 + HO_2$ (R5.14)

The rate of *n*-butane consumption for [Cl]/[OH] >0.01 will be dominated by Cl atoms in Arctic regions since at these temperatures (typically around 245 K in Arctic spring) (Cavender et al., 2008), the rate coefficient for reactions of *n*-butane and products with OH radicals are very similar, differing only by a factor of 1.4 (Donahue et al., 1998), while the rate constant for Cl atoms differs by a factor of 7.8 for *n*-butane (Tyndall et al., 1997). This means the ratio of [MEK]/[*n*-butane] can be used as a useful indicator of the [Cl]/[OH] balance of these atmospheric oxidation processes under certain conditions. This balance can also be monitored by [*iso*-butane]/[*n*-butane] ratios since this ratio is unaffected by OH chemistry but is by Cl atom chemistry. At 245 K the rates of reaction with OH only differ by 1.006 (Donahue et al., 1998) while reactions with Cl atoms at the same temperature differ by a factor

of 1.65 with values of 1.30 and 2.15 × 10^{-10} molecule^{-1}s^{-1}cm^3 for *iso*-butane and *n*-butane respectively (Hooshiyar and Niki, 1995, Tyndall et al., 1997). Therefore an increase in this ratio can be ascribed to rapid Cl atom processing of [*n*-butane], and this ratio, together with [MEK]/[*n*-butane] has been used a marker in several field campaigns in the Arctic to account for the Cl atom and OH oxidation processes occurring in the polar regions (Cavender et al., 2008).

Butanes and pentanes are commonly present in the troposphere in concentrations ranging from 0 – 0.5 ppm (Fehnsenfeld et al, 1992; Singh and Zimmerman, 1992). The main sources of alkanes in the troposphere are primarily industrial processes including fossil fuel production (Atkinson and Arey, 2003b). Depending on their atmospheric lifetimes, these hydrocarbon emissions can disperse and are primarily removed based on their different rates of reaction with oxidants such as OH and Cl atoms in the troposphere. Significant inferred Cl atom concentrations in marine boundary layer, polar regions and more recently in urban mainland continental regions have shifted the balance of the main oxidants (OH and Cl) responsible for the removal of these hydrocarbons in the troposphere, and their atmospheric lifetimes. These Cl atoms represent a significant sink and these uncertainties in sources of Cl atoms (primarily stored in the atmosphere as HOCl and $ClNO_2$) have led to Cl atom chemistry to be revisited (Thornton et al., 2010, von Glasow, 2010b, von Glasow, 2010a).

Numerous room temperature relative rate ratios have been reported for *n*-butane and *iso*-butane reactions with Cl atoms, differing by 20% between different authors (Wallington et al. 1988; Atkinson and Aschmann 1985) as has been reported by both Tyndall et al. and Beichert et al. (Tyndall et al., 1997, Stutz et al., 1998, Beichert et al., 1995) and shown in Table 5.1. Some Cl atom reactions with butanes have been reported over high temperature ranges (Pilgrim et al., 1997) but only few have been performed over low temperatures (Hickson et al., 2010). Kinetic data for Cl reactions with *n*-pentane and *iso*-pentane at 298 K were found to be scarcely mentioned in the literature (Qian et al., 2001) and to our knowledge no previous temperature dependent studies have been reported for these alkanes. Pentanes as well as butanes have been monitored in several campaigns (Yates et al., 2010, Hellen et al., 2012, Li et al., 2005, Pozzer et al., 2010, Hopkins et al., 2002).

5.2.2 Experimental

Cl atom experiments were carried out using the same experimental setup and procedure described for relative rate experiments in Section 4.2.1. Chlorine atoms were generated by UV irradiation of mixtures of hydrocarbons and chlorine. The photolysis rate was controlled by switching all eight photolysis lamps on and off every ~100s. This has been previously found to yield a [Cl] concentration of around 7×10^7 molecule cm^{-3} in HIRAC.

Experiments were all carried out in laboratory grade nitrogen. HIRAC was first filled to ~970 mbar with departmental nitrogen and the hydrocarbon (~2 - 5 ppm), chlorine (~20 - 40 ppm) and reference compound (~2 - 5 ppm) were added after and 5 minutes were allowed for adequate mixing in the chambers. The chemicals used in these experiments were acquired from the following commercial sources: ethane (Sigma Aldrich, 98%), *n*-pentane, *neo*-pentane, *iso*-pentane, *n*-butane, *iso*-butane (Sigma Aldrich, 99%) and chlorine (Sigma Aldrich, 99.5%). All the above gases were used as obtained from the supplier, while *n*-pentane and *iso*-pentane liquids were prepared in a vacuum line and purified prior to delivery into the chamber by successive freeze-pump-thaw cycles to remove any impurities that may cause interferences in the spectroscopic and chromatographic analyses.

An Agilent HP 6890 GC-FID (described in chapter 2) with a CP-Sil-5CB 100% dimethylpolysiloxane column (50 m length, 0.25 μm film and 0.32 mm internal diameter) was used for all experiments. The GC column was maintained at a temperature of 300 K for all experiments which was about the same as the boiling point of the most volatile hydrocarbon used in these experiments. HIRAC's multipass FTIR described in chapter 2 was also used for both the butanes and pentanes to further investigate the mechanism behind these reactions and compare results obtained with gas chromatographic end product analysis. FTIR analysis was however only carried out for the butanes given the higher complexity (larger number of products) for the analysis of the pentanes.

Rate coefficients were measured for the reaction of *n*-butane, *iso*-butane, *n*-pentane, *neo*-pentane and *iso*-pentane with Cl, using ethane as a reference compound for all experiments. This reference compound's reaction with Cl atoms (7.05×10^{-11}

exp(-60/T) cm^3 $molecule^{-1}$ s^{-1}) has been reviewed by IUPAC (Atkinson et al., 2006a) and has also been used in previous studies as a reference for similar systems (Tyndall et al., 1997, Sarzynski and Sztuba, 2002). The reactions investigated are shown from R5.15 – 5.21:

$Cl + CH_4 \rightarrow$ products (R5.15)
$Cl + C_2H_6 \rightarrow$ products (R5.16)
$Cl + n\text{-}C_4H_{10} \rightarrow$ products (R5.17)
$Cl + i\text{-}C_4H_{10} \rightarrow$ products (R5.18)
$Cl + n\text{-}C_5H_{12} \rightarrow$ products (R5.19)
$Cl + i\text{-}C_5H_{12} \rightarrow$ products (R5.20)
$Cl + neo\text{-}C_5H_{12} \rightarrow$ products (R5.21)

Methane was used as an internal standard in all experiments (R5.15). The rate constant for reaction of methane with Cl atoms is $k < 10^{13}$ cm^3 $molecule^{-1}$ s^{-1} (Atkinson et al., 2001), over three orders of magnitude slower than the expected reaction of Cl atoms with butanes and pentanes. The methane can therefore be considered to decrease in concentration in the reaction chamber only through dilution. Any significant changes in methane during the experiment would account for any dilution effects, and this has been a useful indicator in several relative rate chamber studies (Atkinson, 1990a). Rate coefficients were determined using the relative rate technique which monitors the relative decay of an organic and a reference compound in the presence of a reactive species.

Experiments were carried out in the HIRAC chamber at 292 ± 3 K and at 1000 mbar in departmental (laboratory grade) nitrogen. The same UV B medical therapy lamps used previously for Cl atom experiments with oxygenates in HIRAC were used for irradiation of Cl_2, and four stainless steel fans ensured mixing of reactants within 60 s of their introduction into the chamber. Provided the alkanes and the reference compound used are only removed by Cl atoms:

Cl + alkane → products (R5.22)
Cl + ethane → products (R5.23)

then:

$$\ln\left(\frac{[\text{alkane}]_0}{[\text{alkane}]_t}\right) = \left(\frac{k}{k_{\text{ref}}}\right) \ln\left(\frac{[\text{ethane}]_0}{[\text{ethane}]_t}\right) \quad \text{(Eq 5.1)}$$

The ratio $k/k_{ref,}$ obtained experimentally is used in order to derive the relative rate coefficients using the known rate coefficient for the reference compound as has been already elaborated in previous chapters.

5.2.3 Kinetics of Cl atoms with a series of butanes and pentanes

This section focuses on the results obtained for *n*-butane, *iso*-butane, *n*-pentane, *iso*-pentane and *neo*-pentane reactions with Cl atoms in the HIRAC chamber. Table 5.1 shows a summary of the results obtained for the reactions of chlorine atoms with butanes and pentanes compared with their respective literature values (IUPAC recommendations were only available for *n*-butane and *iso*-butane). Both FTIR and GC measurements were reported for butanes, however FTIR analysis was not possible for the pentanes given the greater number of products and the difficulty in obtaining suitable reference spectra for their analysis using the Quant2 software developed Fred Winiberg (School of Chemistry, University of Leeds). This software is briefly described in Section 5.3.2.

A comparison of the rate coefficients obtained in HIRAC for the GC and FTIR measurements are within error for both *n*-butane and *iso*-butane. Results obtained for all hydrocarbons are within good agreement (to within ~10%) of the literature values. Experimental ratios obtained are placed on an absolute basis using a rate coefficient for Cl atoms with ethane of $k = (5.80 \pm 0.29) \times 10^{-11} cm^3\ molecule^{-1}\ s^{-1}$ (Atkinson et al., 2006a). The errors quoted are the cumulative of the systematic errors from the relative rate plot obtained through a linear regression of the data obtained from plotting the data and corresponding errors in Regres2 software (Brauers and Finlayson-Pitts, 1997) and the error reported for the reference (Atkinson et al., 2006a). High accuracy for the majority of relative rate plots ($r^2 \geq 0.99$) ensures the reliability of the data obtained and the relative rate method used in HIRAC.

Hydrocarbon	k/k_{ref}(GC)	k/k_{ref} (FTIR)	k / 10^{-10} cm^3 molecule^{-1} s^{-1}			Reference
			GC	FTIR	Literature	
n-butane	3.32 ± 0.04	3.23 ± 0.05	1.95 ± 0.25	1.90 ± 0.31	2.05 ± 0.10	(Atkinson et al., 2006a)
iso-butane	2.35 ± 0.03	2.52± 0.03	1.38 ± 0.18	1.47 ± 0.25	1.41 ± 0.08	(Atkinson et al., 2006a)
n-pentane	5.11 ± 0.05	-	2.96 ± 0.31	-	2.83 ± 0.34	(Wallington et al., 1988c)[a]
					2.35 ± 0.12	(Qian et al., 2001)[b]
iso-pentane	3.88 ± 0.04	-	2.25 ± 0.24	-	1.93 ± 0.08	(Anderson et al., 2006)[b]
					2.08 ± 0.14	(Qian et al., 2001)[a]
neo-pentane	1.50 ± 0.06	-	0.87 ± 0.04	-	1.11 ± 0.13	(Atkinson and Aschmann, 1985)[a]
					0.98 ± 0.04	(Qian et al., 2001)[b]

Table 5.1: Relative rate ratios and coefficients for Cl atom reactions with butanes and pentanes at 292 ± 3 K and 1000 mbar in the HIRAC chamber ([a] relative rate study, [b]absolute rate study).

All experiments in HIRAC were repeated at least three times to confirm repeatability of the data obtained at room temperature, same as was reported in Tyndall et al.'s work. Better precision was found to be obtained from GC over FTIR measurements as had also been noted previously by Tyndall et al. (Tyndall et al., 1997), although relative rate coefficients obtained using both these techniques are within experimental error of literature values. It must be noted that there were more analysed data sets for GC measurements than FTIR owing to the unavailability of the FTIR mirrors for a short duration of the study.

Figure 5.1 shows the good agreement obtained between the GC and FTIR relative rates obtained for *n*-butane in HIRAC. These results further validate the suitability of this method in HIRAC and validate the integration method used for the FTIR.

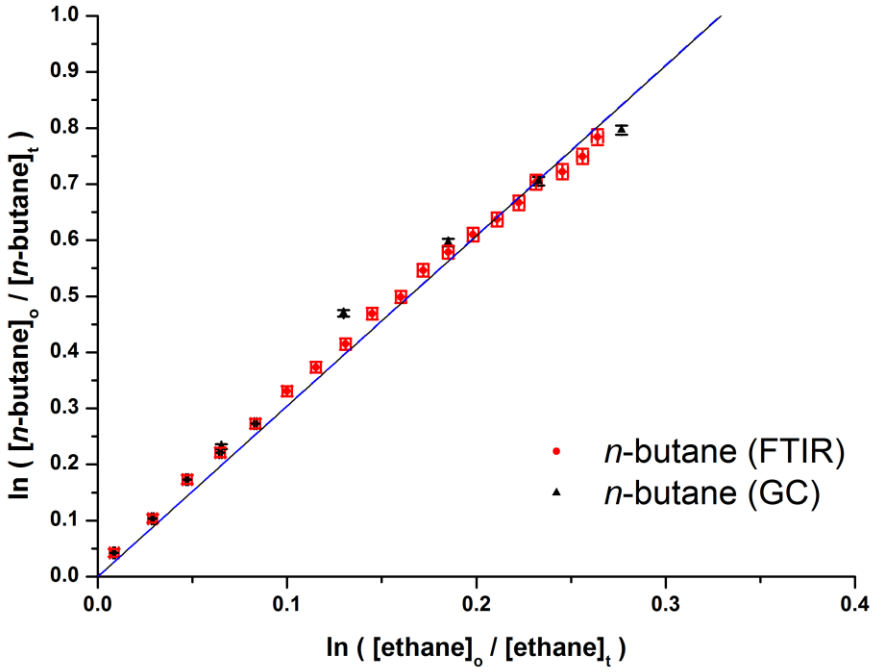

Figure 5.1: A comparison of relative rate plots obtained for reaction of Cl atoms with n-butane in HIRAC at 1000 mbar and 292 ± 3 K. Error bars represent 1σ.

$k_{n\text{-butane}}/k_{ref}$ ratios of 3.32 ± 0.04 and 3.23 ± 0.05 for GC and FTIR measurements respectively in HIRAC are within experimental error of each other and within similar agreement as Tyndall et al.'s work (3.66 ± 0.10 (GC) and 3.85 ± 0.27 (FTIR)). The latter FTIR result by Tyndall et al. was however not obtained directly due to spectral overlap between the C_2H_6 and *n*-C_4H_{10}, and was instead derived by combining different relative rate ratios measured during the same experiment (Tyndall et al., 1997).

All plots shown in Figures 5.1 and 5.2 are linear with the intercepts at the origin, within the experimental error limits, suggesting that the present work is free from complications due to secondary chemistry. Rate coefficients obtained are generally within good agreement (to within ~10%), except for *neo*-pentane (to within ~15%). The experiments involving *neo*-pentane were carried out at a later stage in order to complete the full series of pentanes and butanes investigated.

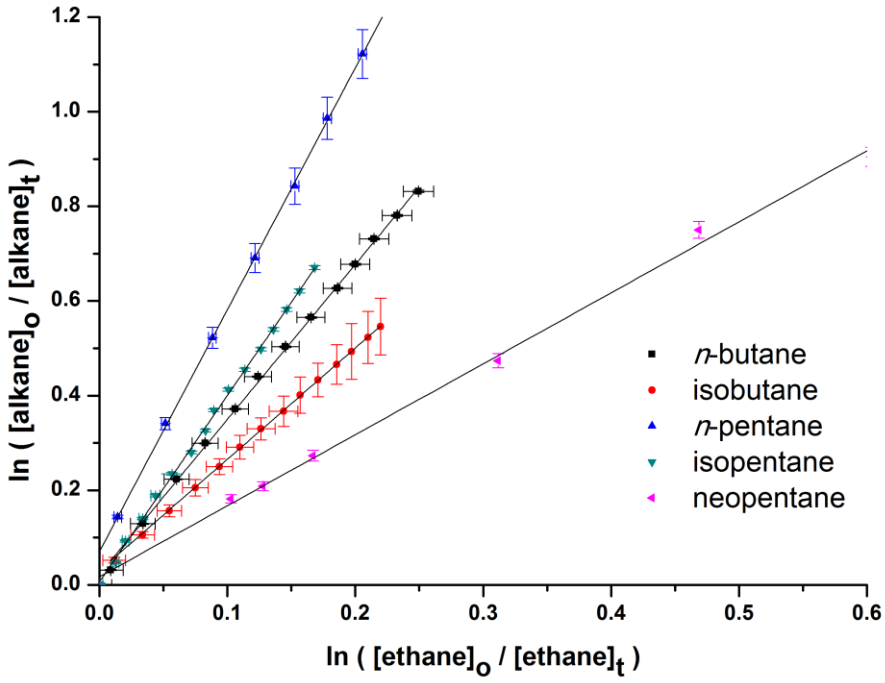

Figure 5.2: Relative rate results using GC-FID measurements obtained for reaction of Cl atoms with butanes and pentanes in HIRAC at 1000 mbar and 292 ± 3 K. Error bars represent 1σ.

For the reaction of Cl atoms with alkanes, structure-reactivity relationships have been proposed which consider H-atom abstraction from $–CH_3$, $-CH_2-$ and >CH- groups (k_{prim}, k_{sec} and k_{tert} respectively), with substituent factors to take into account the influence of neighbouring primary, secondary and tertiary groups (Aschmann and Atkinson 2012). The order of reactivity for butanes and pentanes agreed well with the literature (*iso*-butane < *n*-butane < *iso*-pentane < *n*-pentane < *neo*-pentane). The reactivity of branched alkanes is less than straight chain alkanes. Results for *n*-butane and *iso*-butane were analysed using both GC and FTIR data, and the rate coefficient measurements for both were within error of each other (*n*-butane: $(1.90 \pm 0.08) \times 10^{-10}$ (GC), $1.76 \pm 0.10 \times 10^{-10}$ (FTIR); *iso*-butane: $1.36 \pm 0.05 \times 10^{-10}$ (GC), $1.20 \pm 0.10 \times 10^{-10}$ (FTIR) cm^3 $molecule^{-1}$ s^{-1}), which confirms the suitability of the relative rate method used in HIRAC for the temperature dependence and product studies to follow.

5.2.4 Temperature dependence of Cl atom reactions with butanes and pentanes

Cl atom abstraction reactions with both ethane and propane are known to exhibit prominent curvature in their Arrhenius plots due to a temperature dependence of the Arrhenius parameters (Lewis et al., 1980); this has been backed by transition state analysis (Taatjes, 1999). As has already been stressed, there have been limited studies regarding the temperature dependence of larger hydrocarbon reactions with Cl atoms, particularly pentanes. For the temperature dependent study performed for *n*- and *iso*- butanes and pentanes, the main goal was to further confirm the suitability of the recently installed temperature control system in HIRAC as well as obtain new important information on the temperature dependence of pentanes over tropospheric conditions in light of recent use of pentanes as tracers for Cl atom chemistry in the Arctic (Dhanya, Pushpa and Naik 2012).

The suitability of HIRAC to carry out such experiments following the setting up and validation of a new temperature control system described in chapter 3 meant these reactions could be investigated in greater depth in our atmospheric simulation chamber. The precision of the relative rate method demonstrated from previous results obtained for oxygenated hydrocarbons in chapter 4 confirm the suitability of this method to carry out such experiments.

Table 5.2 shows the relative rate results obtained in HIRAC for the *n*- and *iso*- butanes and pentanes. Plots of the Arrhenius relationships of these rate coefficients with temperature are displayed in Figures 5.3 and 5.4 for butanes and pentanes respectively, with the Arrhenius parameters and activation energies being quoted in Table 5.3 for each of the four hydrocarbons investigated in this study.

Hydrocarbon	**Temperature/ ± 3 K**	***Number of runs***	***k*/ k_{ref}**	***k* (T)/ 10^{-10} cm^3 $molecule^{-1}$ s^{-1}**
n-butane	320	3	3.61 ± 0.03	2.19 ± 0.10
	292	3	3.94 ± 0.04	2.32 ± 0.11
	271	3	3.92 ± 0.04	2.25 ± 0.10
	251	3	4.91 ± 0.05	2.74 ± 0.12
	236	3	4.61 ± 0.04	2.50 ± 0.11
	223	2	4.07 ± 0.07	2.34 ± 0.14
iso-butane	320	3	2.26 ± 0.02	1.37 ± 0.16
	292	3	2.53 ± 0.02	1.49 ± 0.16
	271	3	2.88 ± 0.02	1.65 ± 0.16
	251	3	2.73 ± 0.03	1.52 ± 0.18
	236	3	2.69 ± 0.02	1.46 ± 0.14
	222	2	2.99 ± 0.02	1.58 ± 0.14
n-pentane	320	3	5.08 ± 0.06	3.09 ± 0.17
	292	3	5.08 ± 0.06	2.99 ± 0.17
	271	3	5.77 ± 0.07	3.31 ± 0.19
	251	3	5.28 ± 0.06	2.94 ± 0.17
	236	3	5.54 ± 0.07	3.01 ± 0.17
	220	2	5.07 ± 0.06	2.68 ± 0.16
iso-pentane	320	3	3.63 ± 0.03	2.21 ± 0.11
	292	3	3.88 ± 0.04	2.28 ± 0.12
	271	3	4.03 ± 0.05	2.31 ± 0.12
	251	3	4.57 ± 0.04	2.55 ± 0.11
	236	3	4.81 ± 0.04	2.61 ± 0.12
	220	2	5.11 ± 0.05	2.69 ± 0.14

Table 5.2: Experimentally determined relative rate ratios (*k*/ k_{ref}) and relative rate coefficients (*k* (T)/ 10^{-10} cm^3 $molecule^{-1}$ s^{-1}) for *n*- and *iso*- butane and pentane over a temperature range of 220 – 320 K and at 1000 mbar in HIRAC. Errors represent averaged results from GC/FTIR measurements for three separate runs and averaged errors to standard deviation of 1σ.

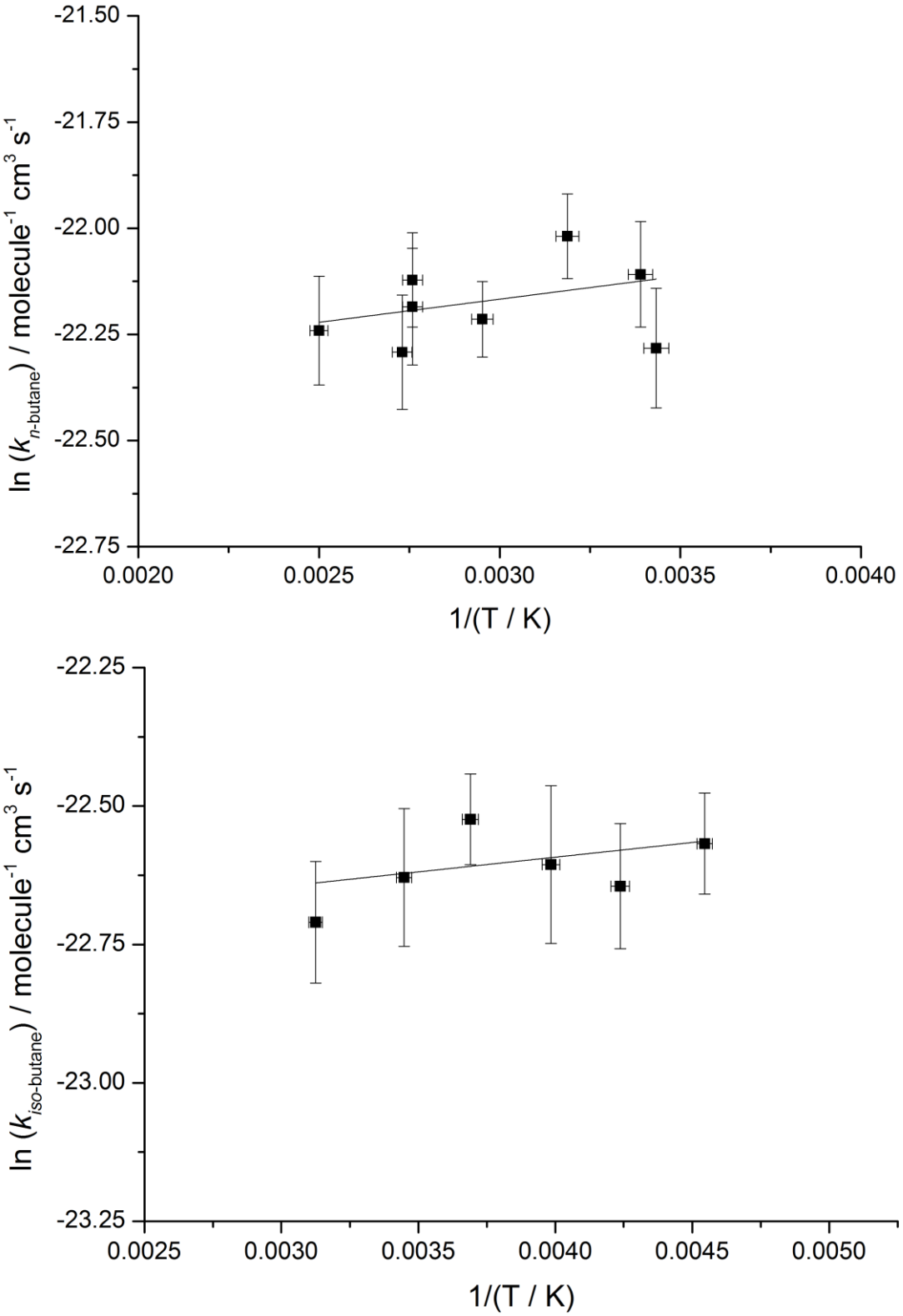

Figure 5.3: Arrhenius plots for *n*-butane and *iso*-butane at 1000 mbar and over a temperature range of 220 - 320 K. Error bars represent 1σ.

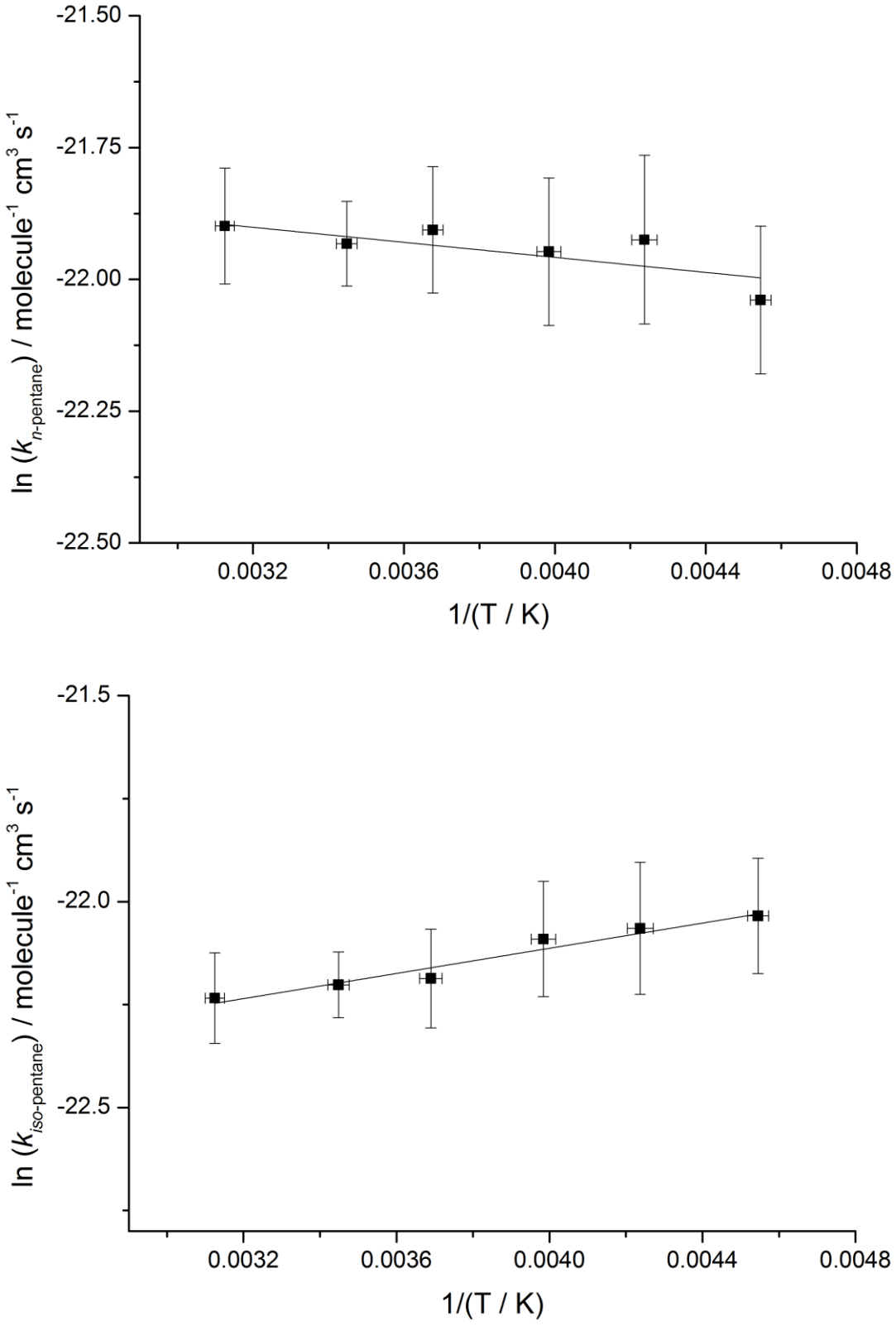

Figure 5.4: Arrhenius plots for *n*-pentane and *iso*-pentane at 1000 mbar and over a temperature range of 220 - 320 K. Error bars represent 1σ.

Table 5.3 shows the Arrhenius parameters obtained in HIRAC for these reactions compared with literature values.

	A (10^{11} cm^3 molecule^{-1} s^{-1})	**E_a/R (K)**	**Reference**
n-butane	21.5 ± 1.0	12 ± 26	(Lewis et al., 1980)
	21.4 ± 1.0	140 ± 140	(Tyndall et al., 1997)
	22.8 ± 2.9	151.3 ± 94.5	(Sarzynski and Sztuba, 2002)
	22.5 ± 0.4	109 ± 118	This work
iso-butane	22.5 ± 3.2	56 ± 53	(Sarzynski and Sztuba, 2002)
	22.8 ± 0.2	53.2 ± 59.0	This work
n-pentane	21.7 ± 0.1	-71.3 ± 28.0	This work
iso-pentane	22.7 ± 0.1	153.9 ± 17.0	This work

Table 5.3: A summary of Arrhenius parameters for *n*- and *iso*- butane and pentane obtained over a temperature range of 220 – 320 K and at 1000 mbar in HIRAC. Error bars represent 1σ.

The Arrhenius plots shown in Figure 5.3 for both butanes show slight positive gradients *i.e.* negative temperature dependence. The reaction of Cl atoms with *n*-butane shows a slight negative temperature dependence of the overall rate coefficients however the large error bars for these results, in particular from the large uncertainty in the lower temperature rate coefficient (223 K), would outweigh this and support the essentially zero activation energy reported first by Lewis et al. (1980) and supported by other authors (Tyndall et al., 1997, Sarzynski and Sztuba, 2002). Excluding this anomalous result at 223 K, the relationship exhibits clear temperature independence for this reaction. Good agreement was observed for the Arrhenius parameters reported in Table 5.3 for *n*-butane with the study by Sarzynski and Sztuba (2002), and other work by Lewis et al. (1980) and Tyndall et al. (1997) were also within error of the values obtained in HIRAC.

In the case of the reaction of Cl atoms with *iso*-butane, a similar outcome as that for *n*-butane was observed, with a slight temperature curvature which is not so definite given the large error bars associated with the result. The positive gradient of the Arrhenius plot in Figure 5.3 is more defined than that for *n*-butane, however the errors associated with the activation energy value outweigh the result. According to Sarzynski and Sztuba (2002), this reaction was found to have significant temperature dependence in the individual hydrogen abstraction pathways available (*i.e.* primary and tertiary abstractions). Sarzynski and Sztuba reported significant negative temperature dependence for the tertiary abstraction processes and slight positive

temperature dependence for the primary abstraction process, giving overall temperature independence over the temperature range for their measurements (298 – 467 K). Excellent agreement was obtained for the E_a/R value obtained in HIRAC of 53 ± 59 K with the result reported by Sarzynski and Sztuba of 56 ± 53 K.

The reaction of Cl atoms with the pentanes showed more defined temperature dependences than the butanes. The results obtained for *iso*-pentane showed definite slight negative temperature dependence, while definite slight positive temperature dependence was observed for the reaction with *n*-pentane. A positive E_a/R of 153.9 ± 17.0 K was obtained for the reaction with *iso*-pentane while a negative E_a/R of -71 ± 28 K was obtained for *n*-pentane. This indicates that temperature dependence is influenced strongly by the structure of these pentanes. As has been reported by Sarzynski and Sztuba for *n*-butane and *iso*-butane, the secondary and tertiary hydrogen atom abstractions have a more negative temperature dependence when compared to primary hydrogen abstractions. Unfortunately the chloropentanes could not be analysed in this study, however the temperature dependence of the chlorobutane product formation is further interpreted in Section 5.4.3 and 5.4.4.

The implications of these findings can be significant in field investigations that used pentanes as a tracer for Cl atom concentrations in the atmosphere (Boundries and Bottenheim, 2000; Jobson et al., 1994), as depending on the temperature at which the monitoring was carried out the results for *iso*-pentane reactivity could have changed from anything between 5 – 25% based on the results obtained in HIRAC.

5.3 Product study and branching ratios of Cl reactions with *n*-butane and *iso*-butane

5.3.1 Introduction

Product branching ratios have long been known to be important in determining the overall rate of a reaction through the measurement of rates of product formations in multichannel reactions (Seakins, 2007). Such investigations have found practical applications in both atmospheric and combustion modelling, as well as in the fundamental understanding of the mechanisms of such chemical processes.

Hydrogen atom abstraction from reactions of Cl atoms with hydrocarbons are known to form HCl and this has been used by several authors to derive kinetic data for Cl atom reactions with hydrocarbons (Taatjes, 1999, Choi et al., 2006). Several authors have determined the contribution of the abstraction of primary and secondary or tertiary hydrogen atoms from *n*-butane and *iso*-butane by Cl atom attack under room temperature conditions. Two of these studies used an indirect relative rate approach similar to the experiments performed in HIRAC (Tyndall et al., 1997, Sarzynski and Sztuba, 2002), while other authors have used direct flash photolysis studies (Choi et al., 2006) and theoretical calculations based on structure activity relationships (Atkinson, 1987).

Temperature dependence of the chlorobutane product yields has been previously reported by Tyndall et al. (1997) Choi et al. (2006) and Sarzynski and Sztuba (2002) but has to our knowledge not been investigated under lower tropospheric temperatures (220 – 290 K) for both *n*-butane and *iso*-butane. The only reported temperature dependent product yields for *iso*-butane were reported over a temperature range of 298 – 470 K by Sarzynski and Sztuba (2002) and at 195 and 295 K by Choi et al. (2006). The latter investigations were direct measurements of the HCl product by IR diode laser absorption, using normal and selectively deuterated systems to determine the ratios (Choi et al., 2006). Sarzynski and Sztuba reported only gas chromatographic end product analysis while HIRAC measurements are reported here using both GC and FTIR analysis. The results obtained in HIRAC are the first low temperature site selective rate coefficients of these reactions.

Seakins and Choi concluded that as temperature increased abstraction from the primary position of the *iso*-butane increased. Owing to the limited data on all aspects of Cl atom C-H abstractions from hydrocarbons at low temperatures, this study in HIRAC was also aimed at examining further the hydrogen abstraction of butanes over this tropospherically relevant temperature range. Data were obtained using both GC and FTIR and experiments were carried out in HIRAC over a temperature range of 220 – 320K.

5.3.2 Product analysis

A Cl atom hydrogen abstraction rate coefficient for alkanes has been obtained for abstraction from primary, secondary and tertiary C-H groups. FTIR spectra for the experimental chlorobutane products were analysed using an FTIR software tool programmed on LabView. Quant2 has been developed by Fred Winiberg (School of Chemistry, University of Leeds) in order to analyse multi-component FTIR spectra obtained during experiments carried out in HIRAC using the long-path FTIR system described in Chapter 2.

Gas phase FTIR spectrometry has been widely used in atmospheric chambers as it is a fast and robust method of obtaining kinetic and mechanistic data of relevance to atmospheric chemistry (Barnes et al., 1983, Barnes et al., 1994, Cavalli et al., 2002, Blanco et al., 2010, Oksdath-Mansilla et al., 2009, Schutze et al., 2010b). The inherent problem with obtaining FTIR spectra during a reaction in HIRAC lies in the difficulty to analyse these multi-component spectra owing to many species absorbing in the same IR regions of the spectrum. A brief overview of this quantitative analysis technique as well as all the requirements necessary for the software is detailed in this section.

The Beer-Lambert law shows that a given species' absorption, *A*, is directly proportional to the concentration, [*c*], assuming a constant path length, *l*, and absorption cross section, σ.

$$A = \ln\left(\frac{I}{I_0}\right) = \sigma [c]\, l \qquad \text{(Eq 5.2)}$$

Where I and I_o are the intensity of light before and after the sample respectively. It is this linear relationship that is used in order to quantify FTIR spectra using a number of different methods. These convoluted (or overlapping) spectra obtained in HIRAC were analysed using a spectral subtraction method. This latter method can be utilised for separation of multivariate spectra by the determination of scaling factors rather than using the integration of peak areas or heights.

The quality and accuracy of the quantitative data are dependent upon several factors. A disadvantage of this method is that beyond binary and tertiary systems, subsequent subtractions are difficult to assess, owing to the accumulation of systematic errors in the method. This will often result in a distorted or non-zero residual. This method is dependent upon the quality of reference and sample spectra used and accurate concentrations of the sample and reference components in order to accurately analyse the convoluted spectra. The wrong choice of spectra for this subtraction method would result in inaccuracies in the quantitative analysis of sample spectra (Griffith, 1996).

Reference spectra were acquired by introducing known volumes of reference compounds into HIRAC under similar conditions as the experiments carried out. All primary products where obtained from commercial sources for the purpose of recording reference spectra in HIRAC for analysis using Quant2. Unfortunately this was not possible for the pentanes due to the difficulty encountered in obtaining all the necessary chloropentane products from the supplier. Moreover, no reference spectra were found in the FTIR database therefore only chlorobutane product ratios have been analysed in this work.

FTIR databases such as HITRAN, NIST or PNNL can be easier and faster to use for the purpose of obtaining reference spectra, however environmental and instrumental parameters must be taken into consideration and when possible, a spectrum taken with the same HIRAC experimental apparatus would be better due to the path length and band width as well as the environmental conditions. When a spectrum is taken from a database, or donated by another university all relevant data must be included so that the spectra can be corrected for apodisation, pressure, and temperature.

The quantitative analysis of these chlorobutanes has been carried out by exporting the experimental sample spectra using a saved method file in the OPUS v.5.5 software. This saves all experimental and measurement parameters and in doing so ensures both reference and sample spectra used in future experiments contain the same standardised parameters thus facilitating their spectral analysis using the Quant2 software.

Figure 5.5 shows the Quant2 user interface used for the analysis of the chlorobutane branching ratios over a temperature range of 235 – 320 K. The top panel illustrates the subtraction of all 7 reference spectra (1-chloro-2-methylpropane, 2-chloro-2-methylpropane, methane, chloroethane, ethane, HCl and *iso*-butane) between the selected ranges of 2825 – 3075 cm^{-1}. A flat residual following spectral subtraction demonstrates the analysis has been successfully carried out using this software and that all components inputted as reference and experimental spectra have been taken into account. The bottom panel shows the profiles of all the different reactants and products present during the experiment, which is also outputted as a text file.

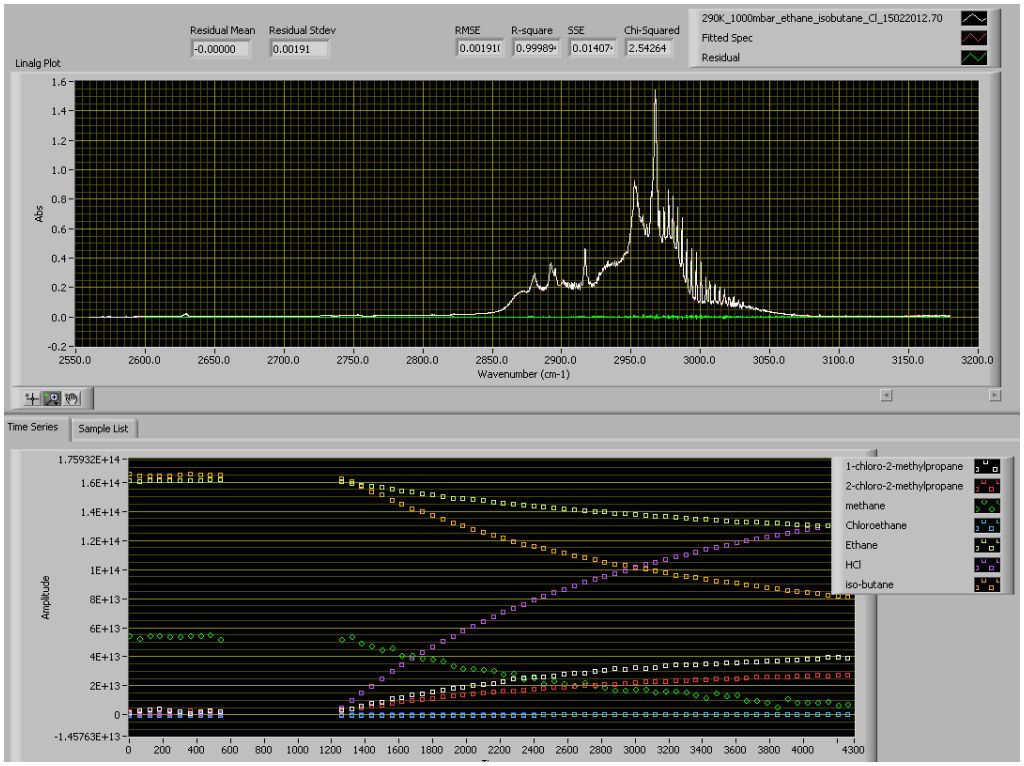

Figure 5.5: FTIR software used for chlorobutane branching ratio analysis. (a) Shows fitting of spectral analysis between 2800 – 3100 cm^{-1} and (b) Shows profiles for reactants and products for reaction of *iso*-butane with Cl over at 320 K

The output file containing the absolute concentrations of the different reactants and products were then analysed in Microsoft Excel and results were compared with the measurements obtained using the HIRAC GC. Similarly, reference chromatograms were obtained simultaneously with the FTIR reference spectra, and absolute concentrations were worked out for reference compounds using the FTIR measurements. GC measurements were carried out for a number of experiments and were used as a comparison for the computed FTIR spectra, although the main focus on this analysis was to make use of the FTIR and test its potential for analysing product ratios in HIRAC which had previously never been attempted using this instrument.

A comparison of the profiles of the FTIR data outputted from the Quant2 software with the analysed GC data are shown in Figures 5.6 and 5.7 for *n*-butane and *iso*-butane respectively carried out in HIRAC at 320 K. Further discussion of this work is divided into Sections 5.3.3 and 5.3.4 for *iso*-butane and *n*-butane respectively.

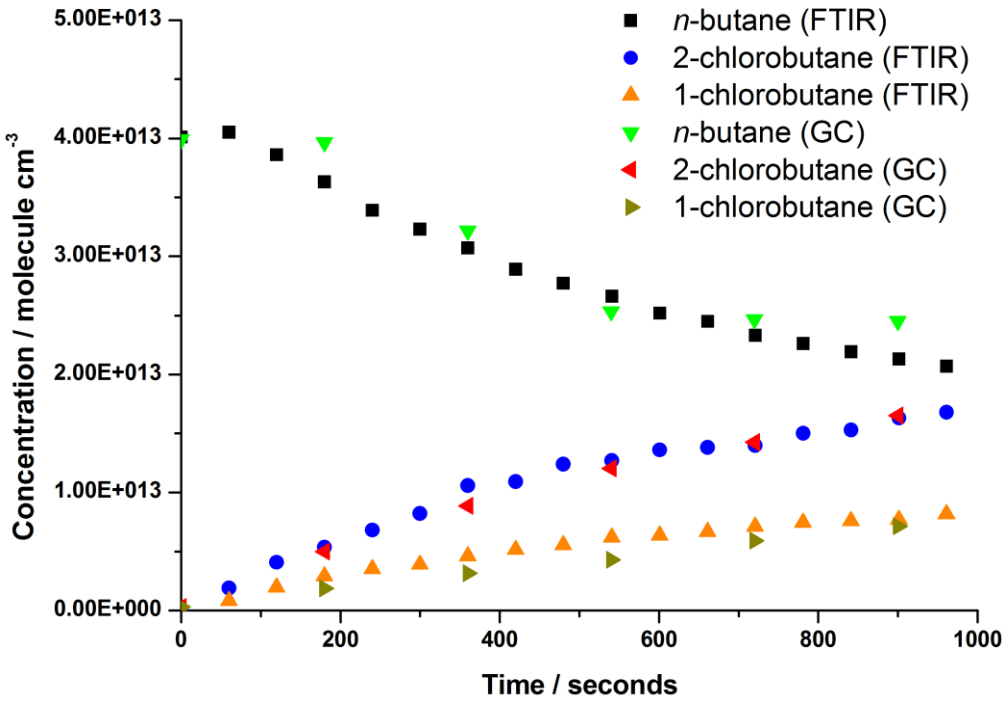

Figure 5.6: Concentration profiles of reactants and products for the reaction of *n*-butane with Cl atoms in HIRAC at 320 K using both FTIR and GC measurements.

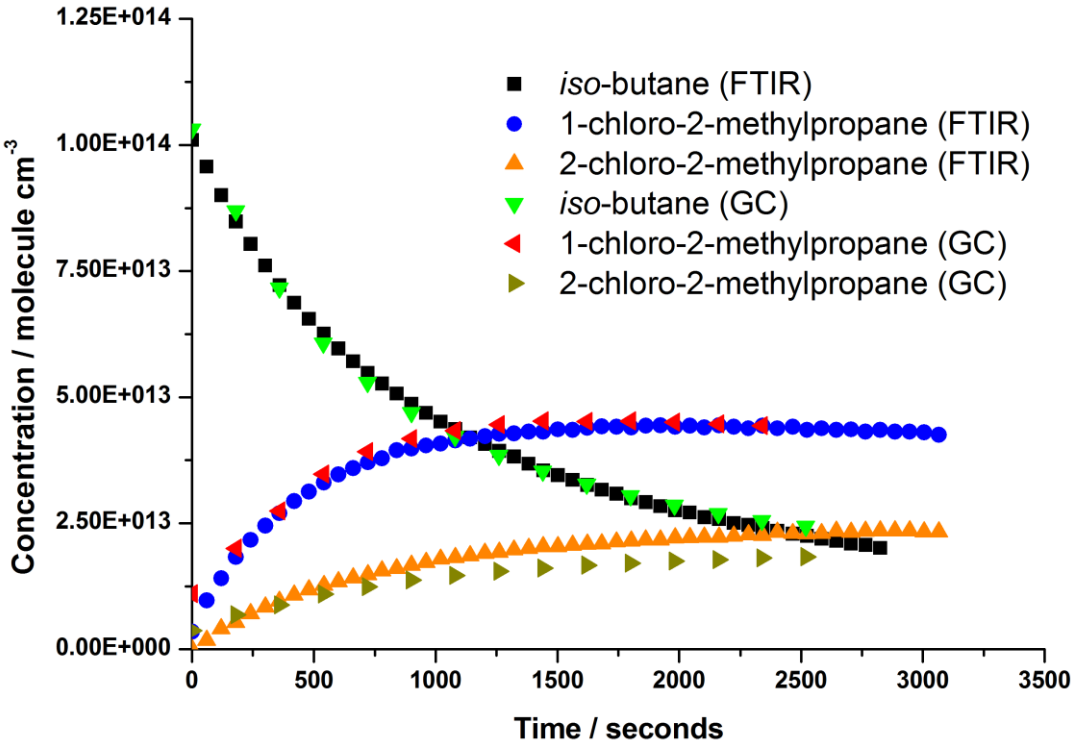

Figure 5.7: Concentration profiles of reactants and products for the reaction of *iso*-butane with Cl atoms in HIRAC at 320 K using both FTIR and GC measurements.

Due to poor signal on the GC, no low temperature product ratios could be obtained using the GC data. However given the good agreement of the GC data with FTIR data in HIRAC, FTIR results obtained at these temperatures were considered to be sufficient to understand the temperature dependence of these hydrogen abstraction reactions over the entire temperature range studied.

5.3.3 Branching ratios for *iso*-butane with Cl between 235 – 320 K

In the case of the reaction of Cl atoms with *iso*-butane, the primary chlorinated products expected are 1-chloro-2-methylpropane (R5.24) and 2-chloro-2-methylpropane (R5.25):

$$CH_3CH(CH_3)CH_3 + Cl \rightarrow CH_3CH(CH_3)CH_2 + HCl \xrightarrow{Cl2} CH_3CH(CH_3)CH_2Cl \quad (R5.24)$$

$$\rightarrow CH_3C(CH_3)CH_3 + HCl \xrightarrow{Cl2} CH_3(CCl)(CH_3)CH_3 \quad (R5.25)$$

The hydrogen abstraction pathways possible are either *via* a primary or tertiary hydrogen on the *iso*-butane molecule. Further reaction with chlorine molecules present in excess in HIRAC would lead to further chlorination of products (R5.26). These products were observed using both the GC and FTIR instruments, and for this reason only the first 5 - 10% conversion of [*iso*-butane] was taken into consideration for these product studies. Also, the accuracy of the Quant2 software outputs would be diminished owing to likely poorer residuals due to unknown components present in the analysis.

$$CH_2ClCH(CH_3)CH_3 \rightarrow\rightarrow CH_2ClCH(CH_3)CH_2Cl \quad (R5.26)$$

Plots of the concentration profiles of the 1-chloro-2-methylpropane and 2-chloro-2-methylpropane are shown over a temperature range of 235 – 320 K in Figures 5. 8 – 5. 10.

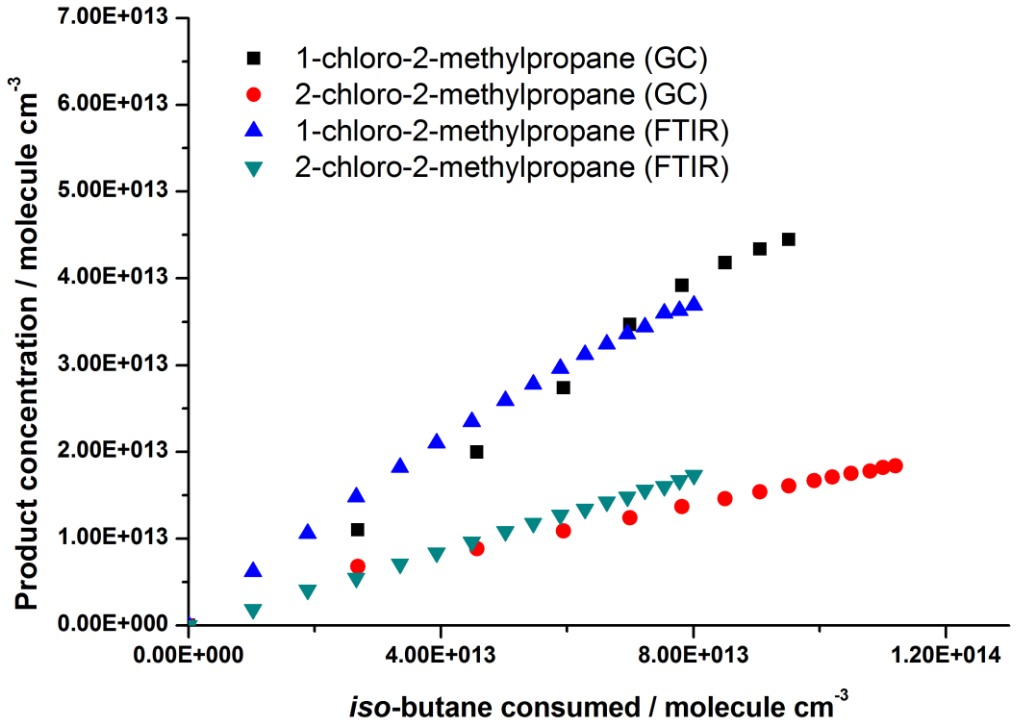

Figure 5.8: Concentration profiles for 1-chloro-2-methylpropane and 2-chloro-2-methylpropane from the reaction of *iso*-butane (1.3×10^{14} molecule cm^{-3}) with Cl atoms in HIRAC at 320 K.

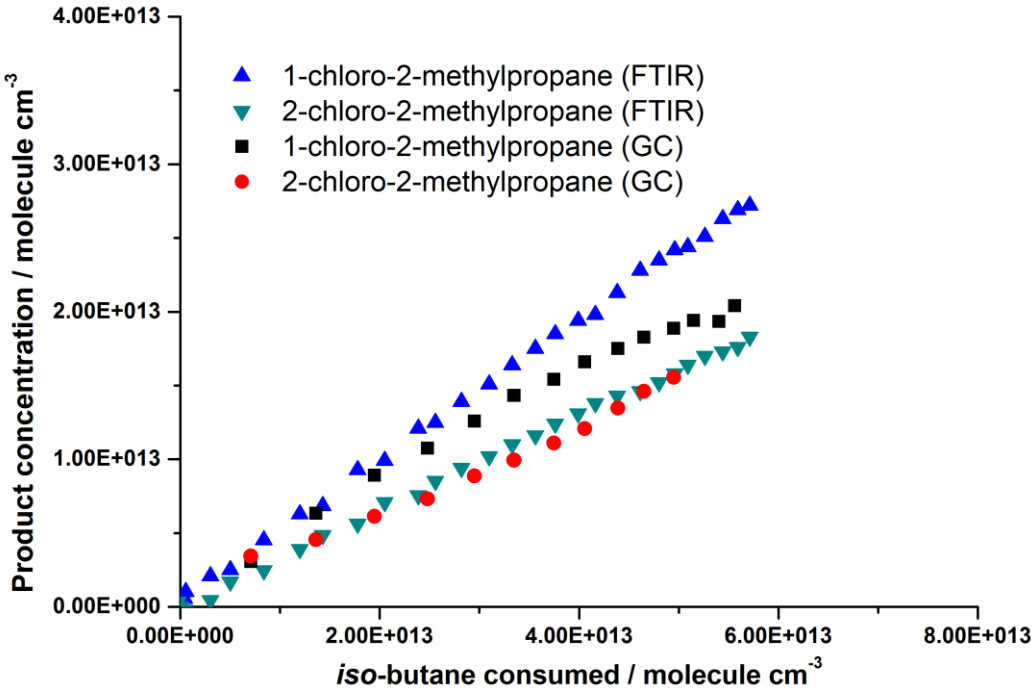

Figure 5.9: Concentration profiles for 1-chloro-2-methylpropane and 2-chloro-2-methylpropane from the reaction of *iso*-butane (1.6×10^{14} molecule cm^{-3}) with Cl atoms in HIRAC at 290 K.

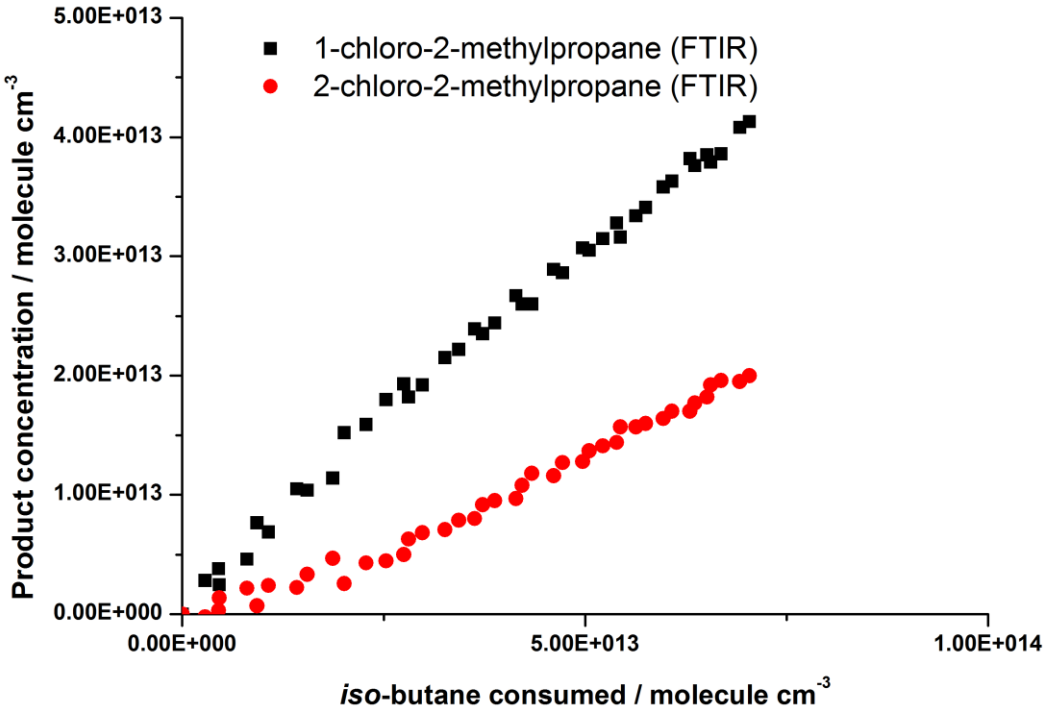

Figure 5.10: Concentration profiles for 1-chloro-2-methylpropane and 2-chloro-2-methylpropane from the reaction of *iso*-butane (2×10^{14} molecule cm^{-3}) with Cl atoms in HIRAC at 235 K.

All plots were recorded against the consumption of [*iso*-butane], and product concentrations were all direct absolute measurements determined from calibration plots in the case of GC, and using the Quant2 software in the case of FTIR. Reference spectra for individual samples and references were both obtained in HIRAC, and spectra and chromatograms were recorded under similar conditions. In the case of the GC calibration, successive dilutions of the chamber were carried out and a calibration plot was obtained from the decrease in signal intensities against concentrations recorded using both instruments. This factor was compared with the FTIR absolute concentrations determined using Beer Lambert's Law discussed in the previous section (R5.15).

Branching ratios reported were taken as the ratio between the two gradients of the plots of product concentration change against disappearance of isobutane concentration (Figures 5.8 – 5.10). The line of best fit (not shown in the above plots) was forced through zero and used as representative of the product ratio. The uncertainties were taken as the standard deviation of the fit. The same work up was used for the analysis of *n*-butane product branching ratios.

From the results obtained from the analysis of the products from the reaction of Cl atoms with *iso*-butane, good agreement between FTIR and GC measurements is noted at the temperatures where both could be analysed from the results obtained in HIRAC.

Some curvature is evident in particular in Figure 5.9 for 1-chloro-2-methylpropane. The GC measurements in this plot show that the concentration of the primary product begins to tail off while for the FTIR measurement this is not as evident. The most likely explanation is that there may have been a flaw in the FTIR analysis and the dichlorinated product forming at this stage of the reaction may have been interpreted as the monochlorinated product hence why there would be no tailing off in the worked out concentrations for 1-chloro-2-methylpropane from the FTIR measurements. As can be observed, the concentrations of these primary products using both GC and FTIR in the majority of the experiments begin to tail off after about 4×10^{13} molecule cm^{-3}. This occurs due to reaction of the chlorinated products with chlorine competing with the production rate of the same chlorinated product. For this reason, the photolysis rate was kept as low as possible by switching the lamps on and off at 100s intervals and only the first 10 – 15% of consumption of the *iso*-butane were considered. Also, given that only the first few data points have been used to derive the branching ratios, the curvature exhibited in some of the plots is not expected to have any effect on these branching ratio results.

Results obtained are tabulated and compared with previous work by Sarzynski and Sztuba (2002) and Choi et al. (2006). Structure activity relationship predictions for this reaction were also derived by Aschmann and Atkinson (1995) for room temperature branching ratios and are shown in Table 5.4.

	Temperature/ (± 3) K	195	235	292	320	365
1-chloro-2-methypropane	**This work (GC)**	**-**	**-**	**62 ± 3**	**66 ± 3**	**-**
	This work (FTIR)	**-**	**60 ± 3**	**63 ± 2**	**67 ± 2**	**-**
	(Sarzynski and Sztuba, 2002)	54[a]	-	65 ± 3	66 ± 4	69 ± 6
	(Choi et al., 2006)	49 ± 4	-	62 ± 5	-	-
	(Aschmann and Atkinson, 1995)	-	-	62	-	-
2-chloro-2-methypropane	**This work (GC)**	**-**	**-**	**36 ± 3**	**32 ± 4**	**-**
	This work (FTIR)	**-**	**40 ± 3**	**37 ± 2**	**32 ± 2**	**-**
	(Sarzynski and Sztuba, 2002)	46[a]	-	35 ± 3	34 ± 4	32 ± 6
	(Choi et al., 2006)	51 ± 4	-	38 ± 4	-	-
	(Aschmann and Atkinson, 1995)	-	-	38	-	-

Table 5.4: GC and FTIR measured branching ratios for Cl atom reactions with *iso*-butane in HIRAC at 1000 mbar. ([a] Extrapolated from Arrhenius plot)

FTIR and GC results obtained in this study are in excellent agreement with each other at 292 and 320 K. Unfortunately no GC data could be analysed at 235 K. Branching ratios obtained are also within error of both Sarzynski and Sztuba (2002) and Choi et al. (2006). A slight temperature dependence of primary hydrogen abstraction is observed, and a similar trend to the Arrhenius plots by Sarzynski and Sztuba were observed in this study. GC and FTIR errors quoted in Table 5. 4 were all derived from the regression of the branching ratio plots obtained for each individual product. Systematic errors were not accounted for in this analysis; however a 10 – 15% error is estimated for the FTIR results based on the subtraction method used and the qualities of the fittings.

The results obtained are relevant to the numerous field campaigns in the polar regions and during colder temperatures from a mechanistic point a view, as the understanding of the chemistry of these reactions is important should the Cl atom concentrations be deduced from these hydrocarbon decays in the atmosphere. These reactions are also atmospherically relevant since subsequent atmospheric oxidation of these butyl radicals would lead to production of aldehydes or ketones which have very different OH reactivities and photolysis rates and would therefore influence the HO_x cycle differently (Choi et al. 2006).

5.3.4 Branching ratio results for *n*-butane with Cl over 235 – 320 K

The following primary chlorinated products are expected from the reaction of *n*-butane with Cl atoms:

$$CH_3CH_3CH_3CH_3 + Cl \rightarrow \quad CH_3CH_2CH_2CH_2 \rightarrow CH_2ClCH_3CH_3CH_3 \qquad (R5.27)$$

$$\rightarrow \qquad CH_3CH_2CHCH_3 \rightarrow CH_3CH_2ClCH_3CH_3 \qquad (R5.28)$$

As can be seen, 1-chlorobutane (R5.27) and 2-chlorobutane (R5.28) are the two expected products from the hydrogen abstraction process, with competition being between a primary or secondary hydrogen of *n*-butane. Further reaction leads to further chlorination of products by chlorine molecules present in excess in HIRAC, as is shown in R5.29 for 2-chlorobutane:

$$CH_3CH_2ClCH_3CH_3 \rightarrow\rightarrow CH_2ClCH_2ClCH_3CH_3 \qquad (R5.29)$$

Figure 5.11 shows the comparison of branching ratios obtained experimentally for n-butane using FTIR and GC detection at 320 K.

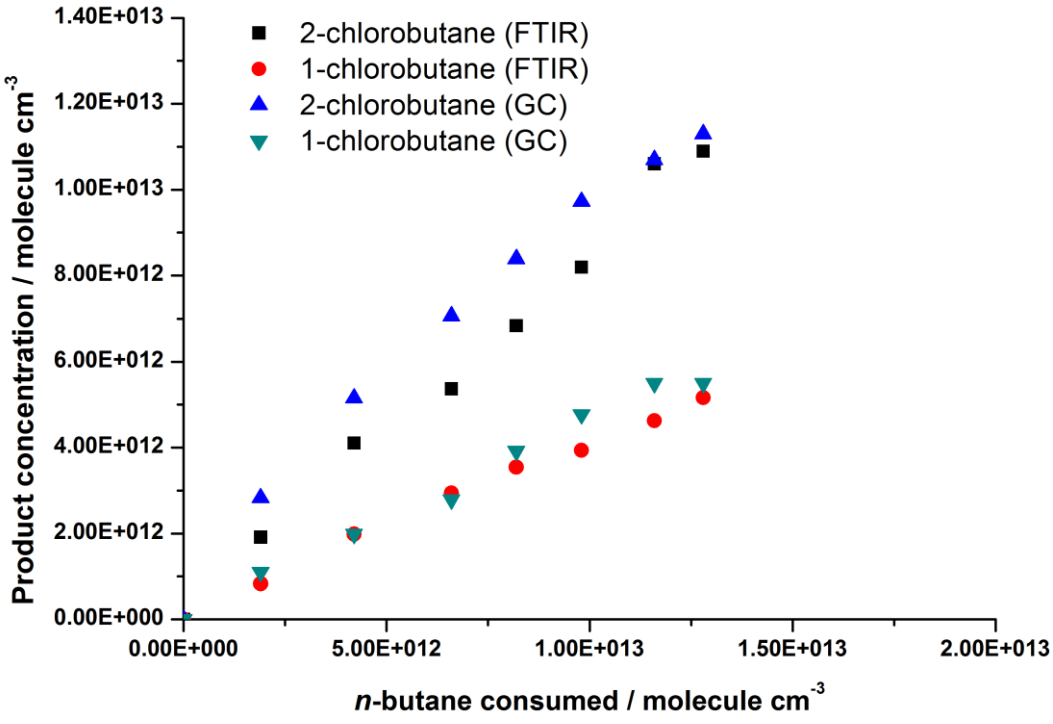

Figure 5.11: Concentration profiles for 1-chlorobutane and 2-chlorobutane from the reaction of *n*-butane (4×10^{13} molecule cm^{-3}) with Cl atoms in HIRAC at 320 K.

The same degree of curvature as for 1-chloro-2-methylpropane is shown here for 2-chlorobutane. In this case it is clear to note that both GC measurements show tailing off at 1×10^{13} molecule cm^{-3} while this is not apparent for the FTIR measurements pointing towards a possible overlap of the dichloroproduct which has been noted and discussed for the *iso*-butane products previously. Importantly however, this does not influence the branching ratios reported given that the first few data points that show linearity have been used to derive these values.

The results obtained show good agreement between the GC and FTIR measurements in HIRAC. Table 5.5 compares the results obtained with those reported by Tyndall et al. (1997) and Sarzynski and Sztuba (2002).

	Temperature/ (± 3) K	**235**	**292**	**320**	**365**
1-chlorobutane	**This work (GC)**	**-**	**30 ± 3**	**31 ± 3**	**-**
	This work (FTIR)	**37 ± 4**	**29 ± 2**	**33 ± 3**	**-**
	(Sarzynski and Sztuba, 2002)	-	29 ± 2	30 ± 4	31 ± 6
	(Tyndall et al., 1997)	-	29 ± 2	-	-
2-chlorobutane	**This work (GC)**	**-**	**71 ± 3**	**69 ± 3**	**-**
	This work (FTIR)	**63 ± 4**	**71 ± 2**	**67 ± 3**	**-**
	(Sarzynski and Sztuba, 2002)	-	71 ± 4	69 ± 4	68 ± 6
	(Tyndall et al., 1997)	-	71 ± 3	-	-

Table 5.5: % Branching fractions ($k_{product}/k_{RH}$) for Cl atom reactions with n-butane in HIRAC at 1000 mbar.

The results obtained for the product branching fractions for the reaction of Cl atoms with *n*-butane are all in excellent agreement with the room temperature results by Tyndall (295 K) and Sarzynski and Sztuba (292 K). As had been noted for the temperature dependence study, the branching fractions obtained by FTIR measurements in HIRAC at 235 K appear to be anomalous since they are in disagreement with the trend observed at higher temperatures. Unfortunately there were very few data sets that could be analysed for *n*-butane at this temperature, given the slower rates at which products appeared at 235 K. As such, the results reported at this temperature had only been obtained from a single experimental data set, therefore there is a possibility the experimental uncertainties for this run may have been underestimated.

The branching fractions obtained in HIRAC for the reaction of Cl atoms with *n*-butane are found to be temperature independent as had been initially predicted by Lewis et al. (1980) from Cl atom experiments carried out with propane over a temperature of 298 – 598 K. This temperature independence has also been supported by Tyndall et al. (1997), while Sarzynski and Sztuba reported weak temperature dependence in the branching ratios of *n*-butane, which is in agreement with the derived conclusions from this study.

5.4 Conclusion

The understanding of Cl atom chemistry is of increased importance due to higher concentrations of Cl atoms being reported in urban atmospheres resulting in competition with OH radicals. This study has investigated several aspects of Cl atom chemistry and revisited several topics of interest.

The kinetics data determined in HIRAC for Cl atom reactions with hydrocarbons were all within good agreement of the literature values for butanes and pentanes. All relative rate coefficients obtained were within 10% of the literature values for rate coefficients measured at room temperature.

Moreover, the order of reactivity for butanes and pentanes agreed well with the literature (*iso*-butane <*n*-butane <*iso*-pentane <*n*-pentane). As can be noted the reactivity of branched alkanes is less than straight chain alkanes. Results for *n*-butane and *iso*-butane were analysed using both GC and FTIR data, and the relative rate coefficients for both were within error of each other: *n*-butane: $1.90 \pm 0.08 \times 10^{-10}$ (GC), $1.76 \pm 0.10 \times 10^{-10}$ (FTIR); *iso*-butane: $1.36 \pm 0.05 \times 10^{-10}$ (GC), $1.20 \pm 0.10 \times 10^{-10}$ (FTIR), which confirms the precision of the results obtained in HIRAC. The results also confirm the suitability of the relative rate method used in HIRAC for the temperature dependence and product studies to follow.

From surveying the literature it was found that very few have investigated pentanes in reasonable detail, and in particular their temperature dependence. For the temperature dependent study performed for *n*- and *iso*- butanes and pentanes, the main goal was to further confirm the suitability of the recently installed temperature control system in HIRAC as well as obtain new important information on the temperature dependence of pentanes over tropospheric conditions in light of recent use of pentanes as tracers for Cl atom chemistry in the Arctic (Hellen et al., 2012).

The results obtained are within good agreement of the literature values for *n*-butane and *iso*-butane. Both butanes exhibited temperature independence for their reaction with Cl atoms, with possibly a slight negative temperature dependence for *iso*-butane as can be seen from the slight positive gradient of the Arrhenius plot in Figure 5.3. There are several interpretations to this phenomenon, the most credible

explanation being the fast kinetics of these reactions resulting in a barrier-less reaction not influenced by temperature. The results obtained for *n*-butane were more scattered than *iso*-butane, likely to have been due to problems in some of the experiments when introducing *n*-butane into HIRAC.

The investigation of the temperature dependence of *n*-pentane and *iso*-pentane showed a similar trend for the butanes, with a slight negative temperature dependence being exhibited for *iso*-pentane, and temperature independence for *n*-pentane. The implications of these findings may be important in field investigations that used pentanes as a tracer for Cl atom concentrations in the atmosphere, as depending on the temperature at which the monitoring was carried out the results for *iso*-pentane reactivity could have changed from anything between 5 – 25% based on the results obtained in HIRAC.

A chlorobutane product study for *n*-butane and *iso*-butane was aimed at looking further into the difference not just in the kinetics but also mechanistic behaviour of these Cl+ hydrocarbon reactions. Unfortunately difficulties were encountered in analysing the pentane experiments due to the greater number of products and very limited availability of these products from the supplier, required for identification and calibration purposes. Hopefully, should suitable reference spectra become available for these products, along with the improvement of the current FTIR software, these experiments could be reinvestigated and the product yields deduced from this work for the pentanes over a temperature range, enhancing the information available for these reactions.

The temperature dependence for chlorobutane product yields obtained would be relevant to the numerous field campaigns in the polar regions and during colder temperatures from a mechanistic point of view, since the understanding of the chemistry of these reactions is important should the Cl atom concentrations be deduced from these hydrocarbon decays in the atmosphere. Results obtained for *n*-butane at room temperature (292 ± 3 K) are in excellent agreement with both Sarzynski and Sztuba and with Tyndall et al. (primary/secondary: 29%/71%). While temperature independence was observed for *n*-butane it can be noted that a slight temperature dependence in the branching fractions was found from the study of *iso*-butane. Room temperature branching fractions here were also in excellent agreement

with literature data (primary/tertiary: 63%/37%). The *t*-butoxy radical formed from the reaction of Cl atoms with *iso*-butane has no α-hydrogens as it is a tertiary hydrogen abstraction process. This ultimately is known to decompose to form acetone and a methyl radical (Blitz et al., 1999). In the atmosphere such radicals can also react with oxygen to form a carbonyl and HO_2.

In the case of the primary abstraction pathway for *iso*-butane the isobutoxy radical formed can either react with oxygen to give the respective aldehyde or decompose to give formaldehyde and *iso*-butene. There is some uncertainty as to which of the two pathways predominates in the atmosphere, however in conclusion these branching ratios have been crucial in understanding whether these abstraction reactions ultimately lead to the formation of either an aldehyde (primary abstraction) or a ketone (tertiary abstraction).

Chapter 6 – Hydrogen abstraction reaction of Cl atoms with ethanol

6.1 Introduction

The rising costs of petroleum and desire for greater energy security where fossil fuel resources are depleting has resulted in an increasing interest in biofuels as an alternative source of energy. The use of biofuels has already been highlighted in Chapter 4 in the section on the kinetics and reactivity of esters. The discussion dealt with the biofuel commonly called biodiesel, and this type of biofuel is produced primarily from plant oils and fats that convert into long-chain fatty acids referred to as FAMEs (fatty acid methyl esters). The other main type of biofuel in common use is ethanol (or bioethanol). Ethanol is of great importance as a source of energy from biomass, and is also used directly as a fuel. These energy options are being driven owing to the environmental and energy securities from these methods (Farrell et al., 2006). Biofuels can offer an opportunity to prolong the lifetime of finite petroleum resources, as biological systems have been shown to be very good at converting sunlight to biomass, making biofuels a suitable candidate for future energy needs. There is, however, a greater need to understand and assess their potential and combustion characteristics in greater detail before they can be fully accepted by society, and a lot of work is currently being carried out to address this (Demirbas, 2010, Selvam and Vadivel, 2013, Tuccar and Aydin, 2013, Lapuerta et al., 2008, Agarwal, 2007).

Product studies for reactions of alcohols are of importance for the understanding of urban atmospheric chemistry. Only a few studies have characterised the product yields of ethanol oxidation reactions in detail, with more kinetic studies being carried out for reaction with Cl atoms possibly due to the ease to carry out the Cl atom studies compared to OH (Taatjes et al., 1999, Seakins et al., 2004, Crawford et al., 2004, Nelson et al., 1990, Carter et al., 1979, Garzon et al., 2006). Cl atoms react 25-50 times faster than the OH radical does (Nelson et al., 1990, Wallington et

al., 1988c, Carr et al., 2011) with alcohols resulting in higher product yields in most cases when compared to OH over the same reaction times (Grosjean, 1997).

Despite this greater reactivity of Cl atoms over OH radicals, the latter are present in higher concentration and are the primary contributor to the degradation of atmospheric ethanol. This has been discussed in Section 5.2.1. Both reactions of OH and Cl atoms with alcohols proceed *via* hydrogen abstraction from either a C-H or O-H bond. In the case of ethanol reactivity, this can occur *via* either primary or secondary C-H abstraction (α and β abstraction respectively) or O-H as is shown in R6.1 – 6.3:

$$Cl\ (OH) + CH_3CH_2OH \rightarrow CH_3CHOH + HCl\ (H_2O) \quad (R6.1)$$
$$Cl\ (OH) + CH_3CH_2OH \rightarrow CH_2CH_2OH + HCl\ (H_2O) \quad (R6.2)$$
$$Cl\ (OH) + CH_3CH_2OH \rightarrow CH_3CH_2O + HCl\ (H_2O) \quad (R6.3)$$

Recently published work on the reaction of methanol with OH has suggested that alcohol oxidation plays an important role at low temperatures despite the presence of an activation barrier (Shannon et al., 2013). Reaction kinetics is governed by the details of potential energy surfaces upon which reactions take place. Figure 6.1 illustrates the PES of the reaction of OH with ethanol (Xu and Lin, 2007). A reaction is likely to proceed if there is sufficient energy to overcome the overall activation barrier ending in products. The Arrhenius equation, described in Chapter 5, shows the relationship of temperature with the rate coefficient, *k*, and includes two other parameters, the Arrhenius (*A*) parameter (related to the rate of collisions and geometry of reaction) and the activation energy (the overall barrier).

Kinetic studies indicate that during alcohol reactions with OH or Cl atoms, the hydrogen abstraction from the C-H bond is the major pathway, rather than from the O-H bond (Nelson et al., 1990). This is expected given there are more C-H sites than O-H sites to attack, and it also is consistent with theory given the bond strength of the O-H bond is greater than that for C-H (104 kcal mol^{-1} compared to 94 kcal mol^{-1} in methanol) (Hess and Tully, 1989).

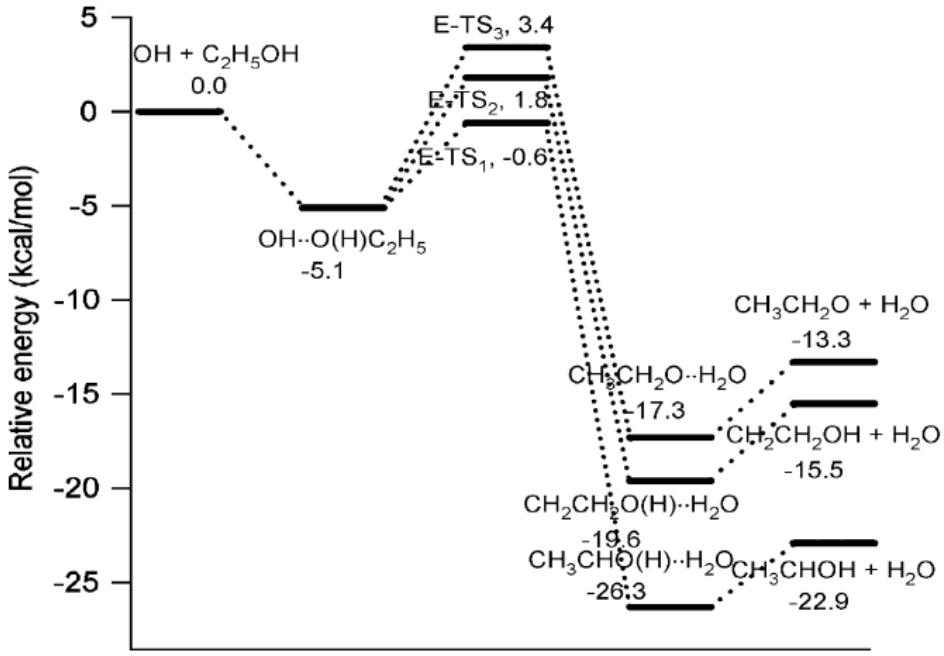

Figure 6.1: Potential energy surfaces for the three possible channels for the reaction of OH with ethanol (Xu and Lin, 2007).

The above PES for the reaction of OH with ethanol shows three possible pathways (i.e.: R6.1 – R6.3) for the reaction due to the OH being able to abstract one of the two methylene hydrogens, one of three methyl group hydrogens or one hydroxyl hydrogen. All pathways proceed *via* a pre-reaction complex formation $OH\cdots O(H)C_2H_5$. According to the work by Xu and Lin, the three possible transition states have activation barriers of −0.6, 1.8 and 3.4 kcal mol^{-1} for α, β and hydroxyl hydrogen abstraction respectively (Xu and Lin, 2007). All pathways result in fragmentation of the complex to form $H_2O + CH_3CHOH$, $H_2O + CH_2CH_2OH$ and $H_2O + CH_3CH_2O$ with overall heats of reaction: −22.9, −15.5, and −13.3 kcal/mol (Xu and Lin, 2007).

The atmospheric oxidation of ethanol leads to important secondary pollutants such as acetaldehyde, peroxyacetylnitrate (PAN), formaldehyde and ozone (Seakins et al., 2004) with the primary oxidation product being acetaldehyde (0.80 ± 0.15) (Carter et al., 1979). Acetaldehyde is formed from the hydroxyethyl radical which is formed in R6.1 from the abstraction of the α-hydrogen from ethanol. This radical reacts with molecular oxygen by hydrogen abstraction as is shown in R6.4:

$$O_2 + CH_3CHOH \rightarrow CH_3CHO + HO_2 \qquad \text{(R6.4)}$$

The alternative pathway from C-H hydrogen abstraction (from β-hydrogen in R6.5) leads to an alkyl radical CH_2CH_2OH which reacts with oxygen to form a peroxy radical that in the presence of NO forms an alkoxy radical:

$$O_2 + CH_2CH_2OH \rightarrow OOCH_2CH_2OH \quad \text{(R6.5)}$$
$$NO + OOCH_2CH_2OH \rightarrow NO_2 + OCH_2CH_2OH \quad \text{(R6.6)}$$

Further oxidation of this alkoxy radical will lead to hydroxyacetaldehyde. R6.7 competes with decomposition of this alkoxy radical to anα-hydroxyalkyl radical and formaldehyde (R6.8), the former radical reacting with oxygen to give formaldehyde (R6.9):

$$O_2 + OCH_2CH_2OH \rightarrow HC(O)CH_2OH + HO_2 \quad \text{(R6.7)}$$
$$OCH_2CH_2OH \rightarrow CH_2OH + HCHO \quad \text{(R6.8)}$$
$$O_2 + CH_2OH \rightarrow HCHO + HO_2 \quad \text{(R6.9)}$$

The kinetics and mechanism of propanol (Yamanaka et al., 2007), *n*-butanol (Hurley et al., 2009, Andersen et al., 2010, McGillen et al., 2013), *iso*-butanol (Ballesteros et al., 2007, McGillen et al., 2013) and *n*-pentanol (Hurley et al., 2008) have all been extensively investigated in recent years stressing the increased interest in the oxidation processes of alcohols, and the importance of this information to atmospheric chemistry and the implications due to the shifts of energy utilisation.

The importance of Cl atom reactions with alcohols and their atmospheric relevance has fuelled interest in more general aspects of Cl atom reactivity. Site selectivity of Cl atom reactions is important not just for a better understanding of atmospheric chemistry, but also since Cl atoms are widely used as selective sources of radicals in kinetic experiments (Taatjes et al., 1999). This chapter will focus on outlining work carried out in HIRAC to better understand the way hydrogen atom abstractions from C-H bonds occur in the reactions of Cl atoms with ethanol and some of its deuterated isotopologues (CD_3CH_2OH, CH_3CD_2OH, CD_3CD_2OH).

Site-specific rate data was determined for ethanol and its isotopologues (CD_3CH_2OH, CH_3CD_2OH and CD_3CD_2OH). Similar studies were carried out previously by a number of authors (Taatjes et al., 1999, Seakins et al., 2004, Crawford et al., 2004), however none had previously reported HCl:DCl product ratios and obtained mechanistic information of these reactions from these ratios, which is what will be reported in this chapter. The only previous isotopic study to our knowledge on

the branching ratios to products of the reaction of Cl atoms with ethanol were reported by Taatjes et al. (Taatjes et al., 1999) who measured HCl yields, therefore these would be the first reported investigations using HCl/DCl ratios, and would also serve as a test of the capabilities of HIRAC (as well as chambers in general) to obtain absolute rate data using the FTIR which has previously not been attempted in HIRAC or in any chamber to our knowledge for isotopic investigations of this kind. Branching ratios are needed for the modelling and understanding of alcohol chemistry and to probe the impact of the increased use of ethanol in combustion. A description of the methodology used and some preliminary results will follow.

6.2 Experimental

DCl and HCl branching fractions are reported in this section for the reaction of Cl atoms with ethanol and its isotopologues (CD_3CH_2OH, CH_3CD_2OH and CD_3CD_2OH). The significance of these reactions as well as the scarcity of site selective information has triggered an interest in reinvestigating these reactions in HIRAC. The methodology will be described in this section.

The gases and liquids used in the present work were obtained from different sources. Chlorine (Sigma Aldrich, 98%), HCl (Sigma Aldrich, 99%) and DCl (Fluka, 99%) gases were used as received. HCl and DCl were used to obtain reference spectra on the FTIR. Ethanol and its isotopologues were all supplied from Sigma Aldrich and had stated purities of CH_3CH_2OH (99.5%), CD_3CD_2OH (99% atom D), CH_3CD_2OH (99% atom D), CD_3CH_2OH (99.5% atom D). The small 1% impurities (presumably unidentified organic contaminants) could be a significant error for the study of HCl:DCl ratios. For this reason repeat freeze-pump-thaw cycles were performed prior to introducing into HIRAC to minimise this likely uncertainty. Relative rate kinetic experiments using GC-FID and FTIR were performed for ethanol, CD_3CH_2OH and CH_3CD_2OH at 292 ± 3 K. This is discussed in the preliminary results section to follow, and is accompanied by an isotopic branching ratio study probing HCl and DCl products. Measurements of HCl and DCl were performed to obtain isotopic branching ratios for the reaction of Cl atoms with ethanol and its isotopologues at atmospheric

pressure and temperature. The reactions R6.11 – R6.14 have been investigated in this study:

$$Cl_2 + h\upsilon\ (\leq 320\ nm) \rightarrow Cl + Cl \qquad (R6.10)$$

$$CH_3CH_2OH + Cl \rightarrow CH_3CHOH + HCl \qquad (R6.11)$$
$$CH_3CH_2OH + Cl \rightarrow CH_2CH_2OH + HCl \qquad (R6.12)$$

$$CD_3CH_2OH + Cl \rightarrow CD_2CH_2OH + DCl \qquad (R6.13)$$
$$CH_3CD_2OH + Cl \rightarrow CH_3CDOH + DCl \qquad (R6.14)$$
$$CD_3CD_2OH + Cl \rightarrow CD_2CD_2OH + DCl \qquad (R6.15)$$
$$CD_3CD_2OH + Cl \rightarrow CD_3CDOH + DCl \qquad (R6.16)$$

Chlorine atoms (R6.10) were generated similarly to the methodology described in the previous two chapters using Philips TLK40W/05 actinic UV blacklamps and chlorine gas as the precursor. In the case of these experiments only two lamps were used to initiate photolysis. This would keep the Cl atom production rate low to better distinguish the initial HCl and DCl evolutions on the FTIR. GC-FID measurements were used during relative rate experiments to monitor the ethanol and its isotopologues and reference compound concentrations. Typical concentrations used were $(1 – 5) \times 10^{13}$ molecule cm^{-3} chlorine gas, $(0.8 – 2) \times 10^{14}$ molecule cm^{-3} ethanol and its isotopologues, and 5×10^{13} molecule cm^{-3} ethane (reference compound). Experimental determination of the HCl:DCl ratios is possible with quantification of HCl and DCl by an FTIR spectrometer (Brucker IFS/66, MIR source, in conjunction with a modified multipass Chernin cell (Glowacki et al., 2007b) path length ~172 m, Happ-Genzell apodisation, 32 averaged scans, 0.5 cm^{-1}).

Figure 6.2 shows the FTIR spectra obtained in HIRAC which were used as references, in order to attempt at calibrating for the DCl and HCl absorbances recorded during the isotopic studies. This was, however, difficult to obtain owing to exchange of DCl into HCl during delivery into HIRAC, which was found difficult to account for. For this reason, and given the fact that only ratios of the two were of interest, a numerical calculation was used in order to correct for the different magnitudes of their respective vibration-rotational transitions.

$$A/B = 8\pi h\nu^3/c^3 \qquad (Eq6.1)$$

Literature values for the HCl A factor (40.21 s^{-1}) for the 1-0 band (J=0 to J=0) and DCl A factor (11.038 s^{-1}) for the same transition (Arunan et al., 1992) were used

in order to calculate the HCl:DCl ratio from the following derived relationship which links the emission and absorption coefficients *via*:.

$$A(HCl)/A(DCl) = B(HCl)/B(DCl)\ (\nu^3(HCl)/\nu^3(DCl)) \qquad (Eq6.2)$$

Where ν is the frequency (s^{-1}). The ratio of A values for 1-0 transitions for DCl and HCl obtained was used in order to correct the absorbances obtained for the ratio of HCl and DCl during experiments in HIRAC. A value of 3.64 was obtained for the transition at 2727.43cm^{-1} for HCl and the corresponding transition at 2010.85cm^{-1} DCl, both being 1-0 transitions on the P7 branch of the vibration-rotational spectra. Figure 6.3 shows the HCl evolution from the reaction of Cl atoms with CD_3CH_3OH. FTIR spectra were analysed using the peak analysis package available in the OPUS software. The vibration-rotation transition analysed for DCl was the P7 branch transition at 2010.85 cm^{-1}, and the corresponding transition for HCl was analysed at 2727.43cm^{-1}.

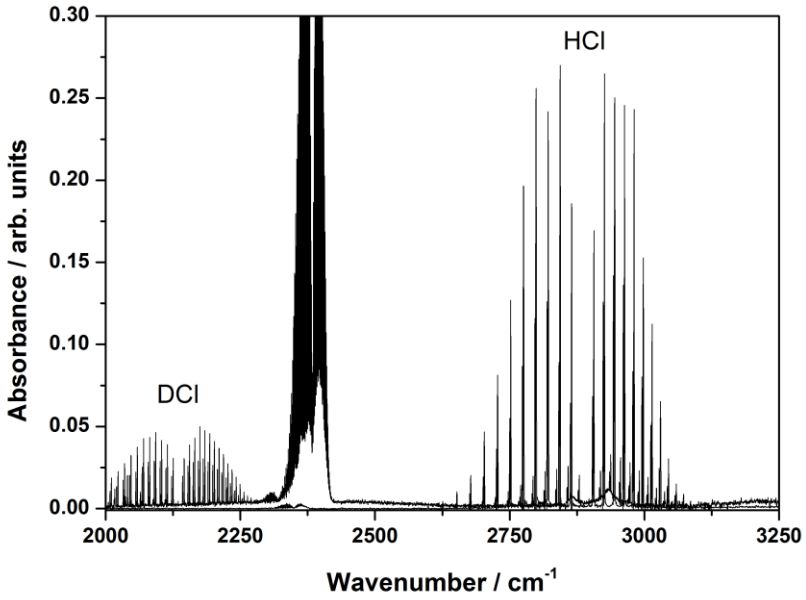

Figure 6.2: FTIR spectra of HCl and DCl in HIRAC at 292 K and 1000 mbar in OFN nitrogen bath gas.

The analysis involved setting up a method in the OPUS v5.5 platform and defining the region of the spectrum that would be analysed for the different experimental spectra available. Peak heights were recorded and these results were corrected using the ratio obtained previously.

Carbon monoxide was a problem for DCl analysis, as it absorbed in a similar region and overlapped with DCl. For this reason the P7 (7^{th} vibration-rotational transition on the P) branch of DCl was chosen for analysis. Some isotopologues of ethanol also absorbed close to 2000 cm^{-1}, and therefore the lowest possible P-branch transition where no overlap occurred was selected. The signal-to-noise ratio was slightly poorer at this range; however it was sufficient for these experiments. A validation of the method was carried out by analysing the respective isotopic peaks, verifying the ratios were the same for a number of sets of data that were analysed. The results confirmed the analysis method being used was repeatable for the different isotope transitions not overlapping with any other species for the FTIR spectra of both HCl and DCl.

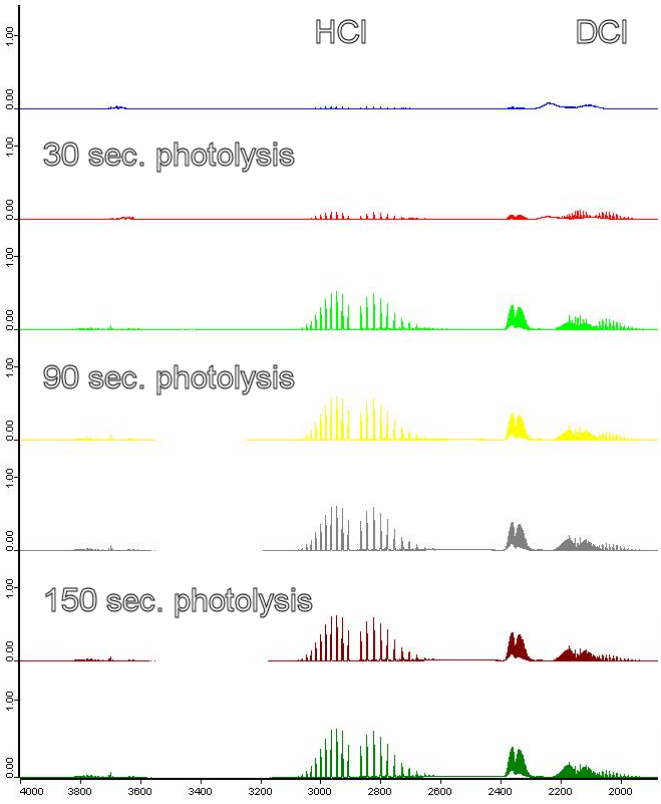

Figure 6.3: Infrared spectra of the analysed portion of the spectra, containing HCl (2600 – 3100 cm^{-1}) and DCl (1900 – 2100 cm^{-1}) for the reaction of Cl atoms with CD_3CH_2OH in HIRAC. Irradiation was turned on and off every 120 – 150 s. The presence of CO_2 (2400 cm^{-1}) and CO (2200 cm^{-1}) is also noted in these spectra.

HCl:DCl ratios were derived by plotting the relative changes of Δ[HCl] against Δ[DCl] from the evolution of these two products during the experiment. The [HCl] evolving from chamber walls was not subtracted, as it was assumed to be

constant for the sets of experiments that were carried out over the same day. This, however, is likely to contribute to a large undetermined uncertainty in the [HCl] being produced from the reaction of Cl atoms with ethanol. It was difficult to obtain a factor to subtract this residual HCl since the rate was not found to be constant during the experiment and also changes from day to day based on the exposure of the chamber walls to organics and other compounds.

This study would assess the suitability of the HIRAC FTIR system for obtaining these isotopic branching ratios, and several tests were initially carried out to assess the optimum chamber conditions to use. The effect of the purity of the bath gas used was tested using the FTIR to determine its influence on the residual HCl from the chamber walls. Figure 6.4 shows a comparison of the two bath gases that were tested. A higher purity source of nitrogen was found to be more suitable for these experiments, since residual organics present in impure bath gases would contribute to residual HCl in the chamber. It was found that both OFN (BOC, Oxygen Free) and UHP (Ultra High Purity) nitrogen both gave similar residual HCl for runs of chlorine gas photolysis only in HIRAC. OFN nitrogen being more economical to use was selected as the bath gas of choice for these experiments.

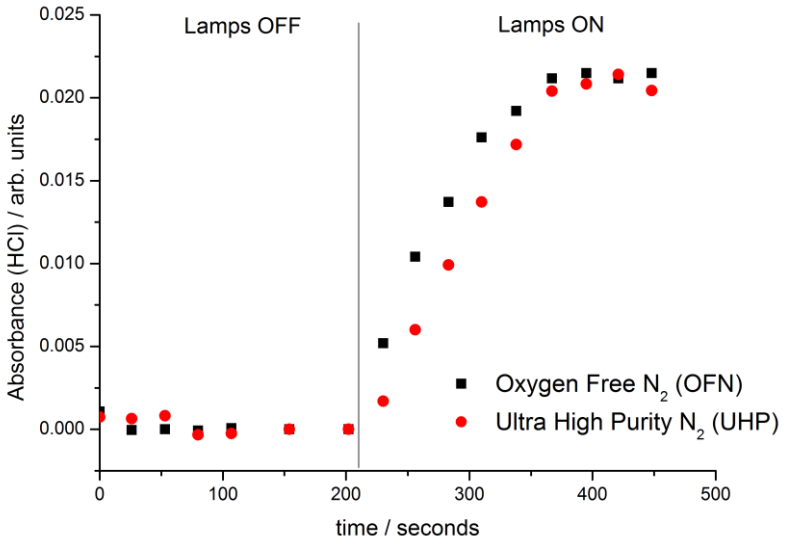

Figure 6.4: A comparison of residual HCl recorded at the start of the experiment in HIRAC using Oxygen-free and Ultra High Purity N_2.

Experiments were performed in the HIRAC chamber using the long-path FTIR instrument described in Section 2.4.1. All experiments were carried at 292 ± 3 K and

1000 mbar in laboratory grade nitrogen. Chlorine gas ((1 – 5) × 10^{13} molecules cm^{-3}) was used as a precursor for all experiments and irradiation was performed using two TL 40W/12 RS SLV UV-B medical therapy lamps. Cl atoms were generated by successive "lamps on" and "lamps off" periods (100 second cycles). The use of only two lamps ensured the photolysis rate was kept low since only primary products (HCl and DCl) were being assessed, and therefore slowing the chemistry down would ensure more of the initial chemistry is recorded.

A fans test was also assessed given the possible influence from disturbances of the chamber walls resulting in possible evolution of HCl which is not from reaction of Cl atoms with ethanol and which would influence HCl:DCl measurements. Isotopic exchange of the deuterium in the DCl was also likely to occur on the walls of HIRAC and several diagnostic tests were carried out using FTIR detection to monitor the relative decays of HCl and DCl. Figure 6.5 confirms that with fans on, exchange of DCl to HCl occurs at a fast rate due to faster mixing and results in few data points (2 – 3) obtained in this experiment shown for reaction of Cl atoms with CH_3CD_2OH, and more uncertainty is predicted due to difficulty in quantifying the exchange rate, which would be dependent on several experimental conditions, in particular the conditioning of the HIRAC walls.

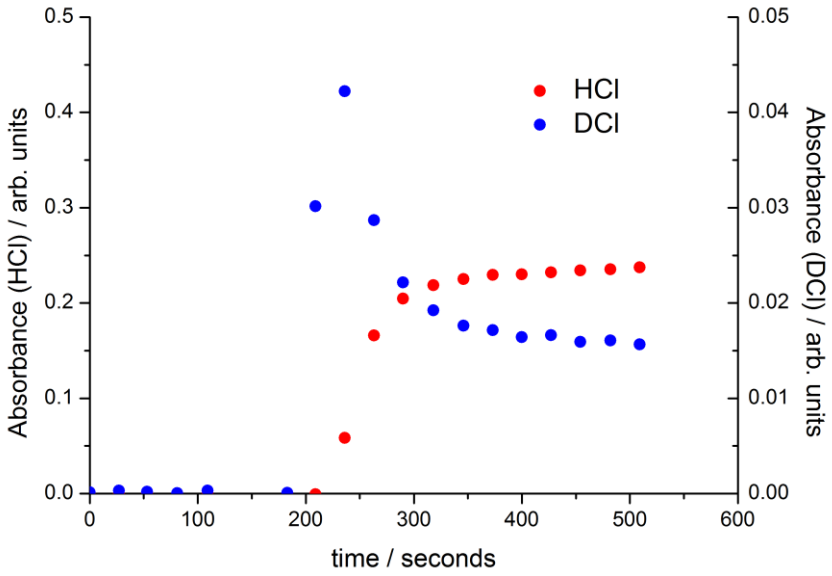

Figure 6.5: Fans on experiment for reaction of CH_3CD_2OH (2 ppmv) with Cl atoms (20 ppmv) at 292 ± 3 K and 1000 mbar in HIRAC.

Fans off experiments were carried out using all isotopologues in order to assess the possibility of carrying out the experiments without fans to decrease the rate at which isotope exchange occurs at the chamber walls. This latter effect could not be fully characterised given that the effects of chamber walls, in particular stainless steel, are influenced by environmental conditions and conditioning of the walls, therefore for the purpose of these experiments this could not be carried out. In order to achieve this it was first necessary to first determine the effect no fans would have on the method being used.

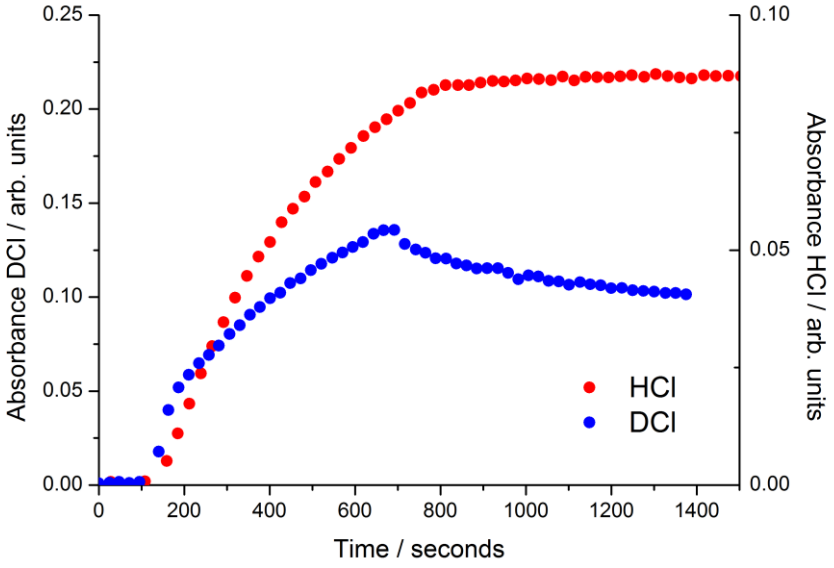

Figure 6.6: Fans off experiment for CH_3CD_2OH+Cl (2ppmv) with Cl atoms (20 ppmv) at 292 ± 3 K and 1000 mbar in HIRAC.

Figure 6.6 shows that for a fans off experiment for reaction of Cl atoms with CH_3CD_2OH, the deuterium exchange is delayed enough to be able to obtain more data points for DCl formation before conversion to HCl than with fans on. Fans on experiments lead to faster exchange to the chamber walls and this is likely due to faster mixing occurring in HIRAC. For this reason it was more appropriate to carry out these experiments with fans off to delay the exchange from occurring.

These data would only be valid, however, provided the contents of HIRAC are adequately mixed prior to the start of the reaction, and therefore before photolysis was initiated it was ensured that all concentrations of reactants were stable in HIRAC. This

is what is regularly carried out during experiments in HIRAC when using fans (highlighted in chapter 2) to ensure that none of the reactants are reacting with precursors or being lost to walls. In the case of these fans off experiments, more time was allowed (15 – 30 minutes) for equilibration of these compounds.

6.3 Preliminary Results

6.3.1 Relative rate method for the study of the reaction of Cl atoms with ethanol and CD_3CH_2OH

A validation of the FTIR setup used for studying Cl atom reactions with ethanol and its isotopologues was considered useful to assess any potential uncertainties such as unnoticed anomalies in the FTIR spectra. This was a concern given the integration of the spectra was not carried out as for the investigation of chlorobutanes product yields in the previous chapter. This was due to the lack of reliable reference spectra for DCl and any of the deuterated isotopologues and their respective products, for which further work is required to have suitable reference spectra made available.

Calibration of methodology and the apparatus used would be achieved by obtaining the kinetics of reaction of Cl atoms with ethanol and its isotopologues. Using the GC-FID as a comparison ensured the FTIR system was suitable for obtaining not just kinetics but also mechanistic information. This was achieved by comparing how both instruments performed and their inter-comparison for studying the kinetics of the reaction of chlorine with ethanol, as had been investigated before in previous chapters, as well as by previous workers in HIRAC for different systems using both instruments (Malkin, 2010).

Relative rate experiments were carried out using the same method as had been reported in previous chapters 4 and 5 for experiments carried out in HIRAC. These relative rate experiments were all carried out in OFN nitrogen bath gas. HIRAC was first filled to ~970 mbar with nitrogen and the ethanol (~2 - 5 ppmv), chlorine (~20 - 40 ppmv) and ethane (~2 - 5 ppmv) were introduced *via* a delivery vessel and ~5

minutes was allowed for adequate mixing in the chamber. Ethane was used as a reference compound and the rate coefficient used for determination of the relative rate coefficient for these ratios was that recommended by IUPAC, and mentioned in chapter 5 ($(5.80 \pm 0.20) \times 10^{-11}$ molecule^{-1} cm^3 s^{-1}) (Atkinson et al., 2006b). Reference spectra were obtained for each individual isotopologue in HIRAC. These are shown in Figure 6.7.

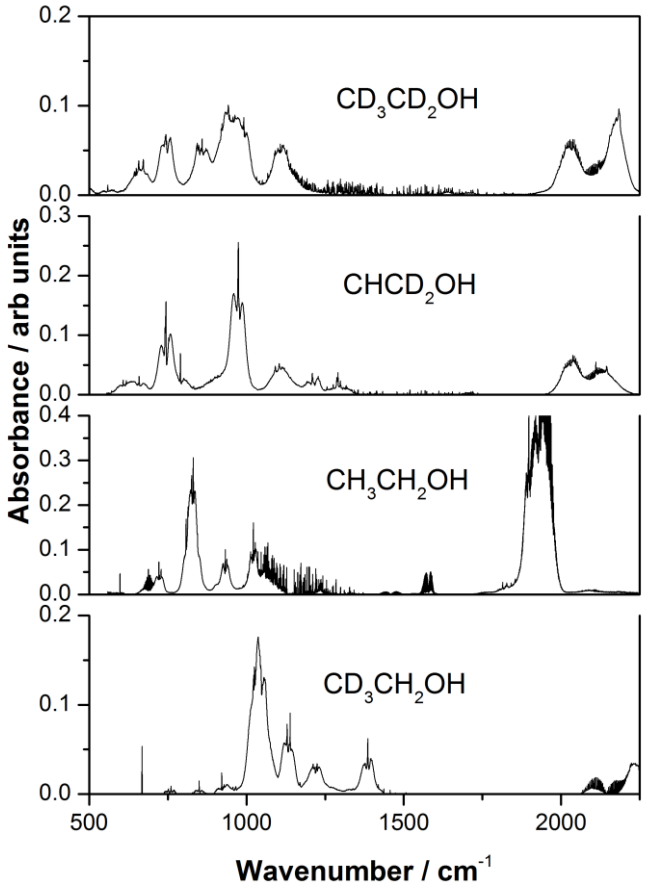

Figure 6.7: FTIR spectra of isotopologues of ethanol (2 ppm) in HIRAC at 292 K and 1000 mbar in OFN nitrogen bath gas.

The chemicals used in these experiments were acquired from the following commercial sources: CH_3CH_3 (Sigma Aldrich, 98%), CH_3CH_2OH, CD_3CH_2OH, CH_3CD_2OH and CD_3CD_2OH (Sigma Aldrich, 99.5+%) and Cl_2 (Sigma Aldrich, 99.5%). The presence of small impurities for ethanol and their isotopologues would significantly affect the results for the HCl:DCl ratios calculated, and all the liquids

were prepared in a vacuum line and purified by several successive freeze-pump-thaw cycles to remove any impurities that may cause interferences in the analyses and also contribute to the HCl and DCl yields by reacting with Cl atoms during the experiment. Both these factors were minimised as much as possible by purification and by using the highest purity samples available from the supplier; however a ≤ 1% occurrence of impurities would fall into the random errors of the rate coefficient determinations. According to NMR and GC-FID analysis work by Taatjes (1999), the main impurity for CD_3CH_2OH and CH_3CD_2OH was normal ethanol which reacts similar to its deuterated counterpart. While this was ≤ 1% for CD_3CH_2OH, which had a similar rate coefficient to ethanol, it was noted that the rate coefficient of CH_3CD_2OH may be influenced to a greater degree (1 – 2%) owing to the rate coefficient for this deuterated ethanol being smaller than the ethanol reaction with Cl atoms, however was neglected given it was within random uncertainties of the measurements.

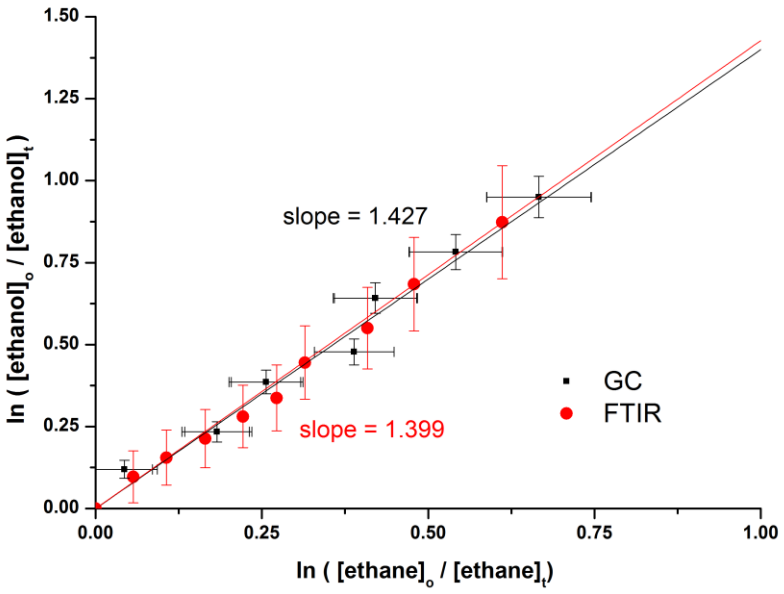

Figure 6.8: Comparison of FTIR and GC relative rates obtained for the reaction of ethanol with Cl atoms using ethane as a reference compound in HIRAC at 292 K and 1000 mbar and nitrogen bath gas (error bars represent 1σ).

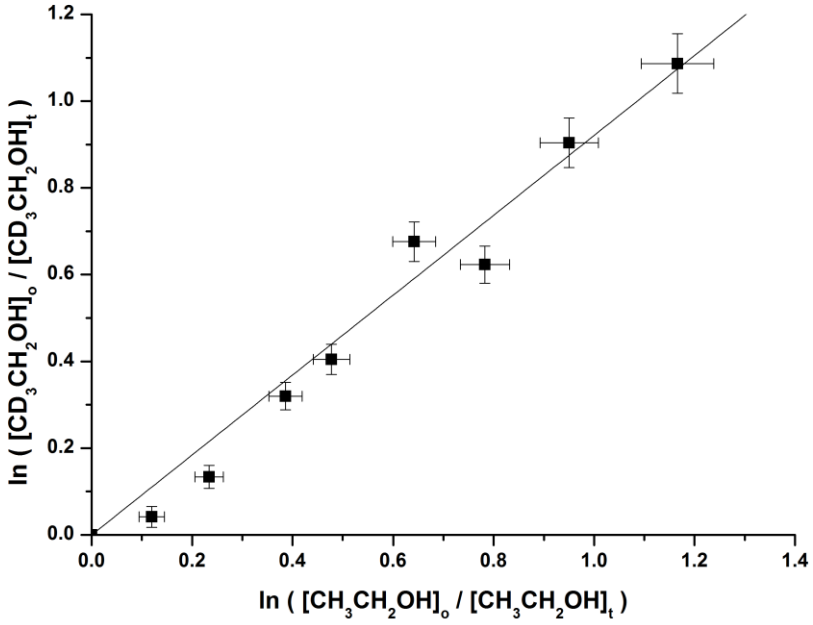

Figure 6.9: GC relative rate obtained for the reaction of CD_3CH_2OH with Cl atoms using ethanol as a reference compound in HIRAC at 292 K and 1000 mbar and nitrogen bath gas (Error bars represent 1σ).

The measured relative rate coefficients for Cl atoms reacting with ethanol, CH_3CD_2OH and CD_3CH_2OH are summarised in Table 6.1 and compared with previously reported literature values. Results obtained for reaction of Cl atoms with ethanol show excellent agreement between GC and FTIR for relative rate measurements (within ≤ 3%). The uncertainties quoted for experimental results were obtained from the linear regression of the relative rate results (using Regres2 software described in chapter 4).

The results obtained compare well with relative rate work by Wallington et al. (1988) and Khatoon et al. (1989), and are within error of the relative rate results by Taatjes et al. (1999). A large discrepancy in the rate coefficient of Cl atoms with ethanol is noticed for absolute rate studies, as was noted by Taatjes et al. (1999), who found the absolute rate coefficient to fall about 15% higher than the relative rate studies. No clear reason was found to explain why there was such a large difference between these two sets of studies, but an estimated uncertainty of ±20% was recommended for the rate coefficient obtained at 298 K (9.5×10^{-11} molecule^{-1} cm^3 s^{-1}).

	k/k_{ethane}	Rate coefficient (k / 10^{-11} molecule^{-1} cm^3 s^{-1})	Study
CH_3CH_2OH	1.48 ± 0.02	8.5 ± 0.2[a]	(Wallington et al., 1988c)
	1.40 ± 0.30	7.8 ± 0.2[a]	(Khatoon et al., 1989)
	-	10.1 ± 0.6[a]	(Nelson et al., 1990)
	-	10.5 ± 0.6[a]	(Crawford et al., 2004)
	-	10.2 ± 0.2[b]	(Seakins et al., 2004)
	-	9.4 ± 0.8[a]	(Taatjes et al., 1999)
	-	10.9 ± 1.2[b]	(Taatjes et al., 1999)
	1.43 ± 0.04	**8.3 ± 0.3[a]**	**This Work (GC)**
	1.40 ± 0.05	**8.1 ± 0.3[a]**	**This Work (FTIR)**
CD_3CH_2OH	1.60 ± 0.08	9.4 ± 1.1[a]	(Taatjes et al., 1999)
	-	9.0 ± 0.9[b]	(Taatjes et al., 1999)
	1.58 ± 0.04	**9.2 ± 0.3[a]**	**This Work (GC)**
CH_3CD_2OH	-	5.4 ± 0.5[b]	(Taatjes et al., 1999)
	1.32 ± 0.04	**7.6 ± 0.3[a]**	**This Work (GC)**

Table 6.1: Relative rate ratios and coefficients for Cl atom reactions with ethanol and its isotopologues at 292 ± 3 K and 1000 mbar in the HIRAC chamber compared with literature values ([a] relative rate study, [b]absolute rate study).

The relative rate work by Wallington et al. (1988) and Khatoon et al. (1989) are shown to differ by ≤ 20% from other relative rate studies by Nelson et al. (1990), and more recently by Seakins, Orlando and Tyndall (2004), Taatjes et al. (1999) and Crawford et al. (2004). The latter three studies are in better agreement with the value quoted by Nelson et al. of (1.1 ± 0.6) × 10^{-10} molecule^{-1} cm^3 s^{-1} (Nelson et al., 1990) and that recommended by IUPAC of (1.0 ± 0.06) × 10^{-10} molecule^{-1} cm^3 s^{-1} (Atkinson et al., 2006b).

It must be noted that the work by Taatjes et al. (1999), which is the most extensive work reported on the chemistry of the reaction of Cl atoms with ethanol, reports absolute measurements for this reaction that are about 15% higher than the relative rate measurements reported for the same study. The reason for this discrepancy was unclear as there is no obvious reason according to Taatjes et al. for these margins and a recommended value of (9.5 ± 1.9) × 10^{-11} molecule^{-1} cm^3 s^{-1} (Taatjes et al., 1999) was reported for this study based on the average of the two studies. This latter result is found to be within error of the results obtained in HIRAC for the reaction of Cl atoms with ethanol, although this would be due to the large estimated uncertainty (±20%) quoted by Taatjes et al..

The relative rate ratio to ethanol of (0.997 ± 0.06) for the reaction of Cl atoms with CD_3CH_2OH analysed using the HIRAC GC is in excellent agreement with the result obtained by Taatjes' study (0.98 ± 0.04). This could only be done based on peak height analysis since there was significant overlap between the two alcohols during this experiment. Unfortunately this could not be analysed using the FTIR due to overlapping spectra for the ethanol and its isotopologue (CD_3CH_2OH).

The importance of this validation was to confirm the suitability of the HIRAC FTIR for the purpose of studying these systems. The excellent agreement obtained between FTIR and GC measurements for the same experiment carried out for the reaction of Cl atoms with CH_3CH_2OH emphasises the suitability of this setup for further investigations of C-H hydrogen abstraction of Cl atoms from ethanol and its isotopologues using the HIRAC FTIR.

6.3.2 Isotopic branching ratios for Cl atom reactions with ethanol

The relative rate investigations confirmed the suitability of the HIRAC FTIR to perform further investigations on these Cl atom reactions with deuterated ethanols. The FTIR was used to measure the HCl and DCl branching yields produced from Cl atom reactions with CD_3CH_2OH, CH_3CD_2OH and CD_3CD_2OH. The study of the latter deuterated ethanol would provide guidance on how well the results for the α and β C-H abstractions obtained are. The O-H abstraction was not considered in this study given the very low abstraction rate from this site (≤ 5%) would be likely to result within the experimental error of the work being carried out given the preliminary nature of the results being presented.

Figure 6.10 shows the profiles of the different changes of HCl and DCl during Cl atom reaction of the three deuterated ethanols. This Figure shows the rough time frame used for working out these HCl:DCl ratios was around 100 – 150 seconds, since isotopic exchange would start to be more significant as the experiment progressed, as can be seen for CH_3CD_2OH profile in Figure 6.10.

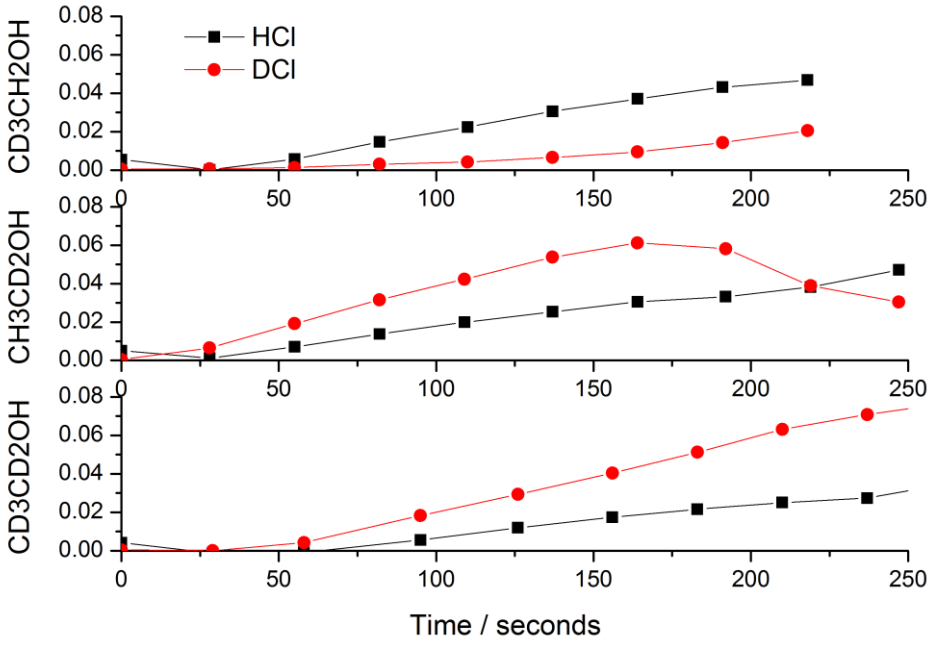

Figure 6.10: FTIR HCl and DCl relative changes of the absorption measurements for reaction of the different ethanol isotopologues with Cl atoms in HIRAC at 292 K and 1000 mbar in OFN nitrogen (fans off).

The outputs of these experiments were reported as HCl:DCl ratios (Δ[HCl]/Δ[DCl]) which are shown in Figure 6.11 and 6.12. The branching ratios were not presented given the large uncertainty in the HCl coming from the walls of HIRAC that could not be accounted for. The same procedure outlined in chapter 5 for the branching ratio calculations of Cl atom reactions with butanes was applied, by fitting a line through the plots shown in Figure 6.12 however a reliable branching ratio could not be obtained from this preliminary work.

The corresponding plots for the HCl:DCl ratios from these experiments are shown in Figure 6.12. Kinetic isotope effects unfortunately could not be derived either given the poor quantification of the results being reported.

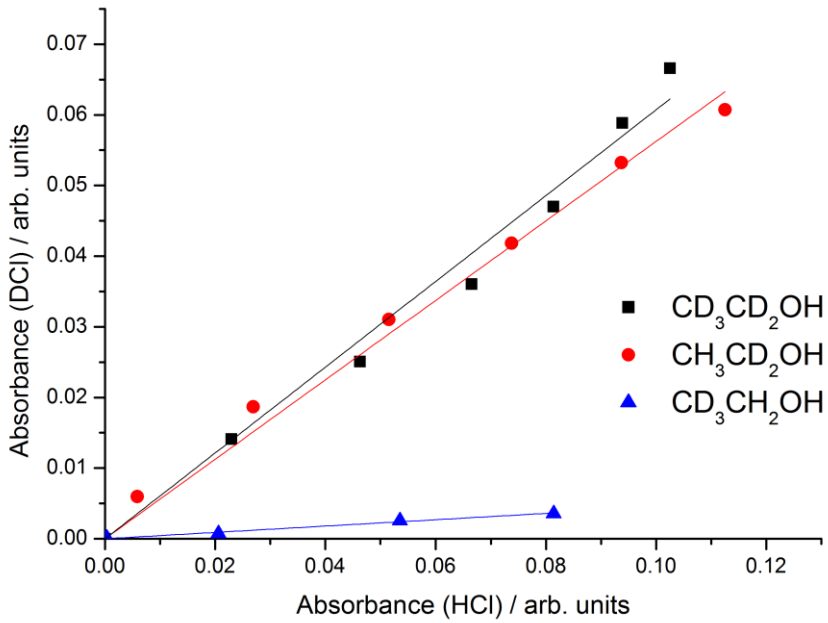

Figure 6.11: Absorbance of DCl versus HCl from reactions of Cl atom with CD_3CD_2OH, CH_3CD_2OH and CD_3CH_2OH in HIRAC at 292 K and 1000 mbar OFN nitrogen bath gas (errors are reported as 1σ).

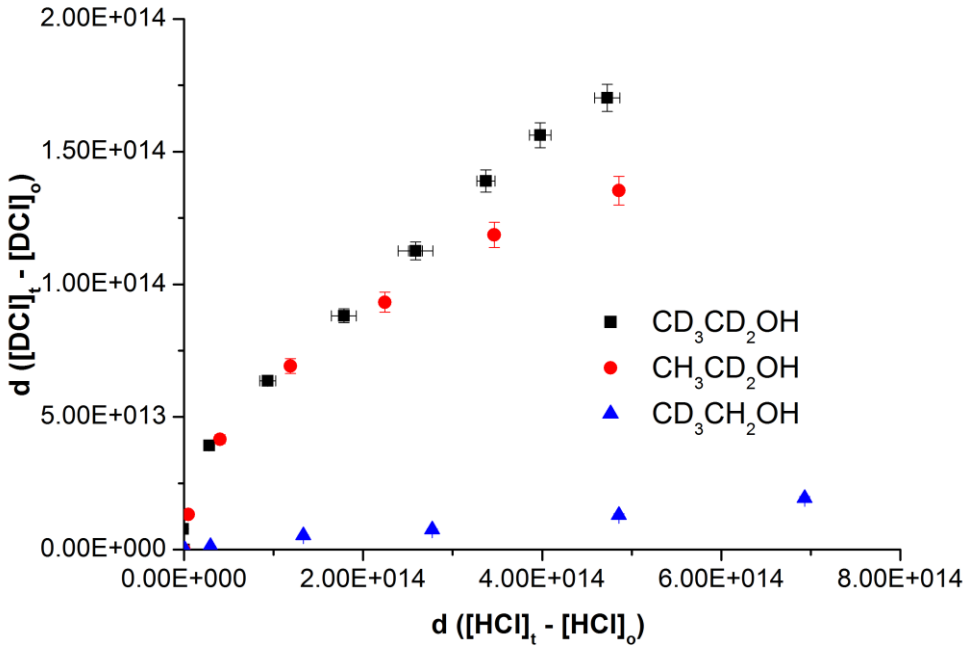

Figure 6.12: Δ[DCl] versus Δ[HCl] from reactions of Cl atom with CD_3CD_2OH, CH_3CD_2OH and CD_3CH_2OH in HIRAC at 292 K and 1000 mbar OFN nitrogen bath gas (errors are reported as 1σ).

Isotopologues	**HCl Yield** (Taatjes et al., 1999)
CD_3CH_2OH (β abstraction)	0.95 ± 0.10
CH_3CD_2OH (α abstraction)	0.16 ± 0.04
CD_3CD_2OH (hydroxyl abstraction)	≤ 0.05

Table 6.2: Taatjes's HCl yields calculated for Cl reactions with selectively deuterated ethanols.

6.4 Discussion and Conclusions

The understanding of Cl atom chemistry is of increased importance due to higher concentrations of Cl atoms being inferred in marine, polar and urban atmospheres resulting in competition with OH for major oxidation reactions (Saiz-Lopez and von Glasow, 2012). Room temperature rate coefficients for Cl atom reactions with ethanol and its isotopologues have been determined in HIRAC from FTIR and GC measurements. The results obtained are in reasonable agreement with some of the relative rate literature values by Taatjes et al. (1999), Wallington et al. (1988) and Khatoon et al. (1989), however differed from absolute rate coefficients reported by different authors. GC-FID and FTIR results obtained in HIRAC for the reaction of ethanol with Cl atoms were in excellent agreement with each other, differing by only 3%. This confirmed the suitability of using the HIRAC FTIR for carrying out further Cl atom studies with ethanol.

The branching fractions for HCl and DCl production during the reaction of Cl atoms with deuterated ethanols could not be determined in HIRAC, however the plots shown in Figure 6.11 and 6.12 give the correct trend that is in agreement with previous work by Taatjes (Taatjes et al., 1999). However due to several difficulties in working out the isotopic branching ratios for these deuterated ethanols as has already been elaborated earlier, these values were considered unreliable. This is primarily due to the poor characterisation of the HCl evolution and isotopic exchange on the chamber walls. As such, one must consider these results to be preliminary in nature, since reliable quantitative data could not be obtained unfortunately from the investigations carried out here. The HCl evolving from the walls of the chamber could be assumed to be constant provided they were carried out over the same day and the chamber had been properly cleaned out between each experiment. If this assumption is correct, then there is no need to subtract the residual HCl formation rate, which is an exponential function in any case, and the ratio could be considered to include an extra quantity of HCl that is not representative of the reaction of ethanol with Cl atoms. Given the ratios of HCl:DCl for the different isotopologues would scale as expected between each other, than it is fair to conclude that the experimental results obtained would be valid, but subject to further work in improving the methodology in order to obtain more quantitative evidence to back these findings.

Another difficulty encountered that would be likely to have an effect on these studies was the volatile organic impurities in the ethanols. In a previous study by Taatjes, the impurities were measured using NMR and corrected for in the measured coefficients and yields, which were however very small influences (≤ 1%). The corrections for measured impurities in CD_3CH_2OH were negligible as the main impurity was found to be normal ethanol, which CH_3CD_2OH may be slightly worse but still 1 – 2% level which is within random uncertainties in measurements. Repeat freeze-pump-thaw exercises ensured this uncertainty was minimised as much as possible.

The final outcome of this work points towards the difficulty in carrying out isotopic experiments of this nature in metal chambers. The chamber wall effects are a major obstacle that are difficult to characterise and as such residual [HCl] could not be accurately determined for the purpose of these studies to quantify the results obtained by subtracting away this HCl formed from a combination of isotopic exchange and chlorine atoms reacting with residual organics coming off the walls. Despite the chamber walls being cleaned before these experiments were carried out, the lamps and chlorine gas only experiments would still result in HCl formation, indicating the difficulty in cleaning such a large metal chamber for experiments of this kind. Nevertheless the suitability and potential of the HIRAC FTIR system has been demonstrated in this chapter, and future similar experiments could be carried out for different branching ratio studies in HIRAC of interest; however caution needs to be taken in assessing the residual HCl.

Chapter 7 – Investigations of OH generation methods under low NO_x conditions

7.1 Introduction

A recent and growing interest in the understanding of the mechanisms of OH oxidation under low NO_x has stemmed from the missing OH source in non-polluted environments. The recycling of OH due to NO_x in urban areas does not occur in the tropics and marine environments, however [OH] measured in these environments has been found to be similar to urban levels implying a potential biogenically driven recycling OH source that has not been fully resolved and results in discrepancies between models and observations (Lelieveld et al., 2008, Stone et al., 2012, Whalley et al., 2012, Stone et al., 2011, Pugh et al., 2010, Hofzumahaus et al., 2009). Isoprene oxidation has been a topic of great interest in recent years owing in particular to the recycling of OH and to the discrepancies in product yields and mechanisms of the reaction of OH radicals with isoprene (Archibald et al., 2011, Malkin et al., 2010, Seakins and Blitz, 2011, Stone et al., 2011, Brune et al., 2013).

The presence or absence of NO_x has a significant effect on the HO_x cycle in the troposphere, as is highlighted in Figure 7.1.

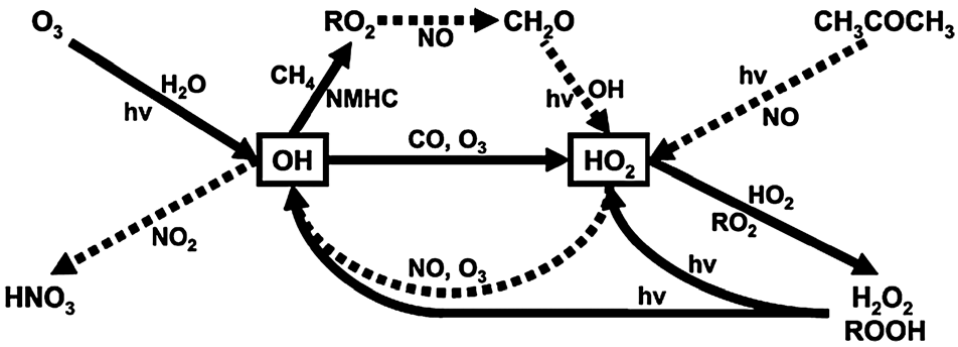

Figure 7.1: Simplified HO_x cycle with high NO_x (polluted) pathway in dashed lines while background conditions are in solid lines (Olson et al., 2006).

Under high NO_x conditions a series of reactions (R7.1 – 7.3) are known to lead to OH recycling:

$$HO_2 + NO \rightarrow OH + NO_2 \quad \text{(R7.1)}$$
$$RO_2 + NO \rightarrow RO + NO_2 \quad \text{(R7.2)}$$
$$RO + O_2 \rightarrow R'CHO + HO_2 \quad \text{(R7.3)}$$

HO_2 formed in R7.3 regenerates OH radicals (R7.4), and subsequent photolysis of NO_2 leads to formation of O_3 which is the main precursor of OH in the troposphere.

$$NO_2 + h\nu\ (\leq 420\ nm) \rightarrow O(^3P) + NO \quad \text{(R7.4)}$$
$$O(^3P) + O_2 + M \rightarrow O_3 + M \quad \text{(R7.5)}$$

Recent modelling studies have shown that the modelled OH under predictions worsened under low NO_x conditions, as a result of biogenically-influenced environments (Stone et al., 2012, Dusanter et al., 2009, Stone et al., 2010). An answer to this may be found by looking into the degradation processes of biogenic VOCs such as isoprene and α-pinene that may contribute to this missing OH precursor.

A recent HO_x-Comp campaign aimed at obtaining HO_2 and OH measurements revealed [OH] measured in low NO_x environments are many times higher than OH expected from models (Elshorbany et al., 2012, Kanaya et al., 2012). A simplified HO_x cycle shown in Figure 7.2 elaborates the pathways under low NO_x in solid lines. Uncertainties in HO_2 measurements resulting from RO_2 interferences are also shown to lead to higher than currently estimated OH in atmospheric models, which implies new OH sources need to be identified for these environments in order to better understand the OH recycling occurring.

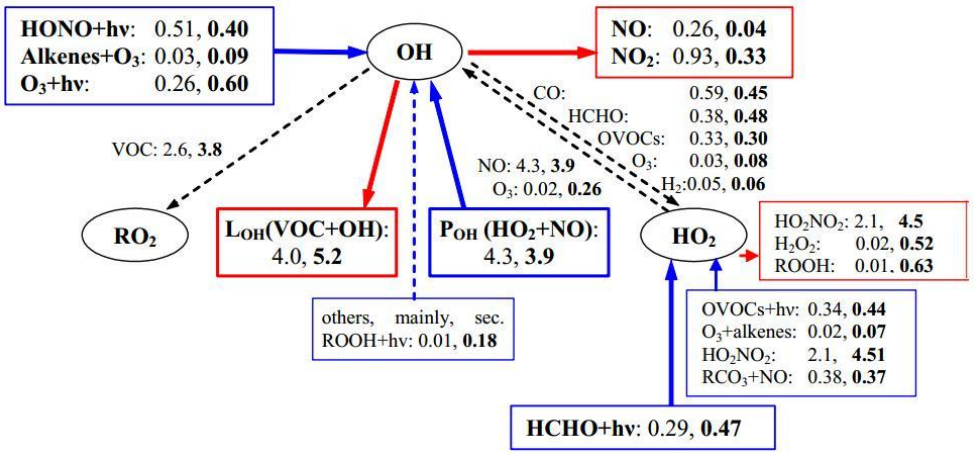

Figure 7.2: Simplified HO_x cycle with high NO_x (polluted) pathway in dashed lines while background conditions are in solid lines (Elshorbany et al., 2012).

A high NO_x OH source has already been characterised in HIRAC by Tamsin Malkin using methyl nitrite photolysis (Malkin, 2010). Large chambers such as the EUPHORE chamber in Valencia and the SAPHIR chamber in Jülich, described in chapter 1, are unable to carry out low NO_x conditions as NO_2 reacts with water to form HNO_2 which adheres to the Teflon chamber walls. In HIRAC this can be remediated by cleaning the walls and evacuating the chamber prior to experiments, however for facilities such as EUPHORE and SAPHIR, which are essentially large Teflon bags, this is not possible. Therefore given its size, HIRAC has the potential that few chambers have to simulate these low NO_x conditions and be able to better understand the source of the missing OH in non-urban environments.

The aim of this chapter is to evaluate the ozonolysis of alkenes, photolysis of alkyl peroxides and acetone in the attempt to identify a viable low NO_x OH generation methods for the purpose of isoprene oxidation studies in HIRAC. The first section will discuss the potential use of a non-photolytic source of OH (ozonolysis of simple alkenes). This will be followed with the discussion of two photolytic sources of OH (UV photolysis of acetone and of peroxides).

7.2 OH sources in chamber studies

OH chemistry has been extensively reviewed in the literature (Atkinson, 1986, Heard and Pilling, 2003), however a full understanding of the products formed during VOC oxidation processes brought about by OH is lacking and is required to understand tropospheric chemistry more fully (Stone et al., 2011, Whalley et al., 2012, Archibald et al., 2011). There have been various OH generation methods reported for chamber studies (Siese et al., 2001, Karl et al., 2004, Albu et al., 2006). Several investigations have been reported using multiple atmospheric simulation chambers.

An example of the different generation methods available is highlighted in a study by Picquet-Varrault et al., on the OH radical oxidation of allyl acetate. The study was performed over three different chambers using three different OH precursors which were chosen based on the construction of the chamber and the suitability of the OH precursor (Picquet-Varrault et al., 2002). Two of these investigations were

performed in the LISA facility in Paris (one experiment in an indoor Teflon film bag and another in an indoor pyrex photoreactor), and the other investigation was carried out in the EUPHORE chamber in Valencia.

The first sets of experiments in the LISA facility were carried out using the photolysis of hydrogen peroxide in purified air. All kinetic results for this study were obtained from these experiments. A mechanistic study was also carried out in the pyrex photoreactor using methyl nitrite or nitrous acid (HNO_2) photolysis as their OH radical generation method in purified air. The outdoor simulation chamber EUPHORE experiments were aimed at obtaining additional mechanistic information from the reaction of OH radical with allyl acetate. In this case OH was generated by the photolysis of nitrous acid formed in chambers by reaction of NO_x with water to walls. The formation of nitrous acid in atmospheric chambers has been known for some time (Besemer and Nieboer, 1985) and is the main method of radical generation in the EUPHORE chamber.

$$2\ H_2O + 2\ NO \rightarrow 4\ HNO_2 \qquad \text{(R7.6)}$$
$$HNO_2 \rightarrow OH + NO \qquad \text{(R7.7)}$$

It is based on the surface area/volume ratio which in principle can be used to roughly estimate the OH radical flux from this photolysis in chambers (Besemer and Nieboer, 1985).

The OH sources investigated in HIRAC and reported in this chapter are three different low NO_x methods: the ozonolysis of alkenes and photolysis of peroxides and acetone. As already mentioned in chapters 1 and 2, the capability of detecting radicals in a chamber the size of HIRAC is what makes it unique (Glowacki et al., 2007a). Alkyl nitrite photolysis has been previously characterised by Tamsin Malkin in HIRAC (Malkin, 2010). Alkyl nitrite photolysis has been used as an OH precursor in kinetic studies involving OH for many years and is a well-established method under high NO_x conditions (Atkinson, 1986, Zhou et al., 2008). The photolysis of methyl nitrite at 300 – 400 nm leads to the generation of OH radicals *via* the following reaction mechanism:

$$CH_3ONO + h\upsilon \xrightarrow{\lambda \geq 290\ nm} CH_3O + NO \qquad \text{(R7.8)}$$
$$CH_3O + O_2 \rightarrow CH_2O + HO_2 \qquad \text{(R7.9)}$$
$$HO_2 + NO \rightarrow OH + NO_2 \qquad \text{(R7.1)}$$

Methyl nitrite photolysis in HIRAC gave OH yields in the order of 10^8 molecule cm^{-3} in HIRAC, however these results have been questioned and recent work by Fred Winiberg on the HIRAC FAGE revealed a possible unknown interference under high NO_x conditions which had previously not been reported. For this reason, and the necessity to conduct reactions under low/zero-NO_x conditions in HIRAC to investigate the missing OH recycling for isoprene oxidation, these three different OH sources have been individually assessed in this chapter.

FAGE measurements would be beneficial in backing up these results and these methods also provide a way of calibrating the instrument in HIRAC. It must be pointed out that the FAGE instrument was out of action due to problems with the FAGE laser system at the time when the majority of these experiments were carried out. The only FAGE results obtained and to be reported in this chapter are for the *tert*-butyl hydroperoxide. This is not the first time an OH yield was determined by FAGE in HIRAC (Malkin et al., 2009). The unavailability of FAGE for a number of these investigations meant that only the relative rate and scavenger methods, to be described in the following section, were available to investigate the OH yields from some of the generation methods investigated.

7.3 Ozonolysis of simple alkenes

7.3.1 Introduction

The ozonolysis of alkenes in the atmosphere has been introduced during the characterisation of the mini photolysis chamber in Chapter 3. The gas phase reactions of O_3 with alkenes and other VOCs containing carbon-carbon double bonds lead to the production of OH radicals (Johnson and Marston, 2008). Being a non-photolytic precursor, this process is regarded as being the major night-time source of OH in the troposphere, and is also the dominant source during the daytime when alkene concentrations are significantly high, such as in urban environments (Paulson and Orlando, 1996).

The mechanism of the ozonolysis of alkenes is complex (Johnson and Marston, 2008) and has been discussed in Chapter 3 during the characterisation of the mini photolysis chamber. The reaction is known to proceed *via* a Criegee intermediate (Criegee and Wenner, 1949) which is either stabilised collisionally or decomposes to give rise to OH radicals as is shown in Figure 7.3.

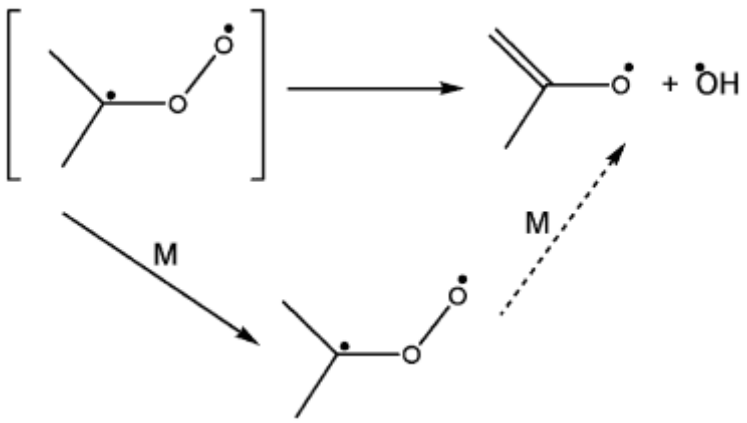

Figure 7.3: Mechanism of OH radical generation *via* Criegee intermediate rearrangement during the ozonolysis of trans-2-butene (Johnson and Marston, 2008).

There is evidence that suggests that a 1, 4-sigmatropic shift in a Criegee followed by bond fission will result in OH radical formation (Martinez and Herron, 1988). The OH yield depends on the alkene. These experiments have been previously investigated by Tamsin Malkin in HIRAC (Malkin, 2010) who carried out experiments for trans-2-butene and isoprene ozonolysis in HIRAC and also obtained absolute OH yields from the ozonolysis of isoprene (Malkin et al., 2009).

Experiments have been carried out again to reinvestigate the suitability of this reaction as an OH source under low NO_x conditions. This method is only suitable as a source of OH when the species being investigated reacts faster with OH than the competing reaction between the alkene and OH. There is also need for the species to have a slow reaction with O_3. An investigation on aerosol aging in a small chamber made use of this generation method as a source of low NO_x OH (Lambe et al., 2007).

7.3.2 Experimental Method

O_3 generation in HIRAC was performed using a mercury pen-ray lamp (Oriel Spectra-Physics, 6035) which photolysed the O_2 introduced in these experiments until 1 – 3 ppmv of [O_3] was generated prior to the introduction of the alkene. O_3 was monitored were determined by a conventional UV photometric O_3 analyser (Thermo Electron Environmental instruments, Model 49C). A standard flow rate of 2 L/minutes sampled continuously from HIRAC with averaging time of 10 s. A detection limit of 1 ppb was determined for this instrument based on previous calibrations by Glowacki using a commercial ozone primary standard (Thermo Electron Corporation 49i-PS) and intercomparison with the HIRAC FTIR (Glowacki et al., 2007b).

All experiments were carried out in 80% departmental nitrogen, and 20% oxygen. All gases were used as provided from the supplier: *n*-butane (Sigma-Aldrich, 99%) and *iso*-butane (Sigma-Aldrich, 99%). Several purification freeze-pump-thaw cycles were carried out for trans-2-butene (Sigma Aldrich, 99.5%) and cyclohexane (Sigma-Aldrich, 98%) to remove any impurities that may react with OH. Typical initial concentrations for relative pair hydrocarbon tracers were ~1 ppmv each, while typical concentrations of cyclohexane scavenger for scavenger experiments were ~400 ppmv. The hydrocarbons were flushed into HIRAC *via* the delivery vessel prior to the introduction of the alkene to record their stability on the GC-FID (Agilent Technologies 6890N Flame Ionisation Detection). This instrument has been described in Chapter 4, and was used to measure the decay of the hydrocarbon and/or scavenger tracers. The instrument was set to sample every 2 minutes, and the oven was maintained at 313 K. Once the alkene was introduced, the ozonolysis reaction commenced and both the O_3 analyser and GC-FID recorded decays of the reactants and hydrocarbon pairs. These are shown in Figures 7.4 and 7.5 for O_3 and trans-2-butene respectively. All four fans were operational during these experiments and were run at 50% of their output speed (1500 rpm).

The OH generated from these methods could be estimated using one of two known techniques: relative rate tracer pair and scavenger technique. These two methods, albeit indirect, both provide evidence of OH generation during the experiments. The main criteria for the selection of the hydrocarbons used for both

methods are dependent on their reactivity towards OH radicals but relative unreactivity towards any other reactive species present in the chamber. The relative rate tracer pair makes use of the same principles highlighted in chapter 4 for the relative rate method, and provided the above mentioned criteria are met, the relative changes of these two hydrocarbons should be dictated by the relative reactivity with OH being generated. A quantitative way of obtaining OH yields from these experiments would involve use of a scavenger hydrocarbon method, which implies addition of a hydrocarbon in high enough concentrations to react with all the OH being generated in the chamber. The OH generated here could be inferred by quantitatively interpreting the effect of varying concentrations of the scavenger during the experiment.

OH reacts with hydrocarbons present in HIRAC giving several oxidation products. The rate of reaction will depend on the concentration of the hydrocarbon and the OH, which can be inferred from the hydrocarbon decay, provided the hydrocarbon is only removed due to reaction with OH.

$$OH + HC \rightarrow \text{Products} \qquad \text{(R7.10)}$$

$$-\frac{d[HC]}{dt} = k_{OH+HC}[OH][HC] \qquad \text{(Eq 7.1)}$$

$$[OH] = \frac{(-d[HC]/dt)}{k_{OH+HC} \times [HC]} \qquad \text{(Eq 7.2)}$$

where –d [HC]/*dt* is the decay rate of the hydrocarbon and k_{OH+HC} is the rate coefficient for removal of the hydrocarbon with OH. The rate coefficient can be determined from the literature and also obtained using a relative rate during the experiment, and the hydrocarbon concentration [HC] can be measured, the [OH] can be inferred using the Guggenheim method (Bloss et al., 2004). This is first done by calculating the experimental pseudo first order coefficient for hydrocarbon decay:

$$k' = \frac{\ln([HC]_1/[HC]_2)}{(t_2 - t_1)} \qquad \text{(Eq 7.3)}$$

where $[HC]_1$ and $[HC]_2$ are the concentrations at t_1 and t_2 respectively. The mean OH concentration can then be inferred by calculating the following:

$$[OH] = \frac{(k' - k_{dil})}{k_{OH+HC}} \qquad \text{(Eq 7.4)}$$

Where k_{dil} is the dilution rate of the measured [HC] due to FAGE and GC sampling. Saturated hydrocarbon tracer pairs were used to obtain an [OH] estimate from these experiments. An *iso*-butane/*n*-butane hydrocarbon pair was used. The relative rate methodology for these experiments is similar to that described in Chapters 4 and 5. A distinct disadvantage of a scavenger experiment over the relative rate tracer pair method is the mean [OH] will be lowered due to the presence of excess amounts of hydrocarbon scavenger (≤ 100 ppmv) reacting with all the OH being generated. The relative rate tracer pair technique uses smaller concentrations (≥ 1-2 ppmv) of hydrocarbons resulting in a larger more detectable mean [OH].

7.3.3 Results

Results obtained for two sets of experiments on the ozonolysis of trans-2-butene are presented here. Further investigations will take place to fully characterise this generation method in HIRAC, and these results are expected to appear in Fred Winiberg's thesis (2014) and therefore results reported in this section are preliminary. Both experiments carried out used similar starting conditions (2 ppmv O_3, 3 ppmv trans-2-butene, and 1 ppmv of hydrocarbon tracers). One of the experiments included cyclohexane as a scavenger, while the other made use of two relative rate tracers. The decays of the O_3 and trans-2-butene decays from the first experiment are shown in Figures 7.4 and 7.5.

Unfortunately it was not possible to obtain an OH yield from the scavenger experiments given the very small relative stoichiometric change of cyclohexane observed on the GC-FID and the unavailability of the FTIR instrument at the time of the experiments meant cyclohexanone product yields could not be used as a measure of OH as was done previously by Tamsin Malkin in HIRAC (Malkin et al., 2009). Note that in order for the cyclohexane to scavenge at least 99% of the OH generated, about 400 ppmv of cyclohexane was estimated to be introduced in HIRAC prior to the start of the experiment.

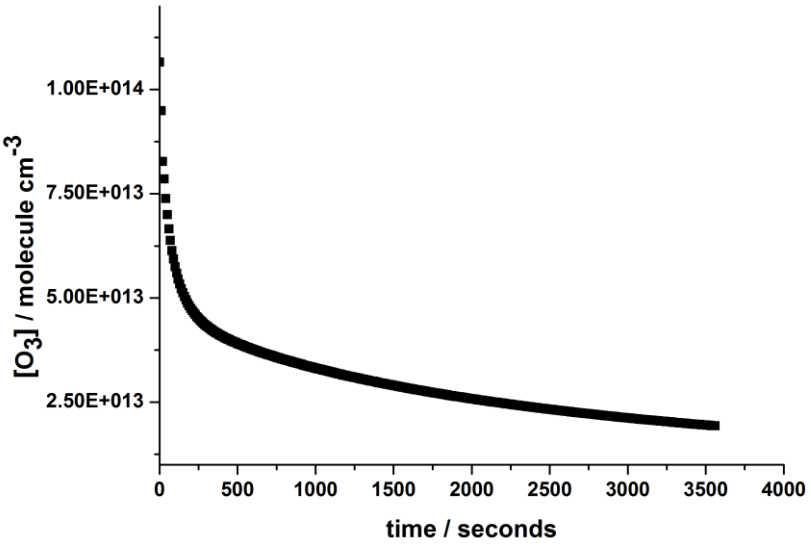

Figure 7.4: $[O_3]$ decay with trans-2-butene, 3 ppmv, in the presence of a cyclohexane scavenger, 500 ppmv, in HIRAC at 1000 mbar and 292 K.

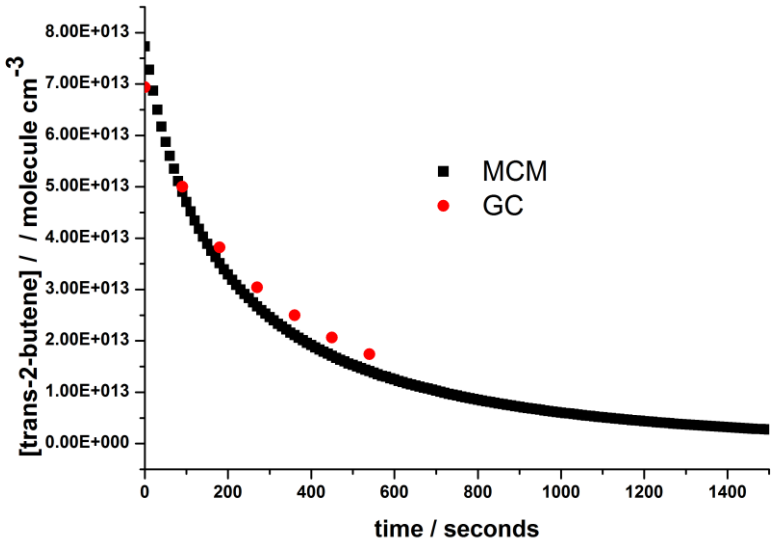

Figure 7.5: Comparison of MCM modelled trans-2-butene decay with experimental decay from reaction of trans-2-butene, 3 ppmv, with O_3, 2 ppmv, in the presence of a cyclohexane scavenger, ~500 ppmv each, in HIRAC at 1000 mbar and 292 K.

A relative rate experiment was also carried out for *iso*-butane/*n*-butane pair during the ozonolysis of trans-2-butene. A relative rate plot for this experiment is shown in Figure 7.6. 1.5 ppmv of *iso*-butane and *n*-butane were used, with n-butane being used as a reference compound in this case given that its reaction with OH has

been reviewed by IUPAC (Atkinson et al., 2006a). The rate coefficient used for the reaction of OH with *n*-butane was (2.35 ± 0.23) × 10^{-12} molecule cm^{-3} s^{-1}.

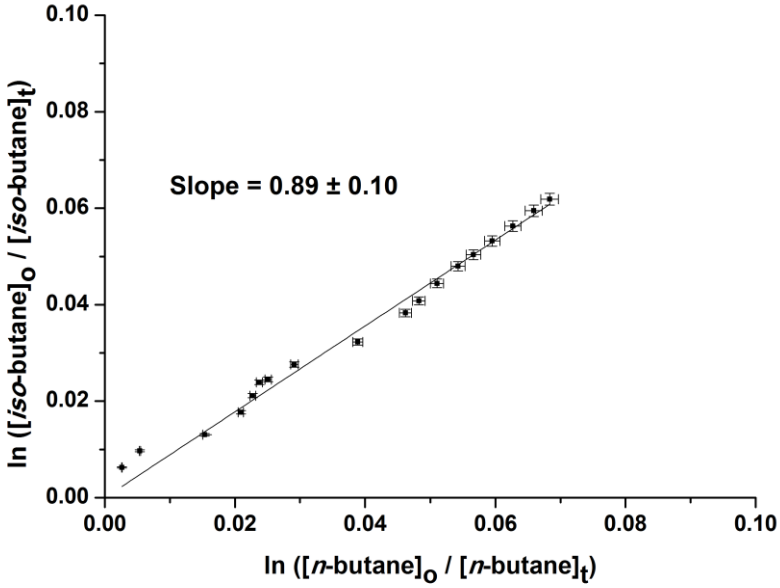

Figure 7.6: Relative hydrocarbon (*n*-butane/*iso*-butane, 1ppmv each) pairs included during trans-2-butene (2 ppmv) with O_3 (3 ppmv) in HIRAC at 1000 mbar and 292 K.

The above relative rate plot demonstrates that OH is being generated in HIRAC from this method. The relative rate ratio obtained for *iso*-butane/*n*-butane is in excellent agreement with ratio from rate coefficients recommended by IUPAC (0.90 ± 0.08) (Atkinson et al., 2006a). The OH generated during this experiment could be estimated from the hydrocarbon tracer pair decays using the methodology detailed in Section 7.3.2. These calculations gave a mean [OH] in HIRAC of 1.1 × 10^6 molecule cm^{-3}, averaged over the hydrocarbon decays measured using the GC-FID. This is lower than what is expected from trans-2-butene (~10^7 molecule cm^{-3}) which has been previously reported to have an OH yield (Y_{OH}) of 0.47. These experiments could not be backed up with FAGE measurements, and therefore a steady state [OH] could not be verified for this OH generation method.

7.3.4 Discussion

The result obtained from this investigation demonstrates the potential of HIRAC and the instruments available to qualitatively generate a low NO_x source of OH. The absence of FAGE during these experiments meant it was not possible to quantify the OH generated. Further characterisation is being carried out to understand the viability of this method as an OH generation method for HIRAC under low NO_x conditions.

The hydrocarbon decays gave a peak [OH] estimates of ~1.1 x 10^6 molecule cm^{-3}. The OH yield (Y_{OH}) had been previously reported by Tamsin Malkin to be 0.47 for this reaction, implying that if this method could be sustained for longer periods of time then it may be a suitable method of generating OH under low NO_x conditions in HIRAC.

This method gives a reasonably high peak [OH], within the detection limits of the FAGE instrument, from small initial concentrations of alkene and ozone in HIRAC. The challenge with this OH generation method is being able to sustain the steady state of OH in HIRAC, which would be dependent on replenishing the alkene and O_3 gradually during the duration of the experiment. There may also be issues regarding reactivity of O_3 in particular if isoprene were to be investigated, and the difficulty in analysing all the products generated from these ozonlysis reactions.

7.4 Low pressure acetone photolysis

7.4.1 Introduction

Acetone, CH_3COCH_3, is the most abundant carbonyl compound in the atmosphere, now regarded as being an important source of OH in the upper troposphere (Sprung and Zahn, 2010). This arises from higher than previously thought concentrations of acetone in these parts of the troposphere (Folkins and Chatfield, 2000).

Photolysis is a significant removal process and a source of HO_x radicals in the upper troposphere (Gierczak et al., 1998). Acetone originates from both natural (vegetation) and anthropogenic (biomass burning) emissions, as well as from the oxidation processes of alkanes (McKeen et al., 1997, Gierczak et al., 1998, Talukdar et al., 2003). The two main pathways of acetone photolysis are shown in R7.11a and R7.11b:

$$CH_3COCH_3 + h\upsilon\ (\leq 338\ nm) \rightarrow CH_3CO + CH_3 \quad \text{(R7.11a)}$$
$$CH_3COCH_3 + h\upsilon\ (\geq 299\ nm) \rightarrow CH_3 + CH_3 + CO \quad \text{(R7.11b)}$$

Acetone photolysis is a suitable method for generating NO_x free OH in chamber studies (Seakins and Blitz, 2011, Carr et al., 2008). It is also readily available as it is used ubiquitously as a solvent. This method of generating OH radicals is considered to be "straightforward" as it does not require any synthesis. The pathway leading to HO_x formation is highlighted from R7.12 – R7.15:

$$CH_3COCH_3 + h\upsilon\ (\geq 299\ nm) + 2O_2 \rightarrow CH_3O_2 + CH_3C(O)O_2 \quad \text{(R7.12)}$$
$$CH_3COCH_3 + h\upsilon\ (\geq 299\ nm) \rightarrow CH_3CO + CH_3 \quad \text{(R7.13)}$$
$$CH_3CO + O_2 \rightarrow OH + CH_2C(O)O \quad \text{(R7.14)}$$
$$CH_2O + h\upsilon + 2O_2 \rightarrow CO + 2HO_2 \quad \text{(R7.15)}$$

The yield of acetylperoxy radicals from R7.14 is known to decrease from >95% at pressures above 135 mbar to about 50% at 8 mbar (Tyndall et al., 1997). Indirect evidence for the formation of OH radicals from the low pressure decomposition has been shown by Tyndall's work. The carbon-containing coproduct of this channel has been recently identified as an alpha lactone by Chen and Lee (2010) that support the concerted mechanism shown in Figure 7.7. This mechanism had been suggested by Tyndall but could not be proved due to the difficulty in identifying the coproduct(s) of the reaction, but Chen and Lee have reported identifying this lactone using transient FTIR (Chen and Lee, 2010).

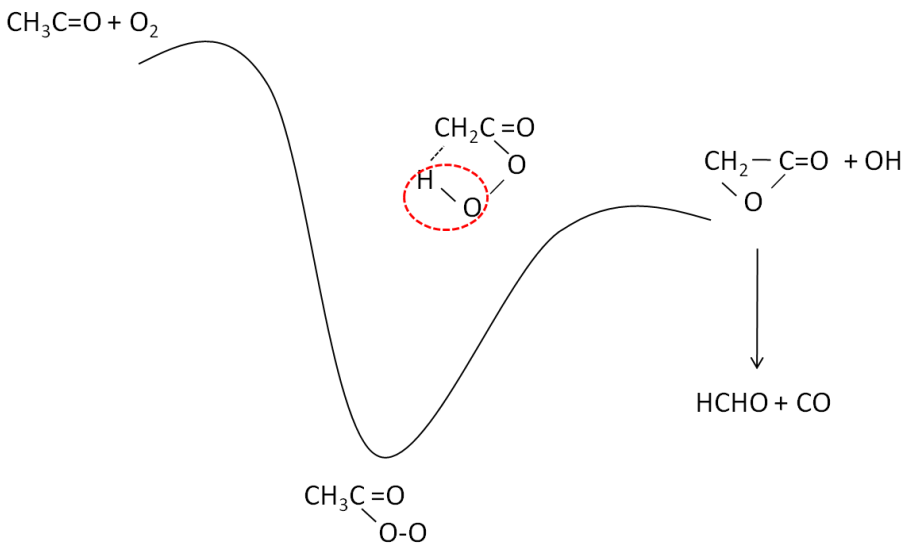

Figure 7.7: Reaction pathway for acetone photolysis under low pressure and the production of OH.

At higher pressures however the OH yield is outcompeted by stabilisation by collision of an excited peroxy radical with other species present in the atmosphere (Arnold et al., 2004, Carr et al., 2008). As a consequence, using this method at high pressures would yield low [OH], thereby being a more suitable source for experiments conducted at lower pressures. The suitability of this method was tested at pressures of ≤ 200 mbar which is relevant to the upper troposphere and therefore not as relevant to biogenic VOCs oxidation which are short-lived in the troposphere.

7.4.2 Experimental Method

These experiments were performed in the recently refurbished mini photolysis chamber detailed in chapter 3 (FAGE is inaccessible for this chamber). Initial experiments and characterisation of this chamber has already been highlighted in chapter 3, and this section follows from the work done on the pressure dependence of acetone photolysis.

The lamps used for these photolysis experiments were two 254 nm Philips 75W/HO TUV T8 UV C lamps and all these experiments were carried out in an air mix made up of 80% departmental N_2 and 20% O_2. All gases were used as provided from the supplier: propane (Sigma-Aldrich, 99%), *n*-butane (Sigma-Aldrich, 99%)

and 2-methylpropene (Sigma-Aldrich, 99%). Several purification freeze-pump-thaw cycles were carried out for liquids used in these experiments: acetone (Sigma Aldrich, 99.5%) and cyclohexane (Sigma-Aldrich, 98%) in order to remove any impurities that may photolyse or have an effect on the chemistry being studied.

Hydrocarbon and acetone decays were monitored using the GC-FID instrument described in chapter 2. The reaction mixture was analysed at 6 minute intervals for approximately 40 minutes prior to photolysis to determine the presence of any potential dark reaction that could be removing any of the reactants. A recently setup LabView 10.1 software has been developed to read the thermocouples in the chamber read ~290 ± 3 K (the uncertainty was taken as the average variation during the duration of the experiments).

Typical starting concentrations used for all these experiments were ~60 – 120 ppmv acetone and ~1 – 5 ppmv hydrocarbons. These proportions were found to be suitable for ensuring 99% of [OH] generated would react with the hydrocarbons used as tracers to quantify the [OH]. This OH generation could be quantified through measurement of hydrocarbon decays on the GC-FID instrument. The relative decay of the two hydrocarbons is a further confirmation that both hydrocarbons are reacting only with the OH radical and no other species that may be present during the experiment.

Calibration of the GC-FID instrument was necessary prior to experiments to confirm validity of sampling and test the recently set up solenoids and LabView software used to automate the sampling process for the mini photolysis chamber. This was carried out by repeat dilutions of a known measured concentration of the acetone and ethane, and measuring the peak areas and peak heights which are expected to scale linearly with concentration. The measured amounts of organics were flushed into the mini photolysis chamber *via* a stream of N_2 through a 4.33×10^{-3} L copper delivery vessel.

During the hydrocarbon decay experiments, repeat GC measurements were taken from the chamber and an OH yield was determined from the photolysis of acetone using the following relationship:

$$[OH] = Y_{OH} \times \Delta\,[Acetone] \qquad \text{(Eq 7.5)}$$

Where Y_{OH} is the OH yield from acetone photolysis during the experiment. The [OH] is experimentally determined based on knowing the concentration of hydrocarbon at the start of the experiment and the loss of hydrocarbon during photolysis would translate into [OH] present in the chamber. A relative rate experiment carried out for these systems would confirm the hydrocarbon being investigated is only reacting with OH radicals based on known rate coefficients for their reaction with OH.

7.4.3 OH estimation from low pressure acetone photolysis

The potential of these reactions as a source of OH radicals for flash photolytic kinetic studies has been investigated by Carr et al. (Carr et al., 2008). The merits of the ketone/oxygen OH source are contrasted with other established precursors. The advantage of using this technique as an OH source in chamber studies in that it is a NO_x free source and it does not require synthesis or problematic storage. The main disadvantage of this technique, more so at high pressures, is its low OH yield, meaning high concentrations of acetone are required to produce comparable OH concentration of the other techniques (~50 ppmv at 1000 mbar).

An average photolysis rate for acetone ($J_{acetone}$) of $(2.21 \pm 0.15) \times 10^{-4}$ s^{-1} was obtained in the mini photolysis chamber over pressures of 150, 175 and 200 mbar (shown in Figure 7.7). All three pressures gave $J_{acetone}$ within error of the average, therefore very little change was observed over this pressure range, further confirming the pressure independence of this process as had already been stated in chapter 3.

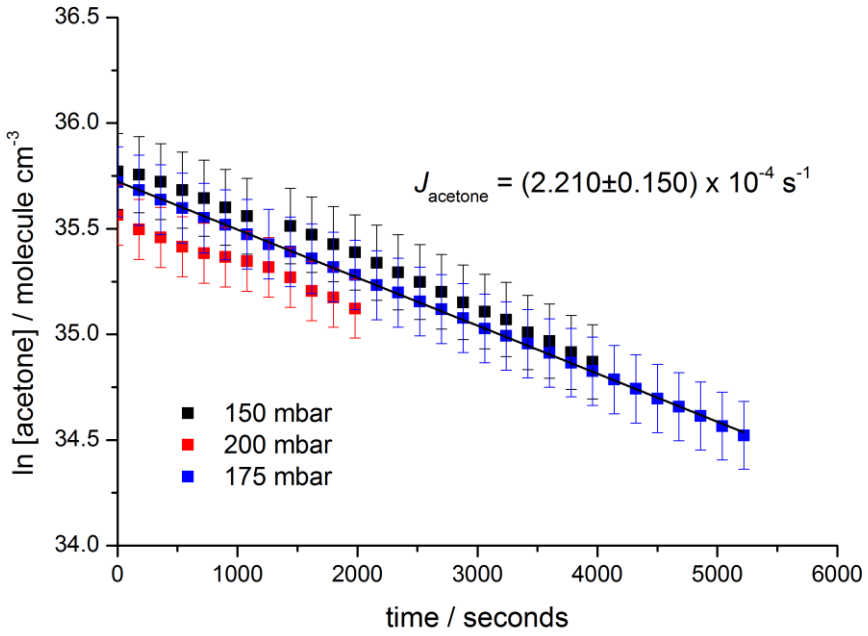

Figure 7.8: Average $J_{acetone}$ for acetone at 290 ± 5 K over a pressure range of 150 – 200 mbar in the mini photolysis chamber.

Scavenger experiments were initially carried out using excess cyclohexane, but as was noted for the alkene ozonolysis experiments, difficulties were encountered in obtaining a detectable change of cyclohexane on the GC-FID. A hydrocarbon tracer experiment was carried out with 1.5 ppmv of propane and *n*-butane being introduced in the mini photolysis chamber at 200 mbar and 292 K. The hydrocarbon decays were monitored using the GC-FID and decays are shown in Figure 7.8.

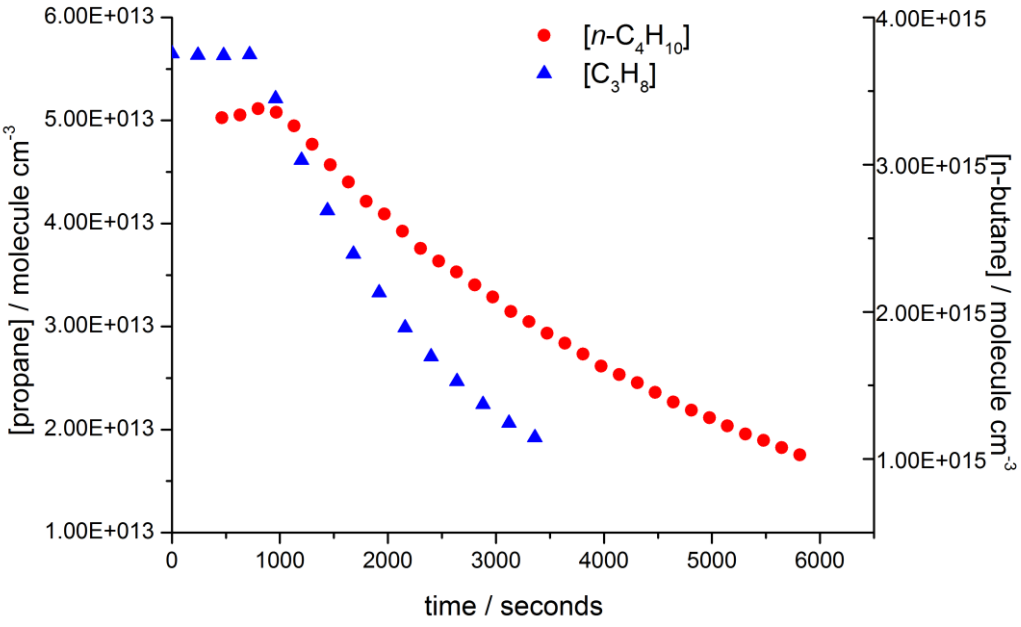

Figure 7.9: Hydrocarbon decays of propane and *n*-butane pairs reaction with OH at 200 mbar in the mini chamber at 292 K.

A relative rate ratio for the two hydrocarbons was derived from these two hydrocarbon decays for this experiment. Estimation of OH formation from the photolysis of acetone was obtained using the same methodology described in Section 7.3.2. The initial concentrations in the chamber on the GC prior to photolysis were used as an estimate of sampling/systematic errors from the GC detection for the mini photolysis chamber. A relative rate ratio of 1.9 ± 0.2 obtained from these decays (shown in Figure 7.9) are within error of the ratio of rate coefficients recommended by IUPAC of 2.2 ± 0.1 (Atkinson et al., 2006a). Uncertainties reported in the relative rate ratio are obtained from a linear regression using Regres2, similar to previously reported relative rate studies in HIRAC. These results confirm the decays observed in the chamber for these hydrocarbons are the result of OH reactivity generated from acetone photolysis.

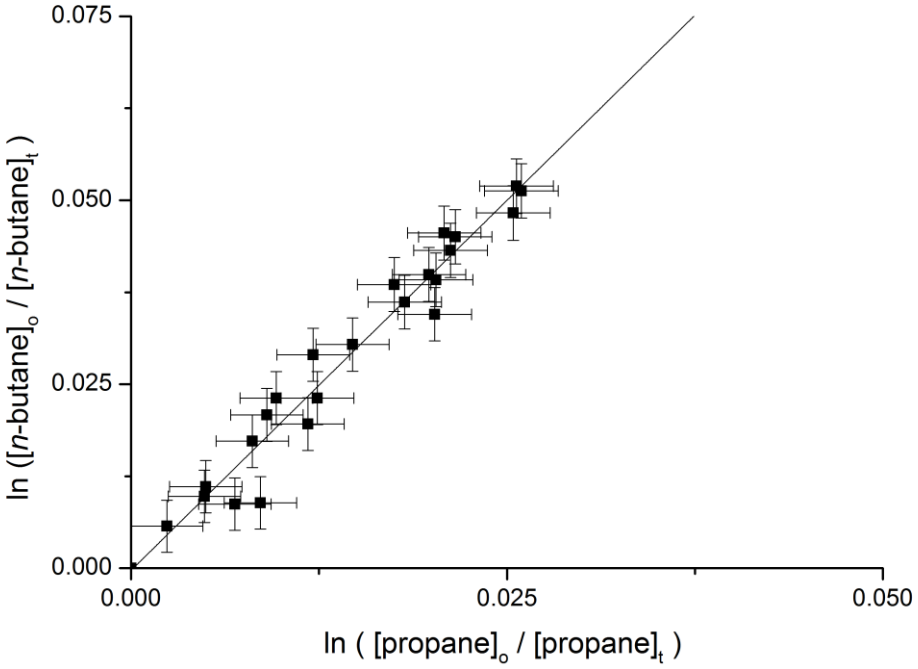

Figure 7.10: Relative rate for acetone photolysis at 200 mbar in the mini chamber at 290 ± 5 K.

From these results [OH] was estimated to be in the region of (1.3 ± 0.5) × 10^7 molecule cm^{-3} based on the average for the two sets of hydrocarbon decays shown in Table 7.1. Quantification from solely using the relative rate approach is not as sufficient evidence to conclude on the large [OH] generated as the steady state [OH] from this generation method can be better obtained when the experiment is coupled with FAGE detection of OH. As with other investigations in this thesis, the comparison of two different techniques and the measuring of different reactants simultaneously offers better reliability in the results reported.

$k_{propane+OH}$	1.09 × 10^{-12}	$k_{n\text{-butane}+OH}$	2.36 × 10^{-12}
[Propane]/ molecule cm^{-3}	2.17 × 10^{13}	[*n*-butane]/ molecule cm^{-3}	3.26 × 10^{13}
gradient	3.85 × 10^{10}	gradient	6.94 × 10^{10}
[OH]/ molecule cm^{-3}	**1.63 × 10^7**	**[OH] / molecule cm^{-3}**	**9.02 × 10^6**

Table 7.1: [OH] estimation from propane and *n*-butane decays at 200 mbar in the mini photolysis chamber.

7.4.4 Discussion

This OH generation method has, to our knowledge, not been previously characterised for chamber studies. The study carried out in the mini photolysis chamber demonstrates the potential of this method to generate high OH yields for kinetic and mechanistic experiments in chambers. Further experiments may be carried out to better assess the OH yield from this method over different pressures. Another possible investigation of interest could be a temperature dependence study of the photolysis of acetone and OH generation, which could be investigated both in the mini photolysis chamber, following the recent installation of a temperature control system which is currently being characterised by Stephanie Orr, as well as in HIRAC, with a working FAGE instrument a vital asset to obtaining OH measurements. It is expected that as the temperature increases the OH yield decreases as there is more stabilisation of the peroxy radical intermediate formed. The only issue faced with carrying out these experiments in the mini photolysis chamber is the low output from the lamps at lower temperatures. The 8 lamps in HIRAC proved sufficient for the photolysis of chlorine during chlorine temperature dependent experiments in Chapter 5, however the output of the lamps was not as crucial in these experiments as it would be for acetone photolysis. If unsuccessful in the mini photolysis chamber, some experiments could also be carried out in HIRAC, with the added benefit of having the FAGE instrument for direct OH measurements.

Another major advantage of this method is the potential for generating OD radicals. As the H atom in the OH radical comes from a methyl group in acetone, it won't be likely to exchange, so photolysis of CD_3COCD_3 should be a good source of OD for laboratory kinetic experiments.

One major disadvantage of this technique however, is the fact that the OH yields are only sufficiently high at pressures that are irrelevant to short-lived VOC oxidation processes of interest, such as isoprene and α-pinene; the only exception being when tropical convections push these latter species in the higher regions of the troposphere (Apel et al., 2012). This generation method would be useful for studying longer-lived emissions which are transported higher up in the troposphere or the chemistry from emissions of aircrafts and volcanoes which are major contributors to VOCs in the upper troposphere in an environment where typical pressures of ~100

mbar and temperatures of ~220 K exist. Given the capabilities available with both HIRAC and the mini photolysis chamber in the wide temperature and pressure ranges that can be studied, these proposed studies could potentially yield some useful information, stressing the advantage of a chamber being able to operate over temperature and pressure ranges relevant to the entire troposphere (Seakins, 2010a).

Another final limitation is the photolysis of products and the fact that the species investigated need to react faster than the competing acetone + OH reaction (1.8×10^{-13} molecule cm^{-3} s^{-1}) (Atkinson et al., 2006a). This method would however be better suited than alkene ozonolysis in the case of isoprene oxidation studies, given isoprene reacts 500 times faster than acetone with OH, however isoprene reacts with ozone.

7.5 Peroxide photolysis

7.5.1 Introduction

This section will assess the use of peroxides as a source of OH under low NO_x conditions in HIRAC. This has previously not been attempted in HIRAC; however other quartz and Teflon chambers have reported use of hydrogen peroxide to study OH chemistry. To our knowledge, no previous chamber studies have utilised *tert*-butyl hydroperoxide, which is characterised for the first time in an atmospheric chamber.

Peroxides are important trace species in the troposphere primarily as HO_x reservoirs which regulate the oxidation capacity of the atmosphere (Gunz and Hoffmann, 1990). Recent reports on atmospheric peroxides have focused on aerosol and cloud formation, primarily through the formation of sulfuric acid. Several organic peroxides are known to exist in the troposphere and these are formed *via* peroxy radical reactions with HO_2 radicals. Hydrogen peroxide (H_2O_2) and hydroxymethyl hydroperoxide ($HOCH_2OOH$) are also known to be formed by the ozonolysis of alkenes in the presence of water vapour (Mertes et al., 2012, Frey et al., 2009, Zhang et al., 2012, Kwan et al., 2012).

Primary sinks for peroxides in the troposphere are reaction with OH radicals and photodissociation in the UV range (Baasandorj et al., 2010). Very few field and laboratory studies have been carried out to date on organic peroxides (Francisco and Eisfeld, 2009, Zhang et al., 2012, Frey et al., 2009) and detailed kinetics and oxidation mechanisms are lacking for these species.

The photochemistry of both hydrogen peroxide (Chu and Anastasio, 2005, Vione et al., 2003) and *tert*-butyl hydroperoxide has been extensively investigated (Baasandorj et al., 2010). The generation of OH from the photolysis of the peroxide is dependent upon Eq 7.6, where $\sigma(\lambda)$ and $\Phi(\lambda)$ are the absorption cross section and OH quantum yield of the peroxide at the photolysis wavelength. During the experiments carried out in HIRAC, the concentration of the *tert*-butyl hydroperoxide is measured from either GC-FID or FTIR.

$$[OH]_o = \sigma(\lambda)\Phi(\lambda)[Peroxide] \quad \text{(Eq 7.6)}$$

UV radiation splits the peroxide bond yielding two OH molecules in the case of H_2O_2 ($\Phi = 2$) and the formation of OH from these peroxides is shown in R7.17 and 7.18.

$$H_2O_2 + h\upsilon \rightarrow 2\ OH \quad \text{(R7.17)}$$
$$(CH_3)_3COOH + h\upsilon \rightarrow OH + (CH_3)_3CO \quad \text{(R7.18)}$$

The alkoxy radical $(CH_3)_3CO$ decomposes to produce acetone and a methyl radical as is shown in R7.19 (Curran, 2006, Orlando et al., 2003):

$$(CH_3)_3CO + M \rightarrow CH_3COCH_3 + CH_3 + M \quad \text{(R7.19)}$$

7.5.2 Experimental Method

Experiments were carried out using the scavenger and relative rate hydrocarbon tracer techniques whereby either one (in excess) or two hydrocarbons that reacted with the OH generated during the experiment were monitored using the HIRAC GC-FID or in some experiments also using the FTIR. [OH] yields from peroxide photolysis was inferred from these decays and compared with OH determined from FAGE detection when FAGE was operational. All FAGE measurements and analysis were carried out by Fred Winiberg.

The methodology used has been described in Section 7.3.2. The mean OH concentration can then be inferred by calculating the following:

$$[OH] = \frac{(k' - k_{dil})}{k_{OH+HC}} \quad \text{(Eq 7.7)}$$

Where k_{dil} is the dilution rate of the measured [HC] due to FAGE and GC sampling.

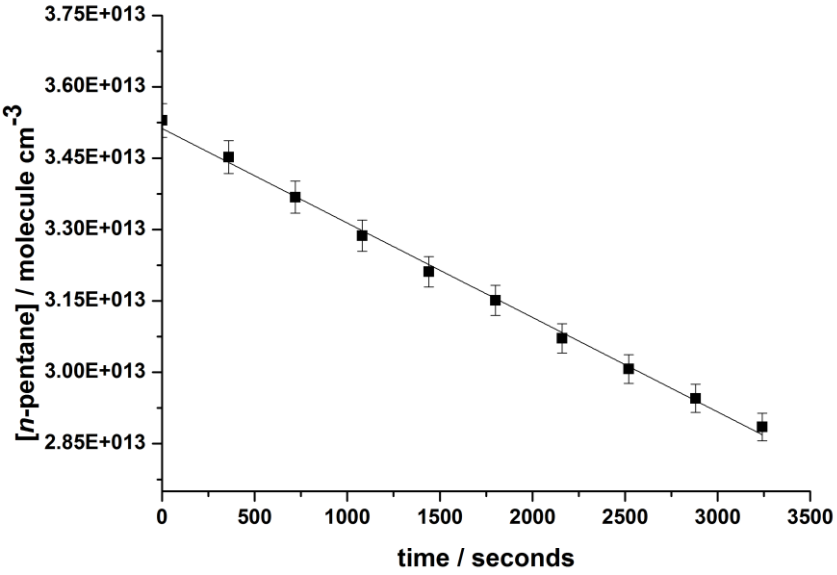

Figure 7.11: Hydrocarbon decay of *n*-pentane measured using the HIRAC GC.

k_{dil} is calculated as a function of the calibrated mass flow controller used to control the dilution flow and the chamber volume (4.5×10^{-5} s^{-1}). An example of hydrocarbon decay for *n*-pentane at 292 K and 1000 mbar in HIRAC is shown in Figure 7.10. The linear rather than exponential shape of this decay plot is indicative of the constant rate at which OH is being produced, implying a steady state is being reached sufficiently high for the purpose of this experiment. The [OH] reacted with the hydrocarbon can be estimated based on the loss of [hydrocarbon] during the experiment, provided the only loss process occurring is the reaction with OH.

The HIRAC FAGE was powered using a new laser system operating at a medium repetition rate and higher energy than the previous FAGE instrument used in HIRAC. Tamsin Malkin used an Nd:YAG (JDSU Q201-HD) pumped dye laser (Sirah Cobra stretch) producing 308 nm light for on-resonance OH detection. The new HIRAC FAGE system was implemented and calibrated by Fred Winiberg and was pumped by an Nd:YAG (Litron, NANO-TRL-50-250) pumped dye laser (Lambda Physik, LPD3000) operating at 200 Hz pulse repetition frequency. A laser pulse energy of 0.24 mJ $pulse^{-1}$ at 308 nm was initially used for on-resonance OH detection. A more in depth description of the laser system and specifications of the HIRAC FAGE instrument will be reported in Fred Winiberg's thesis (Winiberg, 2014).

The lamps used for these experiments were 8 germicidal GE G55T8 / OH 7G UV C lamps that photolyse the peroxide at 254 nm:

$$(CH_3)_3COOH + h\upsilon \rightarrow OH + \text{product} \qquad \text{(R7.20)}$$

A comparison of the typical room temperature absorption cross sections for $(CH_3)_3COOH$ and H_2O_2 is shown in Figure 7.11. Both peroxide and the chosen hydrocarbons were introduced through the vacuum-line delivery system at equal concentrations (~5×10^{13} molecule cm^{-3}). In the case of scavenger experiments, the only difference was the concentration of hydrocarbon introduced was higher, depending on the peroxide concentration introduced and reactivity of the peroxide with OH. The amount introduced would be based on the chosen hydrocarbon's rate coefficient with OH in comparison with the precursors, and the concentration would be required to be high enough to out-compete the precursor by reacting with 99% of the OH generated.

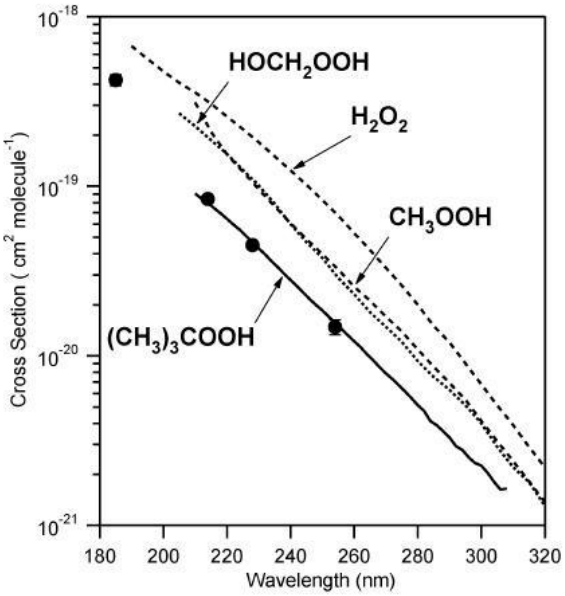

Figure 7.12: UV absorption cross sections of H_2O_2, CH_3OOH, $HOCH_2OOH$ (Sander et al., 2010) and $(CH_3)_3COOH$ measured at 296 K (Baasandorj et al., 2010).

This method however would result in a lower OH steady state and give very small decay measurements. The preferred relative rate technique allowed for an [OH] steady state of roughly ~5 x 10^6 molecule cm^{-3} which is a measurable quantity on the HIRAC FAGE instrument. The hydrocarbon concentrations used in this method also gave more adequate relative changes for the GC-FID to measure. These hydrocarbon

concentrations and the precursor concentration were measured using the HIRAC GC-FID (0.53 mm i.d. column coated with a 50 m, operated at 305 K coated with 100% dimethylpolysiloxane (J and W, DB-1)) at a time resolution of 6 minutes.

Cyclohexane (99.9% Sigma Aldrich), *iso*-butene and *n*-pentane (99.9%, Sigma Aldrich) were chosen as suitable hydrocarbons as they have similar k_{OH+HC} to *tert*-butyl hydroperoxide (70% in H_2O Sigma Aldrich), are well understood and cyclohexane has been used previously, giving accurate sensitivity measurements.

7.5.3 Hydrogen Peroxide

Hydrogen peroxide, H_2O_2, photolysis was tested in HIRAC since the photolysis is known to only yield two OH radicals (Gunz and Hoffmann, 1990, Vione et al., 2003) while tert-butyl hydroperoxide photolysis produces OH and a *tert*-butyl radical which results in further products (Baasandorj et al., 2010).

Several difficulties were encountered with H_2O_2 in HIRAC. One of the most problematic was that the contents of the H_2O_2 solution provided from the supplier (Sigma Aldrich: 30% H_2O_2: 70% H_2O) meant that every experiment carried out in HIRAC introduced copious amounts of water in the chamber. Distillation of the water prior to introduction into HIRAC would be a laborious time consuming process that also posed a safety issue due to the high volatility of H_2O_2. As a result, every introduction of the H_2O_2 resulted in great difficulty in properly pumping down HIRAC after experiments. One of the problems encountered was that the water would settle in the liquid phase making it very energy consuming to remove it by pumping. The only way the water could be completely rid of following hydrogen peroxide experiments was by taking HIRAC apart and cleaning the chamber walls manually. This is not an easy and quick job, but was necessary given the potential corrosive effects the hydrogen peroxide had already caused in HIRAC. The water content also had a significant negative effect on the FTIR background, which when subtracted would result in poor experimental spectra.

The oxidising effects of H_2O_2 on the chamber walls and propensity to go to the walls made it very hard for H_2O_2 to be quantified using the FTIR. Hydrogen

peroxide (H_2O_2) has been previously used as a source of OH in glass chambers (Albu et al., 2006, Klotz et al., 2002, Zhou et al., 2006) but has to our knowledge never been reported for use in steel chambers.

7.5.4 *Tert*-butyl hydroperoxide

The photolysis of *tert*-butyl hydroperoxide was attempted following the unsuccessful attempts of using hydrogen peroxide as an OH source in HIRAC. The methodology used has been described earlier in Section 7.3.2 and is based on previous experiments carried out in EUPHORE (Bloss et al., 2004).

The photolysis rate obtained for *tert*-butyl hydroperoxide using the same equipment detailed in Section 7.5.2 was $(1.45 \pm 0.03) \times 10^{-4}$ s^{-1}. This was obtained in the presence of a scavenger (cyclohexane) that was present in a large excess over *tert*-butyl hydroperoxide ensuring ≥ 99% of OH reacted with the cyclohexane.

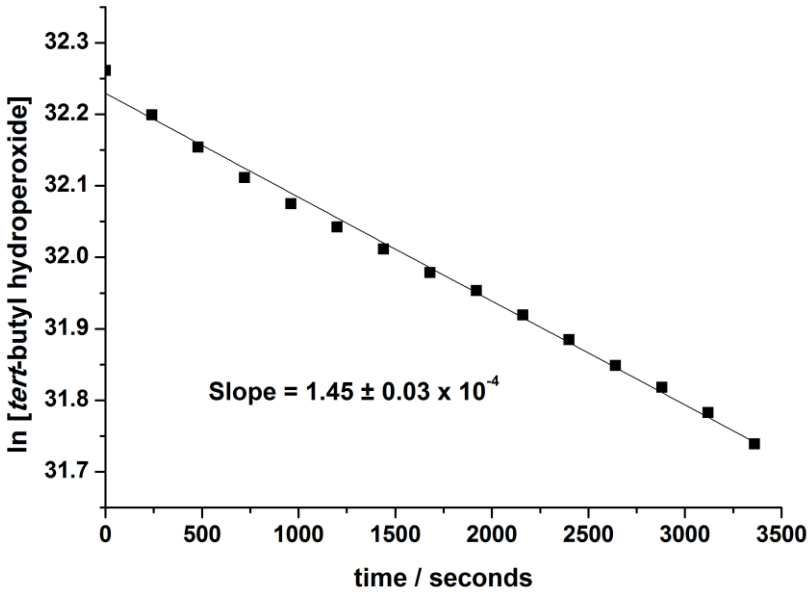

Figure 7.13: *Tert*-butyl hydroperoxide photolysis rate obtained in HIRAC at 1000 mbar and 292 K in the presence of a cyclohexane scavenger.

Hydrocarbon decays were monitored using GC and FTIR for reaction with OH generated from the photolysis of *tert*-butyl hydroperoxide in HIRAC. Figure 7.13

shows a typical set of hydrocarbon decays measured for *iso*-butene and cyclohexane at 1000 mbar and 292 K. Excellent agreement between FTIR and GC-FID measurements for this experiment further validates the hydrocarbon measurements being recorded in HIRAC. Figure 7.14 shows a typical relative rate relationship obtained during the same photolysis of *tert*-butyl hydroperoxide experiment in HIRAC.

This relative rate experiment was used to quantify the OH generated from the relative decays of the tracer *iso*-butene/cyclohexane hydrocarbon pair measured using the GC-FID. Excellent agreement was obtained for the cyclohexane decays using both GC-FID and FTIR instruments demonstrating the accuracy obtained for these hydrocarbon measurements in HIRAC and validating the GC data obtained in other experiments were the FTIR could not be used.

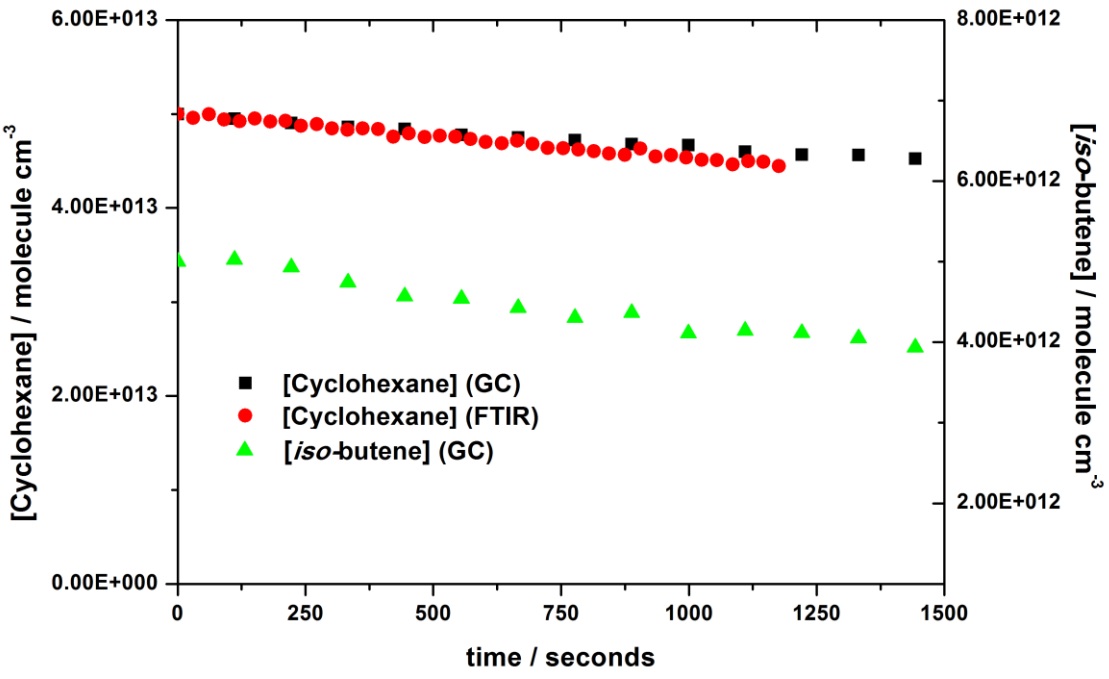

Figure 7.14: Hydrocarbon decays for cyclohexane and *iso*-butene in HIRAC using GC and FTIR detection at 292± 3 K and 1000 mbar. *iso*-butene was below the detection limit on the FTIR and could not be shown.

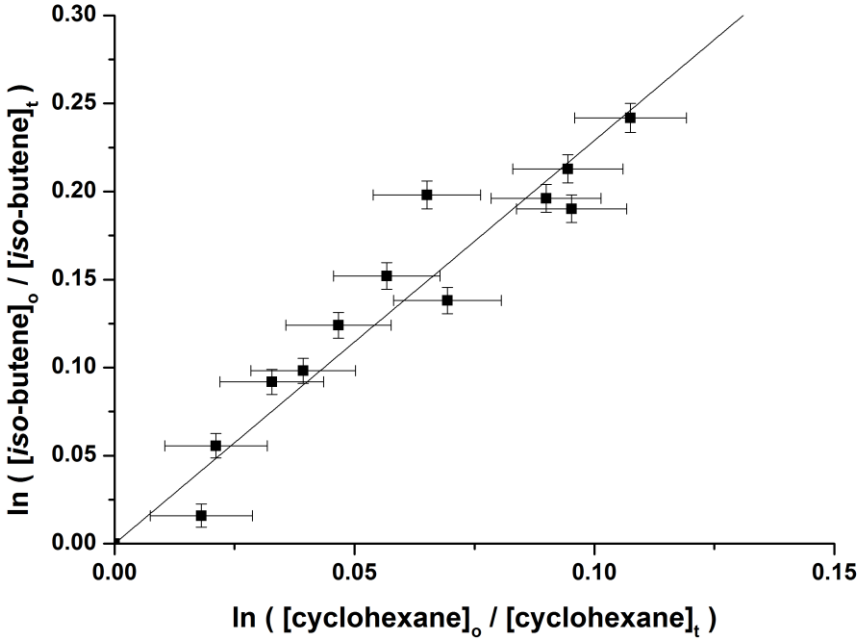

Figure 7.15: Relative rate for the reaction of OH with *iso*-butene and cyclohexane in HIRAC at 292 ± 3 K and 1000 mbar.

A relative rate plot for this hydrocarbon pair is shown in Figure 7.14 for results obtained by GC-FID. A relative rate ratio could not be obtained using FTIR data given the *iso*-butene was below the detection limits in this experiment. A relative rate ratio from the GC-FID measurements of 3.20 ± 0.28 was obtained from this experiment. The relative rate coefficient derived from this ratio using a literature rate coefficient for cyclohexane of (6.9 ± 1.5) × 10^{-12} molecule cm^{-3} s^{-1} (Atkinson, 1986) for *iso*-butene was found to be (2.4 ± 0.22) × 10^{-11} molecule cm^{-3} s^{-1}. This is a factor of two lower than the most recent kinetic data reported by Atkinson for *iso*-butene (5 × 10^{-11} molecule cm^{-3} s^{-1}) (Atkinson et al., 2006a).

A possible reason for the poor agreement for these experimental results with the literature could be the low percentage change for cyclohexane (10%). Alternatively, the low concentrations of *iso*-butene used which meant the *iso*-butene was being measured by the GC-FID within its limits of detection (~1 × 10^{12} molecule cm^{-3}), or that some of hydrocarbon decays could be due to losses to walls. All the experimental conditions for the experiments carried out at 1000 mbar for *n*-pentane and cyclohexane are presented in Table 7.2. Dilution from the HIRAC FAGE instrument was accounted for and would not be expected to be an issue for the relative

rate experiments since the dilution would be expected to be proportional for both hydrocarbons.

	10^{13} molecule cm^{-3}			**10^{8} s^{-1}**	**10^{7} molecule cm^{-3}**		**minutes**
Hydrocarbon (HC)	**[HC1]**	**[HC2]**	**[TbuOOH]**	**[HC] decay**	**mean [OH] GC**	**peak [OH] FAGE**	**GC cycle**
n-pentane	2.00	-	3.00	3.58	0.48	1.10	3
n-pentane	5.00	-	5.00	3.50	0.18	1.10	6
cyclohexane	1.94	-	3.41	2.50	0.10	1.50	1.85
cyclohexane	1.98	-	3.41	2.60	0.10	1.60	1.85
iso-butene/ cyclohexane	0.56	5.30	4.50	2.50	0.08	0.40	1.85

Table 7.2: Experimental conditions in HIRAC for *tert*-butyl hydroperoxide (TbuOOH) photolysis at 292 ± 3 K and 1000 mbar using HIRAC FAGE and GC-FID instruments. Mean [OH] was calculated using Eq 7.2.

Table 7.2 shows results for two sets of hydrocarbon tracer experiments for *n*-pentane and cyclohexane which were performed to demonstrate repeatability in the [OH] being detected using the HIRAC FAGE instrument. Excellent repeatability was obtained for these hydrocarbons with both tracers and an average peak [OH] of ~1 x 10^7 molecule cm^{-3} for experimental conditions of ~1 – 2 ppmv of hydrocarbon and peroxide. A comparison of the hydrocarbons traces using GC-FID and FAGE are shown in Figure 7.15 and 7.16 for *n*-pentane and cyclohexane respectively. Both figures show very good agreement between the [OH] measured by FAGE and that calculated from the hydrocarbon decays from the GC-FID.

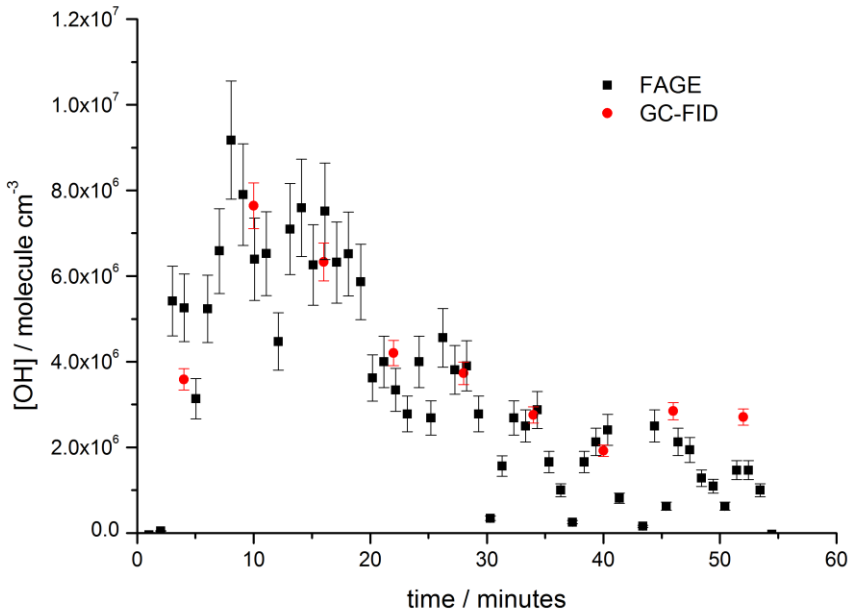

Figure 7.16: Initial *n*-pentane HC decay experiment using FAGE and GC in HIRAC at 292 K and 1000 mbar (measurements corrected for dilution, errors to 1σ).

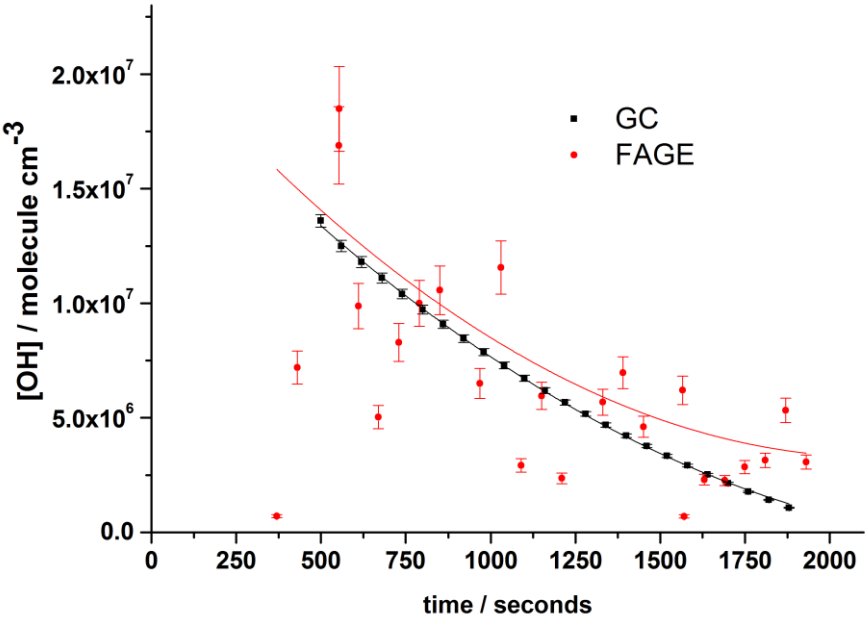

Figure 7.17: [OH] from HC decay (GC) compared with measured [OH] from FAGE for cyclohexane experiment in HIRAC at 292 ± 3 K and 1000 mbar (measurements corrected for dilution, errors to 1σ, non-linear Gaussian fitting used for FAGE measurements).

7.5.5 Discussion

Tert-butyl hydroperoxide photolysis has been successfully characterised in the HIRAC chamber as a suitable OH generation method under low NO_x conditions. Suitable experimental conditions for HIRAC have been obtained that give a peak [OH] of ~1 x 10^7 molecule cm^{-3}, and mean [OH] of ~5 × 10^6 molecule cm^{-3}. The results were backed by direct measurements using the HIRAC FAGE instrument, and the [OH] traces measured over a period of ~30 – 60 minutes agrees well with the calculated [OH] from the hydrocarbon decays measured using the GC-FID.

Aside from being a useful OH generation source, this method has also been tested in HIRAC in order to find an alternate way of calibrating the FAGE instrument. Similar experiments had been carried out in EUPHORE in Valencia to calibrate the FAGE instrument used for OH detection, and avoid relying on a single measurement for determination of [OH] in chambers. The use of a hydrocarbon whose reaction with OH has been well characterised infers an OH concentration from the loss in concentration of the hydrocarbon, assuming the hydrocarbon was lost solely due to reaction with OH. The decay of the hydrocarbon infers the OH which is compared with the FAGE measurement over the same time period.

Pressure dependent calibrations of hydrocarbon decays using *tert*-butyl hydroperoxide have also been in HIRAC obtained as part of this work and will be reported by Fred Winiberg (Winiberg, 2014). HIRAC provides a suitable environment for these pressure dependent experiments as it can cover a large range of pressures, which would be of significance to airborne field instruments.

7.6 Conclusions

OH generation under low NO_x conditions in HIRAC will be important in future to allow for mechanistic studies such as isoprene oxidation as well as other reactions involving OH with other biogenic VOCs under low NO_x conditions. The main criteria for this source of low NO_x OH much desired in HIRAC were to be relatively "easy" to conduct (*i.e.* not requiring much time in preparation for every experiment), sustainable over approximately 30 – 60 minutes (mean timescale for standard HIRAC experiment) and generate [OH] within the detection limits of the HIRAC FAGE instrument (~5×10^5 molecule cm^{-3}).

In this investigation three suitable sources have been examined and their merits will be assessed and contrasted according to the information gathered from the investigations carried out in HIRAC. The goal is to have a clean source of OH radicals with minimal complications caused by other reactive species. Indirectly, [OH] can be calculated using either a scavenger or a relative rate pair technique, while direct measurements may be obtained using FAGE. A combination of these three techniques has been employed and presented in this chapter. Unfortunately the first two techniques discussed in this chapter lacked a working FAGE instrument and so only indirect evidence could be presented.

Table 7.3 highlights the key advantages and disadvantages of the three different methods of OH generation under low NO_x conditions assessed. The first two techniques involve the photolysis of an OH precursor (peroxides and acetone) while the third technique involves the reaction of O_3 with alkenes.

Low NO_x OH Generation Method	Advantages	Disadvantages
Low Pressure Photolysis of Acetone	Acetone is readily available and inexpensive. No preparation or synthesis of any precursors required. Acetone chemistry has been well documented and is understood (McKeen et al., 1997, Gierczak et al., 1998, Talukdar et al., 2003).	Low OH yield at atmospherically relevant pressures. Photolysis at ~300 nm may lead to photolysis of organics being investigated and/or reaction products. Difficult to get lamps with a correct spectral profile, and with sufficient intensity.
Photolysis of peroxides	H_2O_2 and *tert*-butyl hydroperoxide are both readily available and relatively inexpensive to obtain. Photolysis of both these species have been investigated and reported in the literature (Vione et al., 2003, Baasandorj et al., 2010). H_2O_2 photolysis has been used previously in chamber investigations for studying OH chemistry (Klotz et al., 2002, Albu et al., 2006).	Peroxides are supplied in solution with water, and therefore have a tendency to introduce copious amounts of water into the chamber. H_2O_2 has a strong potential for loss to metal chamber walls where it may participate in heterogeneous reactions and corrode/oxidise the lining of the walls. *Tert*-butyl hydroperoxide photolysis is slightly more complex due to more products being formed and due its reaction and product reactions with OH not being easy to avoid.
Simple alkene ozonolysis	A suitable dark source of OH radicals in the absence of NO_x. Alkenes are also readily available, and O_3 generation in chambers is easily carried out, *i.e.:* no requirements for preparation.	Limited to VOCs which do not react with O_3. Competition between the VOC being studied and the alkene for OH radicals limits the reaction of the VOC being studied.

Table 7.3: Advantages and disadvantages of low NO_x OH generation methods available for chamber studies. All methods have the advantage of not having any NO_x chemistry.

As is listed in Table 7.3, all three precursors used are readily available and do not require any complicated synthesis or preparation, which saves on time during OH chemistry experiments in HIRAC. This is advantageous given the average time taken for experiments in HIRAC is around ~2.5 hours taking into account the time required to empty the chamber between runs and filling the chamber at the start of each experiment.

Alkene ozonolysis takes slightly longer to prepare that the other two photolytic sources, since $O_3$is made up in HIRAC prior to introducing the alkene and generating OH in the chamber. This however takes no longer than 30 minutes, although some time is required for the O_3 to properly mix and setup all instruments prior to initiating the chemistry. However, given the presence of O_3 in the system, this technique would be the least suitable given the reactivity of isoprene and other VOCs with O_3. It is also the most complicated given the alkene concentration would need to be sustained during the experiment. Tyndall and Orlando at NCAR have been successful in making use of 2-methyl-2-butene (TME) ozonolysis for the generation of OH in their steel chamber. Due to time constraints this method could not be tried out in HIRAC, however could be characterised in future. One challenge with this method is finding a way of constantly replenishing the fast reacting alkene into HIRAC in order to maintain the mean OH concentration in the chamber as constant as possible.

Acetone photolysis had, to our knowledge, not been previously used as a source of OH in chamber studies. This work represents therefore the first attempts at using acetone photolysis to carry out kinetics experiments. The study carried out in the mini photolysis chamber demonstrated the potential of this method to generate high OH yields for kinetic and mechanistic experiments in chambers. The usefulness of this technique is however debatable given the OH yield drops significantly at higher pressures making this source only useful when pressure dependent studies are being carried out. This generation method would be useful for studying longer-lived emissions which are transported higher up in the troposphere or the chemistry from emissions of aircrafts and volcanoes which are major contributors to VOCs in the upper troposphere in an environment where typical pressures of ~100 mbar and temperatures of ~220 K exist. Given the capabilities available with both HIRAC and the mini photolysis chamber in the wide temperature and pressure ranges that can be studied, these proposed studies could potentially yield some useful information, stressing the advantage of a chamber being able to operate over temperature and pressure ranges relevant to the entire troposphere (Seakins, 2010a). One final limitation includes the fact that the species investigated needs to react faster than the competing acetone + OH reaction (1.8×10^{-13} molecule cm^{-3} s^{-1}) (Atkinson et al., 2006a). This method would however be better suited than alkene ozonolysis in the

case of isoprene oxidation studies, given isoprene reacts 500 times faster than acetone with OH, however isoprene reacts with ozone.

The final generation method assessed in HIRAC was peroxide photolysis. This method was characterised for *tert*-butyl hydroperoxide and mean OH of ~5×10^6 molecule cm^{-3} was measured using the HIRAC FAGE and were monitored using OH tracers by the HIRAC GC-FID and OH chemistry could be noted for periods of up to an hour. The decays of the hydrocarbons were comparable to the OH measured using FAGE over the same time period. The only downfall of this method is the photolysis lamps used (254 nm) would photolyse any of the VOCs produced that absorb within that range, which would account for a vast number of the products of isoprene oxidation which is what is intended to be studied. In order to possibly be able to use this source in HIRAC to study isoprene oxidation in the future, a method needs to be thought of that would require the photolysis lamps to be in for very short periods of time, which would minimise the influence the lamps have over the oxidation reaction being studied.

Chapter 8 – Conclusions and proposed future research

This final section will highlight the original contributions of this work as well as go through recommendations and potential studies that could further the work presented in this thesis. Several aspects of atmospheric chemistry have been investigated, including chlorine reactions with esters (chapter 4), hydrocarbons (chapter 5) and ethanol (chapter 6), ozonolysis of alkenes (chapters 3 and 7), as well as various photolysis studies aimed at characterising a generation method of OH radicals in HIRAC under low NO_x conditions (chapter 7). Improvements have also been made to HIRAC, including the installation of a temperature-control system (chapter 3) which has been characterised and tested in an investigation on the temperature dependence of butanes and pentanes over a temperature range of ~220 – 320 K. Product branching ratios have also been investigated during this study, and have been reported for the first time in HIRAC using measurements made using the GC-FID and FTIR instruments. Initial testing of a cryogenic trap and the setting up of this instrument for potential use in isoprene oxidation studies has been mentioned (chapter 2), the setting up and characterisation of a mini photolysis chamber as a test-bed for investigations to be carried out in HIRAC (chapter 3), as well as the characterisation of a low NO_x source of OH in HIRAC using GC-FID and FAGE. All these investigations, their outcomes, and future recommendations are to be individually assessed here.

The first achievement to be highlighted in this summary is the successful **installation and characterisation of a temperature control system** in the HIRAC chamber. The installation, insulation and temperature profiling of HIRAC was carried out together with Shona Smith and Fred Winiberg. Successful experiments of the ozonolysis of propene over a temperature range of ~233 – 323 K presented in chapter 3 confirmed the suitability of this system for studying temperature dependent kinetics. This system now enables HIRAC to study reactions of interest to tropospheric chemistry over temperatures of ~220 – 320 K and a pressure range of ~50 – 1000 mbar. This is of importance as it represents the entire range of conditions occurring in the troposphere. Suggestions on future studies that can be carried out in HIRAC over

these temperature limits include the study of product ratios for tropospherically relevant reactions of organics. Such an example has already been presented in chapter 5, where the temperature dependence of butanes and pentanes reactions with Cl atoms was investigated. The findings from these investigations were novel for the reaction of Cl atoms with pentanes at low temperatures. The mechanisms of these processes were also investigated and identification and quantification of product ratios using both GC-FID and FTIR have been presented over a temperature range. A slight negative temperature dependence recorded for the reaction of Cl atoms with *iso*-pentane has notable atmospheric implications in that the rate coefficient was found to vary by 15 – 20% over 220 – 320 K. These findings are particularly significant in field measurements where pentanes have been used as a hydrocarbon tracer for Cl atoms in the Arctic regions. *Iso*-pentane is however not as abundant as other NMHCs (~10 pptv) (Hellen et al., 2012) but the 15 – 20% change in its rate coefficient may still be significant should Cl atom chemistry be a more significant driver of oxidation on a global scale than initially perceived.

Given the successful use of this system in HIRAC, and improvements made at addressing problems encountered during characterisation, including condensation in the quartz tubes housing the lamps, and over-heating of the lamps when HIRAC was heated to higher temperatures, this system now has the potential to be used for several other temperature dependent studies of interest to the troposphere. Similar to Cl atom chemistry, reactions of atomic bromine are known to play a significant role in the marine and polar regions (Jobson et al., 1994). Br atom reactions with hydrocarbons have been sparsely reported in the literature (Laine et al., 2012), and recent BrO measurements in Polar regions during ozone depletion has shown that concentrations can be as high as ~5×10^7 atoms cm^{-3} (Liao et al., 2011b, Liao et al., 2011a). Given the interest to understand the chemistry in environments where temperatures vary quite significantly (Arctic temperatures vary from ~220 – 300 K), HIRAC could provide a suitable platform for the study of these sparsely investigated reactions of importance and help in better understanding of VOC oxidation processes in marine and polar environments. There are concerns regarding the introduction of a corrosive liquid into a metal atmospheric chamber, and in particular the corrosive effects it may have on the FTIR mirrors. Much consideration needs to be taken into account before performing such experiments. Bromine reacts vigorously with metals

particularly in the presence of water, and results in the formation of bromides; therefore it is important to evaluate the suitability of carrying out such experiments in HIRAC, perhaps a good way of doing this is to first carry out some tests in **the mini photolysis chamber** described in chapter 3. The availability of a smaller scale chamber in the HIRAC lab will offer increased potential in carrying out experiments quicker and in testing any experiments that may pose a certain risk of corrosion for instance, such as these proposed Br atom experiments.

Another achievement and original contribution to be noted is the **relative rate and structure activity relationships obtained for Cl atom reactions with propionates**. The increased interest in esters stemming from the increased use of biofuels has led to the investigation of the kinetics of these species that are likely to be generated from the combustion of biofuels. Given the limited number of reports on the chemistry of these species, chapter 4 aimed at addressing this and investigated further these compounds and their kinetics with Cl atoms in HIRAC. This was also seen as a continuation of the work already performed in HIRAC on acetates by Tamsin Malkin and Khuanjit Hemavibool(Hemavibool, 2009, Malkin, 2010). The reactivity trends obtained for the different propionates were similar to those previously reported by Malkin (Malkin, 2010)and stress the importance of obtaining such SARs. Chamber studies provide the advantage of obtaining temperature and pressure dependent SARs that could be useful in predicting the rates of oxidation processes of higher organics, although extrapolation of these kinetic calculations has had some scrutiny over the years.

Finally the increased importance of the missing OH source in rural environments (Hard et al., 1986, Archibald et al., 2011, Di Carlo et al., 2004, Stone et al., 2012) has led to the increased interest in studying OH chemistry under low NO_x conditions. Chamber studies provide a suitable environment for such investigations, and work on low NO_x isoprene oxidation in HIRAC has been happening over the past year. An important necessity for these experiments to be successful was **a suitable precursor of OH radicals in chambers under low NO_x conditions**. Several methods were tested in HIRAC and reported in the final chapter of this thesis (chapter 7).The findings from this chapter have demonstrated the potential for all three methods to yield a detectable concentration of OH radicals in HIRAC; however each method was found to have its limitations. In the case of the ozonolysis of alkenes, the major

drawback would be sustaining the OH concentrations for a long enough time period for an experiment to be carried out in HIRAC (30 – 60 minutes). Devising a way of continuously injecting the alkene into the chamber in order to keep the generation of OH going is crucial in obtaining a useful low NO_x source of OH in chambers out of this method. This method also struggles from the fact that the presence of O_3 chemistry would create complications in the understanding and modelling of the chemistry in the chamber given the presence of multiple reactive oxidants, and the greater difficulty in assessing the products from each individual oxidation pathway.

The other two generation methods were two photolytic methods which in terms of what were achieved, could potentially be useful in future. Acetone photolysis did yield a detectable amount of OH in the mini photolysis chamber, the first to our knowledge to be reported in an atmospheric chamber. The OH yields obtained are however only sufficiently high at pressures that are irrelevant to short-lived VOC oxidation processes of interest, such as isoprene and α-pinene. Future proposed work include a temperature dependence study of the photolysis of acetone and OH generation, which could be investigated both in the mini photolysis chamber, following the recent installation of a temperature control system, as well as in HIRAC, with a working FAGE instrument always being a vital asset in obtaining OH measurements.

Hydrogen peroxide, being previously used as an OH source in quartz and Teflon chambers, was shown to be unsuitable in metal chambers, and HIRAC got to witness this first hand. Unfortunately the consequences of introducing copious amounts of water (from the hydrogen peroxide supplied) into the chamber and the corrosive effects (adsorbs and oxidises on metals) on the walls have had to be rectified by a thorough manual cleaning of the inside of HIRAC. *Tert*-butyl hydroperoxide was shown to be a sustainable source of OH yielding detectable quantities of OH in HIRAC. The only disadvantage noted for this method is the photolysis at 254 nm would result in the photolysis of any of the VOCs produced that absorb within that range. This would photolyse most of the products of isoprene oxidation which is what is intended to be studied. A possible way of by-passing this is by adapting the method such that the photolysis lamps would only be on for very short periods of time, minimising the influence the lamps have over the oxidation reaction being studied.

References

AGARWAL, A. K. 2007. Biofuels (alcohols and biodiesel) applications as fuels for internal combustion engines. *Progress in Energy and Combustion Science,* 33**,** 233-271.

AGILENT 2000. Agilent 6890 Series Gas Chromatograph *Operating Manual*.

AKIMOTO, H., HOSHINO, M., INOUE, G., SAKAMAKI, F., WASHIDA, N. & OKUDA, M. 1979b. Design and characterization of the evacuable and bakable photochemical smog chamber. *Environmental Science and Technology,* 13**,** 471-475.

ALBALADEJO, J., NOTARIO, A., CUEVAS, C. A., JIMENEZ, E., CABANAS, B. & MARTINEZ, E. 2003. Gas-phase chemistry of atmospheric Cl atoms: a PLP-RF kinetic study with a series of ketones. *Atmospheric Environment,* 37**,** 455-463.

ALBU, M., BARNES, I., BECKER, K. H., PATROESCU-KLOTZ, I., MOCANU, R. & BENTER, T. 2006. Rate coefficients for the gas-phase reaction of OH radicals with dimethyl sulfide: temperature and O_2 partial pressure dependence. *Physical Chemistry Chemical Physics,* 8**,** 728-736.

ALICKE, B., GEYER, A., HOFZUMAHAUS, A., HOLLAND, F., KONRAD, S., PATZ, H. W., SCHAFER, J., STUTZ, J., VOLZ-THOMAS, A. & PLATT, U. 2003. OH formation by HONO photolysis during the BERLIOZ experiment. *Journal of Geophysical Research,* 108**,** 8247.

ANDERSEN, V. F., BERHANU, T. A., NILSSON, E. J. K., JORGENSEN, S., NIELSEN, O. J., WALLINGTON, T. J. & JOHNSON, M. S. 2011. Atmospheric Chemistry of Two Biodiesel Model Compounds: Methyl Propionate and Ethyl Acetate. *Journal of Physical Chemistry A,* 115**,** 8906-8919.

ANDERSEN, V. F., ORNSO, K. B., JORGENSEN, S., NIELSEN, O. J. & JOHNSON, M. S. 2012. Atmospheric Chemistry of Ethyl Propionate. *Journal of Physical Chemistry A,* 116**,** 5164-5179.

ANDERSEN, V. F., WALLINGTON, T. J. & NIELSEN, O. J. 2010. Atmospheric Chemistry of *i*-Butanol. *Journal of Physical Chemistry A,* 114**,** 12462-12469.

ANDERSON, R. S., HUANG, L., IANNONE, R. & RUDOLPH, J. 2006. Measurements of the $^{12}C/^{13}C$ kinetic isotope effects in the gas-phase reactions of light alkanes with chlorine atoms. *The Journal of Physical Chemistry A,* 111**,** 495-504.

APEL, E. C., BRAUERS, T., KOPPMANN, R., BANDOWE, B., BOßMEYER, J., HOLZKE, C., TILLMANN, R., WAHNER, A., WEGENER, R., BRUNNER, A., JOCHER, M., RUUSKANEN, T., SPIRIG, C., STEIGNER, D., STEINBRECHER, R., GOMEZ ALVAREZ, E., MÜLLER, K., BURROWS, J. P., SCHADE, G., SOLOMON, S. J., LADSTÄTTER-WEIßENMAYER, A., SIMMONDS, P., YOUNG, D., HOPKINS, J. R., LEWIS, A. C., LEGREID, G., REIMANN, S., HANSEL, A., WISTHALER, A., BLAKE, R. S., ELLIS, A. M., MONKS, P. S. & WYCHE, K. P. 2008. Intercomparison of oxygenated volatile organic compound measurements at the SAPHIR

atmosphere simulation chamber. *Journal of Geophysical Research,* 113**,** D20307.

APEL, E.C., OLSON, J. R. ,CRAWFORD, J. H.,HORNBROOK, R. S.,HILLS, A. J., CANTRELL,C. A., EMMONS, L. K., KNAPP, D. J., HALL,S., MAULDIN, R. L. , WEINHEIMER,A. J., FRIED,A., BLAKE,D. R., CROUNSE, J. D.,ST. CLAIR, J. M., WENNBERG,P. O., DISKIN,G. S., FUELBERG,H. E., WISTHALER,A., MIKOVINY,T.,BRUNE, W., AND RIEMER, D. D. 2012. Impact of the deep convection of isoprene and other reactive trace species on radicals and ozone in the upper troposphere. *Atmospheric Chemical Physics,* 12, 1135-1150.

ARANDA, A., DE MERA, Y. D., RODRIGUEZ, A., MORALES, L. & MARTINEZ, E. 2004. Kinetic study of the gas-phase reactions of Cl radicals with 3-pentanone and 3-hexanone. *Journal of Physical Chemistry A,* 108**,** 7027-7031.

ARCHIBALD, A. T., LEVINE, J. G., ABRAHAM, N. L., COOKE, M. C., EDWARDS, P. M., HEARD, D. E., JENKIN, M. E., KARUNAHARAN, A., PIKE, R. C., MONKS, P. S., SHALLCROSS, D. E., TELFORD, P. J., WHALLEY, L. K. & PYLE, J. A. 2011. Impacts of HO_x regeneration and recycling in the oxidation of isoprene: Consequences for the composition of past, present and future atmospheres. *Geophysical Research Letters,* 38.

ARNOLD, S. R., CHIPPERFIELD, M. P., BLITZ, M. A., HEARD, D. E. & PILLING, M. J. 2004. Photodissociation of acetone: Atmospheric implications of temperature-dependent quantum yields. *Geophysical Research Letters,* 31.

ARUNAN, E., SETSER, D. W. & OGILVIE, J. F. 1992. Vibration-rotational Einstein coefficients for HF/DF and HCl/DCl. *The Journal of Chemical Physics,* 97**,** 1734-1741.

ASCHMANN, S. M. & ATKINSON, R. 1995. Rate constants for the gas-phase reactions of alkanes with Cl atoms at 296+/-2 K. *International Journal of Chemical Kinetics,* 27**,** 613-622.

ASCHMANN, S. M. & ATKINSON, R. 2013. Rate constants for the reactions of Cl atoms with a series of C_6-C_{10} cycloalkanes and cycloketones at 297 +/- 2 K. *International Journal of Chemical Kinetics,* 45**,** 52-58.

ATKINSON, R. 1986. Kinetics and mechanisms of the gas-phase reactions of the hydroxyl radical with organic compounds under atmospheric conditions. *Chemical Reviews,* 86**,** 69-201.

ATKINSON, R. 1987. A structure-activity relationship for the estimation of rate constants for the gas-phase reactions of OH radicals with organic compounds. *International Journal of Chemical Kinetics,* 19**,** 799-828.

ATKINSON, R. 1990. Gas-phase tropospheric chemistry of organic compounds - A review. *Atmospheric Environment Part a-General Topics,* 24**,** 1-41.

ATKINSON, R. 1991. Kinetics and mechanisms of the gas-phase reactions of the NO_3 radical with organic compounds. *Journal of Physical and Chemical Reference Data,* 20**,** 459-507.

ATKINSON, R. 1997. Gas-phase tropospheric chemistry of volatile organic compounds: 1. alkanes and alkenes. *Journal of Physical; Chemical Reference Data,* 26**,** 215-290.

ATKINSON, R. 2000. Atmospheric chemistry of VOCs and NOx. *Atmospheric Environment,* 34**,** 2063-2101.

ATKINSON, R. & AREY, J. 2003a. Atmospheric degradation of volatile organic compounds. *Chemical Reviews,* 103**,** 4605-4638.

ATKINSON, R. & AREY, J. 2003b. Gas-phase tropospheric chemistry of biogenic volatile organic compounds: a review. *Atmospheric Environment,* 37**,** S197-S219.

ATKINSON, R. & ASCHMANN, S. M. 1985. Kinetics of the gas-phase reaction of Cl atoms with a series of organics at 296 +/- 2 K and atmospheric pressure. *International Journal of Chemical Kinetics,* 17**,** 33-41.

ATKINSON, R., BAULCH, D. L., COX, R. A., CROWLEY, J. N., HAMPSON, R. F., HYNES, R. G., JENKIN, M. E., ROSSI, M. J. & TROE, J. 2006a. Evaluated kinetic and photochemical data for atmospheric chemistry: Volume II - gas phase reactions of organic species. *Atmospheric Chemical Physics,* 6**,** 3625-4055.

ATKINSON, R., BAULCH, D. L., COX, R. A., CROWLEY, J. N., HAMPSON, R. F., HYNES, R. G., JENKIN, M. E., ROSSI, M. J., TROE, J. & SUBCOMMITTEE, I. 2006b. Evaluated kinetic and photochemical data for atmospheric chemistry: Volume II & gas phase reactions of organic species. *Atmospheric Chemical Physics,* 6**,** 3625-4055.

ATKINSON, R., BAULCH, D. L., COX, R. A., HAMPSON, R. F., KERR, J. A., ROSSI, M. J. & TROE, J. 1997. Evaluated kinetic, photochemical and heterogeneous data for atmospheric chemistry .5. IUPAC Subcommittee on Gas Kinetic Data Evaluation for Atmospheric Chemistry. *Journal of Physical and Chemical Reference Data,* 26**,** 521-1011.

ATKINSON, R., CARTER, W. P. L., DARNALL, K. R., WINER, A. M. & PITTS, J. N. 1980. A smog chamber and modelling study of the gas-phase NO_x-air photooxidation of toluene and the cresols. *International Journal of Chemical Kinetics,* 12**,** 779-836.

BAASANDORJ, M., PAPANASTASIOU, D. K., TALUKDAR, R. K., HASSON, A. S. & BURKHOLDER, J. B. 2010. $(CH_3)_3COOH$ (tert-butyl hydroperoxide): OH reaction rate coefficients between 206 and 375 K and the OH photolysis quantum yield at 248 nm. *Physical Chemistry Chemical Physics,* 12**,** 12101-12111.

BACHER, C., TYNDALL, G. S. & ORLANDO, J. J. 2001. The Atmospheric Chemistry of Glycolaldehyde. *Journal of Atmospheric Chemistry,* 39**,** 171-189.

BAKER, A. K., RAUTHE-SCHÖCH, A., SCHUCK, T. J., BRENNINKMEIJER, C. A. M., VAN VELTHOVEN, P. F. J., WISHER, A. & ORAM, D. E. 2011. Investigation of chlorine radical chemistry in the Eyjafjallajökull volcanic plume using observed depletions in non-methane hydrocarbons. *Geophysical Research Letters,* 38**,** L13801.

BALLESTEROS, B., GARZON, A., JIMENEZ, E., NOTARIO, A. & ALBALADEJO, J. 2007. Relative and absolute kinetic studies of 2-butanol and related alcohols with tropospheric Cl atoms. *Physical Chemistry Chemical Physics,* 9**,** 1210-1218.

BALTENSPERGER, U., KALBERER, M., DOMMEN, J., PAULSEN, D., ALFARRA, M. R., COE, H., FISSEHA, R., GASCHO, A., GYSEL, M., NYEKI, S., SAX, M., STEINBACHER, M., PREVOT, A. S. H., SJOGREN, S., WEINGARTNER, E. & ZENOBI, R. 2005. Secondary organic aerosols from anthropogenic and biogenic precursors. *Faraday Discussions,* 130**,** 265-278.

BANCO, M. B., BARNES, I. & WIESEN, P. 2012. Kinetic Investigation of the OH Radical and Cl Atom Initiated Degradation of Unsaturated Ketones at Atmospheric Pressure and 298 K. *Journal of Physical Chemistry A,* 116**,** 6033-6040.

BARNES, I., BECKER, K. H., FINK, E. H., REIMER, A., ZABEL, F. & NIKI, H. 1983. Rate constant and products of the reaction CS_2 + OH in the presence of O_2. *International journal of chemical kinetics,* 15**,** 631-645.

BARNES, I., BECKER, K. H. & MIHALOPOULOS, N. 1994. An FTIR product study of the photooxidation of dimethyl disulfide. *Journal of Atmospheric Chemistry,* 18**,** 267-289.

BEICHERT, P., WINGEN, L., LEE, J., VOGT, R., EZELL, M. J., RAGAINS, M., NEAVYN, R. & FINLAYSON-PITTS, B. J. 1995. Rate Constants for the Reactions of Chlorine Atoms with Some Simple Alkanes at 298 K: Measurement of a Self-Consistent Set Using Both Absolute and Relative Rate Methods. *The Journal of Physical Chemistry,* 99**,** 13156-13162.

BESEMER, A. C. & NIEBOER, H. 1985. The wall as a source of hydroxyl radicals in smog chambers. *Atmospheric Environment,* 19**,** 507-513.

BLAKE, N., BLAKE, D., 2002. Tropospheric chemistry and composition, doi:10.1006/rwas.2002.0422 (Elsevier Science Ltd.).

BLANCO, M. B., BEJAN, I., BARNES, I., WIESEN, P. & TERUEL, M. A. 2009. Temperature-dependent rate coefficients for the reactions of Cl atoms with methyl methacrylate, methyl acrylate and butyl methacrylate at atmospheric pressure. *Atmospheric Environment,* 43**,** 5996-6002.

BLANCO, M. B., BEJAN, I., BARNES, I., WIESEN, P. & TERUEL, M. A. 2010. FTIR Product Distribution Study of the Cl and OH Initiated Degradation of Methyl Acrylate at Atmospheric Pressure. *Environmental Science and Technology,* 44**,** 7031-7036.

BLITZ, M., HEARD, D. E., PILLING, M. J., ARNOLD, S. R. & CHIPPERFIELD, M. P. 2004. Pressure and temperature-dependent quantum yields for the photodissociation of acetone between 279 and 327.5 nm *Geophysical Research Letters,* 31.

BLITZ, M., J. PILLING, M., H. ROBERTSON, S. & W. SEAKINS, P. 1999. Direct studies on the decomposition of the tert-butoxy radical and its reaction with NO. *Physical Chemistry Chemical Physics,* 1**,** 73-80.

BLITZ, M. A. & SEAKINS, P. W. 2012. Laboratory studies of photochemistry and gas phase radical reaction kinetics relevant to planetary atmospheres. *Chemical Society Reviews,* 41**,** 6318-6347.

BLOSS, W. J., LEE, J. D., BLOSS, C., HEARD, D. E., PILLING, M. J., WIRTZ, K., MARTIN-REVIEJO, M. & SIESE, M. 2004. Validation of the calibration of

a laser-induced fluorescence instrument for the measurement of OH radicals in the atmosphere. *Atmospheric Chemistry and Physics,* 4**,** 571-583.

BOHN, B., CORLETT, G. K., GILLMANN, M., SANGHAVI, S., STANGE, G., TENSING, E., VREKOUSSIS, M., BLOSS, W. J., CLAPP, L. J., KORTNER, M., DORN, H. P., MONKS, P. S., PLATT, U., PLASS-DULMER, C., MIHALOPOULOS, N., HEARD, D. E., CLEMITSHAW, K. C., MEIXNER, F. X., PREVOT, A. S. H. & SCHMITT, R. 2008. Photolysis frequency measurement techniques: results of a comparison within the ACCENT project. *Atmospheric Chemistry and Physics,* 8**,** 5373-5391.

BORGERDING, A. J. & WILKERSON, C. W. 1996. A Comparison of Cryofocusing Injectors for Gas Sampling and Analysis in Fast GC. *Analytical Chemistry,* 68**,** 2874-2878.

BORRAS, E. & TORTAJADA-GENARO, L. A. Determination of oxygenated compounds in secondary organic aerosol from isoprene and toluene smog chamber experiments. *International Journal of Environmental Analytical Chemistry,* 92**,** 110-124.

BOUNDRIES, H. & BOTTENHEIM, J.W. 2000. Cl and Br Atom Concentrations During a Surface Boundary Layer Ozone Depletion Event in the Canadian High Arctic, *Geophysical Research Letters,* 27, 4, 517-520.

BRAUERS, T. & FINLAYSON-PITTS, B. J. 1997. Analysis of relative rate measurements. *International Journal of Chemical Kinetics,* 29.

BRETTELL, T. A. & GROB, R. L. 1985a. CRYOGENIC TECHNIQUES IN GAS-CHROMATOGRAPHY .1. *American Laboratory,* 17**,** 19-21.

BRETTELL, T. A. & GROB, R. L. 1985b. CRYOGENIC TECHNIQUES IN GAS-CHROMATOGRAPHY .2. CRYOFOCUSING AND CRYOGENIC TRAPPING. *American Laboratory,* 17**,** 50-54.

BREWER, D. A., AUGUSTSSON, T. R. & LEVINE, J. S. 1983. The photochemistry of anthropogenic nonmethane hydrocarbons in the troposphere. *Journal of Geophysical Research,* 88**,** 6683-6695.

BROWN, S. S., DIBB, J. E., STARK, H., ALDENER, M., WHITLOW, M. V. A., WILLIAMS, E. J., LERNER, B. M., JAKOUBEK, R., M.MIDDLEBROOK, A., DEGOUW, J. A., WARNEKE, C., GOLDAN, P. D., C.KUSTER, W., ANGEVINE, W. M., SUEPER, D. T., QUINN, P. K., MEAGHER, T. S. B. J. F., FEHSENFELD, F. C. & RAVISHANKARA, A. R. 2004. Nighttime removal of NO_x in the summer marine boundary layer. *Geophysical Research Letters,* 31**,** 1-5.

BROWN, S. S., STARK, H. & RAVISHANKARA, A. R. 2002. Cavity ring-down spectroscopy for atmospheric trace gas detection: application to the nitrate radical (NO3). *Applied Physics B-Lasers and Optics,* 75**,** 173-182.

BRUHL, X., POSCHL, U., CRUTZEN, PJ., STEIL B. 2000, Acetone and PAN in the upper troposphere: impact on ozone production from aircraft emissions, *Atmospheric Environment,* 34, 3931-3938, 2000.

BUSER, H. U., SODER, R. & WIDMER, H. M. 1982. Influence of a sophisticated cold trap on the shape of capillary chromatography peaks. *Journal of High Resolution Chromatography,* 5**,** 156-157.

HUNTER, M.C., BARTLE, K.D., SEAKINS, P.W. & LEWIS, A.C. 1999. Direct measurement of atmospheric formaldehyde using gas chromatography-pulsed discharge ionisation detection. *Analytical Communications,* 36**,** 101-104.

CABANAS, B., BAEZA, M. T., MARTIN, P., SALGADO, S., VILLANUEVA, F., MONEDERO, E. & WIRTZ, K. 2005. Products and mechanism of the NO3 reaction with thiophene. *Journal of Atmospheric Chemistry,* 51**,** 317-335.

CALVERT, J., MELLOUKI, A. & ORLANDO, J. 2011. *Mechanisms of Atmospheric Oxidation of the Oxygenates*, Oxford University Press, USA.

CARPENTER, L. J. 2003. Iodine in the marine boundary layer. *Chemical Reviews,* 103**,** 4953-4962.

CARR, S. A., BAEZA-ROMERO, M. T., BLITZ, M. A., PRICE, B. J. S. & SEAKINS, P. W. 2008. Ketone photolysis in the presence of oxygen: A useful source of OH for flash photolysis kinetics experiments. *International Journal of Chemical Kinetics,* 40**,** 504-514.

CARR, S. A., BLITZ, M. A. & SEAKINS, P. W. 2011. Site-Specific Rate Coefficients for Reaction of OH with Ethanol from 298 to 900 K. *Journal of Physical Chemistry A,* 115**,** 3335-3345.

CARTER, W. P. L., COCKER(III), D. R., FITZ, D. R., MALKINA, I. L., BUMILLER, K., SAUER, C. G., PISANO, J. T., BUFALINO, C. & C.SONG 2005. A new environmental chamber for evaluation of gas-phase chemical mechanisms and secondary aerosol formation. *Atmospheric Environment,* 39**,** 7768–7788.

CARTER, W. P. L., DARNALL, K. R., GRAHAM, R. A., WINER, A. M. & PITTS, J. N. 1979. REACTIONS OF C2 AND C-4 ALPHA-HYDROXY RADICALS WITH OXYGEN. *Journal of Physical Chemistry,* 83**,** 2305-2311.

CAVALLI, F., BARNES, I. & BECKER, K. H. 2001. FT-IR kinetic and product study of the OH radical and Cl-atom - Initiated oxidation of dibasic esters. *International Journal of Chemical Kinetics,* 33**,** 431-439.

CAVALLI, F., BARNES, I., BECKER, K. H. & WALLINGTON, T. J. 2000. Atmospheric Oxidation Mechanism of Methyl Propionate. *The Journal of Physical Chemistry A,* 104**,** 11310-11317.

CAVALLI, F., GEIGER, H., BARNES, I. & BECKER, K. H. 2002. FTIR kinetic, product, and modeling study of the OH-initiated oxidation of 1-butanol in air. *Environmental Science & Technology,* 36**,** 1263-1270.

CAVENDER, A. E., BIESENTHAL, T. A., BOTTENHEIM, J. W. & SHEPSON, P. B. 2008. Volatile organic compound ratios as probes of halogen atom chemistry in the Arctic. *Atmospheric Chemistry and Physics,* 8**,** 1737-1750.

CHAPMAN, S. 1930. On ozone and atomic oxygen in the upper atmosphere. *Philosophical Magazine,* 10**,** 369-383.

CHEN, S.Y., LEE, Y.P. 2010. Transient infrared absorption of t-CH3C(O)OO, c-CH3C(O)OO, and alpha-lactone recorded in gaseous reactions of CH3CO and O2. *Journal of Chemical Physics*, 132, 11.

CHERNIN, S. M. 2001. Development of optical multipass matrix systems. *Journal of Modern Optics,* 48**,** 619-632.

CHILTZ, G., JOHNSTON, H. S., HUYBRECHTS, G., GOLDFINGER, P., MEYERS, L., VERBEKE, G. & ECKLING, R. 1963a. Kinetic Isotope Effect in Photochlorination of H_2, CH_4, $CHCl_3$, and C_2H_6. *Journal of Chemical Physics,* 38**,** 1053-1059.

CHILTZ, G., MARTENS, G., HUYBRECHTS, G., GOLDFINGER, P. & VERBEKE, G. 1963b. Atomic chlorination of simpe hydrocarbon derivatives in gas phase. *Chemical Reviews,* 63**,** 355-360.

CHOI, N., PILLING, M. J., SEAKINS, P. W. & WANG, L. 2006. Studies of site selective hydrogen atom abstractions by Cl atoms from isobutane and propane by laser flash photolysis/IR diode laser spectroscopy. *Physical Chemistry Chemical Physics,* 8**,** 2172-2178.

CHRISTENSEN, L. K., BALL, J. C. & WALLINGTON, T. J. 1999. Atmospheric Oxidation Mechanism of Methyl Acetate. *The Journal of Physical Chemistry A,* 104**,** 345-351.

CHU, L. & ANASTASIO, C. 2005. Formation of Hydroxyl Radical from the Photolysis of Frozen Hydrogen Peroxide. *The Journal of Physical Chemistry A,* 109**,** 6264-6271.

COCKER, D.R., FLAGAN, R.C., SEINFELD, J.H., 2001a. State-of-the-art chamber facility for studying atmospheric aerosol chemistry. *Environmental Science & Technology*, 35, 2594–2601.

CRAWFORD, M. A., LI, Z. J., HEUERMAN, H. A. & KINSCHERFF, D. 2004. A kinetic and product study of reaction of chlorine atom with CH_3CH_2OD. *International Journal of Chemical Kinetics,* 36**,** 584-590.

CRIEGEE, R. 1975. Mechanism of ozonolysis. *Angewandte Chemie-International Edition in English,* 14**,** 745-752.

CRIEGEE, R. & WENNER, G. 1949. Die Ozonisierung des 9,10-Oktalins. *Justus Liebigs Annalen der Chemie,* 564**,** 9-15.

CROSLEY, D. R. 1995. The Measurement of OH and HO_2 in the Atmosphere. *Journal of the Atmospheric Sciences,* 52**,** 3299-3314.

CRUTZEN, P. J. 1971. Ozone production rates in oxygen-hydrogen-nitrogen oxide atmosphere. *Journal of Geophysical Research,* 76**,** 7311-7327.

CUEVAS, C. A., NOTARIO, A., MARTINEZ, E. & ALBALADEJO, J. 2004. A kinetic study of the reaction of Cl with a series of linear and ramified ketones as a function of temperature. *Physical Chemistry Chemical Physics,* 6**,** 2230-2236.

CUEVAS, C. A., NOTARIO, A., MARTINEZ, E. & ALBALADEJO, J. 2005a. Influence of temperature in the kinetics of the gas-phase reactions of a series of acetates with Cl atoms. *Atmospheric Environment,* 39**,** 5091-5099.

CUEVAS, C. A., NOTARIO, A., MARTÍNEZ, E. & ALBALADEJO, J. 2005b. Influence of temperature in the kinetics of the gas-phase reactions of a series of acetates with Cl atoms. *Atmospheric Environment,* 39**,** 5091-5099.

CURRAN, H. J. 2006. Rate constant estimation for C_1 to C_4 alkyl and alkoxyl radical decomposition. *International Journal of Chemical Kinetics,* 38**,** 250-275.

DEMIRBAS, B. 2010. Biomass business and operating. *Energy Education Science and Technology Part a-Energy Science and Research,* 26**,** 37-47.

DHANYA, S., PUSHPA, K. K. & NAIK, P. D. 2012. Measurement of kinetic parameters of gas-phase reactions relevant to atmospheric chemistry. *Current Science,* 102**,** 452-459.

DILLON, T.E., CROWLEY, J.N. 2008.Direct detection of OH formation in the reactions of HO2 withCH3C(O)O2 and other substituted peroxy radicals. *Atmospheric Chemical Physics*,8, 4877–4889.

DI CARLO, P., BRUNE, W. H., MARTINEZ, M., HARDER, H., LESHER, R., REN, X., THORNBERRY, T., CARROLL, M., YOUNG, V., SHEPSON, P., RIEMER, D., APEL, E. & CAMPBELL, C. 2004. Missing OH reactivity in a forest: Evidence for unknown reactive biogenic VOCs. *Science Magazine,* 304**,** 722-725.

DONAHUE, N. M., CLARKE, J. S. & ANDERSON, J. G. 1998. Predicting radical-molecule barrier heights: The role of the ionic surface. *Journal of Physical Chemistry A,* 102**,** 3923-3933.

DORN, H. P., APODACA, R. L., BALL, S. M., BRAUERS, T., BROWN, S. S., CROWLEY, J. N., DUBÉ, W. P., FUCHS, H., HÄSELER, R., HEITMANN, U., JONES, R. L., KIENDLER-SCHARR, A., LABAZAN, I., LANGRIDGE, J. M., MEINEN, J., MENTEL, T. F., PLATT, U., PÖHLER, D., ROHRER, F., RUTH, A. A., SCHLOSSER, E., SCHUSTER, G., SHILLINGS, A. J. L., SIMPSON, W. R., THIESER, J., TILLMANN, R., VARMA, R., VENABLES, D. S. & WAHNER, A. 2013. Intercomparison of NO3 radical detection instruments in the atmosphere simulation chamber SAPHIR. *Atmospheric Measurement Technology,* 6**,** 1111-1140.

DUSANTER, S., VIMAL, D., STEVENS, P. S., VOLKAMER, R., MOLINA, L. T., BAKER, A., MEINARDI, S., BLAKE, D., SHEEHY, P., MERTEN, A., ZHANG, R., ZHENG, J., FORTNER, E. C., JUNKERMANN, W., DUBEY, M., RAHN, T., EICHINGER, B., LEWANDOWSKI, P., PRUEGER, J. & HOLDER, H. 2009. Measurements of OH and HO2 concentrations during the MCMA-2006 field campaign - Part 2: Model comparison and radical budget. *Atmospheric Chemistry and Physics,* 9**,** 6655-6675.

EHHALT, D. H. 1998. Atmospheric chemistry - Radical ideas. *Science,* 279**,** 1002-1003.

EHHALT, D. H., ROHRER, F., WAHNER, A., PRATHER, M. J. & BLAKE, D. R. 1998. On the use of hydrocarbons for the determination of tropospheric OH concentrations. *Journal of Geophysical Research-Atmospheres,* 103**,** 18981-18997.

ELSHORBANY, Y. F., KLEFFMANN, J., HOFZUMAHAUS, A., KURTENBACH, R., WIESEN, P., BRAUERS, T., BOHN, B., DORN, H. P., FUCHS, H., HOLLAND, F., ROHRER, F., TILLMANN, R., WEGENER, R., WAHNER, A., KANAYA, Y., YOSHINO, A., NISHIDA, S., KAJII, Y., MARTINEZ, M., KUBISTIN, D., HARDER, H., LELIEVELD, J., ELSTE, T., PLASS-DÜLMER, C., STANGE, G., BERRESHEIM, H. & SCHURATH, U. 2012. HOx budgets during HOxComp: A case study of HOx chemistry under NOx-

limited conditions. *Journal of Geophysical Research: Atmospheres,* 117**,** D03307.

EZELL, M. J., WANG, W., EZELL, A. A., SOSKIN, G. & FINLAYSON-PITTS, B. J. 2002. Kinetics of reactions of chlorine atoms with a series of alkenes at 1 atm and 298 K: structure and reactivity. *Physical Chemistry Chemical Physics,* 4**,** 5813-5820.

FARRELL, A. E., PLEVIN, R. J., TURNER, B. T., JONES, A. D., O'HARE, M. & KAMMEN, D. M. 2006. Ethanol Can Contribute to Energy and Environmental Goals. *Science,* 311**,** 506-508.

FAXON, C. B. & ALLEN, D. T. 2013. Chlorine chemistry in urban atmospheres: a review. *Environmental Chemistry,* 10**,** 221-233.

FERNANDEZ-RAMOS, A., MARTINEZ-NUNEZ, E., MARQUES, J. M. C. & VAZQUEZ, S. A. 2003. Dynamics calculations for the Cl + C_2H_6 abstraction reaction: Thermal rate constants and kinetic isotope effects. *The Journal of Chemical Physics,* 118**,** 6280-6288.

FINLAYSON-PITTS, B. J. 2010. Atmospheric Chemistry. *Proceedings of the National Academy of Sciences,* 107**,** 6566-6567.

FINLAYSON-PITTS, B. J., EZELL, J. & PITTS, J. N. 1989. *Formation of chemically active chlorine compounds by reactions of atmospheric NaCl particles with gaseous N2O5 and ClONO2*, *Nature* **337**, 241 - 244.

FINLAYSON-PITTS, B. J. & PITTS, J. N. 1986. *Atmospheric chemistry: fundamentals and experimental techniques,* Wiley.

FINLAYSON-PITTS, B. J. & PITTS, J. N. J. 2000. *Chemistry of the Upper and Lower Atmosphere. Theory, Experiments and Applications,* San Diego, Academic Press.

FINLEY, B. D. & SALTZMAN, E. S. 2006. Measurement of Cl_2 in coastal urban air. *Geophysical Research Letters,* 33**,** L11809.

FOLKINS, I. & CHATFIELD, R. 2000. Impact of acetone on ozone production and OH in the upper troposphere at high NO_x. *Journal of Geophysical Research-Atmospheres,* 105**,** 11585-11599.

FRANCISCO, J. S. & EISFELD, W. 2009. Atmospheric Oxidation Mechanism of Hydroxymethyl Hydroperoxide. *Journal of Physical Chemistry A,* 113**,** 7593-7600.

FREEMAN, R. R. 1979. *High resolution gas chromatography,* Hewlett-Packard.

FREY, M. M., HUTTERLI, M. A., CHEN, G., SJOSTEDT, S. J., BURKHART, J. F., FRIEL, D. K. & BALES, R. C. 2009. Contrasting atmospheric boundary layer chemistry of methylhydroperoxide (CH_3OOH) and hydrogen peroxide (H_2O_2) above polar snow. *Atmospheric Chemistry and Physics,* 9**,** 3261-3276.

FUCHS, H., BRAUERS, T., DORN, H. P., HARDER, H., HÃ¤SELER, R., HOFZUMAHAUS, A., HOLLAND, F., KANAYA, Y., KAJII, Y., KUBISTIN, D., LOU, S., MARTINEZ, M., MIYAMOTO, K., NISHIDA, S., RUDOLF, M., SCHLOSSER, E., WAHNER, A., YOSHINO, A. & SCHURATH, U. 2010. Technical Note: Formal blind intercomparison of HO_2 measurements in the atmosphere simulation chamber SAPHIR during the HO_x Comp campaign. *Atmospheric Chemical Physics,* 10**,** 12233-12250.

FUENTES, J. D., LERDAU, M., ATKINSON, R., BALDOCCHI, D., BOTTENHEIM, J. W., CICCIOLI, P., LAMB, B., GERON, C., GU, L., GUENTHER, A., SHARKEY, T. D. & STOCKWELL, W. 2000. Biogenic hydrocarbons in the atmospheric boundary layer: A review. *Bulletin of the American Meteorological Society,* 81**,** 1537-1575.

GARZON, A., CUEVAS, C. A., CEACERO, A. A., NOTARIO, A., ALBALADEJO, J. & FERNANDEZ-GOMEZ, M. 2006. Atmospheric reactions $Cl+CH_3-(CH_2)(n)$-OH (n=0-4): A kinetic and theoretical study. *Journal of Chemical Physics,* 125**,** 10.

GEYER, A., BÄCHMANN, K., HOFZUMAHAUS, A., HOLLAND, F., KONRAD, S., KLÜPFEL, T., PÄTZ, H.-W., PERNER, D., MIHELCIC, D., SCHÄFER, H.-J., VOLZ-THOMAS, A. & PLATT, U. 2003. Nighttime formation of peroxy and hydroxyl radicals during the BERLIOZ campaign: Observations and modeling studies. *Journal of Geophysical Research,* 108**,** 8249-8263.

GIERCZAK, T., BURKHOLDER, J. B., BAUERLE, S. & RAVISHANKARA, A. R. 1998. Photochemistry of acetone under tropospheric conditions. *Chemical Physics,* 231**,** 229-244.

GILMAN, J. B., BURKHART, J. F., LERNER, B. M., WILLIAMS, E. J., KUSTER, W. C., GOLDAN, P. D., MURPHY, P. C., WARNEKE, C., FOWLER, C., MONTZKA, S. A., MILLER, B. R., MILLER, L., OLTMANS, S. J., RYERSON, T. B., COOPER, O. R., STOHL, A. & DE GOUW, J. A. 2010. Ozone variability and halogen oxidation within the Arctic and sub-Arctic springtime boundary layer. *Atmospheric Chemistry and Physics,* 10**,** 10223-10236.

GLOWACKI, D. R. 2008. *Investigation of Atmospheric Chemical Mechanisms Using Experiments and Theory*, University of Leeds (School of Chemistry).

GLOWACKI, D. R., GODDARD, A., HEMAVIBOOL, K., MALKIN, T. L., COMMANE, R., ANDERSON, F., BLOSS, W. J., HEARD, D. E., INGHAM, T., PILLING, M. J. & SEAKINS, P. W. 2007a. Design of and initial results from a Highly Instrumented Reactor for Atmospheric Chemistry (HIRAC). *Atmospheric Chemical Physics,* 7**,** 5371-5390.

GLOWACKI, D. R., GODDARD, A. & SEAKINS, P. W. 2007b. Design and performance of a throughput-matched, zero-geometric-loss, modified three objective multipass matrix system for FTIR spectrometry. *Applied Optics,* 46**,** 7872-7883.

GOLDSTEIN, A. H. & GALBALLY, I. E. 2007. Known and unexplored organic constituents in the earth's atmosphere. *Environmental Science & Technology,* 41**,** 1514-1521.

GRAEDEL, T. E. & KEENE, W. C. 1995. Tropospheric budget of reaction chlorine. *Global Biogeochemical Cycles,* 9**,** 47-77.

GRAEDEL, T. E. & KEENE, W. C. 1996. The budget and cycle of Earth's natural chlorine. *Pure and Applied Chemistry,* 68**,** 1689-1697.

GREENBERG, J. P., GUENTHER, A., ZIMMERMAN, P., BAUGH, W., GERON, C., DAVIS, K., HELMIG, D. & KLINGER, L. F. 1999. Tethered balloon measurements of biogenic VOCs in the atmospheric boundary layer. *Atmos. Environ.,* 33**,** 855-867.

GRIFFITH, D. W. T. 1996. Synthetic Calibration and Quantitative Analysis of Gas-Phase FT-IR Spectra. *Applied Spectroscopy,* 50**,** 59-70.

GROB, R. L. & BARRY, E. F. 2004. *Modern practice of gas chromatography*, Wiley-Interscience.

GROSJEAN, D. 1997. Atmospheric chemistry of alcohols. *Journal of the Brazilian Chemical Society,* 8**,** 433-442.

GUICHERIT, R. 1997. Traffic as a source of volatile hydrocarbons in ambient air. *ScienctificTotal Environment,* 205**,** 201-213.

GUNZ, D. W. & HOFFMANN, M. R. 1990. Atmospheric chemistry of peroxides - A review. *Atmospheric Environment Part a-General Topics,* 24**,** 1601-1633.

HAGMAN, A. & JACOBSSON, S. 1988. Trapping efficiency of capillary cold traps. *Journal of Chromatography A,* 448**,** 117-126.

HAHN, J., LUTHER, K. & TROE, J. 2000. Experimental and Theoretical Study of the Temperature and Pressure Dependences of the Recombination Reactions $O+NO_2(+M) \rightarrow NO_3(+M)$ and $NO_2+NO_3(+M) \rightarrow N_2O_5(+M)$. *Physical Chemistry Chemical Physics.***,** 5098 - 5104.

HALLETT, J. 2002. Climate change 2001: The scientific basis. Edited by J. T. Houghton, Y. Ding, D. J. Griggs, N. Noguer, P. J. van der Linden, D. Xiaosu, K. Maskell and C. A. Johnson. Contribution of Working Group I to the Third Assessment Report of the Intergovernmental Panel on Climate Change, Cambridge University Press, Cambridge. 2001. 881 pp. ISBN 0521 01495 6. *Quarterly Journal of the Royal Meteorological Society,* 128**,** 1038-1039.

HAMILTON, J. F. 2010. Using Comprehensive Two-Dimensional Gas Chromatography to Study the Atmosphere. *Journal of Chromatographic Science,* 48**,** 274-282, 10A-11A.

HAMILTON, J. F., LEWIS, A. C., BLOSS, C., WAGNER, V., HENDERSON, A. P., GOLDING, B. T., WIRTZ, K., MARTIN-REVIEJO, M. & PILLING, M. J. 2003. Measurements of photo-oxidation products from the reaction of a series of alkyl-benzenes with hydroxyl radicals during EXACT using comprehensive gas chromatography. *Atmospheric Chemistry and Physics,* 3**,** 1999-2014.

HARD, T. M., CHAN, C. Y., MEHRABZADEH, A. A., PAN, W. H. & O'BRIEN, R. J. 1986. Diurnal cycle of tropospheric OH. *Nature,* 322**,** 617-620.

HARD, T. M., OBRIEN, R. J., CHAN, C. Y. & MEHRABZADEH, A. A. 1984. Tropospheric free-radical determination by FAGE. *Environmental Science & Technology,* 18**,** 768-777.

HARRIS, D. C. 2003. *Quantitative Chemical Analysis*, W.H. Freeman and Company.

HARRIS, G. W., CARTER, W. P. L., WINER, A. M., PITTS, J. N., PLATT, U. & PERNER, D. 1982. Observations of nitrous acid in the Los Angeles atmosphere and implications for predictions of ozone-precursor relationships. *Environmental Science & Technology,* 16**,** 414-419.

HARRY, C., AREY, J. & ATKINSON, R. 1999. Rate constants for the reactions of OH radicals and Cl atoms with di-n-propyl ether and di-n-butyl ether and their deuterated analogs. *International Journal of Chemical Kinetics,* 31**,** 425-431.

HASSON, A.S.., TYNDALL, G.S., ORLANDO, J.J. 2004.A product yield study of the HO2 radicals with ethyl peroxy, acetyl peroxy and acetonyl peroxy radicals. *Journal of Physical Chemistry A,* 108, 5979-5989.

HAUSMANN, M., HOLLAND, F., KOHLMANN, J.-P., ROHRER, F. & EHHALT, D. H. On the dependence of the OH radical concentration on its precursors: Results of the POPCORN field campaign. 23rd EGS Conference, 1998 Nice.

HEARD, D. E. 2006. Atmospheric field measurements of the hydroxyl radical using laser-induced fluorescence spectroscopy. *Annual Review of Physical Chemistry,* 57**,** 191-216.

HEARD, D. E., CARPENTER, L. J., CREASEY, D. J., HOPKINS, J. R., LEE, J. D., LEWIS, A. C., PILLING, M. J., SEAKINS, P. W., CARSLAW, N. & EMMERSON, K. M. 2004. High levels of the hydroxyl radical in the winter urban troposphere. *Geophysical Research Letters,* 31.

HEARD, D. E. & PILLING, M. J. 2003. Measurement of OH and HO_2 in the troposphere. *Chem Rev,* 103**,** 5163-98.

HELLEN, H., LECK, C., PAATERO, J., VIRKKULA, A. & HAKOLA, H. 2012. Summer concentrations of NMHCs in ambient air of the Arctic and Antarctic. *Boreal Environment Research,* 17**,** 385-397.

HEMAVIBOOL, K. 2009. *Formaldehyde and hydrocarbon measurements in ambient air and in an environmental chamber,* University of Leeds (School of Chemistry).

HESS, W. P. & TULLY, F. P. 1989. Hydrogen atom abstraction from methanol by OH. *Journal of Physical Chemistry*. 93**,** 1944-1947.

HICKSON, K. M., BERGEAT, A. & COSTES, M. 2010. A low temperature study of the reactions of atomic chlorine with simple alkanes. *Journal of Physical Chemistry A,* 114**,** 3038-3044.

HOFZUMAHAUS, A., ROHRER, F., LU, K. D., BOHN, B., BRAUERS, T., CHANG, C. C., FUCHS, H., HOLLAND, F., KITA, K., KONDO, Y., LI, X., LOU, S. R., SHAO, M., ZENG, L. M., WAHNER, A. & ZHANG, Y. H. 2009. Amplified Trace Gas Removal in the Troposphere. *Science,* 324**,** 1702-1704.

HOOSHIYAR, P. A. & NIKI, H. 1995. Rate constants for the gas-phase reactions of Cl atoms with C_2 - C_8 alkanes at T = 296 +/- 2 K. *International Journal of Chemical Kinetics,* 27**,** 1197-1206.

HOPKINS, J. R., JONES, I. D., LEWIS, A. C., MCQUAID, J. B. & SEAKINS, P. W. 2002. Non-methane hydrocarbons in the Arctic boundary layer. *Atmospheric Environment,* 36**,** 3217-3229.

HOPKINS, J. R., STILL, T., AL-HAIDER, S., FISHER, I. R., LEWIS, A. C. & SEAKINS, P. W. 2003. A simplified apparatus for ambient formaldehyde detection via GC-pHID. *Atmospheric Environment,* 37**,** 2557-2565.

HOWARD, C. J. 1979. Kinetic measurements using flow tubes. *Journal of Physical Chemistry,* 83**,** 3-9.

HUBSCHMANN, H. J. 2009. *Handbook of GC/MS: fundamentals and applications,* Wiley-VCH.

HUNTER, M. C., BARTLE, K. D., LEWIS, A. C., MCQUAID, J. B., MYERS, P., SEAKINS, P. W. & VAN TILBURG, C. 1998. The Use of the Helium Ionization Detector for Gas Chromatographic Monitoring of Trace Atmospheric Components. *Journal of High Resolution Chromatography,* 21**,** 75-80.

HURLEY, M. D., WALLINGTON, T. J., BJARRUM, M., JAVADI, M. S. & NIELSEN, O. J. 2008. Atmospheric chemistry of 3-pentanol: Kinetics, mechanisms, and products of Cl atom and OH radical initiated oxidation in the presence and absence of NO_X. *Journal of Physical Chemistry A,* 112**,** 8053-8060.

HURLEY, M. D., WALLINGTON, T. J., LAUIRSEN, L., JAVADI, M. S., NIELSEN, O. J., YAMANAKA, T. & KAWASAKI, M. 2009. Atmospheric Chemistry of n-Butanol: Kinetics, Mechanisms, and Products of Cl Atom and OH Radical Initiated Oxidation in the Presence and Absence of NOx. *Journal of Physical Chemistry A,* 113**,** 7011-7020.

JENKIN, M. E., HURLEY, T.J.&WALLINGTON, T. J. 2007. Investigation of the radical product channel of the $CH_3C(O)O_2 + HO_2$ reaction in the gas phase. *Physical Chemistry Chemical Physics,*9**,**3149-3162.

JENKIN, M. E., SAUNDERS, S. M. & PILLING, M. J. 1997. The tropospheric degradation of volatile organic compounds: a protocol for mechanism development. *Atmospheric Environment,* 31**,** 81-104.

JIA, L., XU, Y. F., GE, M. F., DU, L., WANG, G. C. & ZHUANG, G. S. 2006. Kinetic study of the gas-phase ozonolysis of propylene. *Acta Physico-Chimica Sinica,* 22**,** 1260-1265.

JOBSON, B. T., NIKI, H., YOKOUCHI, Y., BOTTENHEIM, J., HOPPER, F. & LEAITCH, R. 1994. Measurements of C2-C6 hydrocarbons during the Polar Sunrise1992 Experiment: Evidence for Cl atom and Br atom chemistry. *J. Geophys. Res.,* 99**,** 25355-25368.

JOHNSON, D. & MARSTON, G. 2008. The gas-phase ozonolysis of unsaturated volatile organic compounds in the troposphere. *Chemical Society Reviews,* 37**,** 699-716.

JOHNSTON, H. S. & GOLDFINGER, P. 1962. Theoretical interpretation of reactions occurring in photochlorination. *Journal of Chemical Physics,* 37**,** 700-706.

KAISER, E. W. & WALLINGTON, T. J. 2007. Rate Constants for the Reaction of Cl with a Series of C4 to C6 Ketones Using the Relative Rate Method. *The Journal of Physical Chemistry A,* 111**,** 10667-10670.

KANAYA, Y., HOFZUMAHAUS, A., DORN, H. P., BRAUERS, T., FUCHS, H., HOLLAND, F., ROHRER, F., BOHN, B., TILLMANN, R., WEGENER, R., WAHNER, A., KAJII, Y., MIYAMOTO, K., NISHIDA, S., WATANABE, K., YOSHINO, A., KUBISTIN, D., MARTINEZ, M., RUDOLF, M., HARDER, H., BERRESHEIM, H., ELSTE, T., PLASS-DULMER, C., STANGE, G., KLEFFMANN, J., ELSHORBANY, Y. & SCHURATH, U. 2012. Comparisons of observed and modeled OH and HO2 concentrations during the ambient measurement period of the HOxComp field campaign. *Atmospheric Chemistry and Physics,* 12**,** 2567-2585.

KARL, M., BRAUERS, T., DORN, H.-P., HOLLAND, F., KOMENDA, M., POPPE, D., ROHRER, F., RUPP, L., SCHAUB, A. & WAHNER, A. 2004. Kinetic Study of the OH-isoprene and O_3-isoprene reaction in the atmosphere simulation chamber, SAPHIR. *Geophysical Research Letters,* 31**,** L05117.

KERDOUCI, J., PICQUET-VARRAULT, B. & DOUSSIN, J. F. 2010. Prediction of Rate Constants for Gas-Phase Reactions of Nitrate Radical with Organic Compounds: A New Structure-Activity Relationship. *Chemical Physics Chemistry,* 11**,** 3909-3920.

KHALIL, M. A. K., MOORE, R. M., HARPER, D. B., LOBERT, J. M., ERICKSON, D. J., KOROPALOV, V., STURGES, W. T. & KEENE, W. C. 1999. Natural emissions of chlorine-containing gases: Reactive Chlorine Emissions Inventory. *Journal of Geophysical Research: Atmospheres,* 104**,** 8333-8346.

KHATOON, T., EDELBUTTELEINHAUS, J., HOYERMANN, K. & WAGNER, H. G. 1989. Rates and mechanisms of the reactions of ethanol and propanol with fluorine and chlorine atoms. *Berichte Der Bunsen-Gesellschaft-Physical Chemistry Chemical Physics,* 93**,** 626-632.

KIESER, B. N., BOTTENHEIM, J. W., SIDERIS, T. & NIKI, H. 1993. Spring 1989 observations of lower tropospheric chemistry in the canadian high arctic. *Atmospheric Environment Part a-General Topics,* 27**,** 2979-2988.

KLEFFMANN, J., GAVRILOAIEI, T., HOFZUMAHAUS, A., HOLLAND, F., KOPPMANN, R., RUPP, L., SCHLOSSER, E., SIESE, M. & WAHNER, A. 2005. Daytime formation of nitrous acid: A major source of OH radicals in a forest. *Geophysical Research Letters,* 32**,** L05818.

KLOTZ, B., VOLKAMER, R., HURLEY, M. D., ANDERSEN, M. P. S., NIELSEN, O. J., BARNES, I., IMAMURA, T., WIRTZ, K., BECKER, K.-H., PLATT, U., WALLINGTON, T. J. & WASHIDA, N. 2002. OH-initiated oxidation of benzene Part II.Influence of elevated NO concentrations. *Physical Chemistry Chemical Physics,* 4**,** 4399-4411.

KOLB, B., LIEBHARDT, B. & ETTRE, L. 1986. Cryofocusing in the combination of gas chromatography with equilibrium headspace sampling. *Chromatographia,* 21**,** 305-311.

KROMIDAS, S., NEUE, U. D., CHENG, Y.-F. & LU, Z. 2008. Fundamentals of Optimization: Sections 1.1 and 1.2. *HPLC Made to Measure.* Wiley-VCH Verlag GmbH & Co. KGaA.

KWAN, A. J., CHAN, A. W. H., NG, N. L., KJAERGAARD, H. G., SEINFELD, J. H. & WENNBERG, P. O. 2012. Peroxy radical chemistry and OH radical production during the NO3-initiated oxidation of isoprene. *Atmospheric Chemistry and Physics,* 12**,** 7499-7515.

KWOK, E. S. C. & ATKINSON, R. 1995a. Estimation of hydroxyl radical reaction rate constants for gas-phase organic compounds using a structure-reactivity relationship: An update. *Atmospheric Environment,* 29**,** 1685-1695.

LAINE, P. L., SOHN, Y. S., NICOVICH, J. M., MCKEE, M. L. and WINE, P. H. 2012. Kinetics of Elementary Steps in the Reactions of Atomic Bromine with Isoprene and 1,3-Butadiene under Atmospheric Conditions. *Journal of Physical Chemistry A,* 116**,** 6341-6357.

LAM, K. Y., DAVIDSON, D. F. and HANSON, R. K. 2012. High-Temperature Measurements of the Reactions of OH with a Series of Ketones: Acetone, 2-Butanone, 3-Pentanone, and 2-Pentanone. *Journal of Physical Chemistry A,* 116**,** 5549-5559.

LAMBE, A. T., ZHANG, J. Y., SAGE, A. M. and DONAHUE, N. M. 2007. Controlled OH radical production via ozone-alkene reactions for use in aerosol aging studies. *Environmental Science and Technology,* 41**,** 2357-2363.

LAPUERTA, M., ARMAS, O. & RODRIGUEZ-FERNANDEZ, J. 2008. Effect of biodiesel fuels on diesel engine emissions. *Progress in Energy and Combustion Science,* 34**,** 198-223.

LAWLER, M. J., FINLEY, B. D., KEENE, W. C., PSZENNY, A. A. P., READ, K. A., VON GLASOW, R. and SALTZMAN, E. S. 2009. Pollution-enhanced reactive chlorine chemistry in the eastern tropical Atlantic boundary layer. *Geophysical Research Letters,* 36**,** L08810.

LEE, J. D., MCFIGGANS, G., ALLAN, J. D., BAKER, A. R., BALL, S. M., BENTON, A. K., CARPENTER, L. J., COMMANE, R., FINLEY, B. D., EVANS, M., FUENTES, E., FURNEAUX, K., GODDARD, A., GOOD, N., HAMILTON, J. F., HEARD, D. E., HERRMANN, H., HOLLINGSWORTH, A., HOPKINS, J. R., INGHAM, T., IRWIN, M., JONES, C. E., JONES, R. L., KEENE, W. C., LAWLER, M. J., LEHMANN, S., LEWIS, A. C., LONG, M. S., MAHAJAN, A., METHVEN, J., MOLLER, S. J., MULLER, K., MULLER, T., NIEDERMEIER, N., O'DOHERTY, S., OETJEN, H., PLANE, J. M. C., PSZENNY, A. A. P., READ, K. A., SAIZ-LOPEZ, A., SALTZMAN, E. S., SANDER, R., VON GLASOW, R., WHALLEY, L., WIEDENSOHLER, A. & YOUNG, D. 2010. Reactive Halogens in the Marine Boundary Layer (RHaMBLe): the tropical North Atlantic experiments. *Atmospheric Chemistry and Physics,* 10**,** 1031-1055.

LELIEVELD, J., BUTLER, T. M., CROWLEY, J. N., DILLON, T. J., FISCHER, H., GANZEVELD, L., HARDER, H., LAWRENCE, M. G., MARTINEZ, M., TARABORRELLI, D. & WILLIAMS, J. 2008. Atmospheric oxidation capacity sustained by a tropical forest. *Nature,* 452**,** 737-740.

LELIEVELD, J., PETERS, W., DENTENER, F. J. & KROL, M. C. 2002. Stability of tropospheric hydroxyl chemistry. *Journal of Geophysical Research-Atmospheres,* 107, 23, ACH171-11.

LEVART, A. & VEBER, M. 2001. Determination of aldehydes and ketones in air samples using cryotrapping sampling. *Chemosphere,* 44**,** 701-708.

LEWIS, A. C., CARSLAW, N., MARRIOTT, P. J., KINGHORN, R. M., MORRISON, P., LEE, A. L., BARTLE, K. D. & PILLING, M. J. 2000. A larger pool of ozone-forming carbon compounds in urban atmospheres. *Nature,* 405**,** 778-781.

LEWIS, R. S., SANDER, S. P., WAGNER, S. & WATSON, R. T. 1980. Temperature-dependent rate constants for the reaction of ground-state chlorine with simple alkanes. *The Journal of Physical Chemistry,* 84**,** 2009-2015.

LI, Y., CAMPANA, M., REIMANN, S., SCHAUB, D., STEMMLER, K., STAEHELIN, J. & PETER, T. 2005. Hydrocarbon concentrations at the Alpine mountain sites Jungfraujoch and Arosa. *Atmospheric Environment,* 39**,** 1113-1127.

LIANG, P., MU, Y. J., DAELE, V. & MELLOUKI, A. 2010. Rate Coefficients for Reactions of OH and Cl with Esters. *Chemphyschem,* 11**,** 4097-4102.

LIAO, J., HUEY, L. G., TANNER, D. J., BROUGH, N., BROOKS, S., DIBB, J. E., STUTZ, J., THOMAS, J. L., LEFER, B., HAMAN, C. & GORHAM, K. 2011a. Observations of hydroxyl and peroxy radicals and the impact of BrO at Summit, Greenland in 2007 and 2008. *Atmos. Chem. Phys.,* 11**,** 8577-8591.

LIAO, J., SIHLER, H., HUEY, L. G., NEUMAN, J. A., TANNER, D. J., FRIESS, U., PLATT, U., FLOCKE, F. M., ORLANDO, J. J., SHEPSON, P. B., BEINE, H. J., WEINHEIMER, A. J., SJOSTEDT, S. J., NOWAK, J. B., KNAPP, D. J., STAEBLER, R. M., ZHENG, W., SANDER, R., HALL, S. R. & ULLMANN, K. 2011b. A comparison of Arctic BrO measurements by chemical ionization mass spectrometry and long path-differential optical absorption spectroscopy. *Journal of Geophysical Research: Atmospheres,* 116**,** D00R02.

MALKIN, T. L. 2010. *Detection of Free-radicals and Other Species to Investigate Atmospheric Chemistry in the HIRAC Chamber*, University of Leeds (School of Chemistry).

MALKIN, T. L., GODDARD, A., HEARD, D. E. & SEAKINS, P. W. 2009. Measurements of OH and HO2 yields from the gas phase ozonolysis of isoprene. *Atmospheric Chemistry and Physics Discussions,* 9**,** 17579-17631.

MALKIN, T. L., GODDARD, A., HEARD, D. E. & SEAKINS, P. W. 2010. Measurements of OH and HO2 yields from the gas phase ozonolysis of isoprene. *Atmospheric Chemistry and Physics,* 10**,** 1441-1459.

MARSTON, G. 1999. Chapter 8. Atmospheric chemistry. *Annual Reports Section "C" (Physical Chemistry),* 95**,** 235-276.

MARTINEZ, R. I. & HERRON, J. T. 1988. Stopped-Flow Studies of the Mechanisms of Ozone-Alkene Reactions in the Gas Phase: trans-2-Butene. *Journal of Physical Chemistry. A.,* 92**,** 644-4648

MCGILLEN, M. R., ARCHIBALD, A. T., CAREY, T., LEATHER, K. E., SHALLCROSS, D. E., WENGER, J. C. & PERCIVAL, C. J. 2011a. Structure-activity relationship (SAR) for the prediction of gas-phase ozonolysis rate coefficients: an extension towards heteroatomic unsaturated species. *Physical Chemistry Chemical Physics,* 13**,** 2842-2849.

MCGILLEN, M. R., BAASANDORJ, M. & BURKHOLDER, J. B. 2013. Gas-Phase Rate Coefficients for the OH plus *n*-, *i*-, *s*-, and *t*-Butanol Reactions Measured Between 220 and 380 K: Non-Arrhenius Behavior and Site-Specific Reactivity. *Journal of Physical Chemistry A,* 117**,** 4636-4656.

MCGILLEN, M. R., GHALAIENY, M. & PERCIVAL, C. J. 2011b. Determination of gas-phase ozonolysis rate coefficients of C_{8-14} terminal alkenes at elevated temperatures using the relative rate method. *Physical Chemistry Chemical Physics,* 13**,** 10965-10969.

MCKEEN, S. A., GIERCZAK, T., BURKHOLDER, J. B., WENNBERG, P. O., HANISCO, T. F., KEIM, E. R., GAO, R. S., LIU, S. C., RAVISHANKARA, A. R. & FAHEY, D. W. 1997. The photochemistry of acetone in the upper troposphere: A source of odd-hydrogen radicals. *Geophysical Research Letters,* 24**,** 3177-3180.

MCNAIR, H. M. & MILLER, J. M. 2009. *Basic Gas Chromatography*, John Wiley & Sons.

MEHRAN, M. F., NICKELSEN, M. G., GOLKAR, N. & COOPER, W. J. 1990. Improvement of the purge- and -trap technique for the rapid analysis of volatile organic pollutants in water. *Journal of High Resolution Chromatography,* 13**,** 429-433.

MELLOUKI, A., LE BRAS, G. & SIDEBOTTOM, H. 2003. Kinetics and mechanisms of the oxidation of oxygenated organic compounds in the gas phase. *Chemical Reviews,* 103**,** 5077-5096.

MERTES, P., PFAFFENBERGER, L., DOMMEN, J., KALBERER, M. & BALTENSPERGER, U. 2012. Development of a sensitive long path absorption photometer to quantify peroxides in aerosol particles (Peroxide-LOPAP). *Atmospheric Measurement Techniques,* 5**,** 2339-2348.

MIELKE, L. H., FURGESON, A. & OSTHOFF, H. D. 2011. Observation of ClNO2 in a Mid-Continental Urban Environment. *Environmental Science & Technology,* 45**,** 8889-8896.

MILLER, B. & WALLING, C. 1957. The displacement of aromatic substituents by halogen atoms. *Journal of the American Chemical Society,* 79**,** 4187-4191.

MÖHLER, O., STETZER, O., SCHAEFERS, S., LINKE, C., SCHNAITER, M., TIEDE, R., SAATHOFF, H., KRÄMER, M., MANGOLD, A., BUDZ, P., ZINK, P., SCHREINER, J., MAUERSBERGER, K., HAAG, W., KÄRCHER, B. & SCHURATH, U. 2003. Experimental investigation of homogeneous freezing of sulphuric acid particles in the aerosol chamber AIDA. *Atmospherical Chemical Physics,* 3**,** 211-223.

MOLINA, M. J. & ROWLAND, F. S. 1974. Stratospheric sink for clourofluoromethanes: chlorine atom catalysed destruction of ozone. *Nature,* 249**,** 810.

MONKS, P. S., GRANIER, C., FUZZI, S., STOHL, A., WILLIAMS, M. L., AKIMOTO, H., AMANN, M., BAKLANOV, A., BALTENSPERGER, U., BEY, I., BLAKE, N., BLAKE, R. S., CARSLAW, K., COOPER, O. R., DENTENER, F., FOWLER, D., FRAGKOU, E., FROST, G. J., GENEROSO, S., GINOUX, P., GREWE, V., GUENTHER, A., HANSSON, H. C., HENNE, S., HJORTH, J., HOFZUMAHAUS, A., HUNTRIESER, H., ISAKSEN, I. S. A., JENKIN, M. E., KAISER, J., KANAKIDOU, M., KLIMONT, Z., KULMALA, M., LAJ, P., LAWRENCE, M. G., LEE, J. D., LIOUSSE, C., MAIONE, M., MCFIGGANS, G., METZGER, A., MIEVILLE, A., MOUSSIOPOULOS, N., ORLANDO, J. J., O'DOWD, C. D., PALMER, P. I., PARRISH, D. D., PETZOLD, A., PLATT, U., POSCHL, U., PREVOT, A. S. H., REEVES, C. E., REIMANN, S., RUDICH, Y., SELLEGRI, K., STEINBRECHER, R., SIMPSON, D., TEN BRINK, H., THELOKE, J., VAN DER WERF, G. R., VAUTARD, R., VESTRENG, V., VLACHOKOSTAS, C. and VON GLASOW, R. 2009. Atmospheric composition change - global and regional air quality. *Atmospheric environment,* 43**,** 5268-5350.

MONTSKA S.A, & REIMANN S. 2010, Ozone-Depleting Substances (ODSs) and Related Chemicals – Scientific Assessment of Ozone Depletion: 2010; World Meteorological Organization, Global Ozone Research and Monitoring Project – Report No. 52.

NELSON, L., RATTIGAN, O., NEAVYN, R., SIDEBOTTOM, H., TREACY, J. & NIELSEN, O. J. 1990. Absolute and relative rate constants for the reactions of hydroxyl radicals and chlorine atoms with a series of aliphatic alcohols and ethers at 298 K. *International Journal of Chemical Kinetics,* 22**,** 1111-1126.

NILSSON, E. J. K., ESKEBJERG, C. & JOHNSON, M. S. 2009. A photochemical reactor for studies of atmospheric chemistry. *Atmospheric Environment,* 43**,** 3029-3033.

NOTARIO, A., LE BRAS, G. & MELLOUKI, A. 1998. Absolute Rate Constants for the Reactions of Cl Atoms with a Series of Esters. *The Journal of Physical Chemistry A,* 102**,** 3112-3117.

NOTARIO, A., MELLOUKI, A. & LE BRAS, G. 2000. Rate constants for the gas-phase reactions of chlorine atoms with a series of ketones. *International Journal of Chemical Kinetics,* 32**,** 62-66.

OKSDATH-MANSILLA, G., PENENORY, A. B., ALBU, M., BARNES, I., WIESEN, P. & TERUEL, M. A. 2009. FTIR relative kinetic study of the reactions of $CH_3CH_2SCH_2CH_3$ and $CH_3CH_2SCH_3$ with OH radicals and Cl atoms at atmospheric pressure. *Chemical Physics Letters,* 477**,** 22-27.

OLSON, J. R., CRAWFORD, J. H., CHEN, G., BRUNE, W. H., FALOONA, I. C., TAN, D., HARDER, H. & MARTINEZ, M. 2006. A reevaluation of airborne HOx observations from NASA field campaigns. *Journal of Geophysical Research-Atmospheres,* 111.

ORLANDO, J. J. & TYNDALL, G. S. 2002. Mechanisms for the Reactions of OH with Two Unsaturated Aldehydes: Crotonaldehyde and Acrolein. *Journal of physical chemistry A,* 106**,** 12252-12259.

ORLANDO, J. J., TYNDALL, G. S., BURKHOLDER, J. B., BERTMAN, S. B. & CHEN, W. 2002. The atmospheric chemistry of the unsaturated aldehydes methacrolein, acrolein, and crotonaldehyde. *Abstracts of Papers American Chemical Society,* 223**,** 96.

ORLANDO, J. J., TYNDALL, G. S. & WALLINGTON, T. J. 2003. The atmospheric chemistry of alkoxy radicals. *Chemical Review,* 103**,** 4657-4689.

ORR, S. 2012. A kinetic and mechanistic study of atmospheric oxidation chemistry using the highly instrumented reactor for atmospheric chemistry. *Transfer report,* School of Chemistry, University of Leeds.

PANKOW, J. F. 1983. Cold trapping of volatile organic compounds on fused silica capillary columns. *Journal of High Resolution Chromatography,* 6**,** 292-299.

PARKER, J. K., PAYNE, W. A., CODY, R. J., NESBITT, F. L., STIEF, L. J., KLIPPENSTEIN, S. J. & HARDING, L. B. 2007. Direct measurement and theoretical calculation of the rate coefficient for Cl+CH3 in the range from T=202-298 K. *Journal of Physical Chemistry A,* 111**,** 1015-1023.

PAULSEN, D., J. DOMMEN M. KALBERER, PREVOT, A.S.H., RICHTER, R.. SAX M., STEINBACHER M., WEINGARTNER M., and BALTENSPERGER.U. 2005. Secondary Organic Aerosol Formation by Irradiation of 1,3,5-Trimethylbenzene-NO_x-H_2O in a New Reaction Chamber for Atmospheric Chemistry and Physics, Environmental Science and Technology 39, 2668-2678.

PAULSON, S. E. & ORLANDO, J. J. 1996. The reactions of ozone with alkenes: An important source of HO_x in the boundary layer. *Geophysical Research Letters,* 25**,** 3727-3730.

PEETERS, J., NGUYEN, T. L. & VEREECKEN, L. 2009. HO_x radical regeneration in the oxidation of isoprene. *Physical Chemistry Chemical Physics,* 11**,** 5935-5939.

PHILLIPS, G. J., TANG, M. J., THIESER, J., BRICKWEDDE, B., SCHUSTER, G., BOHN, B., LELIEVELD, J. & CROWLEY, J. N. 2012. Significant concentrations of nitryl chloride observed in rural continental Europe associated with the influence of sea salt chloride and anthropogenic emissions. *Geophysical Research Letters,* 39.

PICQUET-VARRAULT, B., DOUSSIN, J. F., DURAND-JOLIBOIS, R., PIRALI, O., CARLIER, P. & FITTSCHEN, C. 2002. Kinetic and Mechanistic Study of the Atmospheric Oxidation by OH Radicals of Allyl Acetate. *Environmental Science & Technology,* 36**,** 4081-4086.

PILGRIM, J. S., MCILROY, A. & TAATJES, C. A. 1997. Kinetics of Cl atom reactions with methane, ethane, and propane from 292 to 800 K. *Journal of Physical Chemistry A,* 101**,** 1873-1880.

PINELLI, D., BUJALSKI, W., NIENOW, A. W. & MAGELLI, F. 2001. Comparison of experimental techniques for the measurement of mixing time in gas-liquid systems. *Chemical Engineering & Technology,* 24**,** 919-923.

PLATT, U. & HONNINGER, G. 2003. The role of halogen species in the troposphere. *Chemosphere,* 52**,** 325-338.

POUTSMA, M. L. 1968. Chlorination studies of unsaturated materials in nonpolar media - Ionic chlorination of some simple allenes. *Journal of Organic Chemistry,* 33**,** 4080-4087.

POUTSMA, M. L. 2013. Evolution of Structure-Reactivity Correlations for the Hydrogen Abstraction Reaction by Chlorine Atom. *Journal of Physical Chemistry A,* 117**,** 687-703.

POZZER, A., POLLMANN, J., TARABORRELLI, D., JOCKEL, P., HELMIG, D., TANS, P., HUEBER, J. & LELIEVELD, J. 2010. Observed and simulated global distribution and budget of atmospheric C_2-C_5 alkanes. *Atmospheric Chemistry and Physics,* 10**,** 4403-4422.

PRATHER, M. J., MCELROY, M. B. & WOFSY, S. C. 1984. REDUCTIONS IN OZONE AT HIGH-CONCENTRATIONS OF STRATOSPHERIC HALOGENS. *Nature,* 312**,** 227-231.

PRATT, K. A., CUSTARD, K. D., SHEPSON, P. B., DOUGLAS, T. A., POEHLER, D., GENERAL, S., ZIELCKE, J., SIMPSON, W. R., PLATT, U., TANNER, D. J., HUEY, L. G., CARLSEN, M. & STIRM, B. H. 2013. Photochemical production of molecular bromine in Arctic surface snowpacks. *Nature Geoscience,* 6**,** 351-356.

PSZENNY, A. A. P., FISCHER, E. V., RUSSO, R. S., SIVE, B. C. & VARNER, R. K. 2007. Estimates of Cl atom concentrations and hydrocarbon kinetic reactivity in surface air at Appledore Island, Maine (USA), during International Consortium for Atmospheric Research on Transport and

Transformation/Chemistry of Halogens at the Isles of Shoals. *Journal of Geophysical Research,* 112**,** D10S13.

PSZENNY, A. A. P., KEENE, W. C., JACOB, D. J., FAN, S., MABEN, J. R., ZETWO, M. P., SPRINGER, YOUNG, M. & GALLOWAY, J. N. 1993. Evidence of inorganic chlorine gases other than hydrogen chloride in marine surface air. *Geophysical Research Letters,* 20**,** 699-702.

PUGH, T., MACKENZIE, A. R., HEWITT, C. N., LANGFORD, B., EDWARDS, P. M., FURNEAUX, K. L., HEARD, D. E., HOPKINS, J., JONES, C. E., KARUNAHARAN, A., LEE, J. D., MILLS, G., MISZTAL, P., MOLLER, S., MONKS, P. S. & WHALLEY, L. K. 2010. Simulating atmospheric composition over a South-East Asian tropical rainforest: performance of a chemistry box model. *Atmospheric Chemistry and Physics,* 10**,** 279-298.

QIAN, H. B., TURTON, D., SEAKINS, P. W. & PILLING, M. J. 2001. A laser flash photolysis/IR diode laser absorption study of the reaction of chlorine atoms with selected alkanes. *International Journal of Chemical Kinetics,* 34**,** 86-94.

RAFF, J. D., NJEGIC, B., CHANG, W. L., GORDON, M. S., DABDUB, D., GERBER, R. B. & FINLAYSON-PITTS, B. J. 2009. Chlorine activation indoors and outdoors via surface-mediated reactions of nitrogen oxides with hydrogen chloride. *Proceedings of the National Academy of Sciences,* 106**,** 13647-13654.

RAVISHANKARA, A. R. 2005. Chemistry-climate coupling: the importance of chemistry in climate issues. *Faraday Discussions,* 130**,** 9-26.

RAVISHANKARA, A. R. 2009. Are chlorine atoms significant tropospheric free radicals? *Proceedings of the National Academy of Sciences,* 106**,** 13639-13640.

RAVISHANKARA, A. R., DAWSON, J. P. & WINNER, D. A. 2012. New Directions: Adapting air quality management to climate change: A must for planning. *Atmospheric Environment,* 50**,** 387-389.

READ, K. A., LEWIS, A. C., SALMON, R. A., JONES, A. E. & BAUGUITTE, S. P. 2007. *OH and halogen atom influence on the variability of non-methane hydrocarbons in the Antarctic Boundary Layer,* 59, 1, 22-38.

READ, K. A., MAHAJAN, A. S., CARPENTER, L. J., EVANS, M. J., FARIA, B. V. E., HEARD, D. E., HOPKINS, J. R., LEE, J. D., MOLLER, S. J., LEWIS, A. C., MENDES, L., MCQUAID, J. B., OETJEN, H., SAIZ-LOPEZ, A., PILLING, M. J. & PLANE, J. M. C. 2008. Extensive halogen-mediated ozone destruction over the tropical Atlantic Ocean. *Nature,* 453**,** 1232-5.

REN, X., VAN DUIN, D., CAZORLA, M., CHEN S., MAO J., ZHANG L., BRUNE WH., FLYNN JH, GROSSBERG N., LEFER BL., RAPPENGLUCK B., WONG K.W., TSAI C., STUTZ J., DIBB JE., JOBSON BT., LUKE WT. & KELLEY P. 2013. Atmospheric oxidation chemistry and ozone production: Results from SHARP 2009 in Houston, Texas. *Journal of Geophysical Research of Atmosphere,* 118, 5770-5780.

RIEDEL, T. P., BERTRAM, T. H., CRISP, T. A., WILLIAMS, E. J., LERNER, B. M., VLASENKO, A., LI, S. M., GILMAN, J., DE GOUW, J., BON, D. M., WAGNER, N. L., BROWN, S. S. & THORNTON, J. A. 2012. Nitryl Chloride

and Molecular Chlorine in the Coastal Marine Boundary Layer. *Environmental Science & Technology,* 46**,** 10463-10470.

RIEMER, D., APEL, E., ORLANDO, J., TYNDALL, G., BRUNE, W., WILLIAMS, E., LONNEMAN, W. & NEECE, J. 2008. Unique isoprene oxidation products demonstrate chlorine atom chemistry occurs in the Houston, Texas urban area. *Journal of Atmospheric Chemistry,* 61**,** 227-242.

ROBERTS, J. M. 1990. The atmospheric chemistry of organic nitrates. *Atmospheric Environment. Part A. General Topics,* 24**,** 243-287.

RODRIGUEZ, A., RODRIGUEZ, D., SOTO, A., BRAVO, I. N., DIAZ-DE-MERA, Y., NOTARIO, A. & ARANDA, A. 2012. Products and mechanism of the reaction of Cl atoms with unsaturated alcohols. *Atmospheric Environment,* 50**,** 214-224.

ROHRER, F., BOHN, B., BRAUERS, T., BRUNING, D., JOHNEN, F. J., WAHNER, A. & KLEFFMANN, J. 2004. Characterisation of the photolytic HONO-source in the atmosphere simulation chamber SAPHIR. *Atmospheric Chemistry and Physics,* 5**,** 2189-2201.

ROHRER, F., BOHN, B., BRAUERS, T., BRÜNING, D., JOHNEN, F. J., WAHNER, A. & KLEFFMANN, J. 2005. Characterisation of the photolytic HONO-source in the atmosphere simulation chamber SAPHIR. *Atmospheric Chemical Physics,* 5**,** 2189-2201.

SAIZ-LOPEZ, A. & VON GLASOW, R. 2012. Reactive halogen chemistry in the troposphere. *Chemical Society Reviews,* 41**,** 6448-6472.

SANDER, S. P., FRIEDL, R. R., BARKER, J. R., GOLDEN, D. M., KURYLO, M. J., WINE, P. H., ABBATT, J., BURKHOLDER, J. B., KOLB, C. E., MOORTGAT, G. K., HUIE, R. E. & ORKIN, V. L. 2010. Chemical Kinetics and Photochemical Data for Use in Atmospheric Studies.

SARZYNSKI, D. & SZTUBA, B. 2002. Gasp-phase reactions of Cl atoms with propane, n-butane, and isobutane. *International Journal of Chemical Kinetics,* 34**,** 651-658.

SAUNDERS, S. M., JENKIN, M. E., DERWENT, R. G. & PILLING, M. J. 2003. Protocol for the development of the Master Chemical Mechanism, MCM v3 (Part A): tropospheric degradation of non-aromatic volatile organic compounds. *Atmospheric Chemistry and Physics,* 3**,** 161-180.

SCHLOSSER, E., BOHN, B., BRAUERS, T., DORN, H.-P., FUCHS, H., HÄSELER, R., HOFZUMAHAUS, A., HOLLAND, F., ROHRER, F., RUPP, L., SIESE, M., TILLMANN, R. & WAHNER, A. 2007. Intercomparison of Two Hydroxyl Radical Measurement Techniques at the Atmosphere Simulation Chamber SAPHIR. *Journal of Atmospheric Chemistry,* 56**,** 187-205.

SCHLOSSER, E., BRAUERS, T., DORN, H. P., FUCHS, H., HÃ¤SELER, R., HOFZUMAHAUS, A., HOLLAND, F., WAHNER, A., KANAYA, Y., KAJII, Y., MIYAMOTO, K., NISHIDA, S., WATANABE, K., YOSHINO, A., KUBISTIN, D., MARTINEZ, M., RUDOLF, M., HARDER, H., BERRESHEIM, H., ELSTE, T., PLASS-DULMER, C., STANGE, G. and SCHURATH, U. 2009. Technical Note: Formal blind intercomparison of OH

measurements: results from the international campaign HOxComp. *Atmospheric Chemistry and Physics,* 9**,** 7923-7948.

SCHUTZE, N., ZHONG, X., KIRSCHBAUM, S., BEJAN, I., BARNES, I. & BENTER, T. 2010a. Relative kinetic measurements of rate coefficients for the gas-phase reactions of Cl atoms and OH radicals with a series of methyl alkyl esters. *Atmospheric Environment,* 44**,** 5407-5414.

SEAKINS, P. W. 2007. Product branching ratios in simple gas phase reactions. *Annual Reports Section "C" (Physical Chemistry),* 103**,** 173-222.

SEAKINS, P. W. 2010a. A brief review of the use of environmental chambers for gas phase studies of kinetics, chemical mechanisms and characterisation of field instruments. *In:* BOUTRON, C. (ed.) *Erca 9: From the Global Mercury Cycle to the Discoveries of Kuiper Belt Objects.*

SEAKINS, P. W. 2010b. A brief review of the use of environmental chambers for gas phase studies of kinetics, chemical mechanisms and characterisation of field instruments. *EPJ Web of Conferences,* 9**,** 143-163.

SEAKINS, P. W. & BLITZ, M. A. 2011. Developments in Laboratory Studies of Gas-Phase Reactions for Atmospheric Chemistry with Applications to Isoprene Oxidation and Carbonyl Chemistry. *In:* LEONE, S. R., CREMER, P. S., GROVES, J. T. & JOHNSON, M. A. (eds.) *Annual Review of Physical Chemistry, Vol 62.*

SEAKINS, P. W., ORLANDO, J. J. & TYNDALL, G. S. 2004. Rate coefficients and production of vibrationally excited HCl from the reactions of chlorine atoms with methanol, ethanol, acetaldehyde and formaldehyde. *Physical Chemistry Chemical Physics,* 6**,** 2224-2229.

SEINFELD, J.H, AND PANDIS, S.N.. 1998.*Atmospheric Chemistry and Physics*, Wiley, New York, Atmospheric stability, turbulence.

SELVAM, D. J. P. & VADIVEL, K. 2013. An Experimental Investigation on Performance, Emission, and Combustion Characteristics of a Diesel Engine Fueled with Methyl Esters of Waste Pork Lard and Diesel Blends. *International Journal of Green Energy,* 10**,** 908-923.

SHANNON, R. J., BLITZ, M. A., GODDARD, A. & HEARD, D. E. 2013. Accelerated chemistry in the reaction between the hydroxyl radical and methanol at interstellar temperatures facilitated by tunnelling. *Nature Chemistry, 5, 745-749.*

SHETTER, R. E., DAVIDSON, J. A., CANTRALL, C. A. & CALVERT, J. G. 1987. Temperature variable long path cell for absorption measurements. *Review of scientific instrument,* 58, 1427.

SHIMODA, M. & SHIBAMOTO, T. 1990. Factors affecting headspace analysis by the on-column injection/cryofocusing method. *Journal of High Resolution Chromatography,* 13**,** 518-520.

SIESE, M., BECKER, K. H., BROCKMANN, K. J., GEIGER, H., HOFZUMAHAUS, A., HOLLAND, F., MIHELCIC, D. & WIRTZ, K. 2001. Direct measurement of OH radicals from ozonolysis of selected alkenes: A EUPHORE simulation chamber study. *Environmental Science & Technology,* 35**,** 4660-4667.

SIMMONDS, P. G. 1984. Analysis of trace halocarbons in natural waters by simplified purge cryotrap method. *Journal of Chromatography A,* 289**,** 117-127.

SIMPSON, W. R. 2003. Continuous wave cavity ring-down spectroscopy applied to in situ detection of dinitrogen pentoxide (N_2O_5). *Rev. Sci. Instrum.,* 74.

SIMPSON, W. R., VON GLASOW, R., RIEDEL, K., ANDERSON, P., ARIYA, P., BOTTENHEIM, J., BURROWS, J., CARPENTER, L. J., FRIESS, U., GOODSITE, M. E., HEARD, D., HUTTERLI, M., JACOBI, H. W., KALESCHKE, L., NEFF, B., PLANE, J., PLATT, U., RICHTER, A., ROSCOE, H., SANDER, R., SHEPSON, P., SODEAU, J., STEFFEN, A., WAGNER, T. & WOLFF, E. 2007. Halogens and their role in polar boundary-layer ozone depletion. *Atmospheric Chemistry and Physics,* 7**,** 4375-4418.

SINGH, H., CHEN, Y., STAUDT, A., JACOB, D., BLAKE, D., HEIKES, B. & SNOW, J. 2001. Evidence from the Pacific troposphere for large global sources of oxygenated organic compounds. *Nature,* 410**,** 1078-1081.

SINGH, H. B., O'HARA, D., HERLTH, D., SACHSE, W., BLAKE, D. R., BRADSHAW, J. D., KANAKIDOU, M. & CRUTZEN, P. J. 1994. Acetone in the atmosphere: Distribution, sources, and sinks. *Journal of Geophysical Research.* 99**,** 1805-1819.

SINGH, H. B., SALAS, L. J., CHATFIELD, R. B., CZECH, E., FRIED, A., WALEGA, J., EVANS, M. J., FIELD, B. D., JACOB, D. J., BLAKE, D., HEIKES, B., TALBOT, R., SACHSE, G., CRAWFORD, J. H., AVERY, M. A., SANDHOLM, S. & FUELBERG, H. 2004. Analysis of the atmospheric distribution, sources, and sinks of oxygenated volatile organic chemicals based on measurements over the Pacific during TRACE-P. *Journal of Geophysical Research-Atmospheres,* 109.

SOLOMON, S. 1999. Stratospheric ozone depletion: A review of concepts and history. *Reviews of Geophysics,* 37**,** 275-316.

SPARKMAN, O. D., PENTON, Z. & KITSON, F. G. 2011. *Gas Chromatography and Mass Spectrometry: A Practical Guide,* Elsevier.

SPICER, C. W., CHAPMAN, E. G., FINLAYSON-PITTS, B. J., PLASTRIDGE, R. A., HUBBE, J. M., FAST, J. D. & BERKOWITZ, C. M. 1998. Unexpectedly high concentrations of molecular chlorine in coastal air. *Nature,* 394**,** 353-356.

SPRUNG, D. & ZAHN, A. 2010. Acetone in the upper troposphere/lowermost stratosphere measured by the CARIBIC passenger aircraft: Distribution, seasonal cycle, and variability. *Journal of Geophysical Research-Atmospheres,* 115.

STEPHENS, C. R., SHEPSON, P. B., STEFFEN, A., BOTTENHEIM, J. W., LIAO, J., HUEY, L. G., APEL, E., WEINHEIMER, A., HALL, S. R., CANTRELL, C., SIVE, B. C., KNAPP, D. J., MONTZKA, D. D. & HORNBROOK, R. S. 2012. The relative importance of chlorine and bromine radicals in the oxidation of atmospheric mercury at Barrow, Alaska. *Journal of Geophysical Research-Atmospheres,* 117.

STONE, D., EVANS, M. J., COMMANE, R., INGHAM, T., FLOQUET, C. F. A., MCQUAID, J. B., BROOKES, D. M., MONKS, P. S., PURVIS, R., HAMILTON, J. F., HOPKINS, J., LEE, J., LEWIS, A. C., STEWART, D.,

MURPHY, J. G., MILLS, G., ORAM, D., REEVES, C. E. & HEARD, D. E. 2010. HO_x observations over West Africa during AMMA: impact of isoprene and NO_x. *Atmos. Chem. Phys.,* 10**,** 9415-9429.

STONE, D., EVANS, M. J., EDWARDS, P. M., COMMANE, R., INGHAM, T., RICKARD, A. R., BROOKES, D. M., HOPKINS, J., LEIGH, R. J., LEWIS, A. C., MONKS, P. S., ORAM, D., REEVES, C. E., STEWART, D. & HEARD, D. E. 2011. Isoprene oxidation mechanisms: measurements and modelling of OH and HO_2 over a South-East Asian tropical rainforest during the OP3 field campaign. *Atmospheric Chemistry and Physics,* 11**,** 6749-6771.

STONE, D., WHALLEY, L. K. & HEARD, D. E. 2012. Tropospheric OH and HO2 radicals: field measurements and model comparisons. *Chemical Society Reviews,* 41**,** 6348-6404.

STUTZ, J., EZELL, M. J., EZELL, A. A. & FINLAYSON-PITTS, B. J. 1998. Rate Constants and Kinetic Isotope Effects in the Reactions of Atomic Chlorine with n-Butane and Simple Alkenes at Room Temperature. *The Journal of Physical Chemistry A,* 102**,** 8510-8519.

SUH, I. & ZHANG, R. Y. 2000. Kinetic studies of isoprene reactions initiated by chlorine atom. *Journal of Physical Chemistry A,* 104**,** 6590-6596.

TAATJES, C. A. 1999. Time-resolved infrared absorption measurements of product formation in Cl atom reactions with alkenes and alkynes. *International Reviews in Physical Chemistry,* 18**,** 419-458.

TAATJES, C. A., CHRISTENSEN, L. K., HURLEY, M. D. & WALLINGTON, T. J. 1999. Absolute and site-specific abstraction rate coefficients for reactions of Cl with CH_3CH_2OH, CH_3CD_2OH, and CD_3CH_2OD between 295 and 600 K. *Journal of Physical Chemistry A,* 103**,** 9805-9814.

TAKAHASHI, K., IWASAKI, E., MATSUMI, Y. & WALLINGTON, T. J. 2007. Pulsed Laser Photolysis Vacuum UV Laser-Induced Fluorescence Kinetic Study of the Gas-Phase Reactions of Cl(2P3/2) Atoms with C3-C6 Ketones. *The Journal of Physical Chemistry A,* 111**,** 1271-1276.

TAKETANI, F., MATSUMI, Y., WALLINGTON, T. J. & HURLEY, M. D. 2006. Kinetics of the gas phase reactions of chlorine atoms with a series of ketones. *Chemical Physics Letters,* 431**,** 257-260.

TALUKDAR, R. K., GIERCZAK, T., MCCABE, D. C. & RAVISHANKARA, A. R. 2003. Reaction of hydroxyl radical with acetone. 2. Products and reaction mechanism. *Journal of Physical Chemistry A,* 107**,** 5021-5032.

TANAKA, P. L., OLDFIELD, S., NEECE, J. D., MULLINS, C. B. & ALLEN, D. T. 2000. Anthropogenic sources of chlorine and ozone formation in urban atmospheres. *Environmental Science & Technology,* 34**,** 4470-4473.

TARASOVA, O., KOIDE, H., DLUGOKENCKY, E., MONTZKA, S.A., GRIFFITH, D., BRUNKE, E., SCHEEL, H.E., LAURILA, T., WELLER, R. , BUTLER, J.H. 2013. The state of greenhouse gases in the atmosphere using global observations through 2011. *EGU General Assembly 2013, held 7-12 April, 2013 in Vienna, Austria,* id. EGU2013-2799.

TEMIME, B., HEALY, R. M. & WENGER, J. C. 2007. A Denuder-Filter Sampling Technique for the Detection of Gas and Particle Phase Carbonyl Compounds. *Environmental Science & Technology,* 41**,** 6514-6520.

THERMO ELECTRON CORPORATION. 2005. Model 49i Primary Standard Instruction Manual UV Photometric O_3 Calibrator.

THORNTON, J. A., KERCHER, J. P., RIEDEL, T. P., WAGNER, N. L., COZIC, J., HOLLOWAY, J. S., DUBU, W. P., WOLFE, G. M., QUINN, P. K., MIDDLEBROOK, A. M., ALEXANDER, B. and BROWN, S. S. 2010. A large atomic chlorine source inferred from mid-continental reactive nitrogen chemistry. *Nature,* 464**,** 271-274.

THUNER, L. P., BARDINI, P., REA, G. J. & WENGER, J. C. 2004. Kinetics of the gas-phase reactions of OH and NO_3 radicals with dimethylphenols. *Journal Of Physical Chemistry A,* 108**,** 11019-11025.

TUCCAR, G. & AYDIN, K. 2013. Evaluation of methyl ester of microalgae oil as fuel in a diesel engine. *Fuel,* 112**,** 203-207.

TURPIN, E., FITTSCHEN, C., TOMAS, A. & DEVOLDER, P. 2003. Reaction of OH radicals with acetone: Determination of the branching ratio for the abstraction pathway at 298 K and 1 Torr. *Journal of Atmospheric Chemistry,* 46**,** 1-13.

TYNDALL, G. R. S., ORLANDO, J. J., WALLINGTON, T. J., HURLEY, M. D. 1997. Pressure dependence of the rate coefficients and product yields for the reaction of CH3CO radicals with O-2. *International Journal of Chemical Kinetics,* 29, 9, 655-663.

TYNDALL, G. R. S., ORLANDO, J. J., WALLINGTON, T. J., HURLEY, M. D., GOTO, M. & KAWASAKI, M. 2002. Mechanism of the reaction of OH radicals with acetone and acetaldehyde at 251 and 296 K. *Physical Chemistry Chemical Physics,* 4**,** 2189-2193.

TYNDALL, G. S., ORLANDO, J. J., WALLINGTON, T. J., DILL, M. & KAISER, E. W. 1997. Kinetics and mechanisms of the reactions of chlorine atoms with ethane, propane, and n-butane. *International Journal of Chemical Kinetics,* 29**,** 43-55.

VANDENBERK, S., VEREECKEN, L. & PEETERS, J. 2002. The acetic acid forming channel in the acetone plus OH reaction: A combined experimental and theoretical investigation. *Physical Chemistry Chemical Physics,* 4**,** 461-466.

VASVARI, G., SZILAGYI, I., BENCSURA, A., DOBE, S., BERCES, T., HENON, E., CANNEAUX, S. & BOHR, F. 2001. Reaction and complex formation between OH radical and acetone. *Physical Chemistry Chemical Physics,* 3**,** 551-555.

VENABLES, D. S., GHERMAN, T., ORPHAL, J., WENGER, J. C. & RUTH, A. A. 2006. High Sensitivity in Situ Monitoring of NO3 in an Atmospheric Simulation Chamber Using Incoherent Broadband Cavity-Enhanced Absorption Spectroscopy. *Environmental Science & Technology,* 40**,** 6758-6763.

VIONE, D., MAURINO, V., MINERO, C. & PELIZZETTI, E. 2003. The atmospheric chemistry of hydrogen peroxide: A review. *Annali Di Chimica,* 93**,** 477-488.

VIVANCO, M. G., SANTIAGO, M., MARTINEZ-TARIFA, A., BORRAS, E., RODENAS, M., GARCIA-DIEGO, C. & SANCHEZ, M. 2011. SOA

formation in a photoreactor from a mixture of organic gases and HONO for different experimental conditions. *Atmospheric Environment,* 45**,** 708-715.

VOLKAMER, R., KLOTZ, B., BARNES, I., IMAMURA, T., WIRTZ, K., WASHIDA, N., BECKER, K. H. & PLATT, U. 2002. OH-initiated oxidation of benzene Part I. Phenol formation under atmospheric conditions. *Physical Chemistry Chemical Physics,* 4**,** 1598-1610.

VON GLASOW, R. 2010a. Atmospheric Chemistry - Wider role for airborne chlorine. *Nature,* 464**,** 168-169.

VON GLASOW, R. 2010b. Atmospheric chemistry in volcanic plumes. *Proceedings of the National Academy of Sciences of the United States of America,* 107**,** 6594-6599.

VON SCHNEIDEMESSER, E. & MONKS, P. S. 2013. Air quality and climate - synergies and trade-offs. *Environmental Science-Processes & Impacts,* 15**,** 1315-1325.

WALLINGTON, T. & JAPAR, S. 1989. Fourier transform infrared kinetic studies of the reaction of HONO with HNO_3, NO_3 and N_2O_5 at 295 K. *Journal of Atmospheric Chemistry,* 9**,** 399-409.

WALLINGTON, T. J., DAGAUT, P., LIU, R. & KURYLO, M. J. 1988a. The gas phase reactions of hydroxyl radicals with a series of esters over the temperature range 240–440 K. *International Journal of Chemical Kinetics,* 20**,** 177-186.

WALLINGTON, T. J., HURLEY, M. D. & HARYANTO, A. 2006. Kinetics of the gas phase reactions of chlorine atoms with a series of formates. *Chemical Physics Letters,* 432**,** 57-61.

WALLINGTON, T. J., SKEWES, L. M. & SIEGL, W. O. 1988b. Kinetics of the gas-phase reaction of chlorine atoms with a series of alkenes, alkynes and aromatic species at 295 K. *Journal of Photochemistry and Photobiology a-Chemistry,* 45**,** 167-175.

WALLINGTON, T. J., SKEWES, L. M., SIEGL, W. O., WU, C. H. & JAPAR, S. M. 1988c. Gas-phase reaction of Cl atoms with a series of oxygenated organic species at 295 K. *International Journal of Chemical Kinetics,* 20**,** 867-875.

WANG, J., DOUSSIN, J. F., PERRIER, S., PERRAUDIN, E., KATRIB, Y., PANGUI, E. & PICQUET-VARRAULT, B. 2011. Design of a new multi-phase experimental simulation chamber for atmospheric photosmog, aerosol and cloud chemistry research. *Atmospheric Measurement Techniques,* 4**,** 2465-2494.

WAYNE, R. P. 2000. *Chemistry of Atmospheres,* New York, Oxford University Press.

WAYNE, R.P., BARNES, I., BIGGS,P., BURROWS,J.P., CANOSA - MAS , C.E., HJORTH, J., LE BRAS, G., MOORTGAT, G.K., PERNER, D., POULET,G., RESTELLI, G., SIDEBOTTOM, H. 1991. The nitrate radical: Physics, chemistry, and the atmosphere, Atmospheric Environment. Part A. General Topics, 25, 1, 1-203.WEDEL, A., MULLER, K., RATTE, M. & RUDOLPH, J. 1998. Measurements of Volatile Organic Compounds (VOC) during POPCORN 1994: Applying a new on-line GC-MS-technique. *Journal of Atmospheric Chemisty,* 31**,** 73-103.

WERKHOFF, P. & BRETSCHNEIDER, W. 1987. Dynamic headspace gas chromatography: concentration of volatile components after thermal desorption by intermediate cryofocusing in a cold trap : I. Principle and applications. *Journal of Chromatography A,* 405**,** 87-98.

WETZEL, G., OELHAF, H., KIRNER, O., FRIEDL-VALLON, F., RUHNKE, R., EBERSOLDT, A., KLEINERT, A., MAUCHER, G., NORDMEYER, H. & ORPHAL, J. 2012. Diurnal variations of reactive chlorine and nitrogen oxides observed by MIPAS-B inside the January 2010 Arctic vortex. *Atmospheric Chemistry and Physics,* 12**,** 6581-6592.

WHALLEY, L., STONE, D. & HEARD, D. 2012. New Insights into the Tropospheric Oxidation of Isoprene: Combining Field Measurements, Laboratory Studies, Chemical Modelling and Quantum Theory. *Top Current Chemistry,* Springer, 339, 55-95.

WHALLEY, L. K., LEWIS, A. C., MCQUAID, J. B., PURVIS, R. M., LEE, J. D., STEMMLER, K., ZELLWEGER, C. and RIDGEON, P. 2004. Two high-speed, portable GC systems designed for the measurement of non-methane hydrocarbons and PAN: Results from the Jungfraujoch High Altitude Observatory. *Journal of Environmental Monitoring,* 6**,** 234-241.

WHEELER, M. D., NEWMAN, S. M., ORR-EWING, A. J. & ASHFOLD, M. N. R. 1998. Cavity ring-down spectroscopy. *Journal of the Chemical Society-Faraday Transactions,* 94**,** 337-351.

WHITE, J. U. 1942. Long optical paths of large aperture. *Journal of the Optical Society of America,* 32**,** 285-288.

WINER, A. M., BREUER, G. M., CARTER, W. P. L., DARNALL, K. R. & JR, J. N. P. 1979. Effects of ultraviolet spectral distribution on the photochemistry of simulated polluted atmospheres. *Atmospheric environment*.

WINGENTER, O. W., KUBO, M. K., BLAKE, N. J., SMITH, T. W., BLAKE, D. R. & ROWLAND, F. S. 1996. Hydrocarbon and halocarbon measurements as photochemical and dynamical indicators of atmospheric hydroxyl, atomic chlorine, and vertical mixing obtained during Lagrangian flights. *Journal of Geophysical Research: Atmospheres,* 101**,** 4331-4340.

WINIBERG, F. A. F. 2014. *Development of HOx instrumentation for atmospheric chamber studies*. University of Leeds (School of Chemistry).

WOLLENHAUPT, M., CARL, S. A., HOROWITZ, A. and CROWLEY, J. N. 2000. Rate coefficients for reaction of OH with acetone between 202 and 395 K. *Journal of Physical Chemistry A,* 104**,** 2695-2705.

WYLIE, P. 1986. Headspace analysis with cryogenic focusing: A procedure for increasing the sensitivity of automated capillary headspace analysis. *Chromatographia,* 21**,** 251-258.

XING, J. H., TAKAHASHI, K., HURLEY, M. D. & WALLINGTON, T. J. 2009. Kinetics of the reactions of chlorine atoms with a series of acetates. *Chemical Physics Letters,* 474**,** 268-272.

XU, S. & LIN, M. C. 2007. Theoretical study on the kinetics for OH reactions with CH_3OH and C_2H_5OH. *Proceedings of the Combustion Institute,* 31**,** 159-166.

YAMANAKA, T., KAWASAKI, M., HURLEY, M. D., WALLINGTON, T. J., SCHNEIDER, W. F. & BRUCE, J. 2007. Kinetics and mechanism of the gas phase reaction of chlorine atoms with i-propanol. *Physical Chemistry Chemical Physics,* 9**,** 4211-4217.

YASSAA, N., MEKLATI, B. Y., BRANCALEONI, E., FRATTONI, M. & CICCIOLI, P. 2001. Polar and non-polar volatile organic compounds (VOCs) in urban Algiers and saharian sites of Algeria. *Atmospheric Environment,* 35**,** 787-801.

YATES, E. L., DERWENT, R. G., SIMMONDS, P. G., GREALLY, B. R., O'DOHERTY, S. & SHALLCROSS, D. E. 2010. The seasonal cycles and photochemistry of C-2-C-5 alkanes at Mace Head. *Atmospheric Environment,* 44**,** 2705-2713.

ZHANG, X., HE, S. Z., CHEN, Z. M., ZHAO, Y. & HUA, W. 2012. Methyl hydroperoxide (CH_3OOH) in urban, suburban and rural atmosphere: ambient concentration, budget, and contribution to the atmospheric oxidizing capacity. *Atmospheric Chemistry and Physics,* 12**,** 8951-8962.

ZHAO, Z., HUSKEY, D. T., NICOVICH, J. M. & WINE, P. H. 2008. Temperature-dependent kinetics study of the gas-phase reactions of atomic chlorine with acetone, 2-butanone, and 3-pentanone. *International Journal of Chemical Kinetics,* 40**,** 259-267.

ZHOU, S., BARNES, I., ZHU, T., BEJAN, I. & BENTER, T. 2006. Kinetic Study of the Gas-Phase Reactions of OH and NO_3 Radicals and O_3 with Selected Vinyl Ethers. *Journal of Physical Chemistry A,* 110**,** 7386-7392.

ZHOU, S. M., BARNES, I., ZHU, T., BEJAN, I., ALBU, M. & BENTER, T. 2008. Atmospheric Chemistry of Acetylacetone. *Environmental Science & Technology,* 42**,** 7905-7910.

Appendix A – Gas phase reactions of NO_3 radical in a flow tube using CRDS

Introduction

This section describes the measurement of the rate constants for the reaction of NO_3 with a series of aldehydes and alkenes inside a flow tube using CRDS. This was carried out to assess a suitable source of NO_3 in HIRAC. Preliminary work was carried out in a flow tube.

There are two main methods of NO_3 generation: thermal decomposition of N_2O_5 and reaction of NO_2 + O_3 (to be referred to as the *in situ* method). The most suitable for the study of NO_3 + alkenes is the former method since the latter requires use of O_3 which reacts with alkenes to form OH which will then oxidise alkenes and complicate the chemistry (Malkin, 2010).

Following several unsuccessful attempts at preparation and delivery of N_2O_5 in HIRAC, there was a need to improve the preparation and delivery system. A smaller CRDS system was used in order to better characterise the process of NO_3 generated from N_2O_5 prior to application in the larger volume of the HIRAC chamber. The main focus of this section will be to present a series of flow tube experiments carried out in the Dainton laboratory to study NO_3 generation methods on a smaller scale. This was used to optimise the conditions necessary for NO_3 production using thermal decomposition of N_2O_5 in preparation for subsequent kinetic studies in HIRAC.

Experimental details

Apparatus

An illustration of the CRDS instrument used for these experiments is shown in A.1. It consists of a 10 Hz pulse repetition frequency red light source (laser), an optical cavity and detection system. The light source travels along the length of the

flow tube (of ~ 1 m length) *via* a set of broadband mirrors, that direct the light into the optical cavity through 620 nm high reflectivity mirrors (Los Gatos Research, R = 99.995 %, ROC = 1.0 m, λ = 590 – 650 nm) that are aligned to maximum ring-down. A Nd:YAG (Continuum Powerlite 8010) pumped dye laser (Sirah, precision scan) operating on Rhodamine B, which allows scanning at 615 – 630 nm was used with the output of the dye laser tuned to the desired wavelength light at ~ 623 nm, as NO_3 absorbs strongly at this wavelength, and this is within range of the high reflectivity mirrors used. Argon was used as the purge gas for cleaning the mirrors. The reactants were introduced through a separate port together with U.H.P nitrogen (B.O.C. zero grade) gas acting as the bath gas.

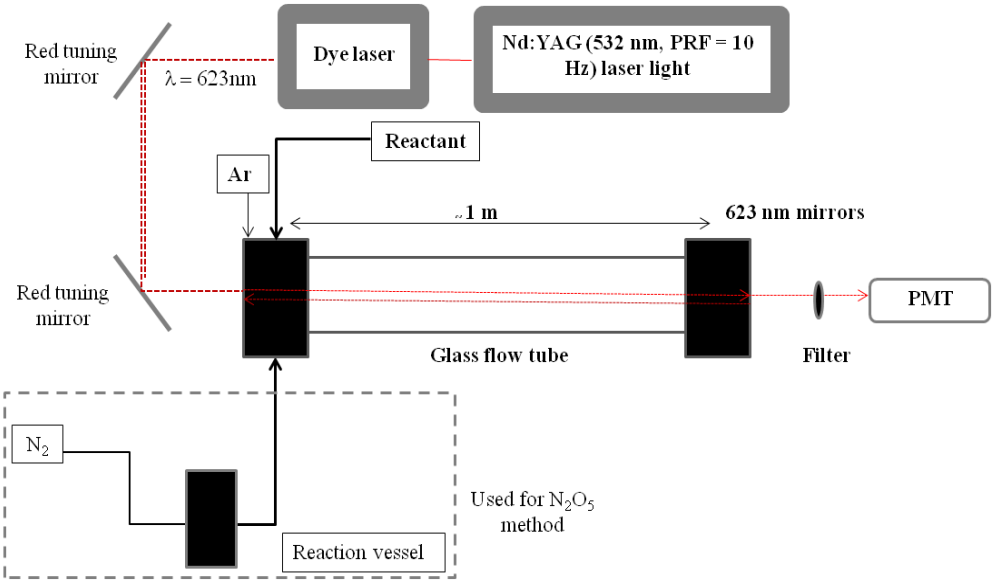

A.1: A sketch of the CRDS flow tube apparatus.

NO_3 generation via an *in situ* method

NO_3 detection using CRDS in flow tube

As has already been mentioned, NO_3 radical detection was successful in HIRAC using the *in situ* method of preparation; however NO_3 from N_2O_5 was not detected. This section will go through the details of NO_3 detection using CRDS, and on the work that has been done in generating NO_3 in this system as well.

660 nm mirrors would have been more ideal for the study of these reactions since absorption of NO_2 and O_3 are less prominent at this wavelength. The influence of NO_2 species present in the study of NO_3-organic kinetics is negligible since the majority of organics have been found to be reactive with NO_2 to a maximum of 10^{-20} molecule^{-1} cm^3 s^{-1}, which is at least a factor of 10^5 smaller than for the NO_3 radical (Atkinson *et al.*, 1984). The presence of O_3 on the other hand does cause problems, as it reacts quite readily with various organics, most notably alkenes. The latter reaction was studied in this work and will be mentioned in the following section. The reactions of NO_3 with aldehydes and with alkenes were also investigated. A summary of the NO_3 reactions carried out with aldehydes and alkenes studied using this CRDS system will follow in later sections.

The signals observed for the NO_3 and O_3 are shown in A.2. The results showed that doubling the NO_2 concentration had a small effect on the NO_3 signal, possibly due to an equilibrium effect ($NO_3 + NO_2 \leftrightarrow N_2O_5$). Based on the results found, a (NO_2) of 10^{12} molecule cm^{-3} was adequate for the purpose of these NO_3 kinetic investigations, since the signal observed was enough for the desired kinetic experiments to be performed, and since the maximum (O_3) was desired to be three orders of magnitude higher than (NO_2) to ensure 100% conversion.

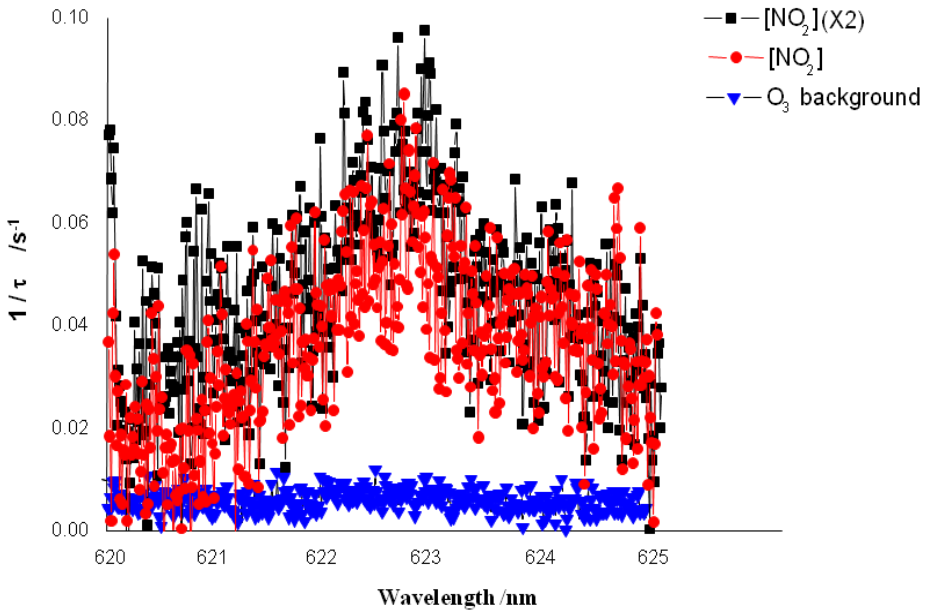

A.2: NO_3 and O_3 CRDS signal scanned over a wavelength range of 620 - 5 nm using different (NO_2).

O_3 + alkenes

O_3 + alkene reactions were studied in order to better characterise the flow tube CRDS system and ensure the setup was suitable for similar investigations using NO_3. The ozonolysis of alkenes are an important process in the atmosphere as they provide a direct oxidation pathway for unsaturated VOCs that competes with OH and NO_3 radical initiated processes and leads to production of important reactive intermediates such as OH and HO_2 (Paulson *et al.*, 1996; Malkin *et al.*, 2009). O_3 cleaves the double bond of alkenes, forming various different products, including OH in the case of some species. The kinetics of the ozonolysis of alkenes has been well reviewed in the literature (Atkinson *et al.*, 2006). The mechanism for the ozonolysis of alkenes was first suggested by Criegee (Criegee, 1975) and is described in A.3.

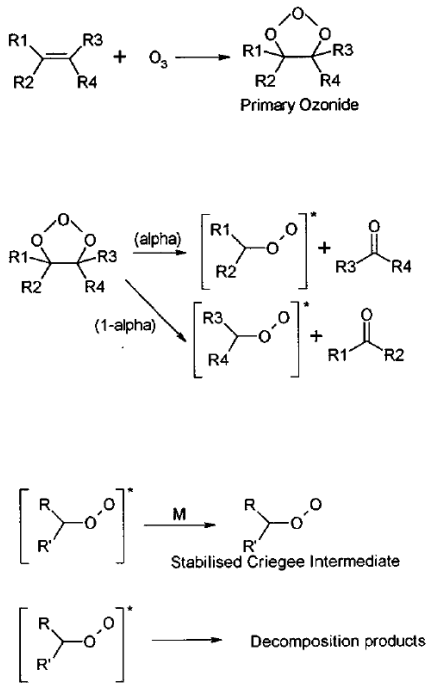

A.3: General mechanism for the reactions of O_3 with alkenes (Marston, 1999).

Experimental details

These experiments were carried out with the alkene (10^{15} – 10^{17} molecule cm^{-3}) being in excess of the O_3 (10^{14} molecule cm^{-3}), in order to obtain the pseudo-first order rate decay:

$$O_3 + \text{alkene} \rightarrow \text{products} \qquad \text{(A1.4)}$$

$$-d\frac{(O_3)}{dt} = k'[O_3] \quad \text{(A1.5)}$$

$$k' = k_{O3+alkene}[alkene] \quad \text{(A1.6)}$$

Where k' is the pseudo-first order rate constant for the O_3 + alkene reaction. The (alkene), being in excess and not being the monitored species, was multiplied by the contact time in the flow tube (~ 2 – 3 seconds – not well determined due to uncertainties in volume and flow in tube). Thus the calculation would be:

$$\ln\frac{(O_3)_t}{(O_3)_o} = k't \quad \text{(A1.7)}$$

$$\text{therefore, } \ln(O_3)_t = k't + \ln(O_3)_o \quad \text{(A1.8)}$$

$$\ln(O_3)_t = k((alkene)\,t) + \ln(O_3)_o \quad \text{(A1.9)}$$

$$\ln(O_3)_t - (O_3)_o = k't \ln(O_3)_t = k't + \ln(O_3)_o \quad \text{(A1.10)}$$

Results

A plot of the natural log of the decay of (O_3) as a function of the (alkene) multiplied by the contact time gives $k_{o3+alkene}$ as the gradient (from equation 5.10). This same method was used for all the experiments carried out in this system, including reaction of O_3 with ethene, propene, and trans-2-butene, reactions of NO_3 with ethanal, propanal and butanal, and reaction of NO_3 with propene. Most of these reactions were studied at room temperature, a flow tube pressure of 50 - 75 Torr, and a total flow of 0.25 SLM. The measured rate constants are shown in A.4. Good agreement was observed with literature values for the reaction of O_3 with ethene and trans-2-butene, however propene was a factor ~ 2 higher than the literature values.

Compound	**This work / molecule cm^{-3} s^{-1}**	**Literature (Experiment) /molecule cm^{-3} s^{-1}**	**Literature (Review) / molecule cm^{-3} s^{-1}**
Ethene	**1.74 (± 0.04) × 10^{-18}**	1.76 (± 0.20) × 10^{-18}	1.58 × 10^{-18}
Propene	**1.96 (± 0.06) × 10^{-17}**	1.05 (± 0.20) × 10^{-17}	1.00 × 10^{-17}
Trans-2-butene	**2.17 (± 0.15) × 10^{-16}**	(1.21 – 2.38)× 10^{-16}	-

A.4: Rate constants for the reaction of O_3 with ethene, propene and trans-2-butene measured by CRDS compared to IUPAC recommendations (Atkinson et al., 2006).

The plots for these reactions are shown in A.5. The ratios of the rate constants were in line with the IUPAC recommendations, however further work is needed in order to understand better the system and be able to calculate and measure the rate constants

of these reactions better. An uncertainty in our system, primarily from the estimation of the contact time, which is not reliably known, is a possible reason why results obtained are out by a factor of 2 or 3.

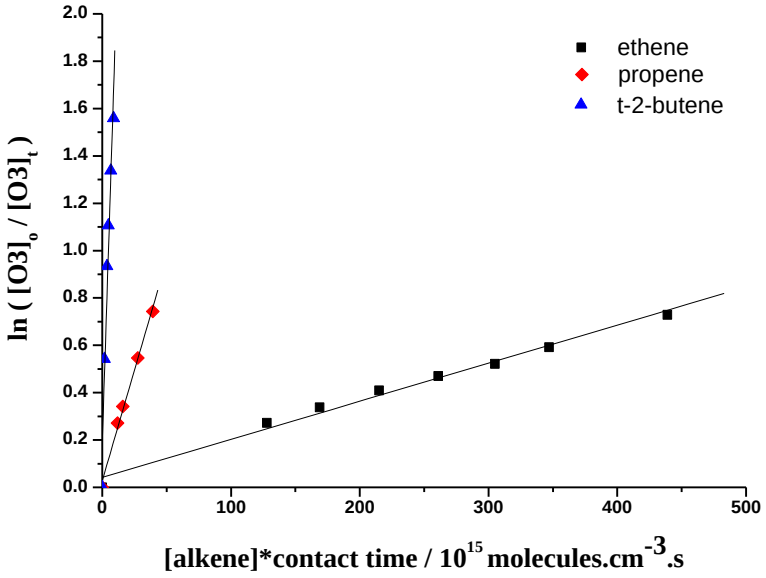

A.5: Pseudo-first order plots for the reaction of O_3 with ethene, propene and butene.

NO_3 generation via thermal decomposition of N_2O_5

Preparation

N_2O_5 is prepared by reaction of NO_2 with O_3 using a trap to isolate the N_2O_5. O_3 is produced using an O_3 generator that converts a flow of oxygen into an ozonised-oxygen mixture by electrical discharge. Two different O_3 generators were tested for the preparation of N_2O_5, the Fischer model 250 produces a maximum of 0.1% O_3 in O_2 whilst the model 500 has a higher energy electrical discharge and produces 1.0% O_3 in O_2.

The setup for preparation of N_2O_5 is shown in A.6. It consists of a vacuum line, a 2 L mixing vessel and a trap contained in a metal Dewar filled with a dry-ice / acetone slurry (195 K). The trap has a vent in order to allow unreacted gases to escape from the system through a bubbler, to the right of the trap.

A.6: N_2O_5 preparation setup.

N_2O_5 was produced by titrating 2 - 20 Torr of NO_2 with a constant slow flow of O_3/O_2 into the 2 L mixing vessel. The amount of NO_2 was typically ~ 2 - 4 Torr for the standard O_3 generator (0.1 % O_3/O_2), and ~ 20 Torr for the higher electric discharge O_3 generator. The flow rate of O_2 in to the O_3 generators was kept to a minimum setting on the O_3 generator in order to achieve maximum conversion to O_3. The flow of O_3/O_2 into the mixing vessel was also slow in order to ensure efficient titration of NO_2 to N_2O_5.

The amount of O_3 flowed into the mixing vessel was judged by eye, as the brown colour in the bulb due to NO_2 vapour slowly becomes colourless upon titration. Subsequently an extra ~ 100 Torr of O_3/O_2 was added to the mixing vessel in order to ensure maximum $NO_2 \rightarrow N_2O_5$ conversion. The mixing vessel at this point still isolated from the trap was raised to atmospheric pressure by flowing departmental nitrogen. The tap between the mixing vessel and the trap, and the vent were simultaneously opened once atmospheric pressure had been reached. The flow of N_2 forced the contents of the bulb into the trap, freezing down the product of titration, *i.e.* white N_2O_5 crystals. The flow rate through the system was kept low by observing the bubbler.

The trap, now containing N_2O_5 crystals was evacuated at room temperature in order to remove any remaining NO_2 and the sequence was repeated several times in order to produce a high yield of N_2O_5. The N_2O_5 produced was stored under vacuum

at 195 K in a Dewar topped with dry ice. An FTIR spectrum of N_2O_5 produced was obtained (A.7) to confirm the product identity and purity.

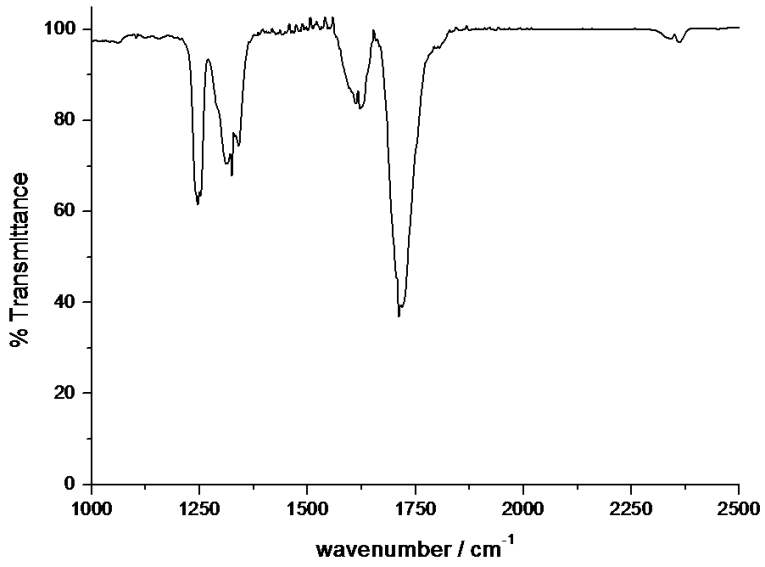

A.7: FTIR spectrum for N_2O_5 sample preparation.

N_2O_5 absorption peaks were observed at 1246 cm^{-1} (υ12 vibration-rotation band), 1350 cm^{-1} and 1750 cm^{-1}. The peaks at 1325cm^{-1} and at 1600cm^{-1} are interferences from HNO_3 and NO_2 respectively present as impurities in the sample (Ballard *et al.*, 1993). NO_2 is used in the preparation of N_2O_5 and is most likely due to decomposition of the N_2O_5 during sample preparation and time it took to take this FTIR, where N_2O_5 decomposes to give NO_3 and NO_2. HNO_3 is most likely present from the reaction of N_2O_5 with H_2O vapour in air, which in our preparation came from the FTIR cell not being sufficiently pumped down prior to taking a sample.

Results

Following successful preparation of N_2O_5, a number of studies were carried out using the flow tube CRDS system. A schematic of our setup is shown in Figure 5.1. Note that the main flow goes through the N_2O_5 only and reagent is injected directly into the cell. The first set of experiments were designed to optimise the method for delivery of N_2O_5 into the system. N_2O_5 was introduced through a port

connected directly to the flow tube thus minimising contact with the walls and therefore loss of NO_3 (Atkinson, 1990). The N_2O_5 was maintained at ~ 195 K until immediately prior to the start of each experiment. At the start of an experiment, the N_2O_5 bulb/trap was elevated from the dry ice Dewar and allowed to warm up. Signals due to NO_3 were observed instantaneously (Figure 5.7) indicating that the N_2O_5 sample was being rapidly consumed. As a result an immersion probe was employed to precisely control the temperature of the Dewar into which the N_2O_5 trap was kept on to using an immersion probe that would control the temperature at which the Dewar containing our trap of N_2O_5 was kept.

Measured change in ring down time observed from this NO_3 production method was at least 5 times greater than in the case of the *in situ* NO_3 generation method (A.8). These investigations were used to optimise the flow of N_2O_5 to obtain a sufficient NO_3 signal for kinetic studies without consuming N_2O_5 too rapidly.

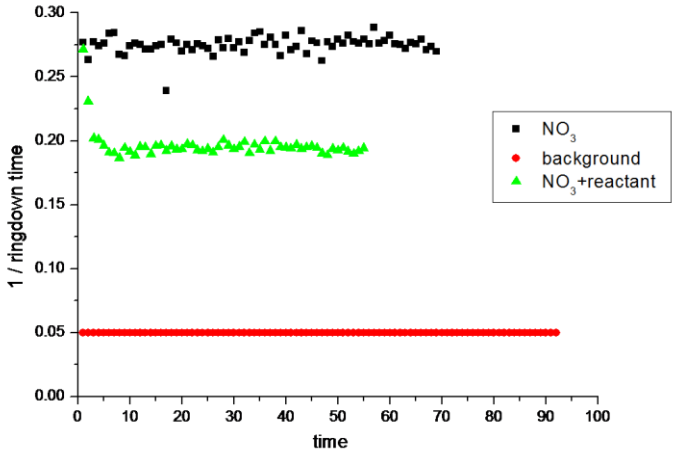

A.8: CRDS NO_3 signal at 623 nm generated from thermal decomposition of N_2O_5.

N_2O_5 decomposition was studied under lower temperature conditions (~ 173 – 233 K) and only a minimum temperature of ~ 203 - 223 K was reached for our experiments giving us a reasonably stable signal without consuming too much N_2O_5. It was also noted that upon increasing the main flow of gas through the N_2O_5, the stability of the NO_3 signal was improved further. The additional flow of N_2 most likely reduced contact of NO_3 with walls of the flow tube and flushes out the excess unreacted NO_2 from the system more rapidly, thus minimising fluctuations in the observed ring-down signal.

NO_3 + aldehydes

Experimental details

The next set of experiments studied using the flow tube CRDS system was the rate of reaction of NO_3 with a series of aldehydes (ethanal, propanal and butanal). Two different methods of NO_3 generation were used to compare the two sets of results. Similar conditions to the O_3 + alkene experiments were used, with (aldehydes) being in excess of the (NO_3) in order to achieve pseudo-first order conditions and allowing derivation of absolute-rate constants. A range of (aldehyde) between 10^{15} – 10^{16} molecule cm^{-3} was used. The flow of nitrogen through the flow tube was kept constant at ~ 200 sccm, and the total flow inside the system was ~ 0.25 SLM giving 130 - 140 Torr total pressure.

Results

NO_3 via thermal decomposition of N_2O_5 generation

The N_2O_5 was prepared on the same day as the experiments were carried out using already described methodology. The results obtained are shown in A.9, and are compared to literature values and previous work performed in HIRAC using the *in situ* method NO_3 generation method (Malkin, 2010). Thermal decomposition of N_2O_5 was achieved using an immersion probe that set the temperature of the bath in which the trap was kept to ~ 220 K.

Compound	$k_{NO3+aldehyde}$ / molecule^{-1} cm^3 s^{-1}	HIRAC (Malkin, 2010) / molecule^{-1} cm^3 s^{-1}	Relative (D'Anna, 2001) / molecule^{-1} cm^3 s^{-1}	Absolute (Cabañas, 2001) / molecule^{-1} cm^3 s^{-1}
Ethanal	**5.83 (± 0.58) × 10^{-15}**	(2.83 ± 0.59) × 10^{-15}	2.60 × 10^{-15}	4.71 × 10^{-15}
Propanal	**6.51 (± 0.21) × 10^{-15}**	(7.17 ± 0.69) × 10^{-15}	6.20 × 10^{-15}	8.97 × 10^{-15}
Butanal	**1.06 (± 0.41) × 10^{-14}**	(1.02 ± 0.10) × 10^{-14}	1.22 × 10^{-14}	1.94 × 10^{-14}

A.9: Rate constants for the reaction of NO_3 with ethanal, propanal and butanal using NO_3 generated from thermal decomposition of N_2O_5 with the flow tube CRDS setup compared to various literature values.

These results were within a factor of two of the literature values. However, excluding the good agreement for the butanal rate constant, the propanal rate constant was just within error and the ethanal rate constant was within error of the absolute-rate measurements and within the combined uncertainties of the HIRAC measurement. Moreover, the trend of the pseudo-first order plots (A.10) shows problems with the ethanal results, since it appears to overlap with the propene and is not reflecting the same ratios observed in the literature for this series of aldehydes.

These experiments were only repeated twice, and thus there may be the need to repeating them a few more in order to ascertain the results reported. Moreover, it is thought that the rate constant obtained for ethanal is a factor of 2 greater than the literature owing to impurities in the sample that was used, that may not have been stored and kept well before use.

Some signs of curvature are also apparent from the plots obtained (Figure 5.8), as was observed for O_3 + alkene experiments, which at first sight points towards problems with our experimental procedure. There may be, however, a possibility of having under-predicted the contact time of the gases in the flow tube, resulting in higher errors in our system. Problems with estimating the contact time in our system have meant that our method of analysis may be inaccurate. Also, from the curved plots obtained for all experiments carried out in this CRDS flow tube system, it is evident that the curvature is real, and that the method of analysis (using reaction 5.11) would need to be reevaluated for this sytem since a better fitting for the data being produced is necessary.

$$\ln (O_3)_t - (O_3)_o = k't \ln (O_3)_t = k't + \ln (O_3)_o \quad \text{(A1.11)}$$

Further studies are however needed in order to compare these findings with other NO_3 reactions in the same system using both NO_3 generation methods where possible, and be able to verify the results obtained.

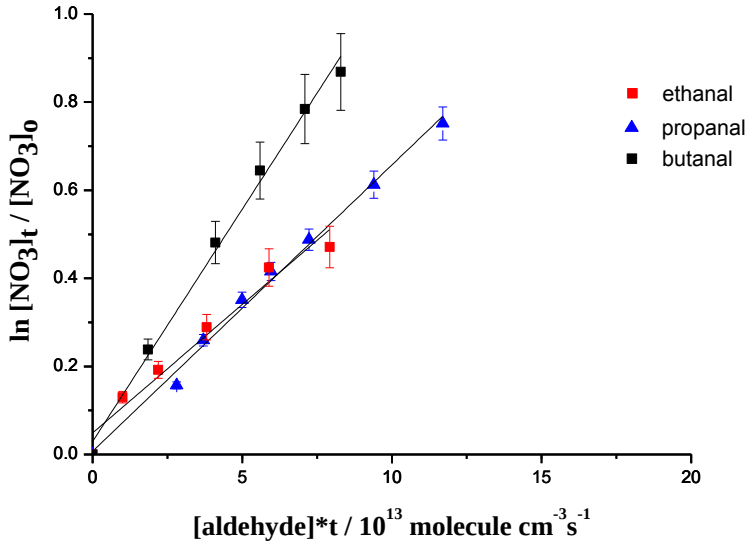

A.10: Pseudo-first order plots for the reaction of NO_3 with ethanal, propanal and butanal using NO_3 generated from thermal decomposition of N_2O_5 in the flow tube CRDS system.

NO_3 *in situ* generation

This kinetic investigation proved to be very curious for several reasons. The rate constants obtained were at least one order of magnitude slower than literature values (Cabañas, 2001; D'Anna, 2001; Malkin, 2010) and the results obtained in HIRAC using this same method by Tamsin Malkin (Malkin, 2010), as can be seen in A.11.

Compound	Mean k_{NO3} / molecule cm^{-3} s^{-1}	HIRAC (Malkin, 2010) / molecule cm^{-3} s^{-1}	Relative - (D'Anna, 2001) / molecule cm^{-3} s^{-1}	Absolute - (Cabañas, 2001) / molecule cm^{-3} s^{-1}
Ethanal	**2.81×10^{-16}**	$(2.83 \pm 0.59) \times 10^{-15}$	2.60×10^{-15}	4.71×10^{-15}
Propanal	**7.22×10^{-16}**	$(7.17 \pm 0.69) \times 10^{-15}$	6.20×10^{-15}	8.97×10^{-15}
Butanal	**1.22×10^{-15}**	$(1.02 \pm 0.10) \times 10^{-14}$	1.22×10^{-14}	1.94×10^{-14}

A.11: Rate constants for the reaction of NO_3 with ethanal, propanal and butanal using NO_3 generated from in situ method compared to those obtained by CRDS in HIRAC (Malkin, 2010) and literature values from Cabañas, 2001 and D'Anna, 2001.

The excess aldehyde appeared to react with the O_3, as the signal given was lower than the background for O_3 at higher concentrations of aldehyde (more so for larger aldehydes, *i.e.* butanal). Similar observations were noted when studies with no NO_2 in the system were carried out, *i.e.* O_3 and aldehyde were only present. From what was observed, it is not clear whether O_3 is reacting with the aldehyde and forming products that do not absorb, or that recycling of NO_3 is taking place, which is reacting more with O_3. The reaction of O_3 with aldehydes is however too slow to be of much significance in our system. Nevertheless, Figure 5.9 aldehyde reaction is so slow that the cavity ring-down signal observed for the reaction of NO_3 with butanal was lower than the O_3 background at a late stage of the experiment, and little is known about why this may be.

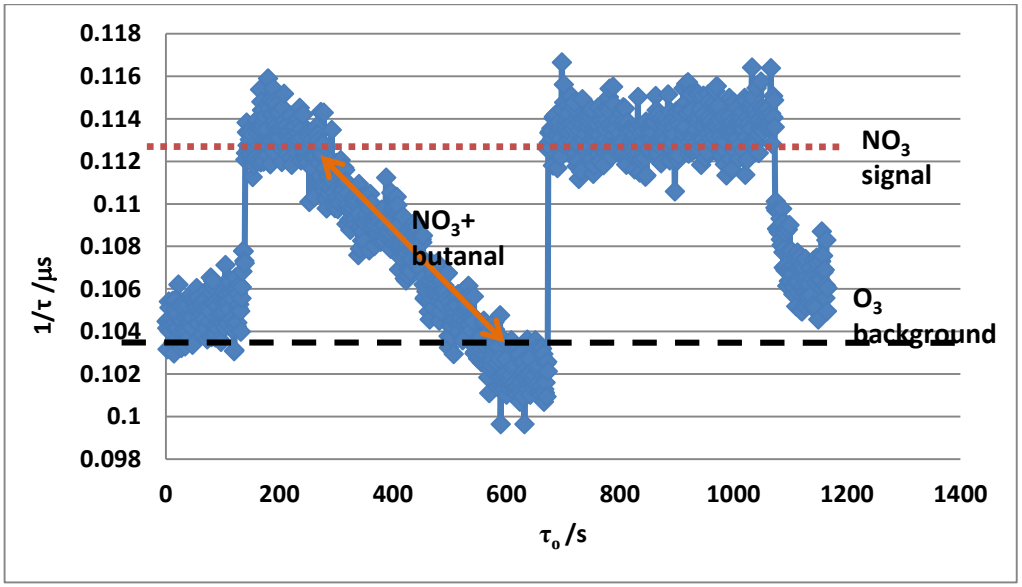

A.12: Cavity ring-down signal for NO_3 + butanal.

Regeneration of NO_3 is very likely, thus reacting further with aldehyde or even O_3. A possible equilibrium effect (A1.12), whereby N_2O_5 is formed, may be predominant over the duration of the experiment. Other possible reactions that may be occurring are reactions A1.13 – A1.15, that however are much slower than the reaction of NO_3 with aldehydes, and are therefore improbable to occur on such a short timescale. Nevertheless there is the possibility of NO_2 accumulating in the system, regenerating NO_3, but this factor might be too small to be noticed in our system.

$$N_2O_5 \leftrightarrow NO_3 + NO_2 \quad \text{(A1.12)}$$

$$NO_3 + O_3 \rightarrow NO_2 \quad \text{(A1.13)}$$

$$NO_3 \rightarrow NO_2 + O_3 \quad \text{(A1.14)}$$

$$NO_3 + RCHO \rightarrow NO_2 \quad \text{(A1.15)}$$

A decision was taken to turn our attention to N_2O_5, and to carry out the experiments using this as our NO_3 precursor rather than $O_3 + NO_2$. These experiments would confirm whether the rate constants obtained using the *in situ* method were true or, if they differ, may give evidence for NO_2 as a possible product from the reaction of NO_3 and aldehydes using this NO_3 generation method.

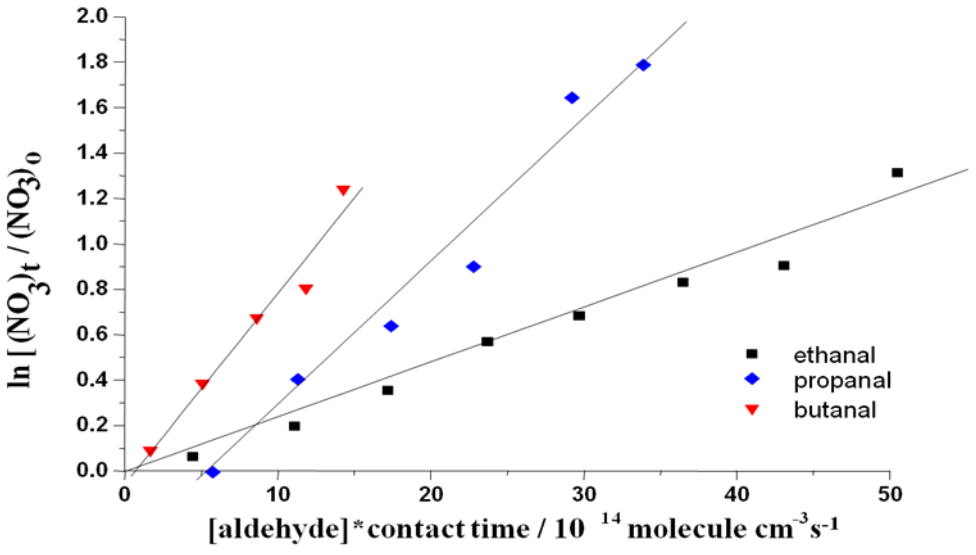

A.13: Plots for the reaction of NO_3 with ethanal, propanal and butanal using NO_3 generated from in situ method in the flow tube CRDS system.

A.13 demonstrates that the results obtained here are also showing signs of curvature, as was the case in the previous results obtained. This further confirm the

curvature is actually caused by our system, and that a different analysis method may be needed to better fit this data.

NO_3 + propene

A study of reaction of NO_3 with propene was carried out using NO_3 generated from the thermal decomposition of N_2O_5. It was unclear from the previous set of results for the reactions of NO_3 with aldehydes whether the method used had been suitable. Studying NO_3 + propene, a more reliably known reaction, would confirm the suitability of the N_2O_5 generation method for future NO_3 kinetic studies. The results obtained from this study are shown in A.14.

Compound	**measured rate constants / molecule^{-1} cm^3 s^{-1}**		**literature $k_{NO3+propene}$ / molecule^{-1} cm^3 s^{-1}**	
	$k_{NO3+propene}$	**$k_{NO3+propene}$**	**(Atkinson *et al.*, 1988)**	**(Atkinson *et al.*, 2006)**
Propene	**9.17 (±0.09) × 10 $^{-15}$**	1.48 (±0.14) × 10^{-14}	9.45 (±0.47) × 10^{-15}	9.50 (±0.20) × 10^{-15}

A.14: NO_3 + propene rate constants using NO_3 from thermal decomposition of N_2O_5.

There is good agreement with the literature for the first set of data, but very poor agreement in the case of the second rate constant. The results obtained were carried out on different days, and this may explain why they are almost a factor of two different from each other. Possible fluctuations in the temperature and pressure of the system during the experiment, or even variations in the flow of gases into our sytem may alter the results obtained. Both results are however found to be within error of the results obtained by Atkinson (Atkinson *et al.*, 1988). Further work is required in order to verify these results. Unfortunately, no other alkenes were studied in time for the submission of this report.

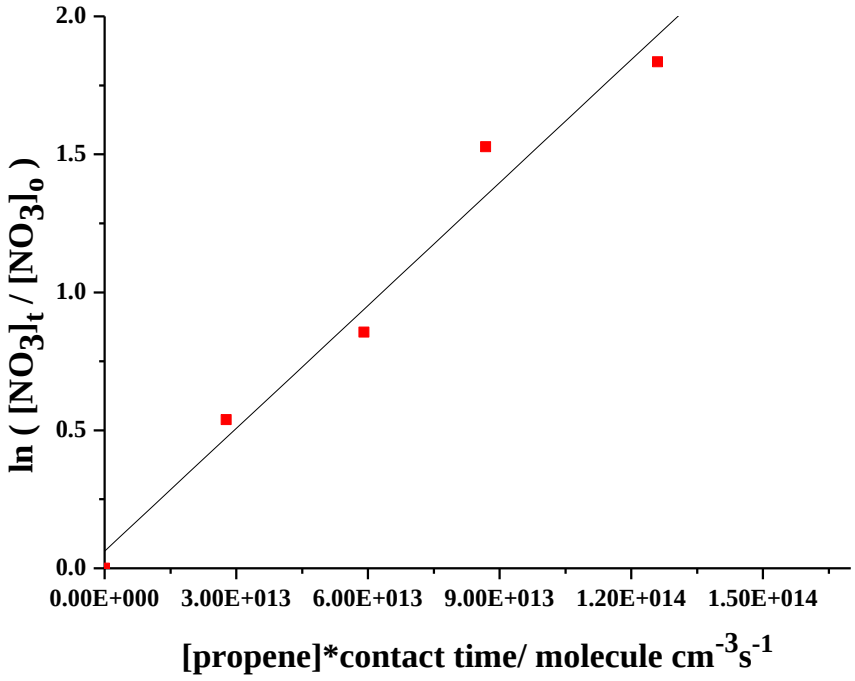

A.15: Pseudo-first order plot for the reaction of NO_3 with propene using NO_3 generated from thermal decomposition of N_2O_5 in the flow tube CRDS system.

The curvature of the plots obtained from all the results reported in this section indicates a possible flaw in our analysis. This was real, and points towards the need to use a different way of fitting our data to obtain a better gradient from our results. The different analysis method proposed is based on the exponential decay of $[O_3]$ in the flow tube:

The absolute rate constant may be derived from the integration of A1.16. This way, we are observing the area under the graph (shown in Figure 5.12) and hence the mean $[O_3]$:

$$(O_3)_t = (O_3)_o \, e^{-kbi\,(R)t} \qquad (A1.16)$$

$$\int (O_3)_t \, dt = \int (O_3)_o \, e^{-kbi\,(R)t} \qquad (A1.17)$$

$$= \frac{(O3)o}{kbi(R)} \left(e^{-kbi(R)t}\right)_o^t \qquad (A1.18)$$

$$= \frac{(O3)o}{kbi(R)} \left(1 - e^{-kbi\,(R)t}\right) \qquad (A1.19)$$

$$(O3) = \frac{areaundergraph}{contacttime} \qquad (A1.20)$$

$$= \frac{(O3)o}{kbi\ (R)t}\ (1 - e^{-kbi\ (R)t}) \qquad \text{(A1.21)}$$

N.B.: plotting ln $\frac{(O3)t}{(O3)o}$ vs [R]t gives initially a linear plot (as observed in data presented) but with significant curvature (as was observed in all cases) at the peak of the plot.

Future proposed research

Following this, the primary objective of these studies would be to continue this work in HIRAC, and thus be able to prepare N_2O_5 in a larger volume. Possible ways of delivery into HIRAC are being thought of. A suitable way would be to use a large glass vessel with a direct connection to the chamber and to the main gas flow (N_2), that would thus minimise contact with walls and also result in a more stable signal, as was observed in the investigations reported here.

N_2O_5*in situ* in the chamber, making use of the chiller system that has been recently installed to carry this out at sufficiently low temperatures (~ 223 - 253 K) is worth investigating; thus being able to isolate and make use of the N_2O_5 shortly after its preparation, and keeping it within the same reaction vessel. The temperature control of the system can be potentially utilised to drive the $N_2O_5 \leftrightarrow NO_2 + NO_3$ equilibrium to NO_3.

Appendix B – Simplified FACSIMILE model for acetone photolysis in HIRAC

```
* MCM3.2 Subset generated for the following species:   ;
* HCHO ;
*;
* Variable definitions.  All species are listed here.;
*;
VARIABLE
CH3COCH3 CH3COCH2O2 CH3COCH2 CH3CO3 CH3CO2 CH3CO CH3COOH CH3OH CH3O2
CH3O HCHO HCO CH3 CO CO2 OH HO2;
*;
PARAMETER
JCH3COCH3 1.65E-4;
*;
PARAMETER  TEMP        PRESSURE    DILUTE
           O2            N2       M        H2O
           KAPHO2;
*                                                                    *;
COMPILE INITIAL ;
 ?TEMP     = 2.95D+02 ;
 ?PRESSURE = 2.42E+02 ;
 ?M = 9.6576E+18*PRESSURE/TEMP ;
 ?N2 = 9.809E-01*M ;
 ?O2 = 0.000E-00*M ;
 ?H2O = 0.00*M ;
*
COMPILE RATES ;                                                      *;
* Generic Rate Coefficients ;
*                                                                    *;
*;
* Complex reactions ;
KAPHO2 = 5.2D-13*EXP(980/TEMP) ;
*;
**;
* ---------------------------------------------------------------------*;
* CH3COCH3 photolysis in N2 at 254nm
* ---------------------------------------------------------------------*;
*;
COMPILE EQUATIONS ;
*;
* Reaction definitions. ;
*;
% JCH3COCH3 : CH3COCH3 = CH3 + CH3 + CO ;
% 8.8E-12*EXP(-1320/TEMP) + 1.7D-14*EXP(423/TEMP) :
CH3COCH3 + OH = CH3COCH2O2 ;
*% 1.0E-30 (TEMP/300)-3.3*N2 : CH3 + O2 + M = CH3O2 + M ;
% 7.4E-13*EXP(-520/TEMP) : CH3O2 + CH3O2 = CH3O + CH3O + O2 ;
% 1.03E-13*EXP(365/TEMP) : CH3O2 + CH3O2 = CH3OH + HCHO + O2 ;
% 2.9E-12*EXP(500/TEMP) :
CH3CO3 + CH3CO3 = CH3CO2 + CH3CO2 + O2 ;
% 1.1E-11 : CH3O2 + CH3CO3 = CH3O + CH3CO2 + O2 ;
% 2.0E-12*EXP(500/TEMP) :
CH3O2 + CH3CO3 = CH3COOH + HCHO + O2 ;
% 8.0E-13 : CH3COOH + OH = CH3O2 + H2O ;
*% 8.8E-12*EXP(-1320/TEMP) + 1.7E-14*EXP(423/TEMP) :
CH3COCH3 + OH = H2O + CH3COCH2 ;
% 5.4E-12*EXP(135/TEMP) : HCHO + OH = H2O + HCO ;
*% 5.1E-12 : CH3CO + O2 + M = CH3CO3 + M ;
% KAPHO2*0.44 : CH3CO3 + HO2 = OH + CH3O2 ;
% 5.4E-12*EXP(135/TEMP) : HCHO + OH = H2O + CO ;
% 5.2E-12*O2 : HCO = HO2 + CO ;
% 1.44D-13*(1+(N2/4.2E+19)) : OH + CO = CO2 + HO2 ;
**;
COMPILE INITIAL;
* Set initial values for variables;
CH3COCH3 = 2.955E17;
**;
* Experimental results;
DATA;
TIME CH3COCH3;
RANGE 1.207E17 2.955E17;
```